Heterogeneous gold and vanadium based catalysts for hydrochlorination and oxidation reactions

Thesis submitted in accordance to the requirements of the University of Cardiff for the degree of Doctor of Philosophy

by

Marco Conte

November 2006

ProQuest LLC
789 East Eisenhower Parkway
P.O. Box 1346
Ann Arbor, MI 48106-1346

Form: PG/R/06/09

CARDIFF UNIVERSITY
PRIFYSGOL CAERDYDD

DECLARATION

This work has not previously been accepted in substance for any degree and is not concurrently submitted in candidature for any degree.

Signed ..... (candidate) Date 04/04/2007

STATEMENT 1

This thesis is being submitted in partial fulfillment of the requirements for the degree of PhD (insert MCh, Md, MPhil, PhD etc, as appropriate)

Signed ..... (candidate) Date 04/04/2007

STATEMENT 2

This thesis is the result of my own independent work/investigation, except where otherwise stated.
Other sources are acknowledged by footnotes giving explicit references.

Signed ..... (candidate) Date 04/04/2007

STATEMENT 3

I hereby give consent for my thesis, if accepted, to be available for photocopying and for inter-library loan, and for the title and summary to be made available to outside organisations.

Signed ..... (candidate) Date 04/04/2007

ABSTRACT

The first examples of gold as the catalyst of choice were the hydrochlorination of acetylene using gold on carbon catalysts and the oxidation of carbon monoxide, both identified around 20 years ago. From that time most research interest has been focused on the use of gold as a catalyst for oxidation reactions, whereas although gold can be an excellent electrophilic agent is some of its oxidation states, few studies are available which display this.

Chlorinated organic compounds are widely manufactured in industry for the production of chemicals that can be used as solvents, glues, anaesthetics, and precursor for plastics. However, the usual industrial conditions applied make use of high pressure and temperature. By focusing attention on the production of commodities like vinyl chloride monomer, and chloroethane we have seen that these kinds of products can be obtained under mild conditions when gold is used as a catalyst, and with high selectivity. Moreover, a tuneable effect can be obtained using different supports, or gold oxidation states.

Although gold as a catalyst for the hydrochlorination of acetylene is known, no literature is available on the effect of adding another metal, either as a bimetallic or an alloy system, on final activity. For this reason, the effect of adding metals such as Pd, Pt, Ru, Rh, Ir has been investigated. Gold alone gives the most stable performance. However, when Au/Pd is used an initial promotional effect is observed. Although this effect is not a long term effect, it has been possible to detect an influence of the gold oxidation state and to identify clearly the gold oxidation state responsible for the hydrochlorination of acetylene and the mechanism of catalyst deactivation.

Using carbon as a support, only carbon-carbon triple bonds are reacted and ethylene is unreactive. For this reason selectivity to vinyl chloride monomer in excess of 99% is achieved. This particular behaviour has been explained by postulating the formation of a C_2H_2/Au/HCl complex, and this hypothesis is supported by the use of deuterated reagents and molecular modelling investigations.

However, we have shown that this effect is unique to carbon, and other supports are largely ineffective. Surprisingly, ZnO as support produces a catalyst that is inactive for acetylene but active for the hydrochlorination of ethylene. Both Au supported on carbon or different metal oxides are ineffective as oxychlorination catalysts. In fact the formation of $ZnCl_2$ has been identified under reaction conditions, and it can be an active catalyst for the hydrochlorination reaction of double C-C bond containing substrates.

In addition the solid state phase transition of a vanadyl orthophosphate species ω-$VOPO_4$ has been investigated during *n*-butane oxidation. This solid phase has, up to now, received little attention due to the difficulty in obtaining it in a pure form and because it exists only at high temperature. It has been possible to demonstrate that reagents like *n*-butane, acetic acid, and CO are able to induce a phase transition of ω-$VOPO_4$ to δ-$VOPO_4$, and this is possible by removal of surface lattice oxygen, but preserving the polymorph nature of the two phases.

SUMMARY

The low temperature CO oxidation is described and discussed, using doped Au/TiO_2 catalysts. It has been possible to demonstrate that the presence of trace amounts of nitrate over Au/TiO_2 can lead to enhanced and long term activity improvements, which are 20-30% better than the undoped catalyst.

In addition hydrochlorination of acetylene using gold and bimetallic gold based catalysts using Pd, Pt, Rh, Ir and Ru on carbon is described. It has been possible to identify an enhanced initial activity for catalysts containing a small amount of Pd and Ir, and a long term enhanced stability when Rh is used, while metals such Pt and Ru do not give reproducible results or increased activity.
Investigations on reaction mechanism of hydrochlorination have been carried out using different triple C-C bond containing substrates, deuterated reactants and molecular modelling investigations. All the collected data suggest a reaction mechanism via alkyne/Au/HCl complex, and this can explain the exceptional selectivity of gold catalysts.

Moreover, hydrochlorination and oxychlorination of double C-C bonds containing substrates using Au/ZnO catalysts have been studied. It has been possible to observe that the reaction is not catalysed by gold, but by $ZnCl_2$ formation on the catalyst surface, and it has been possible to obtain more efficient catalysts by dispersing $ZnCl_2$ on silica, and the catalyst is effective for hydrochlorination only.

Finally, a phase transitions between two different vanadyl orthophosphate, ω-$VOPO_4$ and δ-$VOPO_4$, and their correlation with *n*-butane oxidation, are described and discussed. It has been possible to identify a chemically induced fast solid state transition triggered by removal of surface lattice oxygen.

ACKNOWLEDGMENTS

I wish to thank Prof. Graham Hutchings for giving me the possibility to enjoy this research project in Cardiff, and for the chance to explore different fields of chemistry during these three years. As well as his trust on my skills, and for his supervision both during my research and the writing of this thesis.

Moreover, I like to thank Dr. Philip Landon, for his assistance in supervising and to have patiently contributed to the corrections of this thesis especially on the written style and English, as well as Dr. Dan Enache and Dr. Albert Carley for further supervision.

The work that is reported here would not have been possible with the help of other people. For this reason I am grateful to Prof. Chris Kiely and Andy Herzing that provided me support on TEM analysis and to Dr. David Willock and James Landon for the molecular modelling investigations, as well as to Dr. Frank Girgsdies for a fruitful collaboration in XRD.

I would thank also other teaching and research staff members like Dr. Damien Murphy, Prof. David Knight and Dr. Colin Rhodes with a special thanks to Dr. Stuart Taylor.

In addition, having carried out this research in a chemistry department, also the role of all the technical and clerical staff in Cardiff University has been important. Among others I like to mention: Gary Coleman, Robert Jenkins and John Bowley, with a special thanks to Alun Davis for his endless patience and prompt support.

Finally some special acknowledgments; it is my opinion that life is matter of cycles, and like the pre-Socratics, I think that everything flows and nothing stands still. During my period in Cardiff, I had the chance to meet many people. Like in a journey on a train, we can find people that will stay with us for the entire journey, people only for a part, and people that we could even not to note. To me this is another cycle that is closing; I do not know who of them will be with me to the next rail stop, however I have to thank all the following people that I found during this time or that they were with me from the previous one:

Laura de Francesco	Stefano Ceola	Zi-Rong Tang
Fabrizio Pertusati	Sandra Lavina	Paula Janeiro
Jignesh Khakhar	Davide Bortolato	Tony Lopez
Gerolamo Budroni	Alessandro Ongarato	
Javier Franqueira	Yi-Jun Xu	

As well as my family to have supported my proposal to carry out such PhD experience abroad.

Thank you
Marco Conte

TABLE OF CONTENTS

Chapter 1: CATALYSIS BY GOLD AND VANADIUM PHOSPHORUS OXIDES

1.1 Introduction

This chapter is focused on the description of gold chemistry with specific examples of oxidation, hydrochlorination and oxychlorination reactions, as well as the uses and the properties of vanadium phosphorus oxides towards oxidation reactions.

Both gold and vanadium have been used for heterogeneous catalysis applications, as a consequence, elements of catalysis by surfaces, metal cluster structure, role and effect of supports and catalyst preparation techniques are described

1.2 General aspects of catalysis by gold

Gold has been considered for long time a metal without any particular catalytic activity. However, although this can be true for bulk material, when gold is used in clusters of nanometer size range, it can display surprising catalytic activity [1, 2].
One of the main reasons considered for the absence of activity for gold as a catalyst was the absence of oxidation of the bulk material. In fact, the only characterized oxide of gold is Au_2O_3, but this oxide present a small formation enthalpy of –19.3 kJ mol^{-1} and it is best obtained by heating Au(III) hydroxide at 150 °C [3] and it decomposes to the elements above160 °C [4], whereas oxygen does not react with bulk gold up to the decomposition temperature of the oxide. Nevertheless, when gold clusters are used, gold can be an excellent oxidation catalyst, and probably, the most investigated example is CO oxidation to CO_2 that can occur at temperatures as low as –73 °C [1]. In order to evaluate the role of promoters, this reaction has been investigated in this thesis (chapter 3).

Another parameter generally used to explain the absence of catalytic properties of bulk gold is its electronic configuration, [Xe] $4f^{14}$ $5d^{10}$ $6s^1$, and the extremely high value of the

first ionisation potential 888 kJ mol^{-1}[5]. In addition, the electronegativity value of 2.54, and the standard electrode potential of 1.38 V for the reduction of Au(III) to Au(0) are the highest for all the metals. If this last parameter is used as a term of comparison to evaluate the performance for the hydrochlorination reaction of acetylene among different metal chlorides, gold is able to display the highest conversion values [2]. Investigations into the effect of the simultaneous presence of a second metal with gold for the hydrochlorination reaction have been carried out (chapter 4) as well as new proposal for reaction mechanism (chapter 5).

Further important reactions that are possible to carry out using gold catalysts are: selective oxidation of propene to propene oxide [6], water gas shift reaction [7], NO reduction [8], selective hydrogenation of acetylene [9]. In addition, a gold based catalyst is nowadays considered the best catalyst for the industrial manufacture of vinyl acetate monomer [10], this catalyst is a bimetallic system comprising gold/palladium and its success helped to promote interest in the use of gold as an effective catalyst for industrial applications.

However, although the considerations given above can be useful to explain some properties of gold as catalyst, many other aspects are still unclear. Further factors like: particle size, type of support, structure, preparation methods, and promoters are crucial to obtain a good catalyst. In fact, all these factors are important for every supported metal catalyst, but in the case of gold their importance is higher. It is well known that small variations in the method of synthesis can cause the difference between an excellent and a poor catalyst, and this aspect has been demonstrated from a great number of experiments [11,12]. In order to better understand the behaviour of gold as a catalyst, some effects of these parameters are discussed in more detail in the following paragraphs.

1.2.1 Gold cluster size effect

In catalysis, the term cluster is used to identify aggregates of atoms where the bulk solid,

usually a metal, is in the range of nanometers and the number of atoms is in the range from 3 to 10^4 [13]. Metal clusters exhibit different and distinct properties in comparison with the corresponding bulk solid, such as different optical and electronic properties, and different melting points [14]. A catalyst usually displays its activity by inducing a modification of electronic density of one or more reactants. Consequently, if the metal, or more generally, the material responsible for the catalytic activity is in a physical state where its surface electronic properties are different than that of bulk, it can display different catalytic activity.

However, it is worth noting that there is no agreement on what number of atoms should be called a cluster [14, 15], although the usual upper limit of 10^4 units is accepted. Nevertheless, this is a quite wide range, and different cluster sizes, even under the same conditions can display different catalytic properties such as different conversion or selectivity, or the possibility of changing form one kind of catalysed reaction to another. Moreover, within the same cluster, different catalytic properties can be associated with different cluster faces, due to different saturation levels, i.e. dangling bonds from the surface [16].

A good example is the 'Wulff polyhedron', which is one of the most common geometries observed for metal clusters including gold; see figures 1.1 and 1.2 [17, 18].

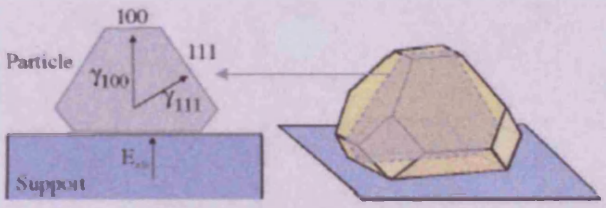

Fig. 1.1: Regular Wulff polyhedron, and identification of crystal planes [17]

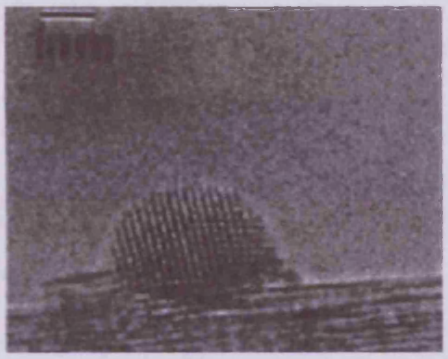

Fig. 1.2: Example of Wulff polyhedron for Au particle on MgO [18]

If a regular Wulff polyhedron consisting of 201 atoms with a face central cubic (fcc) packing is considered, 122 of those atoms are on the surface. Two distinct faces – square (100) and hexagonal (111) - can be identified with different inter-atomic distances and

different reactivity (fig 1.1). Moreover, of these surface atoms 60 are located at edges or corners, leading to a further difference of reactivity. A real example of Wulff polyhedron of Au cluster over MgO is reported in figure 1.2.

Concerning gold, the particle size range for which it can exhibit catalytic activity is still a matter of debate. Indeed, it is possible to find examples of catalytic activity for gold in the range 2 to 3 [19] or 3 to 5 [20] and 7 to 8 nm [21]. However, the proper size range is also dependent on the investigated reaction, and it is possible to find examples of active gold particles in the range 30 to 50 nm [22]. These discrepancies can be explained by taking into account the fact that a reaction can be catalysed by different particle size ranges, moreover it is also possible that cationic gold is participating in the reaction. In this thesis a good example during the hydrochlorination reaction of acetylene will be provided (chapter 4 and 5); although Au(0) is able to catalyse the reaction, and the particle size is in the range of 10 nm, Au(III) is able to perform the reaction more efficiently.
The only agreement among researchers concerning the range of gold particle sizes for activity relates to the upper and lower limits, which are considered to be 50 and 2 nanometers respectively [23].

1.3 Reaction mechanisms over metal surfaces

The most common and accepted reaction mechanisms that can take place over a metal surface are the Langmuir-Hinshelwood (LH) and Eley-Rideal (ER) mechanisms [24]. Although they are limited conditions of kinetic process to a catalyst surface, they are useful to give some indication on how a heterogeneous catalyst can operate. Examples of these two different mechanisms are present in this thesis. The hydrochlorination of acetylene over gold on carbon catalyst (chapter 4 and 5), supports the formation of a complex with both reactants adsorbed on the catalyst surface. It is considered that hydrochlorination reaction of ethylene over gold on zinc oxide catalyst takes place *via* an ER mechanism.

1.3.1 Mechanism proposed by Langmuir and Hinshelwood

If it is considered that in the general case of two reactants A and B which lead to only one product, in the Langmuir-Hinshelwood mechanism it is assumed that both of the reactants A and B are adsorbed on the surface catalyst. The reaction occurs when A and B are able to be in contact, after migration on surface catalyst (fig. 1.3).

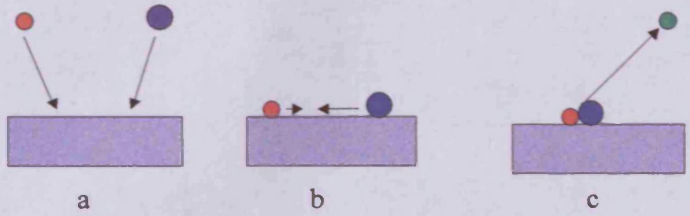

Fig. 1.3: Langmuir-Hinshelwood mechanism: a) approach of both reactants to catalyst surface, b) migration over catalyst surface and c) collision and product formation

Indicating θ_A and θ_B, the surface coverage for A and B respectively, a kinetic constant k, and taking into account that both of them are on the surface, an expected expression rate, r, is equal to:

$$r = k\theta_A\theta_B \qquad \text{(eq. 1.1)}$$

Using macroscopic parameters to define θ_A and θ_B, like the Langmuir isotherm constant K and partial pressure p, it is possible to write:

$$\theta_A = \frac{K_A p_A}{1 + K_A p_A + K_B p_B} \qquad \text{(eq. 1.2)}$$

And

$$\theta_B = \frac{K_B p_B}{1 + K_A p_A + K_B p_B} \qquad \text{(eq. 1.3)}$$

expressions, that can be substituted into 1.1 and lead to:

$$r = \frac{kK_A K_B p_A p_B}{\left(1 + K_A p_A + K_B p_B\right)^2} \qquad \text{(eq. 1.4)}$$

1.3.2 Mechanism proposed by Eley and Rideal

In contrast, in the Eley-Rideal mechanism, only one of the two species is really adsorbed on the catalyst surface, while the other is in a fluid phase. The reaction takes place when the species in the fluid phase encounters the other on the catalyst surface (fig 1.4).

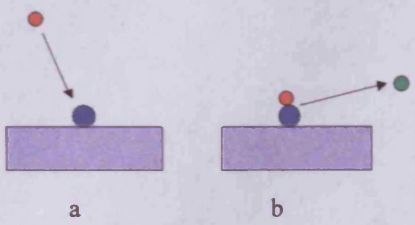

Fig. 1.4: Eley-Rideal mechanism: a) one reactant is already adsorbed on catalyst surface and b) collision on the adsorbed species

Indicating A as the adsorbed species, B as the species in the fluid phase and using the same notation used above, the rate is defined:

$$r = kp_B\theta_A \qquad \text{(eq. 1.5)}$$

In addition, if A follows a Langmuir isotherm of constant K, it is possible to write:

$$r = \frac{kKp_Ap_B}{1+Kp_A} \qquad \text{(eq. 1.5)}$$

In this case, if the catalyst surface is completely covered by the species A, the rate determining step of the catalysed process is the collision between A and the species B in the fluid phase. Whereas, if the surface it is not completely covered, the migration of A on the surface can become important, giving an intermediate situation between the LH and ER mechanisms.

1.4 Role and properties of the catalyst support

In heterogeneous catalysis only the catalyst surface is useful in terms of catalytic activity. This aspect is crucial, and immediately introduces the distinction between supported and non-supported catalysts, and the role of the support for a catalytic reaction.

The first case is when the material itself, i.e. when it is in bulk state, is able to display catalytic activity. For example, some metal oxides or some metals. Since only the surface is active, no other parts of the bulk material contributes to catalyse the reaction [25]. This circumstance has two immediate implications: the first is economic, if the active species is a precious metal, and only the metal surface is active, it is unacceptable to use the active component as bulk. The second aspect, is explained in the figure below (fig 1.5):

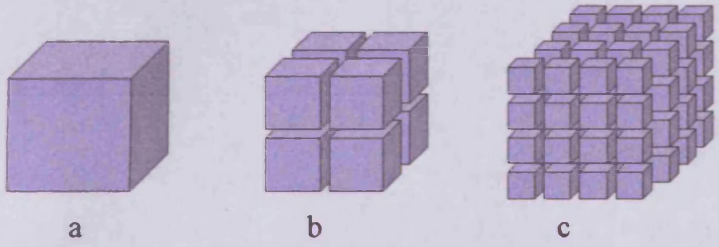

Fig. 1.5: Effect of the increase of surface area moving from a) single particle to b) and c) smaller particles

In the picture above the ideal case of a cube made of metal atoms, broken down into smaller cubes is shown. The sum of the total atoms is obviously the same, but it is possible to increase dramatically the number of atoms on the surface. If the initial cube is totally made of 10^6 atoms, the surface fraction of atoms moves from a) 6% to b) 12% and c) 24%. However, as the surface is responsible for the catalytic activity, it is possible to increase the activity of this metal as a catalyst. When the cluster is very large, the surface atom fraction is too small to display catalytic properties, if a cube of 10^9 atoms is considered only 0.6% of atoms are on surface.

If the described process is carried out to the point where nanometer clusters are formed, it is evident that these clusters are not, and they cannot be, thermodynamically stable [25].

Large crystals are more stable than small crystals, and as a result, the clusters have the tendency to aggregate with each other to reach a more stable thermodynamic condition; this process is named sintering [26], and it is well known in heterogeneous catalysis, because it can irreversibly affect catalytic properties, usually with detrimental results. The crucial role of the support is to disperse the chemically active component to increase the exposed surface area and consequently increase the catalytic activity, but at the same time, to avoid sintering.

The choice of the support is largely determined by the nature of the reaction system. In addition, it should be stable under reaction conditions, and it should not interact with solvent, reactants, or reaction products.

The features required of a material to be a good support are: 1) chemically inert towards secondary unwanted reactions, 2) good mechanical properties (resistant to abrasion, and thermal expansion), 3) high surface area, 4) high porosity and 5) low cost [27].
Properties 2) and 5) are particularly important when industrial application is required. Practically, few materials possess all, or the major part of, the points indicated above. SiO_2, Al_2O_3, TiO_2 and activated carbons are examples of some commonly used supports of precious metals for industrial applications.

1.4.1 Support effects for gold catalysts

In this section, most of the studies described concern the use of gold on supported metal oxides, while specific examples and interactions of gold over carbon will be treated in chapter 4 and its use towards hydrochlorination reactions. As well as the supports mentioned above, other oxides particularly suitable for gold are: Fe_2O_3, CeO_2, ZnO and MgO.

Different supports can have a dramatic effect on the final catalytic performance for both activity and selectivity. A good example is provided in this thesis. Gold on TiO_2 is an

excellent catalyst for low temperature CO oxidation (chapter 3), but it is ineffective for any kind of hydrochlorination reaction (chapter 4 and 6). Similar phenomena are observed when carbon is used as support, it is able to catalyse the hydrochlorination reaction but not CO oxidation; in addition, for hydrochlorination it is effective towards substrates containing triple C-C bonds only (chapter 4 and 6). Moreover, even in the same class of support, if different kinds of carbon are used different results can be obtained (chapter 4). Among carbons it is usually accepted that different carbons can lead to a different cluster formation process, but it is possible to find examples in the literature where, even with similar gold particle sizes different carbon supports can lead to different results [28].

In the case of metals oxides as support, although the matrixes are easier to characterize, they are from some points of view even more intriguing. Indeed it is possible to find examples where not only the support influences the Au cluster final structure, but also Au can affect the support by reducing it as in the cases of CeO_2 and Fe_2O_3 [29, 30]. In addition, and this is true for oxidation reactions, it is assumed that the oxygen necessary for the reaction does not come from the oxidizing atmosphere, but form the support at the interphase region with the gold metal cluster, and some authors consider this route operates for CO oxidation [31].

Nevertheless, although these data indicate clear evidence of the support effect, the matter is far to from being understood. Nørskov and co-workers [32] have recently generated much debate by analysing the results from many other studies concerning the use of Au catalysts for CO oxidation. The effect of the support has been considered in terms of conducting and insulation properties, and this led to the conclusion that although the support can have an influence on catalytic properties this effect has to be considered as minor. Instead the most important parameter is the gold particle size, which governs the number of low-coordinated gold atoms available for reaction (fig. 1.6):

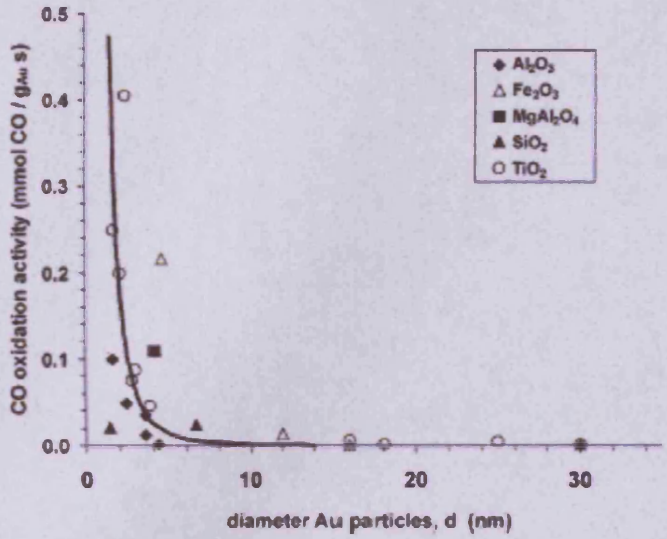

Fig. 1.6: Measured activities (in mmol CO/(gAu) for CO oxidation at 0 °C over different Au-based catalysts as a function of the average particle size. Supports are indicated by the symbol shape. Open symbols are used for reducible supports; solid symbols for irreducible supports [32].

Other authors disagree, because even assuming the absence of a support effect, the support can indirectly participate in the process affecting the cluster formation process, and therefore such arguments are not true. In addition the preparation technique used is crucial, as described in the next section.

1.5 Catalyst preparation method

Taking into account the effect of gold particle size, it is fundamental to have a cluster size distribution as narrow as possible, and this is largely determined by the preparation technique used [33]. For these reasons a brief description of the most common preparation techniques will be presented, with particular attention to the case of gold as an active species.

The most common preparation techniques used to prepare metal supported catalysts are: impregnation, deposition precipitation and co-precipitation. Other methods like sol immobilization techniques [34] have not been used and so they will not be described.

1.5.1 Impregnation technique

The impregnation technique is a simple way to prepare a catalyst, due to the limited number of parameters to control. Substantially, this method consists of dissolving a metal precursor, as a salt, in a solvent with the desired metal loading. This solution is impregnated onto the support, present in the form of powder, pellets, or granules. Afterwards it is possible to follow different procedures. The simplest is to dry the sample at a temperature and for a time sufficient to eliminate the solvent, or to proceed with calcination in the usual temperature range between 200 and 500°C. The calcination temperature is often a crucial parameter. Several publications report that highly active gold catalysts have to be calcined at temperatures above 300 °C [35]. However, other examples are available were increasing calcination temperature leads to a decrease in catalytic activity [36].

An important variation of the impregnation technique is the 'incipient wetness impregnation' [37], which has been used extensively in the present work. In this variation, the amount of solvent is the minimum amount necessary to fill the pore volume of the support. A useful aspect of this method, when compared with the usual impregnation is that the metal loading can be carefully determined and obtained. However, the method can be more affected by gradient phenomena, which can lead to an inhomogeneous product (chapter 4). It is worth mentioning that for industry the wetness impregnation method is preferred due to economic reasons, since only the amount of precious metal needed to reach the desired loading is used [37].

1.5.2 Deposition precipitation technique

The deposition precipitation technique consists of introducing the metal precursor solution, in a slurry containing the support, under stirring. The cluster formation process over the support, is induced by changing the pH value and temperature of this heterogeneous mixture often leading to contradictory results [38, 39].

If compared with impregnation, the deposition precipitation technique is able to lead to a final homogeneous product, if the same batch of catalyst is considered. However, the number of parameters to control is higher, and more difficult to control, especially the pH during the precipitation step, which can lead to more difficult comparison among catalysts from different batches. Moreover, using the wetness impregnation method, the final metal loading can be assumed to be equal to the nominal loading, this is not true when deposition precipitation is used. In this case, only a fraction of the introduced metal really contributes to the formation of the supported clusters, the other fraction stays in solution, with a proportion sometimes equal to 50 %. [40]. For this purpose, it can be useful to observe the following plot (fig 1.7), illustrating the real amount of gold deposited as a function of precipitation pH when TiO_2 is used as support [40].

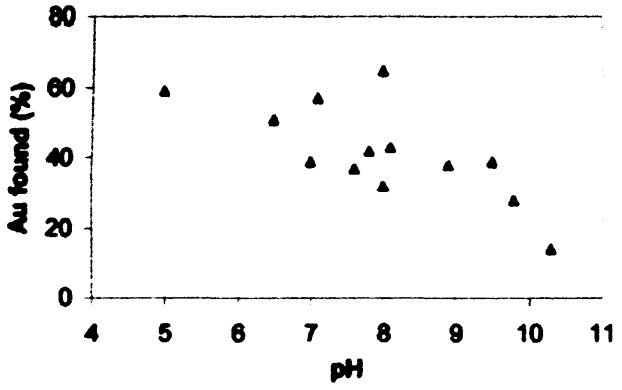

Fig. 1.7: Fraction of gold determined by ICP-AES to be incorporated in samples depends on the pH during precipitation for Au/TiO_2 catalysts with a nominal gold loading of 2.4 wt.% [40].

Low pH values are insufficient for precipitation, and too high values are able to deposit only a small fraction of gold. For this reason, the most common value used to prepare a supported catalyst is around 9. In addition, changes in pH can have a massive effect on the final cluster size as displayed in figure 1.8 below [40] for XRPD analysis of Au/Al_2O_3 samples.

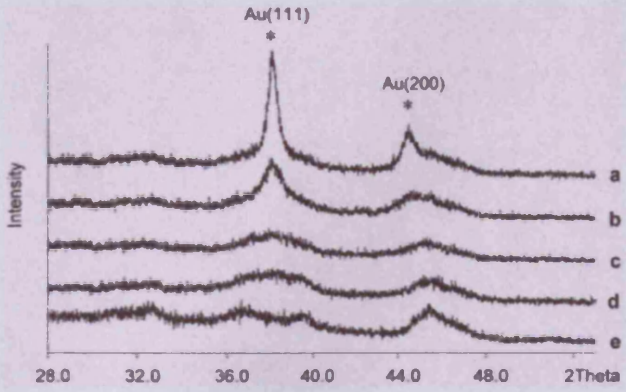

Fig. 1.8: XRPD of a series of Au/Al_2O_3 catalysts precipitated at different pH values: (a) pH 6.3; (b) pH 6.8; (c) pH 7.7; (d) pH 8.1; (e) support. [40]

Even relatively small pH changes from 6.3 to 6.8 have a dramatic effect on the crystallinity of the final products (fig1.8) and pH values above 8 lead to particle sizes not detectable by common XRPD [40].

A further problem can rise from the salt used to adjust the pH value, usually solutions containing NaOH, $NaHCO_3$, Na_2CO_3. If this salt is not removed, or partially removed with a proper washing procedure, the remaining salt can act as a contaminant, with a depressing or a promoting action on the final performance. A good example of these kinds of effects are shown in this thesis, when the influence of traces of nitrates on Au/TiO_2 catalysts for low temperature CO oxidation will be described (chapter 3).

One of the main differences between impregnation and deposition precipitation techniques is the final shape of the metal particles. Over TiO_2, the shape of gold particles is usually spherical for impregnation, and hemispherical for precipitation [41] with consequently different angles and surface contact. Parameters such as the last ones, can be quite important when the reaction takes place at the metal-support interface, or the catalysed reaction is support dependent.

Usually, the precipitation technique leads to a particle size range narrower than impregnation, and this can be quite important when the catalysed reaction takes place only for a limited cluster size range. However, the main difficulty is to be able to preserve all the parameters affecting precipitation from one catalyst batch to another.

1.5.3 Co-precipitation technique and calcination temperature

The co-precipitation technique is probably the more refined way to prepare a catalyst. It can be considered as a variation of deposition precipitation. In this method, metal and support are precipitated together by mixing two different precursor solutions at a given temperature, and effecting the co-precipitation with appropriate pH modification [42]. Most of the time the final product has a poor level of crystallinity, but this can be increased by changing the temperature of the process or the stirring time. If a high level of crystallinity is required, this can usually be achieved by carrying out calcination of the resulting slurry.

With this technique, it is generally possible to obtain a final product with high surface area and high metal dispersion. However, for this technique, because of the high number of parameters to control, it is often difficult do obtain equals performance for different catalyst batches.

In all the techniques discussed above, a calcination step may be required in order to modify the amount of metal in a reduced state, the final cluster size, level of crystallinity and morphology of the support. For the specific case of gold, the thermal treatment can influence the ratio between Au(III) and Au(0), and the final cluster size more easily than with other metals. It is quite important to remember that whereas the melting point of bulk gold is 1073 °C, the melting point of gold particles of 2 nm range is 400 °C [43]. The following picture displays the difference in melting points between bulk and nanoparticlulate gold.

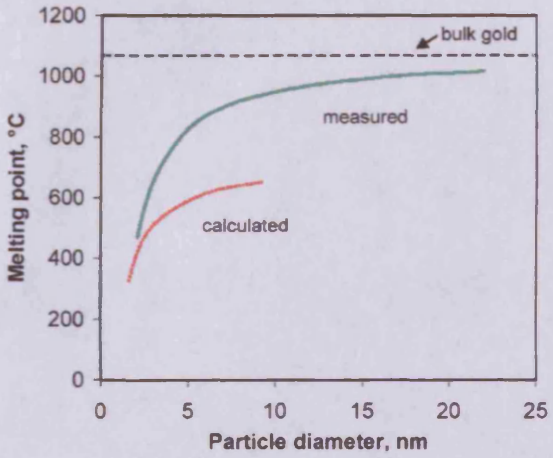

Fig. 1.9: Reduction of melting point with decrease in size of gold nano-particles, showing both theoretical data computed using molecular dynamics and measured data derived from gold nanoparticles encapsulated in silica [43]

The diagram of fig 1.9 is relative for a Au/SiO_2 catalyst, and it is evident why calcination temperatures above 500 °C are not generally used for gold catalysts. Beyond this limit gold melts and complete loss of catalytic properties was observed.

1.6 Chemistry of gold

Although the role of gold clusters has been mainly investigated, it has been possible to demonstrate that Au(III) is involved in hydrochlorination reactions and probably also Au(I) (chapter 4 and 5). Moreover, concerning the hydrochlorination reaction of acetylene all the data collected support the hypothesis of C_2H_2/Au/HCl complex formation. For this reason, considerations concerning gold chemistry are reported independent of whether they are supported species or not.

The precursor used to prepare gold solutions was gold tetrachloroaurate, $HAuCl_4 \cdot xH_2O$, independent of the technique used to deposit it on the support, it is an orange crystalline solid and highly hygroscopic. This salt can be considered the best precursor since it is possible to obtain it in high purity, its solubility in water or acid solutions is high and the high stability of the $AuCl_4^-$ anion [44].

Gold tetrachloroaurate can be directly obtained from bulk gold using concentrated HCl and an oxidizing agent. Usually the oxidizing agent is HNO_3 and the resulting mixture is the well known *aqua regia*. However, the halogen can also display this effect [45] although with very little intensity. Experimental evidence from the behaviour of Au/C catalyst for the hydrochlorination reaction, indicated a regenerative effect by HCl in the gas phase (chapter 5) and the described behaviour could be in agreement with oxidation by HCl on reduced gold after reaction.

Au(III) has a d^8 electronic configuration and so it is isoelectronic with Pd(II) and Pt(II). Both Pd and Pt are well known for their high field energy and so they form tetra-coordinated complexes with square planar geometry [14]. Also Au is able to display this

properties, but in a less marked manner. In fact, the square planar geometry is achieved, but usually the symmetry is lower [46]. Moreover, Pt can reach the oxidation state IV, while for gold the oxidation state III can be considered the limit, therefore Pt can accept a higher number of ligands, which lead to square pyramid or octahedral geometry. However, it is possible to find in the literature some examples of penta-coordination for Au(III), like the Au(dimphen)X_3 (X = Cl, Br) as reported in figure 1.10 below [47]:

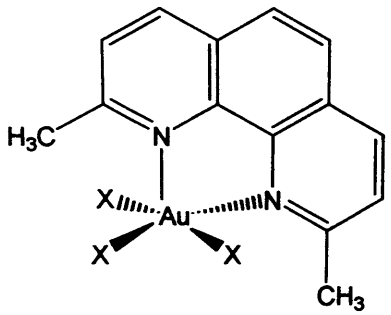

Fig. 1.10: Au(III) complex with square pyramidal geometry: Au(dimphen)X_3 [47]

It is expected that penta-coordination is quite unstable and in fact, in the organometallic complex in fig 1.10 a rigid bidentate ligand coordinating the axial and the equatorial position has been used. Nevertheless, it is an allowed coordination and the existence of a penta-coordinate gold intermediates explains the reactivity of Au(III) towards alkynes as postulated in the present work (chapter 5). More detailed aspects of further coordination chemistry towards alkynes and alkanes will be treated in chapter 5 [48].

1.6.1 Aurophilicity and relativistic effects

A property, which is nowadays accepted to make gold peculiar, when in the cluster state in organometallic compounds, is the so called 'aurophilicity'. This term was used for the fist time by Schmidbaur [49] to indicate the experimental evidence that in many organometallic complexes comprising gold clusters it is possible to observe a short Au-Au distance compared with the homologous compounds obtained from Ag or Cu. In other words, gold tends to lead to a packed structure with its atoms causing distortion of the whole organometallic structure to respect this trend.

One of the most remarkable examples of this phenomenon is reported in the following figure 1.11 [50, 51]:

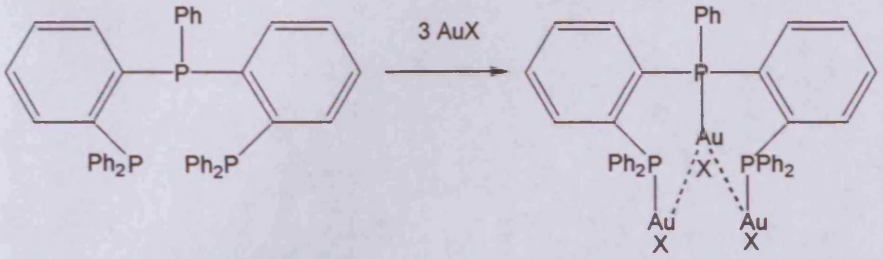

Fig 1.11: The free rotatory motion of the molecular units in the trifunctional phosphine ligand is impeded by strong Au···Au interactions in the trinuclear gold complex after reaction with AuX [50], [51].

In the example above, not is only the Au-Au distance shorter than expected, but even the rotatory motion of the phosphine ligand on the central Au axis is forbidden due to the Au···Au interaction.

This phenomenon is usually considered to be due to the lanthanide contraction [14], observed between the second and the third series of the transition metals, but for gold it is enhanced. This is due to a marked relativistic effect. The *s* electrons that approach the nucleus most closely are attracted strongly by the high nuclear charge and acquire velocities near to the speed of light and to have a substantial, relativistic increase in velocity and mass. This causes contraction of the s shells, and gold is the metal where this effect is highest among metals, as reported in figure 1.12 below [52]:

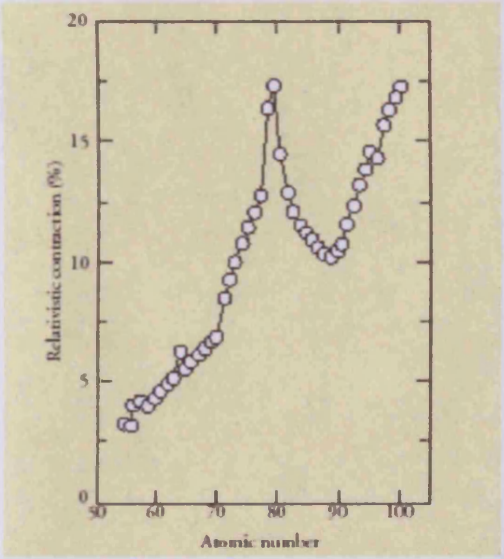

Fig. 1.12: Calculated relativistic contraction of the 6s level as a function of atomic number Z. The actual size of the 6s electron shell for Pt and Au is some 15% smaller than it would be in the absence of the relativistic effect [52]

The phenomenon is present also in the case of Au(I) complexes. Au(I), after Au(II) can be considered the most unstable gold species and if Au(I) salts are dissolved in water it gives an immediate disproportionation reaction leading to Au(0) and Au(III) [45]. Moreover, only arsine and phosphine Au(I) complexes can be considered stable and isolable. However, when ligands such as halogens are used, it is possible to observe a polymerisation process due to the aurophilicity which leads to more stable oligomers, as shown in the figure below (fig 1.13), [51, 53, 54] with short Au-Au distance.

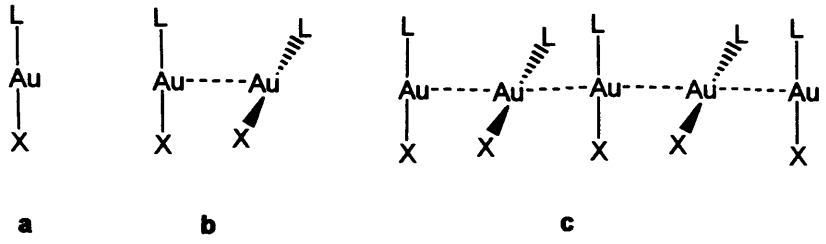

Fig 1.13: Au(I) complexes a) L-Au-X with small ligands L and X (halide) oligimerise to give b) dimers c) chain polymers [51, 53, 54]

1.7 Carbon monoxide oxidation over gold surfaces

Carbon monoxide is well known for its ability to form metal-carbonyl complexes with CO terminally bonded to a single metal atom, or with a bridging structure with two or even three metal atoms (fig. 1.14) [55]:

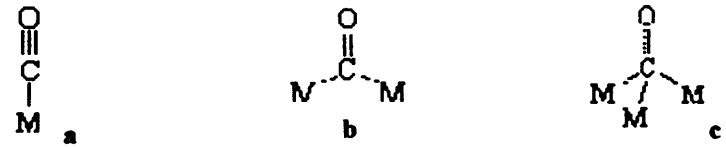

Fig. 1.14: Different modes of CO adsorption on metal surfaces: a) terminal, b) bridge and c) bridge with hollow

In any case, it is accepted that the interaction between CO and metal occurs *via* a dative σ bond from CO to an available orbital on the metal, and a reciprocal π-electron donation from occupied metal orbitals to an unoccupied π-antibonding orbital of CO (Fig. 1.15) [14]:

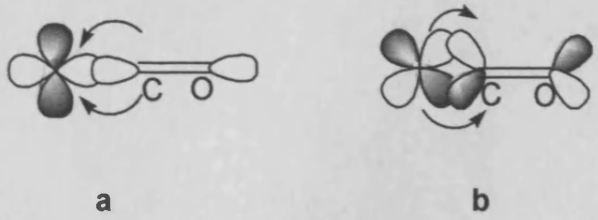

Fig. 1.15: Interaction of metal-CO, a) σ bond from CO to metal and b) reciprocal π donation from metal to CO

Due to this effect, which can also apply to alkenes and alkynes on a metal surface, CO is more strongly adsorbed on the metal surface and the C-O bond becomes weaker, making the molecule more reactive.

This mechanism fits well with metals such as palladium or platinum, which are able to lead to strong CO adsorption, with a dominant role for the back electron donation effect. However, when gold is used as a catalyst, it becomes more difficult to explain such behaviour, due to the weaker CO adsorption over gold surfaces, and the weaker π electron donation which leads to a complex.
For this reason, there is little agreement on the real CO oxidation mechanism over gold surfaces, and the experimental observations can suggest that the reaction between CO and activated oxygen takes place on gold particles, or at the gold/support interface. Both of these hypotheses are present in the literature [56, 57].

It is worth noting that although gold is able to carry out oxidation reactions, the experimental data available shows that gold is not able to dissociate oxygen since it is not possible to cover a gold crystal surface with chemisorbed molecular or dissociated oxygen [58]. Therefore, the effect of gold towards oxidation reactions can be attributed to the coordination of the organic species and subsequent oxidation.

CO oxidation is probably one of the reactions that is most affected by the preparation method and the support used, and the debate is still ongoing. However, it is matter of fact that when using the same support but different crystal structures such as in the case of TiO_2 where the phases can be of anastase or rutile, massive differences in activity can be observed [30]. The simplest explanation is to propose that different phases induce

different particle size distributions. However, in literature examples are reported of catalysts prepared over different supports like TiO_2 and ZrO_2, but with same gold particle size distribution, leading to an active catalyst in case of TiO_2 but to a poor catalyst in case of ZrO_2 [59].

Taking into account that it is not possible to adsorb oxygen on gold, the usual explanation for this effect is that the support is responsible for oxygen dissociation. Behm and co-workers [60] classified supports suitable for CO oxidation as 'reducible' such as Au/Fe_2O_3 and Au/TiO_2, and 'non-reducible' such as Au/Al_2O_3; observing enhanced activity over reducible supports. In this context, a support is defined as reducible if it supplies oxygen to form active oxidic gold sites. In addition, among the non-reducible supports, the activity is lower, but the cluster size effect appears to be dominant.

In closing, although the CO oxidation reaction can be considered relatively simple to investigate due to the simplicity of the substrate and the reaction conditions, an unambiguous answer to explain all the observed variations in activity is far from being reached.

1.8 Gold as a hydrochlorination catalyst

A detailed description of this reaction and the use of bimetallic gold based catalysts will be provided in chapters 4 and 5, while in this paragraph general aspects will be described. In the 1980s Hutchings and co-workers [61] demonstrated that gold can display catalytic activity towards the hydrochlorination reaction of acetylene and that gold supported catalysts can display the highest activity towards acetylene.

Different chlorinated metal species are able to carry out the hydrochlorination of acetylene and, on this concern, one of the most detailed investigations has been performed by Shinoda and co-workers [62]. In this study, 20 metal chlorides supported on carbon were investigated for acetylene hydrochlorination (Fig. 1.16), and it was

proposed that a correlation existed between the catalytic activity and the electron affinity of the metal cation, divided by the metal valence (fig 1.16) [62, 63].

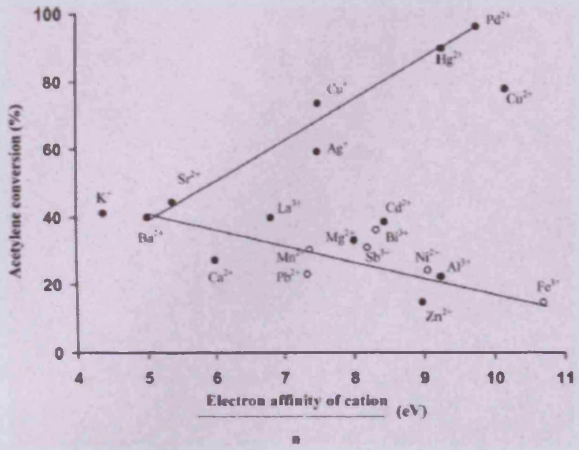

Fig. 1.16: Acetylene conversion for the hydrochlorination reaction versus electron affinity for different metals [62, 63]

This relationship is quite important because it can correlate the catalytic activity with the formation of metal acetylene complexes, acetylides, and so provides information on the possibility of the metal to carry out the reaction. Only metals able to lead to the formation of metastable acetylides would be expected to form an active catalyst; in the plot above the metals able to form the most stable acetylides are Pd(II), Hg(II), Cu(II), and Ag(I).

However, the plot presented in fig 1.16 has two limitations: firstly as the correlation consists of two straight lines it cannot be used predictably, and secondly the correlation parameter used is electron affinity. This last parameter, by definition takes into account only one single electron process. Almost all the metals reported are in oxidation state II, and if the hydrochlorination reaction is postulated to be a $2e^-$ transfer process, an assumption supported in the present thesis, from acetylene to the gold centre, a more suitable correlation could be obtained using the standard electrode potential rather than electron affinity to correlate metals. Plotting the data using this parameter leads to the figure reported below in figure 1.17 [2, 63].

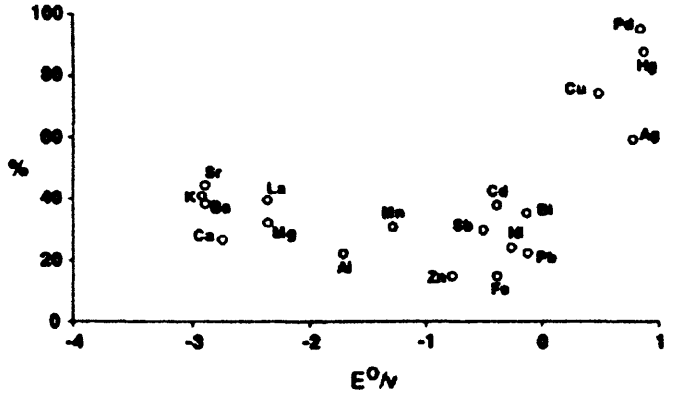

Fig. 1.17: Correlation of activity for acetylene hydrochlorination with the standard electrode potential for the metals in fig 1.16 [2, 63]

In this case a single curve is obtained, moreover it can be used as a predictive model. In fact, metals with higher standard electrode potentials than Pd(II) and Hg (II) should lead to an enhanced activity, and this hypothesis has been confirmed using supported Au(III) catalysts [2].

However, although gold can be considered the best catalyst in terms of initial activity, it is affected by deactivation phenomena, the most important has been identified as Au(III) reduction [64]. This aspect has been investigated in the present thesis, and for catalysts made by gold only it can be considered the main deactivation route. A second deactivation pathway involves oligomer formation, indeed previous observations [64] show that the deactivation rate is minimum at 100-120 °C (fig 1.18), but at this temperature the catalyst is not sufficiently active compared with temperatures of around 180 °C, although reduction can occur. Oligomer formation has been identified as one of the deactivation phenomena for bimetallic catalyst containing Au and Pd (chapter 4).

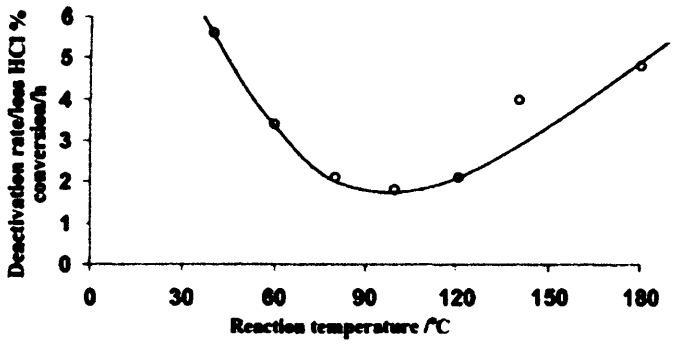

Fig. 1.18: Deactivation rate for the hydrochlorination reaction of acetylene over Au/C catalyst with reaction temperature [64].

Nevertheless, catalysts containing gold only have the interesting properties of being reactivated on line by Cl_2, NO and NO_2 [63]. This experimental evidence also indicates how the reaction can take place. In fact, among all metals and, especially when compared with $HgCl_2$, gold catalysts are able to display the highest selectivity.

Investigations of the kinetics of the hydrochlorination reaction using different metal chlorides lead to the conclusion that the rate determining step is the addition of HCl to a preformed surface acetylene complex, a process that is shown schematically below [65]:

$$MCl_n + HC{\equiv}CH + HCl \rightarrow MCl_n \cdot HC{\equiv}CH \cdot HCl$$

However, it is worth noting that up to now no direct evidence is available for gold. In this thesis the evaluation of the effect of each reactant using inert gas on the catalyst, as well as the use of different substrates and molecular modelling investigations, strongly support this hypothesis (see chapter 5), rejecting the possibility of eventual carbocation formation between Au and acetylene. Moreover, Au/C_2H_2 interactions cannot simply be electrophilic-nucleophilic, as in the case of $HgCl_2$, but a concerted approach involving HCl is needed to form the right activated complex geometry.

1.9 Gold as an oxychlorination catalyst

Oxychlorination is a particular class of hydrochlorination reaction, which leads to chlorinated products if oxygen is used the reaction mixture. Specific examples will be treated in chapter 6; in fact the hydrochlorination product vinyl chloride monomer can be obtained by thermal cracking of 1,2-dichloroethane, obtained using an oxychlorination route. Up to now there are very few examples in the literature concerning the use of gold for this reaction, while it is possible to find extensive studies concerning copper [66].
This absence of literature can be related with the circumstance of a substantial inactivity of gold, which can be maybe related to the already mentioned inability of gold to adsorb oxygen directly. In addition to economic aspects, it is possible to find copper based

catalysts able to give conversion and selectivity values above 98% [67] under industrial conditions, which discourages research into alternatives, apart from the identification of routes able to minimize the formation of deleterious by-products [68].

1.10 Catalysis and solid-state phase transitions on vanadium phosphorus oxides

In contrast to the descriptions so far, involving the use of dispersed metal on a support as the active catalyst, some properties of a class of materials named vanadium phosphorus oxides (VPO) will be described, where the bulk material displays catalytic properties.

Vanadium phosphorus oxides are materials that have been extensively studied due to their importance in the selective catalysis of hydrocarbons, especially *n*-butane to maleic anhydride [69] and the inter conversion of several crystalline phases [70]. Detailed aspects of phase transitions between two different polymorphs of vanadium orthophosphate, ω- and δ-$VOPO_4$, and their correlation with *n*-butane oxidation, will be reported in chapter 7. In the following paragraphs, general aspects concerning the nature of this material and solid-state phase transitions will be described.

1.10.1 Phase transitions among VPO phases

Among VPOs the most investigated phases are the V(IV) species vanadyl hydrogen phosphates $VOHPO_4{\cdot}2H_2O$, $VOHPO_4{\cdot}0.5H_2O$, $VO(H_2PO_4)_2$ and the vanadyl pyrophosphate $(VO)_2P_2O_7$; as well as the V(V) species vanadyl orthophosphates $VOPO_4$ which can exist in seven different polymorph phases named α_I, α_{II}, β, γ, δ, ε and ω (chapter 7) that can be considered as VO_6 distorted octahedra linked by PO_4 tetrahedra. The interest in this phase is related to the fact that the pyrophosphate is considered to be the active species of the industrial catalyst for maleic anhydride manufacture, which is actually a mixture of $(VO)_2P_2O_7$, α_I-$VOPO_4$ and δ-$VOPO_4$ [71].

The vanadyl pyrophosphate $(VO)_2P_2O_7$ can be obtained by vanadyl hydrogen phosphate $VOHPO_4 \cdot 0.5H_2O$ dehydration *via* a topotactic process [72], above 350 °C. This reaction is quite important because it is considered as the activation step for the industrial catalyst, and due to its topological nature has been the object of many investigations, not only in catalysis but also in crystallography. Topotactism is a phenomenon in which the morphology of the final product is controlled by the morphology of the precursor, and as a direct consequence the nature of the active sites. In the specific case of vanadyl hydrogen phosphates and vanadyl pyrophosphate, it has been observed that synthesizing $VOHPO_4 \cdot 0.5H_2O$ in alcoholic solvents crystals with plate-like morphology results in the (001) face being formed. The topotactic dehydration results in $(VO)_2P_2O_7$ with the (020) face of the resulting plate like crystallites being the major crystal face exposed [73].

Scanning electron microscopy (SEM) carried out on precursor and final product gave the images reported in figures 1.19 and 1.20 [73].

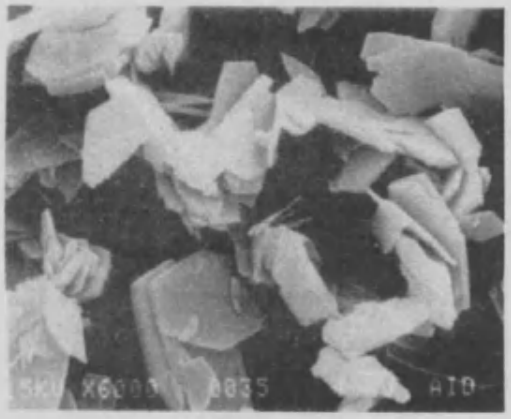

Fig. 1.19: SEM image of $VOHPO_4 \cdot 0.5H_2O$ prepared in butanol solvent [73]

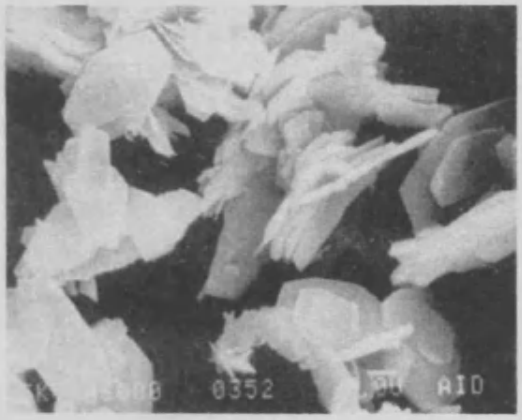

Fig. 1.20: SEM image of $(VO)_2P_2O_7$ after dehydration of the precursor in Fig 1.19 [73]

The dehydration reaction of $VOHPO_4 \cdot 0.5H_2O$ to $(VO)_2P_2O_7$ occurs without altering the apparent size and shape of the individual crystallites.

However, this is not the only phase transition that can occur, in fact by heating the precursor $VOHPO_4 \cdot 0.5H_2O$ in air in the range 400 to 650 °C it is possible to obtain the vanadyl orthophosphate δ-$VOPO_4$, which if it is afterwards heated at 740-780 °C leads to

γ-$VOPO_4$ [74]. Moreover, if the precursor is treated with oxygen at 680 °C is possible to obtain β-$VOPO_4$ [75]. In addition, it is worth noting that if the V(V) vanadyl dihydrate $VOPO_4 \cdot 2H_2O$ is used as precursor, it is possible to obtain, using a thermal treatment in air between 200 and 600 °C, α_I-$VOPO_4$ and afterwards α_{II}-$VOPO_4$ at 750 °C, a phase which can irreversibly convert to γ-$VOPO_4$ at 780 °C. Further phase transitions observed at high temperature are: α_I- to α_{II}- to β-$VOPO_4$ and the δ- to γ- to β-$VOPO_4$ [76] and the phase transition of δ-$VOPO_4$ to α_{II}-$VOPO_4$ during *n*-butane oxidation [77].

A significant and reversible transformation has been observed between β-$VOPO_4$ and $(VO)_2P_2O_7$, indeed by treating β-VOPO4 at 500 °C using a 2% mixture of butane in air is possible to obtain $(VO)_2P_2O_7$, which can be reoxidised to β-$VOPO_4$ using O_2 [78]. These phase transitions are summarized in the scheme below (fig. 1.21):

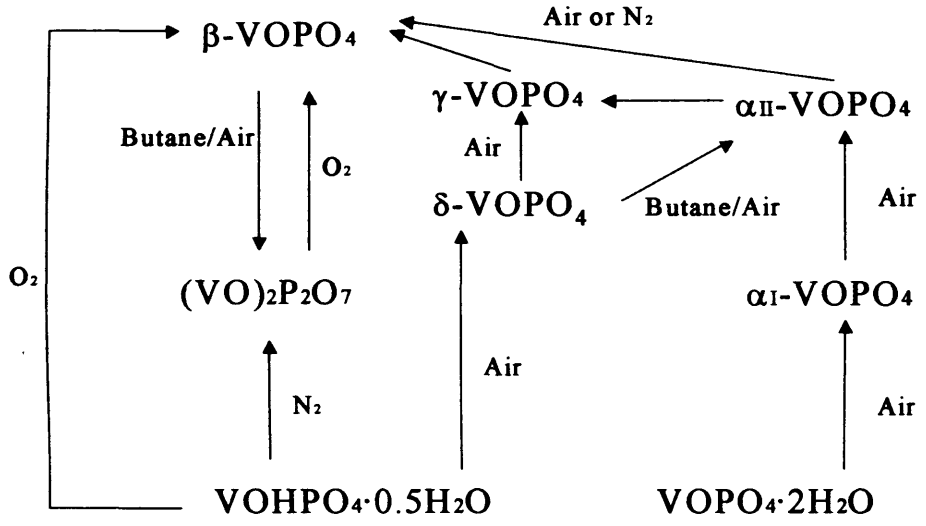

Fig. 1.21: Phase transitions from precursors $VOHPO_4 \cdot 0.5H_2O$ and $VOPO_4 \cdot 2H_2O$ to $(VO)_2P_2O_7$ and vanadyl orthophosphates by different reaction mixtures at high temperature.

The last phase transition between β-$VOPO_4$ and $(VO)_2P_2O_7$ has some common aspects with the phase transition of ω- to δ-$VOPO_4$ described in chapter 7, since it is a reversible process. However, there is the crucial difference in that the transition β-$VOPO_4$ to $(VO)_2P_2O_7$ is a redox process involving a change in stoichiometry, while for the ω- to δ-$VOPO_4$ this does not occur, as it is necessary to preserve the polymorph nature of the two phases ω– and δ-$VOPO_4$.

1.10.2 Bulk and surface oxygen in metal oxides catalysts

Vanadium is not unique in giving such kind of products and structures, molybdenum is another metal that is well known to display similar behaviour [79]. However, investigations of these materials show some general aspects: the preparation and the activation of the catalyst involves reaction of the catalyst bulk and although most reactions in heterogeneous catalysis proceed on the surface of a catalytically active phase, this active phase and its surface may be influenced, or even determined by, the underlying catalyst bulk [80]. Concerning vanadium phosphorus oxides for partial oxidation of butane, recent observations [81] lead to conclusion that the active oxygen species responsible for the reaction is the surface lattice oxygen and that the contribution of either the surface adsorbed oxygen or the bulk lattice oxygen is negligible. Extraction of oxygen from surface lattice oxygen is well known in catalysis, and is called the Mars van Krevelen mechanism [82]. In this case the organic substrate reduces the surface lattice oxide by removal of oxygen, which is subsequently replaced by dioxygen dissociation from the reaction mixture, regenerating the original catalyst form (fig 1.22)

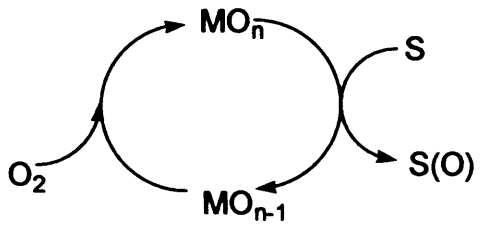

Fig. 1.22: Scheme for Mars – van Krevelen mechanism over metal oxide catalysts: the organic substrate S reduces the metal oxide MO, which is regenerated by O_2 from the reaction mixture.

This is a pure redox mechanism, and a fast change in oxidation state of the metal centre is necessary in order to carry out the catalytic reaction. In addition, the removal of oxygen from the metal oxides is not limited to the top most layer, but also internally due to migration of oxygen species from the bulk to the surface. Some authors assume that this mechanism could be operating when $(VO)_2P_2O_7$ is used for *n*-butane partial oxidation [83].

However, the case of extraction of surface lattice oxygen without a redox pathway but involving surface oxygen mobility, it can be even more complicated. If the process is accompanied by a solid state transition of the bulk, and if the final form is the active catalyst, the kinetics of the solid state transition process involved can affect the selectivity of the catalysed reaction

The extraction of surface lattice oxygen will be treated specifically in chapter 7, and it is considered responsible for the observed phase transition of ω-$VOPO_4$ to δ-$VOPO_4$.

1.11 References

[1] M. Haruta, T. Kobayashi, H. Sano and N. Yamada, *Chem. Lett.*, 405, 1987

[2] G. J. Hutchings, *J. Catal.*, 292, **96**, 1985

[3] R. Lyden, *Z. Anorg. U. Allgem. Chem.*, 157, **240**, 1939

[4] G. Brauer, *Handbook of Preparative Inorganic Chemistry* (Vol. 1, II Ed.), Academic Press, New York, 1963

[5] G. C. Bond, *Catal. Today*, 5, **72**, 2002

[6] T. Hayashi, K. Tanaka and M. Haruta, *J. Catal.*, 566, **178**, 566, 1998

[7] D. Andreeva, V. Idakeiv, T. Tabakova, A. Andreev and R. Giovanoli, *Appl. Catal. A: Gen.*, 275, **134**, 1996

[8] A. Ueda and M. Haruta, *Gold Bull.*, 3, **32**, 1999

[9] G.C. Bond, P.A. Sermon, G. Webb, D. Buchanan and P.B. Wells, *Chem. Comm.*, 444, 1973

[10] D. J. Gulliver and J. S. Kitchen, BP. Chem. Int. Ltd., EU Patent #654301, 1995

[11] C. Mohr and P. Claus, *Sci. Prog.*, 311, **84**(4), 2001

[12] M. Cortie, R. Holliday, A. Laguna, B. Nieuwenhuys and D. Thompson, *Gold Bull.*, 144, **36**, 2003

[13] W. Eberhardt, *Surf. Sci.*, 242, **500**, 2002

[14] J. E. Huheey, E. A. Kieter and R. L. Kieter, *Inorganic Chemistry* (IV ed.), Harper Collins, New York, 1993

[15] F. A. Cotton and G. Wilkinson, *Advanced Inorganic Chemistry* (V ed.), Wiley, New York, 1988

[16] F. E. Wagner, S. Galvagno, C. Milone, A. M. Visco, L. Stievano, S. Calogero *J. Chem. Soc., Faraday Trans.*, 3403, **93**(18), 1997

[17] L. M. Molina and B. Hammer, *Phys. Rev. Lett.*, 206102, **90**(20), 2003

[18] P. M. Ajayan and L.D. Marks, *Phys. Rev. Lett.*, 279, **63**(3), 1989

[19] M. Valden, X. Lai, and D.W. Goodman, *Science*, 1647, **281**, 1998

[20] B.E. Salisbury, W.T. Wallace, and R.L. Whetten, *Chem. Phys.*, 131, **262**, 2000

[21] L. Prati and G. Martra, *Gold Bull.*, 96, **32**(3), 1999

[22] Y. Yuan, A. Kozlova, K. Asakura, H. Wan, K. Tsai, and Y. Isawa, *J. Catal.*, 191, **170**, 1997

[23] H.S. Oh, J.H. Yang, C.H. Costello, Y.M. Wang, S.R. Bare, H.H. Jung, and M.C. Kung, *J. Catal.*, 375, **210**, 2002

[24] P. W. Atkins, *Physical Chemistry* (VI ed.) Oxford University Press, 1998

[25] D. F. Shriver, P. W. Atkins and C. H. Longford, *Inorganic chemistry* (II Ed.), Oxford University Press, 1994

[26] C. T. Campbell, S. C. Parker and D. E. Starr, *Science*, 811, **298**, 2002

[27] J. Haber, J. H. Block and B. Delmon, *Pure & Appl. Chem.*, 1257, **67**(8-9), 1995

[28] C. L. Bianchi, S. Biella, A. Gervasini, L. Prati and M. Rossi, *Catal. Lett.*, 91, **85**, 2003

[29] L. I. Ilieva, D. H. Andreeva, and A. A. Andreev, *Therm. Acta*, 169, **292**, 1997

[30] Q. Fu, A. Weber, and M. Flytzani-Stephanopoulos, *Catal. Lett.*, 87, **77**, 2001

[31] M. Haruta, S. Tsubota, T. Kobayashi, H. Kageyama, M.J. Genet and B. Delmon, *J. Catal.*, 175, **144**, 1993

[32] N. Lopez, T. V. W. Janssens, B. S. Clausen, Y. Xu, M. Mavrikakis, T. Bligaard, and J.K. Nørskov, *J. Catal.*, 232, **223**, 2004

[33] M. Haruta, S. Tsubota, T. Kobayashi, H. Kageyama, M. J. Genet and B. Delmon, *J. Catal.*, 175, **144**, 1993

[34] C. Bianchi, F. Porta, L. Prati and M. Rossi, *Topics Catal.*, 231, **13**(3), 2000

[35] A. P. Kozlova, S. Sugiyama, A. I. Kozlov, K. Asakura and Y. Iwasawa, *J. Catal.*, 426, **176**, 1998

[36] R. M. Finch, N. A. Hodge, G. J. Hutchings, A. Meagher, Q.A. Pankhurst, M. R. H. Siddiqui, F.E. Wagner and R. Whyman, *Phys. Chem. Chem. Phys.*, 485, **1**, 1999

[37] Y. Yamada, T. Akita, A. Ueda, H. Shioyama and T. Kobayashi, *Rev. Sci. Instr.*, 62226, **76**, 2005

[38] E. D. Park and J.S. Lee, *J. Catal.*, 1, **186**, 1999

[39] S. K. Tanielyan, R. L. Augustine, *Appl. Catal. A: Gen.*, 73, **85**, 1992

[40] A. Wolf and F. Schüth, *Appl. Catal. A: Gen.*, 1, **226**, 2002

[41] G. R. Bamwenda, S. Tsubota, T. Nakamura, and M. Haruta, *Catal. Lett.*, 83, **44**, 1997

[42] M. S. Spencer and M. V. Twigg, *Annu. Rev. Mater. Res.*, 427, **35**, 2005

[43] M. B. Cortie and E. van der Lingen, *Mat. Forum*, 1, **26**, 2002

[44] C. Chambers and A. K. Holliday, *Modern Inorganic Chemistry*, Butterworth & Co Ltd, London, 1975

[45] S. A. Cotton, *Chemistry of Precious Metals*, Chapman & Hall, London, 1997

[46] M. I. García-Seijo, A. Habtemariam, S. Parsons, R. O. Gouldb and M. E. García-Fernández, *New J. Chem.*, 636, **26**, 2002

[47] J. Vicente, A. Arcas, P. G. Jones and J. Lautner, *J. Chem. Soc., Dalton Trans.*, 451, 1990

[48] A. S. K. Hashmi *Gold Bull.*, 3, **36**(1), 2003

[49] H. Schmidbaur, *Gold. Bull.*, 11, **23**, 1990

[50] J. Zank, A. Scheir and H. Schmidbaur, *J. Chem. Soc., DaltonTrans.*, 232, 1998

[51] H. Schmidbaur, *Gold. Bull.*, 3, **33**(1), 2000

[52] G. C. Bond, *Gold Bull.*, 117, **34**(4), 2001

[53] K. Angemaier, E. Zeller and H. Schmidbaur, *J. Organomet. Chem.*, 371, **472**, 1994

[54] M. Preisenberger, A. Schier and H. Schmidbaur, *J. Chem. Soc., Dalton Trans.*, 1645, 1999

[55] R. D. Adams, J. E. Babin and M. Tasi, *Inorg. Chem.*, 2618, **27**, 1988

[56] M. Haruta *Cat. Tech.*, 102, **6**(3), 2002

[57] G. C. Bond and D. T. Thompson, *Gold Bull.*, 47, **33**(2), 2000

[58] N.D.S. Canning, D. Outka and R.J. Madix, *Surf. Sci.*, 240, **141**, 1984

[59] J. D. Grunwaldt, C. Kiener, C. Wögerbauer and A. Baiker, *J. Catal.*, 223, **181**, 1999

[60] M. M. Schubert, S. Hackenberg, A.C. van Veen, M. Muhler, V. Plzak and R.J. Behm, *J.Catal.*, 113, **197**, 2001

[61] B. Nkosi, N.J. Coville and G.J. Hutchings, *J. Chem. Soc., Chem. Comm.*, 71, 1988

[62] K. Shinoda, *Chem. Lett.*, 219, 1975

[63] G. J. Hutchings, *Catal. Today*, 11, **72**, 2002

[64] B. Nkosi, N.J. Coville, G.J. Hutchings, M.D. Adams, J. Friedl and F.E. Wagner, *J. Catal.*, 366, **128**, 1991

[65] A.I. Gel'bshtein, G.G. Shceglova and A.A. Khomenko, *Kinetic. Catal.*, 543, **4**, 1964

[66] J. G. Speight, *Chemical and Process Design Handbook*, McGraw-Hill, New York,

2002

[67] F. Casagrande and C. Orsenigo, Sud-Chemie, US Patent 6872684, Appl. N. 791952, Publ. Date 2005-03-29

[68] I. M. Clegg and R. Hardman, US Patent 5763710, Appl. N 797841, Publ. Date 1998-06-09

[69] B. K. Hodnett, *Catal. Today*, 477, **1**, 1987

[70] Z.-Y. Xue and G. L. Schrader, *J. Phys. Chem. B*, 9459, **103**, 1999

[71] K. E. Birkeland, S. M. Babitz, G. K. Bethke, H. H. Kung, G. W. Coulston and S. R. Bare, *J. Phys. Chem. B*, 6895, **101**, 1997

[72] G. J. Hutchings, C. J. Kiely, M. T. Sananes-Schulz, A. Burrows and J. C. Volta, *Catal. Today*, 273, **40**, 1998

[73] J. W. Johnson, D. C. Johnston, A. J. Jacobson, and J. F. Brody, *J. Am. Chem. Soc.*, 8123, **106**, 1984

[74] G.F. Benabdelouahab, J. C. Volta and R. Olier, *J. Catal.*, 334, **148**, 1994

[75] M. G. Willinger, D. S. Su, and R. Schlögl, *Phys. Rev. B*, 155118, **71**, 2005

[76] E. Bordes, *Catal. Today* 499, **1**, 1987

[77] F. B. Abdelouabab, G. R. Olier, F. N. Lefèbvre and J. C. Volta, *J. Catal.* 151, **134**, 1992

[78] E. Lashier and G. L. Schrader, *J. Catal.*, 113, **128**, 1991

[79] T. Ressler, O. Timpe, T. Neisius, J. Find, G. Mestl, M. Dieterle and R. Schlögl, *J. Catal.*, 75, **191**, 2000

[80] X. Bao, M. Muhelr, T. Schedel-Niedrig and R. Schlögl, *Phys. Rev. B*, 2249, **54**, 1996

[81] M. J. Lorences, G. S. Patience, R. Cenni, F. Díez and J. Coca, *Catal. Today*, 45, **112**, 2006

[82] P. Mars and D. van Krevelen, *Chem. Eng. Sci.*, 41, **3**, 1954

[83] G. Centi, E Trifiro, G. Busca, J. R. Ebner, J. T. Gleaves, in: M.J. Phillips, M. Ternan (Eds.), *Proceedings of 9th International Congress on Catalysis*, Calgary, Ottawa, 1538, 1988

Chapter 2: EXPERIMENTAL TECHNIQUES

2.1 Introduction

Several techniques have been used to characterize the catalysts and the reaction products. In this chapter a brief description of the methods used in this thesis work are reported. The techniques include:

1) X-ray photoelectron spectroscopy for surface analysis
2) X-ray diffraction for bulk structured analysis
3) Transmission electron microscopy for particle size determination and morphology
4) Temperature programmed methods for acid/base properties of surfaces and oxidized centres
5) Surface area determination using the Braunauer, Emmett and Teller method
6) Atomic absorption for the determination of the catalyst metal loading
7) Nuclear magnetic resonance for characterization of reaction products

In this chapter the theoretical principles of these instrumental techniques only are described, while catalyst preparation, source of starting materials and the specific instruments used are described in the introduction and experimental sections of chapters 3, 4, 5, 6, and 7. These chapters concern: low temperature CO oxidation, gold based catalysts for the hydrochlorination of acetylene, hydrochlorination reaction mechanism, hydrochlorination of C-C double bond containing substrates and phase transitions in vanadyl orthophosphates respectively.

2.2 X-ray photoelectron spectroscopy

X-ray photoelectron spectroscopy (XPS) is among the most frequently used surface chemical characterization techniques [1, 2] and it provides information on the chemical composition and the oxidation state of the atoms present on the external layers of a solid material.

XPS is based on the photoelectric effect: an atom absorbs a photon of energy $h\nu$ from an X-ray source; next, a core or valence electron with binding energy E_B is ejected with kinetic energy E_{kin}, which is determined by the equation 2.1:

$$E_{kin} = h\nu - E_B - (E_{vac} - E_F) \qquad \text{(eq. 2.1)}$$

Where E_{vac} is the vacuum energy level and E_F is defined as the energy of an electron in the highest occupied molecular orbital in the valence band at 0 K, known as the Fermi level.

The difference between the vacuum and the Fermi level is the so called 'work function' and is usually denoted with the symbol ϕ, and it is an important parameter. In fact the excited electron propagates to the surface and is emitted from the solid into the vacuum, through the surface. This means that the photoemitted electron has to posses enough energy to reach the surface and with a further kinetic energy contribution to leave the surface and be detected. The process is shown in figure 2.1, before (left) and after (right) the excitation process.

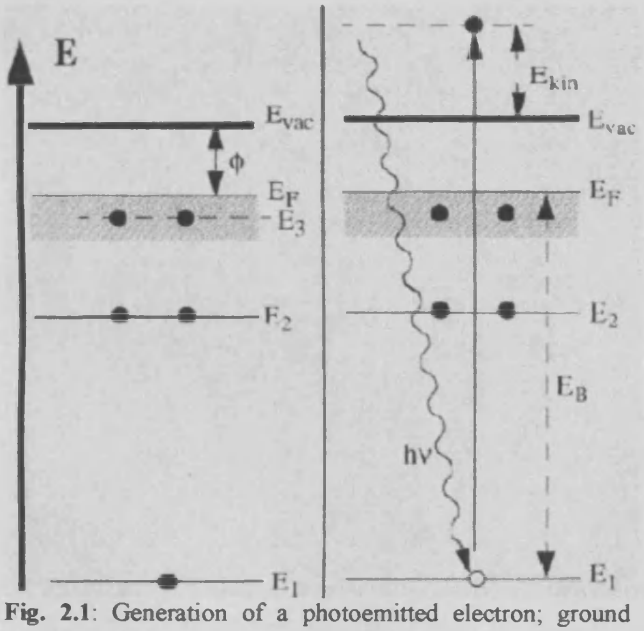

Fig. 2.1: Generation of a photoemitted electron; ground state (left) and excitation process (right)

Therefore, the kinetic energy of the photoemitted electron can be re-written as:

$$E_{kin} = h\nu - E_B - \phi \qquad \text{(eq. 2.2)}$$

And E_B as:

$E_B = E_F - E_i$ (eq. 2.3)

Where the index *i* can have different values, denoting different electron energy levels, as displayed in figure 2.1

The most commonly employed X-rays are the Mg-K_α (1253.6 eV) and the Al-K_α (1486.6 eV), which are produced from a standard X-ray tube and the peaks detected in XPS spectra correspond to the bound core-level electrons of the sample. The intensity of each peak is proportional to the abundance of the emitting atoms in the near-surface region, while the precise binding energy of each peak depends on the chemical oxidation state and local environment of the emitting atoms.

2.2.1 Bulk and surface detection

In paragraph 2.3.1 it will be shown that the use of X-ray radiation as an incident beam is not peculiar to XPS if Cu is used, since it is also possible to carry out X-ray diffraction. In the first case we have a surface technique, while in the second case a bulk technique. Apart from the different energy of the incident beam, the main difference between these two techniques is the radiation analysed after interaction with the sample. In XRD this radiation is again an X-ray, while in XPS only the photoemitted electrons with enough energy to escape from the solid can be analysed, and this last aspect makes XPS a surface method. Photoemitted electrons can be generated in deep solid layers, but due to the low free electron pathway, only photoemitted electron close to the surface can escape to the vacuum and be detected.

In addition, to collect information on the external solid layers, it is necessary to operate at high vacuum, usually of the order of 10^{-10} Torr and at room temperature, which are conditions quite far from the usual reaction conditions of a catalyst. Nevertheless, the

information obtained using XPS analysis is quite useful to give an indication of the metal oxidation state involved in a catalytic process, and to provide some indication of the structure of a catalyst when more than one metal is used in its preparation.

2.2.2 Labelling of photoelectron peaks

Photoelectron peaks are labelled according to the quantum numbers of the level from which the electron originates [3]. An electron coming from an orbital with the main quantum number n, orbital momentum l (0, 1, 2, 3, ... indicated as s, p, d, f, ...) and spin momentum s (+1/2 or –1/2) is indicated as $nl_{l \pm s}$. For every orbital momentum $l > 0$ there are two values of the total momentum: $j = l + 1/2$ and $j = l - 1/2$, each state filled with $2j + 1$ electrons. Most XPS peaks come in doublets and the intensity ratio of the components is $(l + 1)/l$. When the doublet splitting is too small to be observed, the subscript $l + s$ is omitted.

In the case of gold the most intense peak is from the 4f orbital, which leads to the components Au $4f_{7/2}$ and Au $4f_{5/2}$ located for metallic gold at 84 eV and 88 eV respectively. In the case of metal nanoparticles, differences in the expected position can be related to particle size effects and interaction with the support. As a consequence, it is very important to carry out calibration of the XPS spectra. However, it is possible to demonstrate [4] that each surface is contaminated by carbon, which can be detected even in very low amount on the C 1s component at 284.7 eV and this adventitious carbon can be used as an internal standard.

2.3 X-ray diffraction

X-ray diffraction (XRD) is one of the most used bulk techniques that finds a wide range of applications such as [5]:

- Identification of single-phase materials such as minerals, chemical compounds and ceramics
- Identification of multiple phases in microcrystalline mixtures (i.e., rocks)
- Determination of the crystal structure of identified materials
- Identification and structural analysis of clay minerals
- Recognition of amorphous materials in partially crystalline mixtures

As well as:
- Crystallographic structural analysis and unit-cell calculations for crystalline materials
- Determination of crystallite size from analysis of peak broadening

In this thesis the technique has been applied for phase identification of the support (chapter 3 and 6), phase transitions at high temperature (chapter 7), and attempts at particle size determination (chapter 5). However, in this last case the technique has not been informative due to the high surface area of the support (carbon) compared with the low metal loading.

XRD has been developed as a technique to investigate materials in the single crystal state; however, it can also be successfully applied to powder crystalline materials as in this thesis.

2.3.1 X-ray generation and Bragg's law

X-rays can be obtained using three different procedures: 1) by impact of high energy electrons to a metal target, usually made of Cu or Mo, 2) induced X-ray fluorescence (XRF) by a primary X-ray radiation usually on a Pb target and 3) by radioactive decay processes [6]. In this thesis the first method using a Cu target source has been always used. X-ray generation is displayed in figure 2.2 [7]:

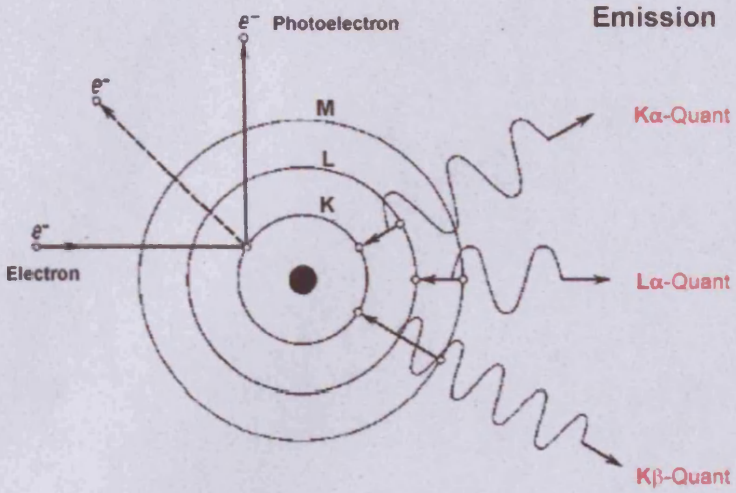

Fig 2.2: X-ray generation process; a primary electron removes an inner electron orbital. An electron in a higher occupied orbital with X-Ray photon emission fills the vacancy.

A high energy electron interacts with electrons in the copper target, removing an electron from an inner orbital. The electronic vacancy is immediately filled by an electron transition of an electron in an outer orbital and during the process generates an X-ray photon of equal quantum energy to the transition.

X-rays follow the same rules for all electromagnetic radiation, as a consequence if an X-ray beam hits a crystal plane then diffraction can be possible. The necessary conditions for diffraction are: spacing among the planes of the solid crystal structure in the same range as the incident radiation and a regular distribution of the planes. Cu and Mo lead to a radiation wavelength for the K_α component of 1.54 and 0.71 Angstrom respectively, which is in the same range as the spacing of atoms in solid materials.

Indicated in figure 2.3 is the principle of Bragg's law [7].

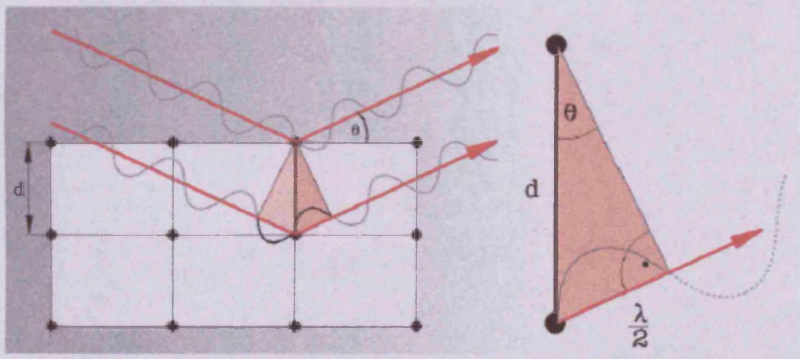

Fig. 2.3: Bragg's law: only diffracted beams with a nλ difference path lead to diffraction

An X-ray beam encounters a three dimensional lattice array of atoms, the X-rays scattered by adjacent atoms can lead to constructive interference only if they have a path difference equal to a whole wavelength number nλ, while for all the other values destructive interference is present. The path difference can be calculated as 2d *sin* θ, where d is the spacing among crystal planes and θ the incident angle of the radiation, therefore Bragg's law (eq. 2.4) can be written as:

$$n\lambda = 2d \sin\theta \qquad \text{(eq. 2.4)}$$

The equation can be applied to both single crystals and crystalline powders. In this last case, due to the random orientation of the crystallites the resulting total diffraction is not a single diffracted beam, but a diffraction cone, as displayed in figure 2.4 below [7]:

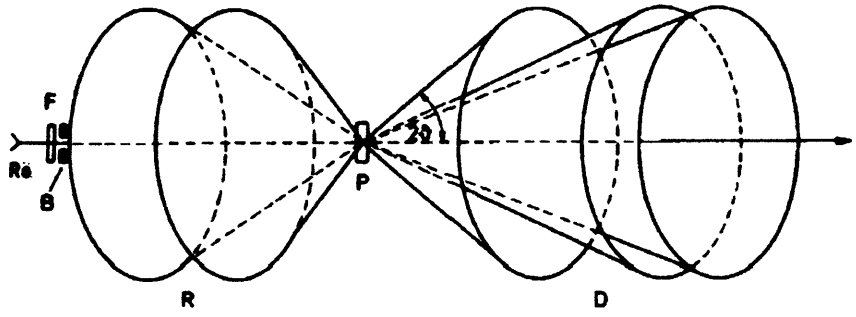

Fig. 2.4: Diffraction cones from a powder crystalline sample P. The primary beam from the source F crosses the sample from R to D

As a consequence of the diffraction pattern being a two dimensional plot, it is actually a section of the generated diffraction cones.

2.3.2 Indexing and crystal planes

Bragg's law immediately introduces the problem of how to identify the different crystal planes and this is solved using the so called Miller indices [5].

Imaging a crystal like an imaginary pattern of points, it is possible to identify points by choosing a point in the lattice as the origin defined as 000, while orthogonal a, b, and c

axes define the directions within the crystal structure with the angular relations defined by the particular crystal system (fig. 2.5) [5]:

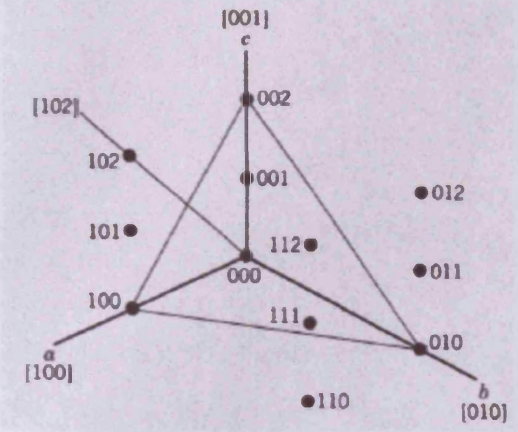

Fig. 2.5: Notation of lattice points, rows and planes

The lattice points are specified without brackets such as: 100, 101, 102, etc. 100 is a point one unit along the *a* axis, 002 is a point two units along the *c* axis, and 101 is a point one unit from *a* and one unit from *c*.

The lattice planes are identified using Miller indices, which are the reciprocals of the intercepts of the planes on the coordinate axes. Again using fig 2.5, the plane show intercepts *a* at 100, *b* at 010 and *c* at 002. The Miller index of the plane is thus calculated as 1/1(*a*), 1/1(*b*), 1/2(*c*), and reduced to integers as 2*a*, 2*b* ,1*c*. Miller indices are by convention given in parentheses, i.e. (221). If the calculations result in indices with a common factor i.e., (442) the index is reduced to the simplest set of integers (221). Such notation has been used in this thesis in chapter 1 and chapter 7.

2.4 Transmission electron microscopy

Electron microscopy techniques are useful tools to investigate the local structure and the chemistry of heterogeneous catalysis from the macroscopic to the atomic scale. Electron

microscopy is a diffraction technique in which the material diffracts electrons in agreement with the Bragg's law (paragraph 2.3.1).

In a conventional transmission electron microscopy (TEM) an electron beam travelling through the sample is used. The interaction between the electron beam and the sample leads to elastic scattered electrons that can be used to generate an image, which is a 2-dimensional projection of the 3-dimensional sample in the direction of the beam as well as a diffraction pattern [8].
If only the primary electron beam is used the resulting image is a so called bright field image, and such analysis has been used in chapter 4 and 6 on Au/C and Au/ZnO samples as well as TEM diffraction pattern for phase identification.

Bright fields images can be used not only to collect information on catalyst morphology, but particularly for cluster size determination and size distributions. This technique provides useful information on the gradient phenomena concerning the preparation of gold on carbon catalyst using the impregnation technique (chapter 4).

During the electron-sample interaction, X-rays can be obtained as a consequence of inelastic scattering of the electrons [9]. The X-rays obtained have an energy which is characteristic of the elements present in the sample, and this property can be used for chemical composition analysis leading to the so called energy dispersive X-ray spectroscopy (EDX) which can be used to create a chemical map of the sample. Such chemical analysis has been used to determine the structure of a Au/Pd catalyst (chapter 4).

The samples are usually analysed at room temperature in high vacuum. The samples can be examined without any particular pretreatment; however, the method usually requires grinding of the sample in high purity ethanol, and depositing a drop of the obtained suspension on a holey carbon grid after evaporation.

2.5 Temperature programmed methods

Temperature programmed methods for thermal analysis are also defined as transient response methods because they can be used for the investigation of kinetics of heterogeneous catalytic reactions. Instead of the reaction system being driven to a steady state, the system is perturbed in a controlled way using a temperature programme. Among the thermoanalytical techniques, temperature-programmed desorption (TPD), temperature-programmed reduction (TPR) and temperature-programmed oxidation (TPO) are the most commonly used tools for heterogeneous catalyst characterization [10, 11]. In this thesis TPD and especially TPR have been used.

In the following table [12] the most common applications for these techniques are reported:

Table 2.1: Types of information obtainable from temperature programmed techniques.

TPD, Temperature-programmed desorption	Characterization of adsorptive properties of materials Characterization of surface acidity Temperature range of adsorbate release, temperatures of rate maxima Total desorbed amount, adsorption capacity, metal surface area and dispersion Surface energetic heterogeneity, binding states and energies of adsorbed molecules Mechanism and kinetics of adsorption and desorption
TPR, Temperature-programmed reduction	Characterization of redox properties of materials, fingerprints of sample Temperature range of consumption of reducing agent, temperatures of rate maxima Total consumption of reducing agent, valence states of metal atoms in zeolites and metal oxides Interaction between metal oxide and support Indication of alloy formation in bimetallic catalysts Mechanism and kinetics of reduction
TPO, Temperature-programmed oxidation	Characterization of redox properties of metals and metal oxides Characterization of coke species in deactivated catalysts

2.5.1 Temperature programmed desorption

Temperature programmed desorption (TPD), also called thermal desorption spectroscopy (TDS), provides information about the surface chemistry such as surface coverage and the activation energy for desorption [13]. In TPD, a clean surface is first exposed to a gaseous molecule that adsorbs. The surface is then quickly heated and the desorbed gas analysed via mass spectrometry, or using a thermal conductivity detector as in the present work. TPD thermograms can give different information such as: 1) identification of the desorbed species if a mass spectrometer is used as analyser 2) the amount of adsorbed species by measuring the area of the TPD peak, and 3) information on the kinetics of the desorption.

In this thesis an example of TPD is described (chapter 4) using gas probe molecules such NH_3 and CO_2 in order to determine acid and basic sites respectively on a carbon matrix.

2.5.2 Temperature programmed reduction

Temperature programmed reduction (TPR) has been used extensively in this thesis, and in this case hydrogen is used to induce reduction of the metal. The method has been used to collect information on the oxidation state of species of supported metals, and to identify metal mixing in the case of alloy formation using bimetallic catalyst (chapter 4).

In fact, using TPR for a metal in an oxidized state the following processes occur: firstly metallic nuclei are generated; afterwards the nuclei then grow until coalition occurs to produce metallic shells encasing cores of unreacted oxide, and finally reaction then proceeds at the metal/metal oxide interfaces until all the oxide in the cores is reduced [14].

This is obtained by submitting the oxidic catalyst precursor to a programmed temperature rise under a flow of hydrogen and the consumption of the reducing agent is continuously

monitored. Multiple reduction rate maxima (or minima) appearing in a thermogram are commonly attributed to occurrence of a multi-step reduction mechanism or to multiple reducing species [12].

2.6 Surface area determination, the Braunauer, Emmett and Teller method

The Braunauer, Emmett and Teller (BET) model is a refinement of Langmuir adsorption in which multiple layers of adsorbates are allowed [15]. In order to measure the surface area, the physical adsorption of a gas is used, and it requires in the determination of the volume of gas, usually N_2 , which leads to monolayer formation over the solid surface. By knowing the surface area of the adsorbed molecule, and the total volume adsorbed it is possible to determine the surface area of the solid.

This method is widely used in catalysis, however the main limit action is the assumption of only having a monolayer of adsorbed species, a condition that sometimes cannot be respected.

The analysis is usually carried out at a temperature close to the boiling point of N_2 (77K), and using a pressure range P below 35% of the P_0 vapour pressure of N_2 at the working temperature.
In these conditions the adsorption isotherm of the volume V versus P can be written as [16]:

$$V = \frac{V_m c P}{(P_0 - P)[1 + (c-1)\frac{P}{P_0}]} \qquad \text{(eq. 2.5)}$$

Where V_m is the volume of the monolayer and c is a constant correlated with the ΔH of the adsorption process.

This equation can be rearranged as:

$$\frac{P}{V(P_0 - P)} = \frac{1}{V_m c} + \frac{c-1}{V_m c}\frac{P}{P_0} \qquad \text{(eq. 2.6)}$$

Knowing P_0 and since P and V are experimental data, it is possible to plot a linear correlation of $\frac{P}{V(P_0 - P)}$ versus $\frac{P}{P_0}$, and from the intercept and the slope to calculate V_m. If the assumption of the method is not respected, deviation form linearity can be present, and the exploration of a different pressure range in order to identify a linear correlation is necessary. This has been the case for the surface area determination of gold on carbon catalysts (chapter 4).

2.7 Atomic absorption spectroscopy

Atomic absorption spectroscopy (AAS) is used to determine the amount of a metal in a solution.

In this method the sample is converted to an atomic gas, using different atomisation sources such as: air/acetylene flames, inductively coupled plasma, electric arc, and graphite furnaces [6]. In the present thesis the flame method has been used.

Using a hollow cathode lamp as the source of radiation and made of the same metal to be analysed, it is possible to determine the amount of metal by measuring the absorbance of the sample and comparing with the absorbance of standard solutions.
The main limitation of this technique is that it requires liquid samples. Consequently, if the amount of precious metal on a catalyst has to be determined the whole catalyst has to be dissolved using HF, or the metal dissolved using an appropriate solvent, usually aqua regia. In addition, it is necessary that the properties of the standard solutions, like acidity and viscosity are as similar as possible to the properties of the sample to analyse to

reduce systematic errors in the determination of the metal. Moreover, particular care is necessary in the case where more metals are present on the same catalyst, a circumstance that can lead to interference phenomena.

2.8 Nuclear magnetic resonance

Nuclear magnetic resonance (NMR) is an experimental technique useful to obtain structural information of a compound, especially organic species, and it has been used in this thesis to identify reaction products.

The principle of the technique is the resonant absorption of radio frequency radiation by nuclei exposed to a magnetic field. In order to be NMR active the nuclei has to have a non zero spin angular momentum I, as for ^{1}H which has I=1/2 as well as ^{13}C, ^{19}F, ^{31}P; and ^{14}N which has I=1. Nuclei like ^{12}C and ^{16}O are not NMR active since I=0 [17].
The nuclei most widely used in NMR are ^{1}H and ^{13}C, in fact these two nuclei are the most abundant in organic compounds, and what is more important is they posses a significant magnetogyric ratio γ which leads to an high NMR signal, and so the possibility of detecting compounds even in trace amounts.

Taking into account the case of a ^{1}H nucleus, if a magnetic field of intensity B_o is applied, a splitting of the energy level of the population of nuclei with angular momentum m_I +1/2 (population α) and m_I-1/2 (population β) is observed, (fig 2.6) [18].

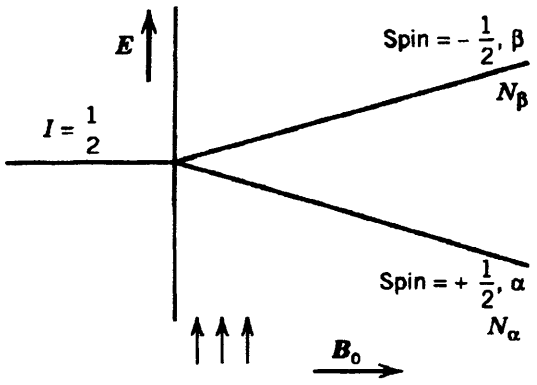

Fig. 2.6: The magnetic field Bo induces energy level splitting between the two populations α s=1/2 and β s=1/2 in a ^{1}H nucleus

The energy splitting is described by the equation:

$$\Delta E = \frac{h\gamma}{2\pi} B_o \qquad \text{(eq. 2.7)}$$

The resonance condition, i.e. the nuclear magnetic absorption for the transition α to β is reached when the energy separation of the levels is equal to the energy of the photons in the electromagnetic field. Denoted as ν_L, the resonance nuclei frequency, and with ν, the frequency of the applied magnetic field, the resonance condition can be expressed by the equation (2.8):

$$\Delta E = h\nu = \frac{h\gamma}{2\pi} B_0 = h\nu_L \qquad \text{(eq. 2.8)}$$

However, and most importantly, the property that nuclear magnetic moments interact with the local magnetic field due to the nucleus environment. In other words the local field can be different from the applied field by an amount called the shielding constant, and it is due to this property that it possible to identify chemical shift, in the specific case of ^{1}H when it is present in different functional groups.

In addition, coupling among nuclei is possible leading to further energy level splitting which can be a useful diagnostic tool. Determination of coupling constants has been performed also in this thesis (chapter 5) to identify products from different possible isomers.

2.9 References

[1] W. N. Delgass, G. L. Haller R. Kellerman and J. H. Lunsford, *Spectroscopy in Heterogeneous Catalysis,* Academic Press, New York, 1979

[2] J. W. Niemantsverdriet, *Spectroscopy in Catalysis, an Introduction,* VCH, Weinheim, 1993

[3] L. Coulier and J. W. Niemantsverdriet, *Surface chemical characterization, Encyclopedia of Chemical Physics and Physical Chemistry,* by N. D. Spencer and J. H. Moore, Vol 2, IOP Publishing Ltd, London, 2001

[4] J. C. Muijsers, J. W. Niemantsverdriet, I. C. M. Wehman-Ooyevaar, D. M. Grove and G. van Koten, *Inorg. Chem.,* 2655, **31** 1992

[5] J. R. Connolly, *Elementary Crystallography for X-Ray Diffraction,* University of New Mexico, Albuquerque, 2005

[6] D.A. Skoog, J.L. Leary, *Principles of Instrumental Analysis (IV Ed.),* Sanders College Publisching, Orlando FL, 1992

[7] Bruker-AXS, *Introduction to Powder X-Ray Diffraction,* Basics in XRD, 2005

[8] P. Hirsh, A. Howie, R. Nicholson, D. W. Pashley and M. J. Whelan, *Electron Microscopy of Thin Crystals* (II Ed.), Krieger, Malabar, FL, 1977

[9] D. C. Joy, A. D. Romig and J. I. Goldstein, *Principles of Analytical Electron Microscopy,* Pleum, New York, 1986

[10] Y. Amenomiya, J. R. Cvetanovic, *J. Phys. Chem.,* 2705, **67,** 1963

[11] S. D. Robertson, B. D. McNicol, J. H. De Baas, S. C. Kloet and J. W. Jenkins, *J. Catal.,* 424, **37,** 1975

[12] J. Kanervo, *Kinetic analysis of temperature-programmed reactions,* Industrial Chemistry Publication Series, Teknillisen kemian julkaisusarja, Espoo 2003 No. 16

[13] D. P. Woodruff and T. A. Delchar, *Modern Techniques of Surface Science* (II Ed.), Cambridge University Press, Cambridge, 1994

[14] S. J. Gentry, N. W. Hurst and A. Jones, *J. Chem. Soc., Faraday Trans.,* 603, **77,** 1981

[15] K. S. W. Sing, D. H. Everett, R. A. W. Haul, L. Mosoul, R. A. Pierotti, J. Rouguerol and T. Siemieniewska, *Pure Appl. Chem.,* 603, **57,** 1985

[16] S. Brunauer, P. H. Emmett and E. Teller, *J. Am. Chem. Soc.*, 309, **60**, 1938

[17] P. W. Atkins, *Physical Chemistry* (VI ed.) Oxford University Press, 1998

[18] R. M. Silverstein and F. X. Webster, *Spectrometric Identification of Organic Compounds* (VI Ed.), John Wiley and Sons, Inc., New York 1998

Chapter 3: LOW TEMPERATURE CARBON MONOXIDE OXIDATION OVER SUPPORTED GOLD CATALYSTS

3.1 Introduction

Low temperature CO oxidation is one of the most widely investigated catalysed chemical reactions on a metal surface, and probably the most studied, when using gold as a catalyst. This is due not only to the fact that the reaction finds a number of industrial application such as automotive emission control [1] and fuel cells applications [2], but also because with the hydrochlorination of acetylene [3] was one of the first two chemical reactions discovered, where gold was able to display catalytic activity [4].

In this chapter, the effect of doping agents, including nitrate ions on a Au/TiO_2 catalyst, is investigated, supporting that the presence of trace amounts of nitrates can lead to enhanced activity.

3.1.1 Carbon monoxide oxidation over gold surfaces

In order to find rational explanations of the observed activity of gold for CO oxidation, several mechanisms has been proposed. The most widely known are those of Haruta [5], Bond [6] and Kung [7]. None of these mechanisms alone are able to explain the activity of gold and effects due to promoters or poisoning, but each of them can explain some experimental evidence. These three mechanisms are briefly reported here; in order to have an inclusive view of this reaction, and to allow insight into the nitrate promotion effect reported here.

3.1.2 Mechanism proposed by Haruta

In this mechanism a crucial role is played by the gold/support interface. Experimental

observations show that carrying out the reaction at different temperatures lead to different kinetics, and that the activity is particle size dependent, although a more consistent correlation exists between the perimeter length of the particle and activity [8]. On this basis the proposed mechanism (Scheme 3.1) is:

1) $*Au + CO \leftrightarrow *Au\cdots CO$
2) $*\square + O_2 + e^- \leftrightarrow O_2^-\cdots *\square$
3) $*Au\cdots CO + O_2^-\cdots *\square \rightarrow *Au + CO_3\cdots *\square + e^-$
4) $CO_3\cdots *\square + *\square \rightarrow CO_2\cdots *\square + O\cdots *\square$
5) $CO_2\cdots *\square \leftrightarrow CO_2 + *\square$
6) $2O\cdots *\square \rightarrow O_2 + 2*\square$

Scheme 3.1: CO oxidation mechanism proposed by Haruta

Where *Au indicates an active gold site, and *□ an active support site. The peculiarity of this mechanism is the formation, as an intermediate, of a bidentate carbonate species adsorbed on the support (step 3 Scheme 3.1).

3.1.3 Mechanism proposed by Bond and Thompson

This mechanism involves, as the previous one, the role of the gold-support interface, but in this case, the gold oxidation state is relevant [6]. Moreover, the peculiarity for this mechanism is the existence of gold-hydroxide groups. This hypothesis is supported by the existence of AuO(OH) species that can be detected by Mössbauer spectroscopy in pre-calcined ferrihydrite-supported catalyst [9]. The proposed mechanism is reported below in Scheme 3.2:

1) $Au(0) + CO \rightarrow Au(0)\cdots CO$
2) $Au(III) + OH^-\square \rightarrow Au(II)\cdots OH$
3) $Au(0)\cdots CO + Au(II)\cdots OH \rightarrow Au(II)\cdots COOH + Au(0)$
4) $O_2 + *^-\square \rightarrow O_2^-\cdots *\square$
5) $Au(II)\cdots COOH + O_2^-\cdots *\square \rightarrow Au(II) + CO_2 + HO_2^-\cdots *\square$
6) $Au(II)\cdots COOH + HO_2^-\cdots *\square \rightarrow Au(II) + CO_2 + 2OH^-\square + *\square$
7) $Au(II) + *\square \rightarrow Au(III) + *^-\square$

Scheme 3.2: CO oxidation mechanism proposed by Bond and Thompson

In this mechanism, the intermediate species is represented by carboxylate group formation (step 3 Scheme 3.2), afterwards O_2^- dehydrogenates it, giving a hydroperoxide ion HO_2^- and restoring the hydroxyl groups on the support surface.

3.1.4 Mechanism proposed by Kung

The mechanism uses both hydroxyl gold species and carbonate formation to explain the activity. In this case the active site is constituted both by Au(0) and Au(I), but with different roles: Au(0) to activate oxygen, and Au(I) to stabilize the carbonate intermediate [7]. A diagram for this mechanism (Scheme 3.5) is displayed here:

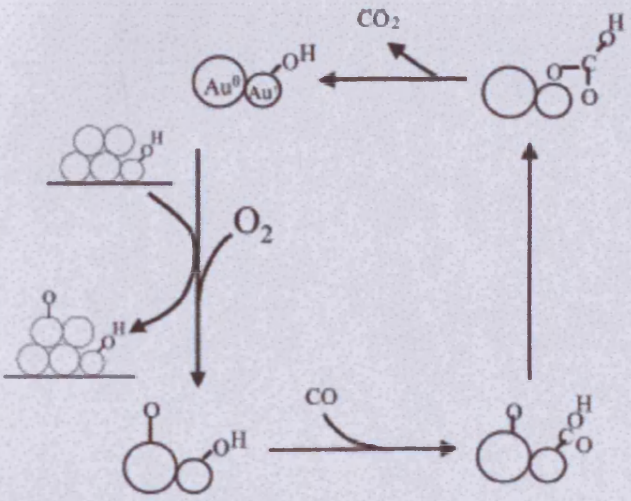

Scheme 3.5: CO oxidation mechanism proposed by Kung

A comparison with the mechanisms proposed by Haruta and Bond reveals that the mechanism proposed by Kung is a compromise, using the assumptions of the other two proposals. An experimental observation that can support it, is the fact that chlorine is a very efficient poison for gold based catalysts for CO oxidation [10]. If it is assumed that the active site is an Au^+-OH^- centre, the presence of chloride can lead to Au^+-Cl^- [7], and this could also be consistent also with Bond's mechanism.

3.2 Au/TiO_2 catalysts for CO oxidation

Several gold metal oxides catalysts are able to perform CO oxidation such as Au/Fe_2O_3, Au/Al_2O_3, Au/TiO_2 and Au/CeO_2, depending also on which technique has been used to prepare them [5].

The most efficient catalyst is probably Au/Fe_2O_3 where conversions of 100 % are often claimed and it is possible to regenerate it, after reaction [8]. However, for this work, Au/Fe_2O_3 has not been used, because of its high efficiency, under the reaction conditions used. The main role of this study was initially related to the evaluation of the effect of alkali metals in very low amounts, in order to identify promoting effects. For this reason it has been chosen to use TiO_2 as support, due to its good conversion values, in order to evaluate the doping effect.

Moreover, Au/TiO_2 has been one of the most investigated catalysts in terms of particle morphology. It has been proved that when gold is deposited on TiO_2 using the deposition precipitation technique, it gives hemispherical particles with their flat planes strongly attached to the TiO_2 support [11]. In contrast, when the impregnation technique is used almost spherical particles on the top of the support are obtained [12]. This difference is quite important because different contact angles lead to different catalytic activity due to the interaction with the support.

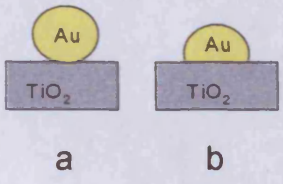

Fig. 3.1 Different shaped gold particles on TiO_2 with different preparation methods. Spherical if impregnation is used (**a**) and hemispherical if deposition precipitation is used (**b**)

In the present work, deposition precipitation has been used to prepare the Au/TiO_2 catalyst, while the impregnation technique has been used to add dopants.

3.3 Experimental

3.3.1 Preparation and doping of Au/TiO_2 catalysts

The Au/TiO_2 catalyst was prepared using deposition precipitation method. TiO_2 (Degussa P25, 3 g) was stirred in deionised water (200 mL) and stirred for 30 min. in order to have a final nominal gold loading of 2.5% wt. A solution of $HAuCl_4 \cdot 3H_2O$ (10 mL) was added dropwise over 10 min subsurface. The slurry was then heated to 80 °C and the pH adjusted to 9 using Na_2CO_3. The slurry was then stirred for 1 h and afterwards cooled and filtered.

The filtrate was tested with $AgNO_3$ solution in order to detect the presence of chloride, and atomic absorption spectrophotometry in order to detect the eventual presence of Na, as Na_2CO_3 solution was used to adjust the pH. A final volume of 5 L of water was necessary to remove all Na traces. Using atomic absorption spectroscopy, a Au loading of 1.4% has been determined. The resulting solid has been dried at 80 °C overnight.

Using the catalyst described above (100 mg aliquots), a new set of catalysts were prepared by impregnation with aqueous solutions of: sodium nitrate, potassium nitrate, sodium acetate and sodium citrate, in order to have a range of alkali metal concentration in the range from 0 to 0.0375% wt.

After addition of the alkali metal solution to the catalyst, the slurry was then stirred for half hour, and then dried at 120 °C for 3 hours.

3.3.2 Catalyst activity tests

In order to evaluate catalyst activity, a fixed bed quartz micro-reactor has been used. The reactor has an internal diameter of 3 mm and for each test catalyst (15 mg) has been employed, operating at atmospheric pressure, at a temperature of 25 °C held constant by

immersing the reactor in a thermostatically controlled water bath.

A reaction mixture of CO/Air (molar ratio 0.5/99.5 at a constant flow of 50 mL min^{-1}) has been used for a total time on line of 10 h. Chromatographic reaction of the products has been carried out using on-line gas chromatography (Porapack Q and Molecular Sieve 5A).

3.4 Results

3.4.1 Effect of $NaNO_3$ and KNO_3 doping over Au/TiO_2

The catalytic activity for Au/TiO_2 and $Au/TiO_2/NaNO_3$ is reported in Fig. 3.2 below:

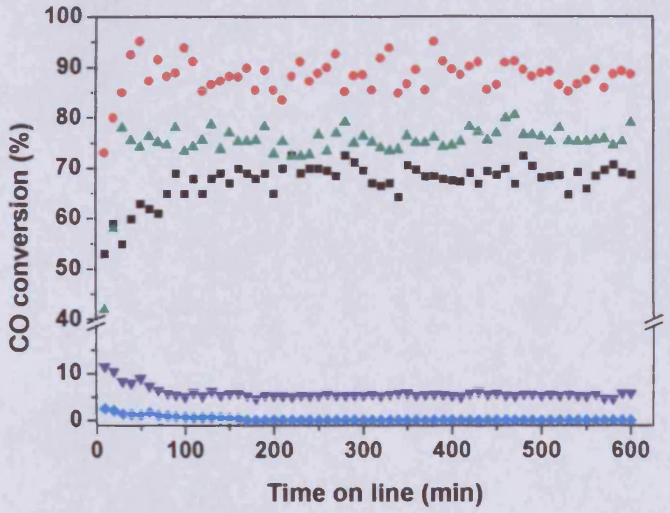

Fig. 3.2 Evolution of the catalytic activity for CO oxidation with the time on line, for sodium nitrate modified Au/TiO_2 catalysts: (■) 0 wt.% Na, (●) 0.00625 wt.% Na, (▲) 0.0125 wt.% Na, (▼) 0.025 wt.% Na and (♦) 0.0375 wt.% Na.

The undoped catalyst, after an induction time, displays an almost constant conversion around 70%. However, the addition of very low amounts of $NaNO_3$ with concentrations of Na equal to 0.00625 and 0.0125 % wt leads to an enhanced activity around 90 and 80% respectively. While a higher concentration leads to a 10% conversion for the 0.025%

wt $NaNO_3$ doped catalyst, and almost a negligible activity for the 0.0375 % wt $NaNO_3$ catalysts. These last two results are not surprising, since sodium is a known poison for this reaction [13].

To determine if the activity trend observed is due to a low amount of Na^+ or to the presence of the counter ion NO_3^-, a different series of experiment using K^+ as cation, and different anions including acetate and citrate has been carried out, and the results are reported in Fig. 3.3:

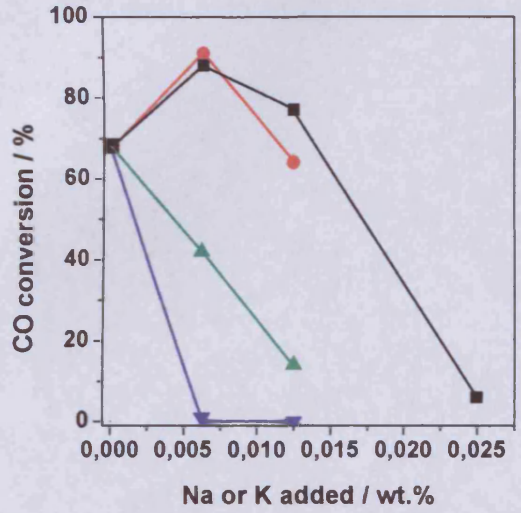

Fig. 3.3 Influence of the alkali metal dopant (Na or K) on the activity for CO oxidation. Alkali source: (■) Na-nitrate, (●) K-nitrate, (▲) Na-citrate and (▼) Na-acetate. Time on line = 500 min.

When Na^+ is used it is evident that acetate, and especially citrate have a deleterious effect on catalytic performance. It could be possible to propose a reducing effect of citrate anion on gold which is a known effect for this salt [14] however XPS spectra do not display significant differences before and after treatment. Nevertheless, when KNO_3 is used, the conversion trend is quite similar to what observed for $NaNO_3$, and in this case, it is not a short term effect, but is consistent for the time on line of the analysis of 10 h.

In order to verify if the trend in Fig. 3.3 could be a function of surface area, the catalysts were analysed using the BET method before and after doping, using a Micromeritics

ASAP 2000 instrument, and the results are reported in Table 3.1:

Table 3.1: Surface areas of Au/TiO_2 catalysts after doping

Cation	Anion	Quantity of cation added (% wt)	BET surface area ($m^2 g^{-1}$)
-	-	-	45
Na^+	NO_3^-	0.00625	45
Na^+	NO_3^-	0.0125	47
Na^+	NO_3^-	0.025	43
Na^+	NO_3^-	0.0375	39
K^+	NO_3^-	0.00625	46
K^+	NO_3^-	0.0125	44
Na^+	CH_3COO^-	0.00625	45
Na^+	CH_3COO^-	0.0125	47
Na^+	$C_6H_5O_7^{3-}$	0.00625	46
Na^+	$C_6H_5O_7^{3-}$	0.0125	48

The impregnation treatment does not affect significantly the surface area of the catalyst, and they are all in the range 40-50 $m^2 g^{-1}$

In addition, to investigate if the promotional effect for $NaNO_3$ and KNO_3 is still observed when another oxidant is used, air has been replaced with N_2O. The results obtained are shown in Fig. 3.4:

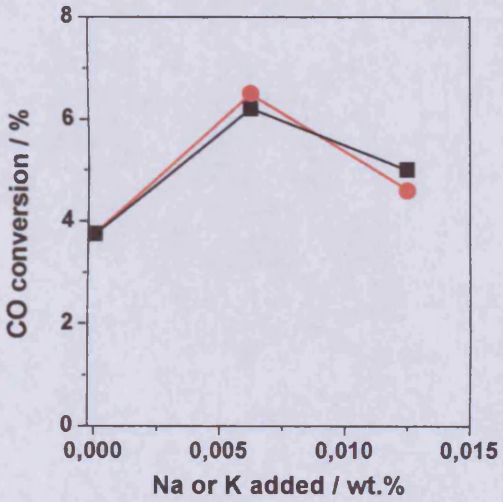

Fig 3.4 Influence of the alkali (Na or K) content on the activity for CO oxidation using N_2O as oxidising agent. Alkali source: (■)Na-nitrate and (●) K-nitrate. Time on line=500 min.

In agreement with previous studies, N_2O is a less efficient oxidizing agent for CO [15], and the conversion values are this time in the range 4 - 7%. However, a significant promotional effect is still observed when low concentrations of sodium and potassium nitrate are used, with a similar degree of promotion for both O_2 and N_2O as oxidants.

3.4.2 Effect of HNO_3 and water on Au/TiO_2

From the data, it is evident that the effect is not induced by the cation. And, since the addition of sodium citrate and sodium acetate has a deleterious effect, it is possible to conclude that Na^+ and/or citrate/acetate act as a poison for the Au/TiO_2 catalyst for CO oxidation, but not the anion nitrate.

In order to test this conclusion directly, and to evaluate the effect of the impregnation on the catalyst, another set of Au/TiO_2 catalysts were prepared, and then impregnated with water and HNO_3 solutions in order to have final NO_3^- loadings of 0.00625 and 0.0125 % wt. It is important to note that the blank catalyst Au/TiO_2 was treated with water as well, and dried at 120 °C for 3 h in the same way as the doped catalyst before use. This is an important precaution, because water is known to be a promoter for this reaction [16]. In our case, we think that water from catalyst preparation should not affect the catalysts, but if it does, it should affect them in the same manner. The results of the tests, for a time on line of 600 min are reported below in figure 3.5:

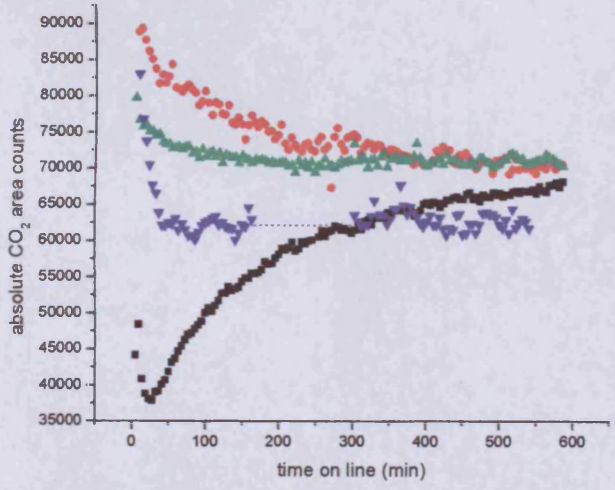

Fig 3.5: Absolute CO_2 counts over the catalysts: (■) Au/TiO_2 2.5% wt, (●) Au/TiO_2 0.00625% HNO_3, (▼) Au/TiO_2 0.125% HNO_3, and (▲) $AuTiO_2$ with water.

The impregnation treatment influences the initial activity trend for the catalyst. For the impregnated catalysts a decrease in activity is observed, and for the untreated catalyst there is an increase, but they are all converging to a similar activity after 10 h. Nevertheless, it is evident that there is an enhanced conversion when HNO_3 is added in very low amounts. Again, the trend observed is very similar to the trend for $NaNO_3$ and KNO_3, proving that nitrate is the promoter.

A comparison between these two sets of catalysts, using the relative ratio of the conversions for the catalysts impregnated with water leads to the following plot (Fig. 3.6):

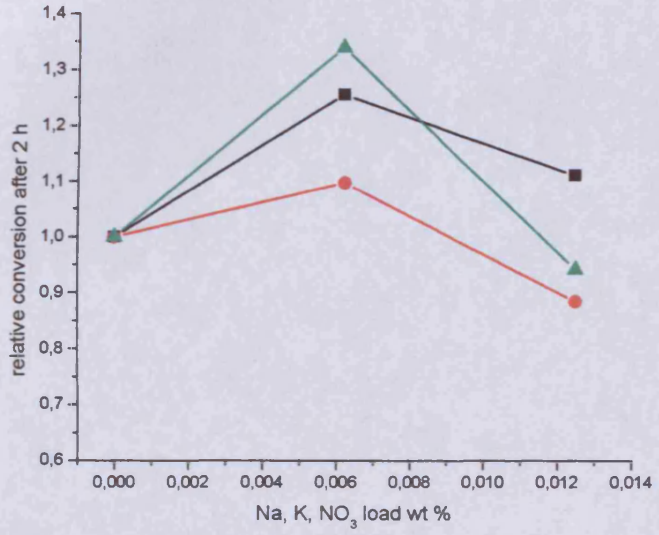

Fig. 3.6: CO relative conversion vs. NO_3 from different sources, Effect of NO_3^- doping from different sources. A promotional effect is detected for low amounts of nitrate independent of its origin (■) $NaNO_3$, (●) HNO_3 and (▲) KNO_3

A promoting effect is observed, which is independent of the nitrate source. The origin of this phenomenon is still unclear, however taking into account the accepted mechanism for CO oxidation previously reported, a possible explanation could involve site blocking, or the formation of new active sites on the gold/support interface. Another explanation could involve electronic effect of nitrates on gold surface; in fact, not all nitrates could be selectively dispersed on the gold/support interface although it is not possible to prove this

assumption with the characterization data collected. In addition, even for the prepared catalyst it is not possible to state which of the three CO oxidation mechanisms described above is operating.

In order to collect further information, X-Ray Powder Diffraction (XRPD) has been carried out on the undoped catalyst impregnated with water (Fig. 3.7) using a Bruker-Nonius FR 590 diffractometer (Cu-K_α X-ray source, 40 KV – 30 mA). X-ray photoelectron spectroscopy of the undoped and $NaNO_3$ doped catalysts has also been performed using a VG EscaLab 220i spectrometer, (AlK_α X-ray source - 300 W - and an analyser pass energy of 20 eV)

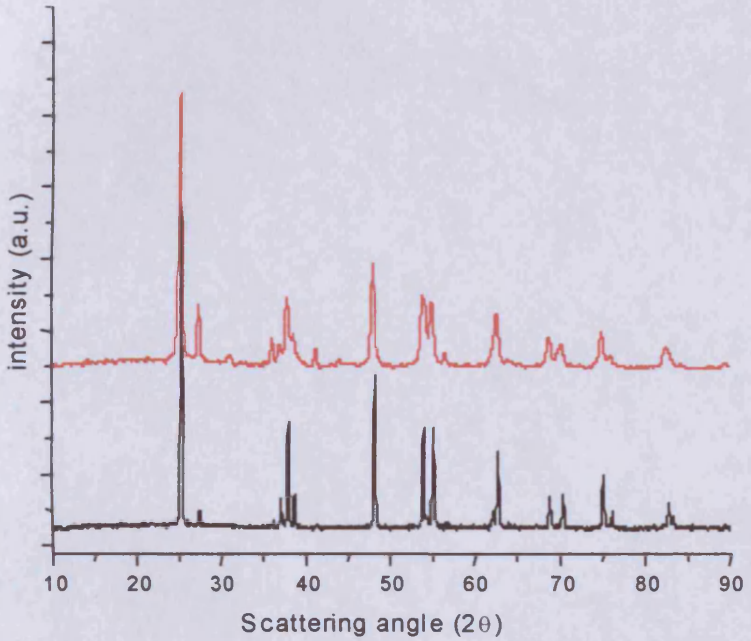

Fig 3.7: XRPD pattern (—) of the support TiO_2, (—) and of the catalyst after gold deposition, and afterwards water impregnation.

The support and catalyst after preparation do not display significant changes in terms of XRD pattern (Fig. 3.7). Moreover, no gold reflections were detected in the pattern shown above - the expected 2θ values for the most intense reflections for gold are at 38.18°, 44.93°, and 64.57° 2θ [17] - probably due to the small gold particle size, expected to be in the range of 2-5 nm [18], which is close to the detection limit for common XRPD.

Concerning XPS spectra of the catalyst as prepared, and after doping with $NaNO_3$, no change in gold oxidation state was detected. Moreover, no nitrates were detected since their concentration is below the detection limit.

The characterization techniques used, did not detect significant differences between the doped and the undoped catalysts. Consequently, the effect of NO_3^- could be related to a site blocking effect or changes in morphology of the perimeter of the gold particles.

3.5 Conclusions

In conclusion, the observation of an enhanced and long term activity improvement, by the addition of trace amounts of nitrate for Au/TiO_2 catalyst for CO oxidation, can be considered as significant for two reasons. The first one is related to the fact that up to now, this is the first example of enhancement of activity of gold supported nanoparticles by the addition of promoters [19]. Consequently, it is reasonable to think that this kind of effect could not be limited to nitrates only. Secondly, the difficulty of reproducibility of active catalysts when gold is used is well known [20]. Since many supported Au catalysts involve precipitation methods using nitrites as one of the components, it is evident that if residual nitrate is not removed, or a variable amount of traces is still present, there is the distinct possibility of a final variable activity. In these studies traces amount of nitrates can give a final improved conversion by 20-30% of the original catalyst. However, this finding could aid the design of improved supported gold catalysts.

3.6 References

[1] A. Ueda, T. Oshima and M. Haruta, *Appl. Catal.*, B 81, **12**, 1997

[2] P. Landon, J. Ferguson, B. E. Solsona, T. Garcia, A. F. Carley, A. Herzing, C. J. Kiely, S. E. Golunskic and G. J. Hutchings, *Chem. Comm.*, 3387, 2005

[3] G. J Hutchings, *J. Catal.*, 292, **96**, 1985

[4] M, Haruta, T, Kobayashi, H. Sano and N. Yamada, *Chem. Lett.*, 405, 1987

[5] M. Haruta, *Chem. Rec.*, 75, **3**, 2003

[6] G. C. Bond and D. T. Thompson, *Gold Bull.*, 47, **33**(2), 2000

[7] H.H. Kung, M.C. Kung and C.K. Costello, *J. Catal.*, 425, **216**, 2003

[8] M. Haruta, *Cat. Tech.*, 102, **6**(3), 2002

[9] R.M. Finch, N.A. Hodge, G.J. Hutchings, A. Meagher, Q.A. Pankhurst, M.R.H. Siddiqui, F.E. Wagner and R. Whyman, *Phys. Chem. Chem. Phys.*, 485, **1**, 1999

[10] H.-S. Oh, J.H. Yang, C.K. Costello, Y. Wang, S.R. Bare, H.H. Kung and M.C. Kung, *J. Catal.*, 375, **210**, 2002

[11] G. R. Bamwenda, S. Tsubota, T. Nakamura, and M. Haruta, *Catal. Lett.*, 83, **44**, 1997

[12] J.M.C. Soares, P. Morrall, A. Crossley, P. Harris and M. Bowker, *J. Catal.*, 17, **219**, 2003

[13] G. C. Bond and D. T. Thompson, *Catal. Rev. Sci. Eng.*, 319, **41**, 1999

[14] J. Turkevitch, P.C. Stevenson and J. Hillier, *Discuss. Faraday Soc.*, 55, **11**, 1951

[15] N.W. Cant and N. J. Ossipoff, *Catal. Today*, 125, **36**, 1997

[16] H. S. Oh, C.K. Costello, C. Cheung, H.H. Kung, M.C. Kung, *Stud. Surf. Sci. Catal.*, 375, **139**, 2001

[17] Swanson and Tatge, Natl. Bur. Stand. (U.S.A. 1953), International Centre for Diffraction Data, Powder Diffraction File, Entry 4-784 (1996)

[18] B.E. Salisbury, W.T. Wallace, and R.L. Whetten, *Chem. Phys.*, 131, **262**, 2000

[19] B. Solsona, M. Conte, Y. Cong, A. Carley and G. Hutchings, *Chem. Comm.*, 2351, 2005

[20] M. Cortie, R. Holliday, A. Laguna, B. Nieuwenhuys and D. Thompson, *Gold Bull.*, 144, **36**, 2003

Chapter 4: GOLD BASED CATALYSTS FOR THE HYDROCHLORINATION OF ACETYLENE

4.1 Introduction

In this chapter, the use of gold based catalysts for the hydrochlorination of acetylene is described. Initially the behaviour of gold on carbon catalyst for hydrochlorination reaction has been investigated, and afterwards moving on to bimetallic catalysts containing Pd, Pt, Rh, Ir, Ru all containing gold as a reference metal.

4.1.1 Hydrochlorination of acetylene

The hydrochlorination reaction of acetylene is one of the most important industrial chemical processes, since the product obtained, vinyl chloride monomer (VCM), which is the building block of polyvinyl chloride (PVC), a plastic material that can find a wide range of application in the building and construction industry, as well as in the electrical, apparel, and packaging industries [1]. PVC degrades relatively quickly for a polymer, but the use of heat, ozone, and ultraviolet stabilizers, can make it a useful polymer. A wide variety of desirable properties can be obtained by using various amounts of plasticisers, leading to both rigid and plasticised PVCs with large markets. Almost 90% of the total production of VCM is destined to the manufacture of PVC [1, 2], while the remaining part is used for production of chlorinated solvents.

For this purpose in 1998 the average VCM production was around 27 millions of tons per year [2], and this explains the efforts carried out in industry to find suitable methods of manufacture. However, interest in this reaction is not only industrial but also academic, given that the use of gold as a catalyst was one of the first examples of activity of this metal as a catalyst [3].

4.1.2 Industrial manufacture of vinyl chloride monomer

Vinyl chloride monomer can be industrially obtained using three different routes, which are the direct hydrochlorination reaction of acetylene [1, 4], the thermal cracking of 1,2 dichloroethane [1, 5], and the 'balance process'[1, 6].

The direct hydrochlorination is:

$CH{\equiv}CH + HCl \rightarrow CH_2{=}CHCl$ (eq. 4.1)

The reaction is thermodynamically favoured (ΔH^o = -99 kJ mol^{-1}) but without a catalyst, no reaction occurs. Industrially the reaction is carried out using mercuric chloride, $HgCl_2$, supported on activated carbon as catalyst at a pressure around 1-2 bar, and temperature in the range of 100-200°C [7]. Nowadays, this kind of route is quite limited, due to the restrictive environmental normative relating to the use of $HgCl_2$ [8], and matters related with the lifetime and the regeneration of the catalyst, due to the phenomena of mercury desorption [9, 10]. However, it is possible to find some example in the patent literature [11] involving the use of bimetallic Au/Pt and Au/Pd catalysts for direct hydrochlorination of acetylene.

The second industrial route uses 1,2 dichloroethane as precursor, and VCM is obtained by thermal dehydrochlorination of the precursor in a temperature range 480 to 510 °C, at a pressure around 3.5 bar [1]:

$CH_2ClCH_2Cl \rightarrow CH_2{=}CHCl + HCl$ (eq. 4.2)

In these conditions the yield is in the range of 50-60%, but industrially VCM can be separated by fractional distillation, and recycling 1,2-dichlroroethane enables to an overall yield above 98%, making this process one of the most efficient available.

Finally, the third industrial route is the so-called 'balance process' [1, 6]. This name is due to the fact that it combines the oxychlorination reaction of ethylene to obtain 1,2

dichloroethane, and subsequent dehydrochlorination, in the same process, and can be shown schematically:

$CH_2=CH_2 + 2\ HCl + O_2 \rightarrow 2\ CH_2ClCH_2Cl + 2\ H_2O$ (eq. 4.3)

$CH_2ClCH_2Cl \rightarrow CH_2=CHCl + HCl$ (eq. 4.4)

Nowadays most VCM is obtained using this last route [1, 12] and this is also due to the circumstance that while ethylene is an oil-derived feedstock, acetylene is a coal-derived feedstock and consequently ethylene can be available in larger amount and lower cost. This reaction will be treated more specifically in chapter 6, while in the present chapter the use of gold based catalysts for direct hydrochlorination of acetylene will be described.

4.1.3 Use of gold based catalysts for hydrochlorination reactions

Different metals, with different efficiency are able to perform the hydrochlorination reaction, remarkably it was observed that metals with higher reduction potentials gave higher catalytic activity [3]. Based on this experimental observation, metals with reduction potentials greater than Hg(II) and Pd(II) should lead to more active catalysts. This hypothesis has been confirmed [3, 13] and led to the demonstration of the role of gold as catalyst. Nevertheless, no literature is available on the effect of adding another metal, either a bimetallic or an alloy system, on final activity. For this reason the effect of adding metals such as Pd, Pt, Rh, Ir, Ru has been investigated, in order to identify a possible synergic effect, and if the use of simple catalyst preparation techniques can lead to an alloy system.

From previous studies [13] it is known that carbon is the best support for this reaction if compared with metal oxides, for this reason all the gold based catalysts described here have been prepared on this material. However, it should be mentioned that the reaction is also carbon type dependent. Consequently, explanations of catalyst preparation procedure and characterization of carbon properties are reported here.

4.2 Experimental

4.2.1 Au/C catalyst preparation

All the gold based catalysts were prepared on carbon using incipient wetness impregnation techniques and *aqua regia* (HCl and HNO_3 using a 3:1 ratio) as solvent. The impregnation cannot be carried out directly on fresh carbon support because it may contain traces of Na, Fe and Cu that are poisons for the hydrochlorination reaction [14]. For this reason washing of the support is necessary, using a dilute solution of HCl (1 mol L^{-1}), heating and mixing the resulting suspension at 70° C for 5 h. Carbon was filtered and washed with distilled water (2 L of water per gram of carbon) and afterwards dried it at 140° C for 18 h.

A solution of $HAuCl_4 \cdot xH_2O$ (Strem, 82 mg, assay 49.7 %) in *aqua regia* (3.7 mL) was added dropwise to carbon (Aldrich, Darco 12-20 mesh, 4 g) with stirring. The final incipient wet product was then dried at 140° C for 18 h.

It appears evident that incipient wetness technique is a rough method to prepare a catalyst, but it is has the advantage that is necessary to control few parameters in contrast with more sophisticated procedures such as deposition precipitation or co-precipitation.

It is well known that small variations in the method of synthesis can cause the difference between a good and a poor catalyst. This aspect has been demonstrated from a great number of experiments [15, 16]. It is also important to remember that one of the targets of this project is to test the reproducibility of the system, and to compare different catalysts. For this reason it is very important to prepare a catalyst using a technique that has small variations of its parameters, so that it can give reproducible results. Moreover, among the impregnation techniques, the method described using *aqua regia* as solvent can lead to the best catalyst in terms of lower metal leaching phenomenon for the hydrochlorination reaction [13].

The repeatability of the preparation method has been tested and will be described later (paragraph 4.4.1). It is worth mentioning, that the phenomena of inhomogeneous concentration gradients have been observed (paragraph 4.10.1).

4.2.2 Micro reactor for the hydrochlorination reaction of acetylene

All the catalytic tests have been carried out on a specifically designed micro reactor, consequently, crucial parameters to control are: temperature, pressure and flow of the reactants.

The hydrochlorination reaction of acetylene is strongly dependent on temperature. In particular we can identify two regions where deactivation of the catalyst can occur. One is at low temperature, between room temperature and 100 °C, and the other one between 120 °C and 180 °C [13]. It should be stated that if a deactivation mechanism can occur at 180 °C, the reaction is conducted just at this temperature, to guarantee a reasonable reaction rate. In the region at higher temperature the reduction of Au(III) to Au(0) is possible, and this has been identified as a deactivation process for a catalyst at higher temperature [13] and this applies for the catalysts prepared in this work. At lower temperature, the deactivation is due to deposition of carbonaceous residues on the catalyst surface. The residues are polymerisation products of vinyl chloride monomer. These polymerisation products have not been observed for the catalyst made using gold only, but they can be present for the other metals used, or after repeated tests on the micro-reactor.

Concerning the flow of reactants, it well known that this is a quite important parameter in heterogeneous catalysis, since the selectivity of a reaction is affected by the contact-time of a chemical species on catalyst surface. Most important is the Gas Hourly Space Velocity (GHSV). Using 200 mg of catalyst, which has a volume of 3.46 ± 0.15 mL g^{-1}, a reactant flow in the range from 5 to 10 mL min^{-1} has been chosen with a consequent GHSV in the range of 430-870 h^{-1}. The pressure of the reactants, both HCl and C_2H_2 was

in the range of 1.1-1.2 bar. This value was chosen both for safety reasons, and to test the catalyst under mild conditions.

A block diagram of the micro reactor used is shown in figure 4.1:

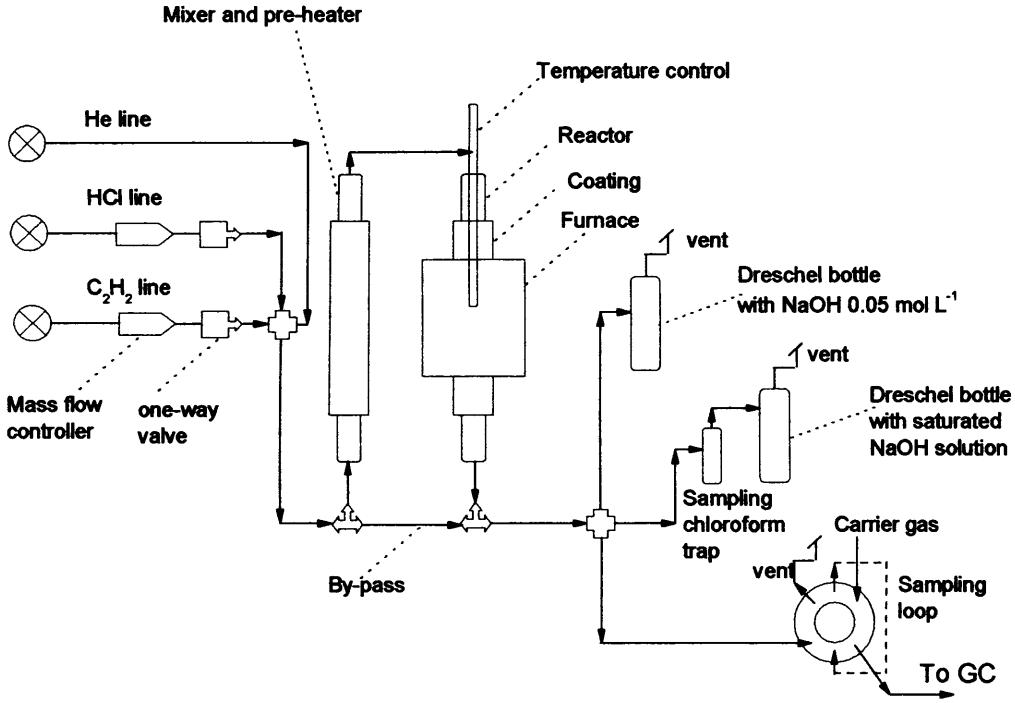

Fig. 4.1 : Diagram for hydrochlorination reactor

In order to have a rigorous control of reactants flow, two flow-mass controllers for HCl and C_2H_2 were used. Before entering the reactor the mixture of reactants passed through a mixer-pre heater. This consisted of a tube containing small glass spheres heated at 70 °C, to guarantee that when the reactants entered the reactor they were well mixed.

At the outlet of the reactor, different options were available. The first option was to flow the gas mixture through a Dreschel bottle containing NaOH at known concentration for a known time. This apparatus can be used to determine the conversion of the reaction. Indeed, knowing the total amount of NaOH, and operating a constant flow of gases for a fixed time, if a fixed amount of NaOH is taken, it is possible *via* back titration with potassium phthalate to determine the amount of unreacted HCl, and so the conversion.

Alternatively, and this was the most used method, before a second Dreschel bottle a sampling port, equipped with a six way valve system enable the gas stream to be analysed by GC.

Measurements based on NaOH titration were very accurate, and they have been used to calibrate the reactant flows in absence of reaction, but for safety reasons, in particular the ascertained carcinogenic nature of VCM, the total conversion has not been calculated based on HCl, but on C_2H_2. Indeed, it is possible to collect the area counts of C_2H_2 for no reaction, by flowing the gases through the by-pass. After making this measurement, the gases were switched from the by-pass to reactor, and by measuring the decrease in the acetylene signal the conversion can be calculated. Moreover, this method has the advantage of enabling all these operations to be carried out on line.

Using a flow of 5 mL min^{-1} for each reactant gives a GHSV of 867 h^{-1} and the number of moles of HCl has been determined to be $6.25 \cdot 10^{-5}$ mol min^{-1}. This can seem an apparently low value, but even assuming a 50% conversion over a catalyst, this leads to a production of 3.9 grams of VCM using a reaction time of 4 h, which is close to the extraction limits of the fume hood. These are not trivial concerns, but are safety measures to take into account. For this reason experimental conditions are determined by efficiency and safety limits due to the well known carcinogenic nature of VCM [2, 17, 18].

In addition, at the outlet of the reactor it is possible to have a chloroform trap in order to collect products for further characterization, or a sampling port for a gas syringe. The trap system has been demonstrated to be more suitable for the required purposes, especially when reactants other than acetylene have been used.

Concerning the reaction temperature a value of 180° C has been chosen, and it is important to add that the reactor must be of inert material such as quartz, since stainless steel is corroded by HCl. Due to the relatively low temperature used, glass is a suitable material for the reactor. Blank tests using an empty reactor filled with quartz wool did not display any kind of catalytic activity, even at 250 °C.

4.2.3 Gas Chromatograph conditions

An initial study has been carried out using a Carbowax 80/20 column, length 6 ft and made of stainless steel. The column allows the identification of the components, which are mainly C_2H_2 and C_2H_3Cl (VCM), however, the chromatographic resolution cannot be considered suitable for a rigorous determination of peak area, even exploring oven temperatures in the range from 40 to 130 °C and relative column inlet pressure in the range from 0.5 to 1.2 bar.

Reported in figure 4.2 is a series of chromatograms obtained using a flow of 1 mL min^{-1} for each reactant in order to identify a steady state regime. A column temperature of 40 °C and a relative inlet pressure of 0.5 bar were used and a FID as detector. The chromatograms indicated (figure 4.11) cover a time of 4 h.

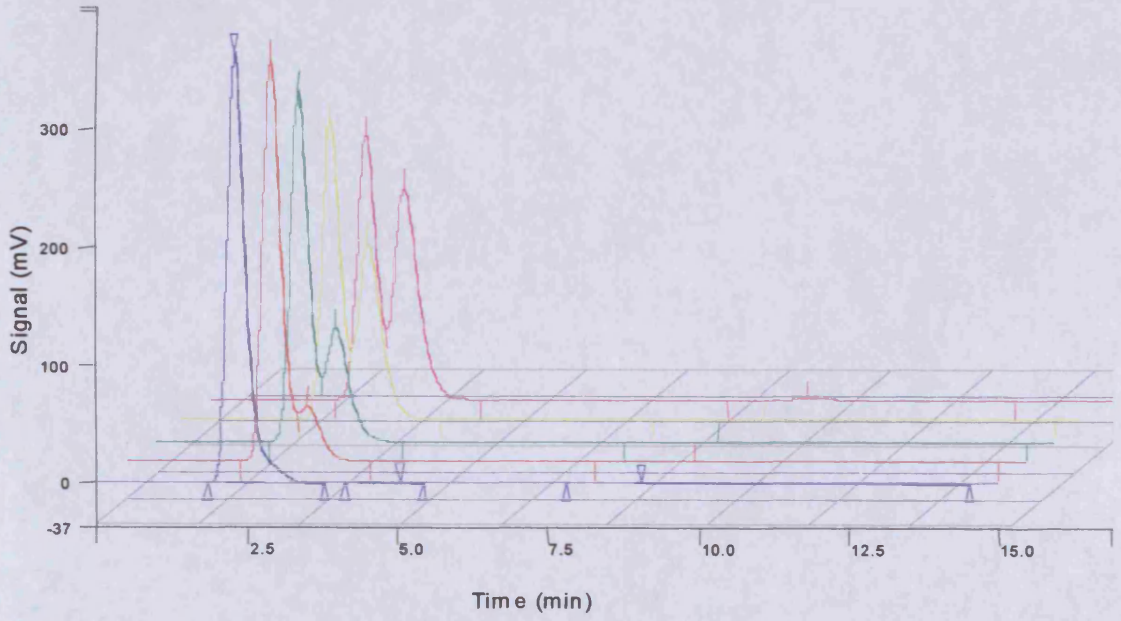

Fig. 4.2: Chromatographic identification of reaction product using a Carbowax 80/20 column. The decreasing peak is the reactant C_2H_2 (2.4 min), while the increasing peak the product CH_2=CHCl (VCM 2.6 min). The chromatograms indicated a relate to the reaction time: (—) 0 h, (—) 1 h, (—) 2h, (—) 3h and (—) 4 h.

As a consequence of these results, a Porapak N column 6 ft length has also been used. In contrast to the Carbowax, which has a stationary phase made by polyethylenglicol polymer, a Porapak N column, has a stationary phase which is based on a styrene-divinyl

benzene polymer [19], and it has been verified this can lead to an enhanced chromatographic resolution of components. Indeed, using a column temperature of 130 °C and helium as carrier gas, if a relative inlet pressure of 0.8 bar is used, it is possible to obtain complete resolution of all the components, including not identified impurities and reaction walls products within 40 minutes. Using a relative inlet pressure of 1.2 bar this could be done in 15 minutes. Examples of chromatograms using these different conditions are reported in figures 4.3 and 4.4.

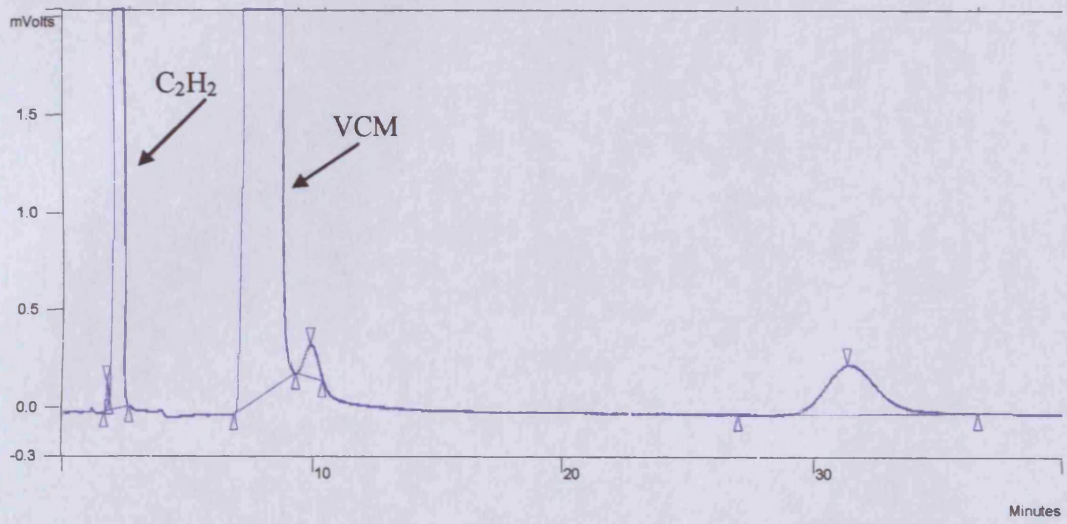

Fig. 4.3: typical chromatogram for reaction in progress using a Porapak N column and a relative inlet pressure of 0.8 bar. The resulting timescale is 40 minutes.

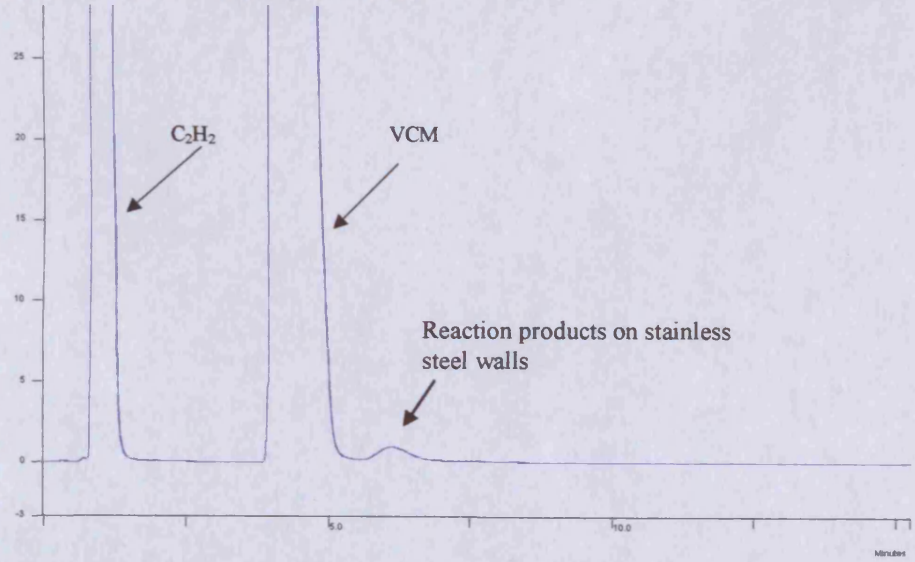

Fig. 4.4: Typical chromatogram with reaction in progress using a Porapak N column and a relative inlet pressure of 1.2 bar. The resulting timescale is 15 minutes.

Reaction walls products are detected, however they represent less than 1% of acetylene conversion. Nevertheless, attempts of characterization of these products have been done and they are specifically treated on appendix A.

An initial series of experiments has been carried out using the lower inlet pressure, later moving to the higher value.
The chromatograms reported above have been obtained using a reactant ratio C_2H_2: HCl equal to 1:1, and it is significant to note that no secondary product is present.
None of the two small impurities detectable on the chromatogram (figure 4.12) are 1,1 dichloroethane. Indeed, injecting on the system a pure sample of 1,1 dichloroethane the corresponding peak is at 42 minutes while the unknown has a retention time of 33 minutes.

This is in agreement with previous experimental observations [20], and is further investigated in this thesis (chapter 5). The expected secondary products 1,1-dichloroethane and 1,2-dichloroethane, are observed for the industrial catalyst $HgCl_2/C$. This leads to conclusion that the selectivity of gold on carbon catalyst can be considered to be virtually 100%, or in the range of 95-98% if experimental error is taken into account.

4.3 Gold on carbon catalyst

4.3.1 Carbon properties and characterization

The activated carbons suitable for catalysis purposes are not simply constituted by C as an element, but they have a more complex structure characterized by the presence of oxygen in the form of carboxylic, esthers, ethers, and lactones groups [21]. Typical carbon structures are shown below in figures 4.5 and 4.6:

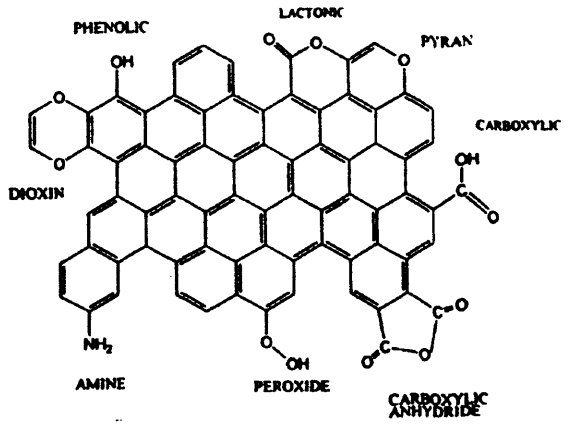

Fig. 4.5: Typical carbon structure which reveals the presence of carboxylic, phenolic, lactonic group, and eventual amine on surface.

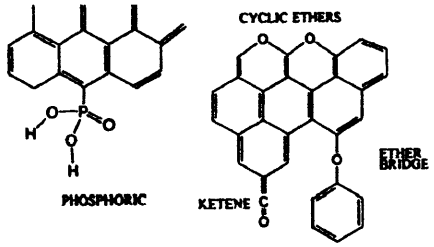

Fig. 4.6: Phosphorus, and ethers bridge on carbon surface.

Heteroatoms can also be present, and if the carbon source is wood, phosphates or amine groups can be present [21] as showed in figure 4.5 and 4.6.

The presence of acid or basic groups on a carbon surface has a direct influence on the metal clusters formation, and as consequence the final catalytic performance. For this reason, parameters such as: pore volume, surface area and acid and base properties have been experimentally determined. The carbon used, where not otherwise specified, is an Aldrich Darco 12-20 mesh (Darco12).

Considering the technique used to prepare the catalyst, it is important to determine the free carbon pore volume accurately. To determine the free carbon pore volume, different and exactly weighed amounts of carbon were taken, and using each sample, with stirring, water was added until a wet final product was obtained. A calibration plot has been constructed using this data (Fig. 4.7). The slope of this line gives the pore volume/g.

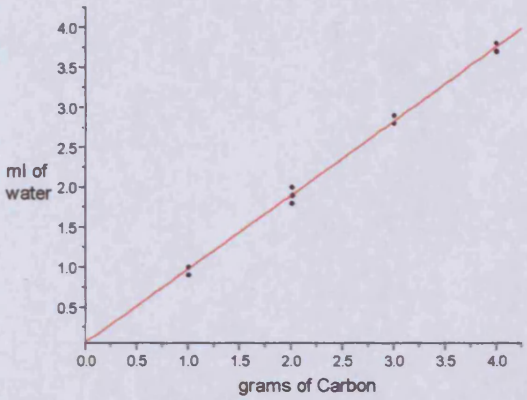

Fig. 4.7: determination of pore volume for carbon Darco 12-20 mesh, pore volume: 0.93 ± 0.02 mL g^{-1}

The second important parameter to determine is the surface area. In order to obtain this quantity, the BET method has been used (chapter 2), using a Micromeritics ASAP 2000 instrument. It has been experimentally observed, that the 5 points BET method, for a relative pressure P/P_0 between 0.1 and 0.3 units, may not be accurate for these samples. It is necessary to use the 20 point BET method exploring a greater region, between 0.01 and 0.4 P/P_0 units, and afterwards to explore the zone at low pressure between 0 and 0.1 P/P_0 units, to perform the measurement in this region. This procedure has been necessary because linear correlations were not observed, likely due to the high micropore volume detected [22]. The measurement gave for the fresh carbon a value of 521 m^2 g^{-1} and for the prepared catalyst a value of: 507 m^2 g^{-1}.

It is important to consider the acid-base properties of the carbon, because the combined effects of hydrophobic carbon and the presence of surface functional groups make them primary adsorption centres [23, 24]. This is an important aspect, because the metal cluster formation process can be summarised as:

1) adsorption of metal on surface functional groups (especially carboxylic)
2) bond formation of other metal atoms to previously adsorbed metal, and consequent cluster formation

As a result, if a great number of functional groups are present, it is expected that the nucleation process leads to small gold particles, otherwise if few functional groups are available, large gold particles may be present.

The most common method to determine the acid-base property of carbon is the Boehm method [25], which uses bases of different strength followed by a back titration with HCl. It has been demonstrated that a potentiometric method using a pH-meter can also be used [26], and this second route has been utilized here.

However, using either method, it is difficult to interpret the results [20], due to the great number of acid-base centres that are possible on carbon e.g. carboxylic, lactones, ether bridge etc.

The titration with NaOH (0.01 mol L^{-1}), followed *via* potentiometric measurement led to the following plots reported in Figs 4.8, 4.9 and 4.10:

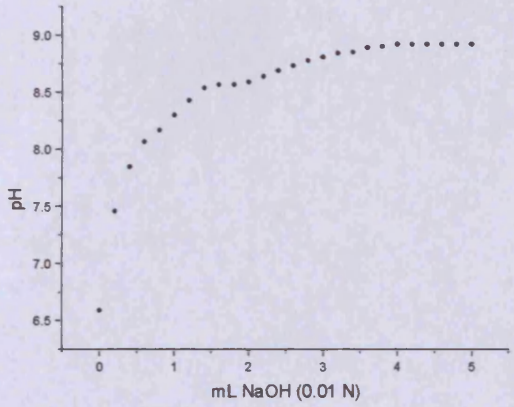

Fig. 4.8: Titration of carbon Darco 12-20, measured pH against volume of NaOH added.

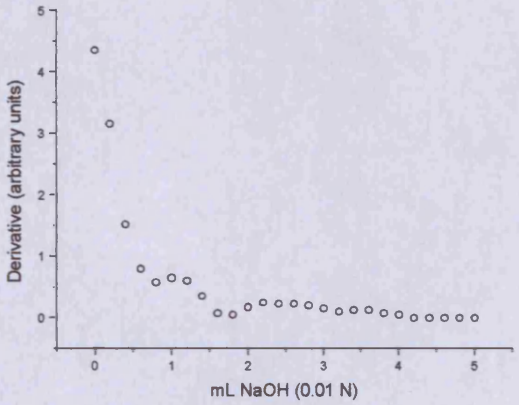

Fig. 4.9: Derivative of previous graph (Fig. 4.8) to identify the equivalent points of titration.

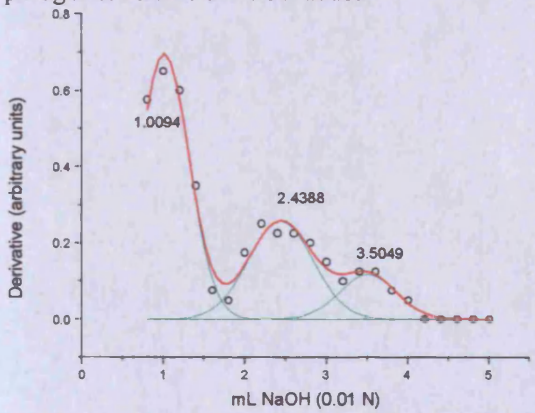

Fig. 4.10: Peak deconvolution, only a portion of the previous graph (Fig. 4.9) has been used to improve the deconvolution procedure

Results: moles of groups/g of carbon:
Lactone: $1 \cdot 10^{-5}$
Phenolic: $1.38 \cdot 10^{-5}$

It is possible to identify three distinct groups for the pH range explored. Comparing tabulated data [27] it seems possible to state that the first peak is a lactone (or possibly a carboxylic) and the second a phenolic. For the third peak the identification is difficult.

Temperature Programmed Desorption (TPD) (chapter 2) has been used to acquire information on carbon acid base properties, using a Micromeritics ASAP 2910 instrument, but the results provided little information.

Using NH_3 as gas probe for acid sites, and CO_2 as gas probe for basic sites, two different TPD have been carried out, using a gas probe flow of 10 mL min^{-1} and a temperature ramp of 10 mL min^{-1} from 40 to 400 °C. The results are reported in figures 4.11 and 4.12:

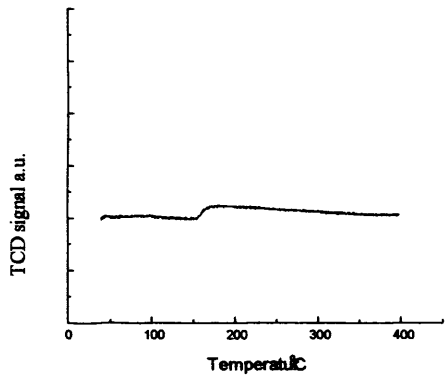

Fig. 4.11: TPD on carbon Darco-12, using CO_2 desorption. No basic sites detected.

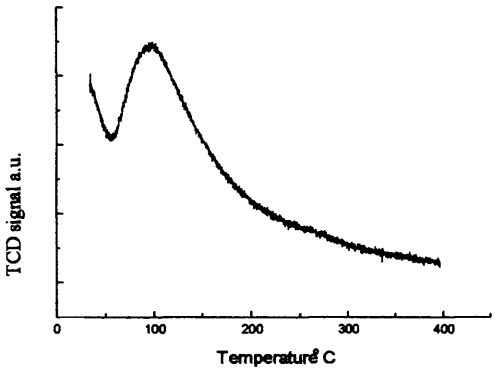

Fig 4.12: TPD on carbon Darco-12 using NH_3 desorption. The resulting peak is broad and this indicates the presence of more than one acid site.

The results obtained are in agreement with the titration, but this last one has to be considered as being more reliable since it is better able to identify the nature of acid groups.

4.3.2 Au/C catalyst characterization

A wide range of characterization techniques have been conducted on the Au/C catalysts in order to determine their properties, and to obtain some correlations with the catalytic

tests described later. Indeed, activated carbon is a matrix, which has proved to be quite difficult to characterize [21, 28] due to its amorphous pore structure and this is also true for metals supported on it.

It is well known that not only the particle size of the supported metal is important but also its oxidation state. For this reason measurements using X-ray photoelectron spectroscopy have been carried out. XPS is an analytical surface technique able to give information about which elements are present on the surface and their oxidation state. In this technique, an electron beam hits the surface and the secondary electron expelled is analysed. The quantitative information obtained is generally good, as well as the qualitative information [29]. X-ray photoelectron spectra were recorded on a VG EscaLab 220i spectrometer, using a standard Al-K_α X-ray source (300 W) and an analyser pass energy of 20 eV. Samples were mounted using double-sided adhesive tape and binding energies are referenced to the C(1s) binding energy of adventitious carbon contamination taken to be 284.7 eV (note: where not differently specified this instrument has been used to carry out all the XPS spectra reported).

In figure 4.13 an XPS spectrum for the Au/C catalyst with 1% wt of gold loading is reported.

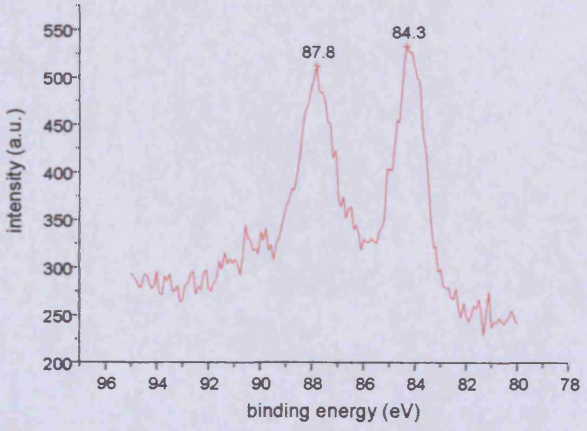

Fig. 4.13: XPS spectra of Au (1% wt) on carbon Darco catalyst. Au 4f peaks, metallic gold is distinctly present.

Tabulated XPS data for metallic gold are 84 eV for Au $4f_{7/2}$ peak and 88 eV for $Au4f_{5/2}$ peak [30]. A significant binding energy shift is observed of 0.3 and 0.2 eV for the two lines position respectively, and this can be partially related with gold particle size [31]. However, it is quite important to note that, the preparation procedure uses $HAuCl_4 \cdot xH_2O$ as precursor and after this step the catalyst is dried at 140 °C for 18 h. Nevertheless, most of the gold is present in oxidation state 0, even if the precursor contains gold in oxidation state III, and no reducing agent has been used during the preparation procedure. This reduction is caused by carbon, which is known to show these properties under thermal treatment [32, 33].
However, the $Au4f_{5/2}$ peak at 88 eV is quite broad, and a small modification in the baseline is present at 90 eV, and these phenomena are diagnostic of the presence of Au(III) [30]. Experimental evidence for the importance of this gold species in term of activity will be provided afterwards, as well as the effect of a second metal on the gold oxidation state.

Additional techniques used to characterize the catalyst include cyclic voltammetry (CV), atomic absorption spectroscopy, X-ray powder diffraction and Raman spectroscopy (chapter 2). However, due to the properties of the carbon these techniques provided little information for different reasons.

Cyclic voltammetry is an analytical method that can give information about the reversibility of a redox couple, and the identification of metal oxides. The principle of method is to subject the sample to different voltages in a given time until a maximum value is obtained, and then return to zero voltage with the same speed. For this purpose, catalysts with 0.5, 1.0, 1.5 wt % gold loading were prepared.
Several attempts were made to make measurements on the catalyst, but with little success. This analytical technique is good for graphite but much more difficult for charcoal carbon of high surface area [34].

Atomic absorption spectroscopy can be used to determine the amount of precious metal on a catalyst. However, carbon does not simply absorb gold, but also stabilizes it.

Attempts to remove gold with *aqua regia* are not fully effective. But this property can be useful, as will be demonstrated later for the purposes of catalyst regeneration (chapter 5).

X-ray powder diffraction measurements have been carried out in order to obtain information on gold particle size using Sherrer equation [35], but it was not possible to detect gold, due to its relative low loading on a support with surface area higher than 500 $m^2 g^{-1}$ leading to a quite low exposed fraction. For this reason it has been necessary to use transmission electron microscopy, in order to obtain this information. A more detailed explanation will be reported on paragraph 4.10.1, the observed average particle size of the order of 10 nm.

Finally, Raman spectroscopy has been uninformative as well, due to the high light absorption properties of the carbon, and the relatively low Au loading.

In conclusion, although the Au/C catalyst is relatively easy to prepare, having few parameters to control, it is nevertheless quite difficult to characterize due to its intrinsic properties. For these reasons XPS has been relied on to provide information on the properties of the supported metal, although a further useful technique, especially for gold supported on carbon could be X-ray fluorescence (XRF) [36].

4.4 Reproducibility and general trends for platinum metal group catalysts

4.4.1 Reproducibility of gold catalyst preparation method and conversion, and catalysts testing data

It has to be reminded that one of the aims of the project is not only to test different bimetallic catalyst, but also the reproducibility of system, and if the incipient wetness impregnation technique used is reliable or not.

In order to obtain information on the reproducibility of system, and if the incipient

wetness impregnation technique used is suitable or not, three catalysts comprising gold on carbon have been prepared using same conditions, with a gold loading of 1% wt. In this context, 'same conditions' means that the same carbon and gold precursor batch have been used, the same *aqua regia* solution and all the catalysts prepared at the same time. Under these conditions, the variance associated with the preparation is minimal, but it is useful as well, indeed if using the most restrictive variability the results should be discordant, the preparation method should be rejected.

The plots presented below (Figs. 4.14, 4.15, 4.16 and 4.17), were obtained using a ratio $HCl:C_2H_2$ about 1.7:1, with a flow of 5 mL min^{-1} of HCl and 2.9 mL min^{-1} of C_2H_2, which gives for the kind of carbon used, a gas hourly space velocity (GHSV) equal to 685 h^{-1}

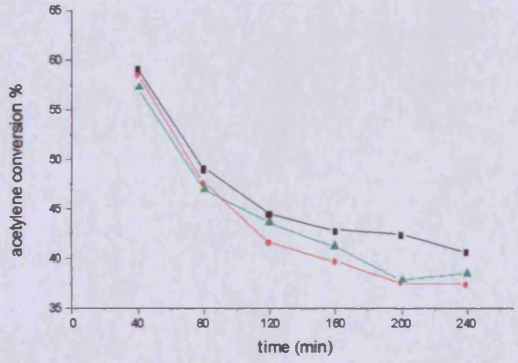

Fig. 4.14: Au/C catalyst, batch 1. Set of repeated measurements, acetylene conversion trend: (-■-) test 1, (-●-) test 2, (-▲-) test 3.

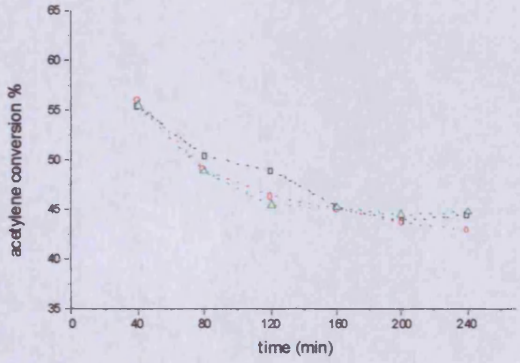

Fig. 4.15: Au/C catalyst, batch 2. Set of repeated measurements, acetylene conversion trend: (·□·) test 1, (·○·) test 2, (·△·) test 3.

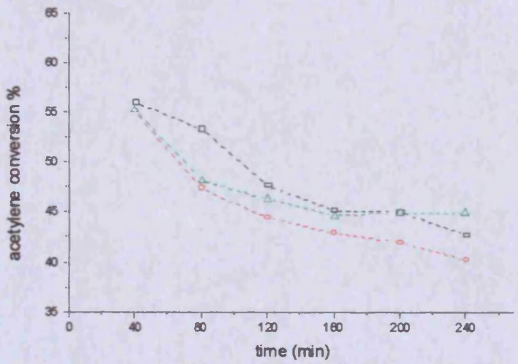

Fig. 4.16: Au/C catalyst, batch 3. Set of repeated measurements, acetylene conversion trend: (-□-) test 1, (-○-) test 2, (-△-) test 3.

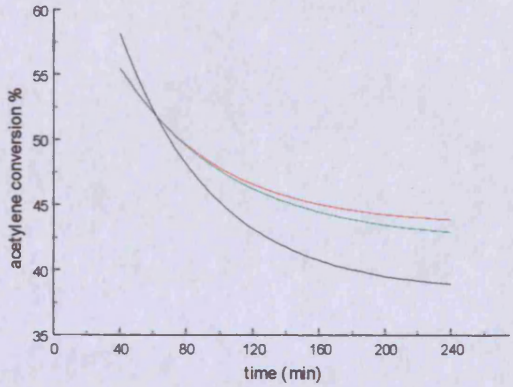

Fig. 4.17: comparison of the average conversion for the three bathes of Au/C catalysts: (—) batch 1, (—) batch 2, (—) batch 3

The behaviour of the three catalysts does not appear very different. If a time of 2 h after the starting of the reaction is taken to compare numerically the catalysts, the statistical analysis leads to the values reported in table 4.1:

Table 4.1: Comparison of conversion values for the three different catalyst batches after 2 h on line.

	Au/C catalyst 1:	Au/C Catalyst 2:	Au/C catalyst 3:
Measurement 1	44.49	48.88	47.64
Measurement 2	41.59	46.28	44.44
Measurement 3	43.64	45.37	46.30
Average	43.24	46.85	46.13
SD	1.48	1.82	1.60
RSD	3.44	3.88	3.48

While BET surface area measurements gave the values: 518, 505 and 512 m^2 g^{-1} respectively.

The reproducibility obtained can be considered to be good, and it is possible to conclude that the incipient wetness impregnation technique, even if rough, can be considered reliable for our purposes. Nevertheless, in the long term this reproducibility has not been confirmed, and this can be correlated with an inhomogeneous concentration gradient that can affect the properties of the final material (for further details see paragraph 4.10.1)

Although secondary products were not detected, a decrease in conversion is clearly evident; as described in paragraph 4.2 this could be due to a reduction of gold from Au(III) to Au(0) or monolayer formation of VCM polymer on the catalyst surface. The data collected and described later, also in comparison with palladium catalysts (paragraph 4.5.3), support the first hypothesis for catalysts comprising gold only.

4.4.2 Activity of platinum metal group metals for the hydrochlorination reaction of acetylene

The metals that have been of interest to study in terms of gold alloys or bimetallic

catalyst are: Pd, Pt, Rh, Ir, and Ru. For this reason, the behaviour of the single metals has been preliminarily investigated focusing most attention on Pd and Rh.

The Au loading of the monometallic catalyst was 1% wt. For comparative purposes, knowing the number of moles of Au, all other metals have been loaded using an equivalent number of moles, and consequently the bimetallic catalysts have the same atomic fraction of metals for a given area of support as the monometallic ones.
For all catalysts the wetness impregnation technique has been used, using *aqua regia* as solvent. The precursors salts were: $PdCl_2$, H_2PtCl_6, $RhCl_3 \cdot 3H_2O$, $IrCl_3 \cdot 3H_2O$, $RuCl_3 \cdot 3H_2O$ (Strem).

The results obtained, in terms of % acetylene conversion, with a 1:1 ratio of C_2H_2 and HCl, with a flow of 5 mL min^{-1} each and 200 mg of catalyst, are presented in Fig. 4.18

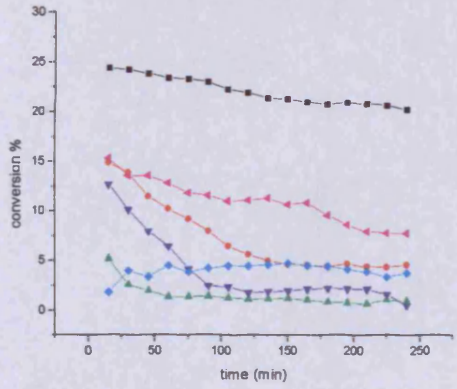

Fig. 4.18: Acetylene conversion using metal chlorinated salts of (■) Au, (▼) Pd, (◆) Pt, (▲) Rh, (●) Ir and (◀) Ru on carbon as catalyst.

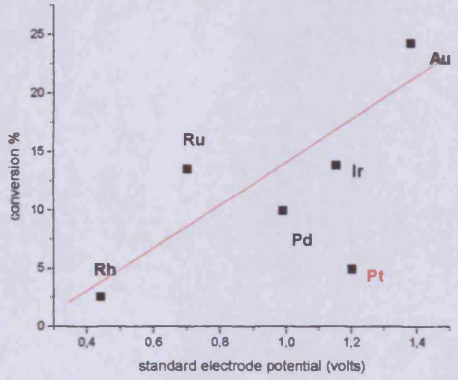

Fig. 4.19: Correlation between initial acetylene conversion (30 min), versus standard electrode potential for the different metals.

It is possible to observe clearly that gold displays a higher activity than the other metals (fig 4.18). Moreover it is possible to identify a rough correlation between initial activity versus standard electrode potential (fig. 4.19). If a trend is possible, in agreement with previous studies [3], i.e. metals with higher standard electrode potential display higher activity, platinum clearly does not fit the data set in this study.

One possible explanation could be that, although standard electrode potentials can provide a good correlation, it is also necessary to take into account the initial metal oxidation state. In this case for Pt it is IV, and if a redox mechanism occurs this would involve the couple Pt(IV)→Pt(II), while for all the other metals the initial oxidation number is II or III. In addition Pt (IV) usually does not form stable complexes with unsaturated species, and it is often considered inert towards alkynes complex formations [37] and this could be a possible indication of the reaction mechanism, although iodo-Pt(IV) complexes can catalyse in acidic aqueous or methanol solutions catalyse acetylene hydroiodination to vinyl iodine [38]. Moreover, mechanically activated salt of K_2PtCl_6 can catalyse the hydrochlorination reaction of acetylene [39], however, these investigations are not exploring the effect of supported species as in the present work.

4.5 Au/Pd on carbon catalysts for the hydrochlorination of acetylene

4.5.1 Initial promotional effect for Au/Pd on carbon catalysts

Catalysts comprising gold and palladium on carbon were prepared at a nominal loading of 1% gold, with $HAuCl_4 \cdot xH_2O$ as the precursor for gold, and $PdCl_2$ for palladium. Both these salts were dissolved in *aqua regia*, and the resulting solution impregnated into carbon.

Bimetallic catalysts containing Au/Pd with a relative palladium loading of: 0, 1, 5, 10, 20, 50, 100% atomic fraction were prepared, for a total metal loading of 1%. However, it is necessary to distinguish clearly between catalysts with low and high palladium loading.
An example of catalytic activity for low palladium loading is reported in figure 4.20, while for high palladium loading is indicated in figure 4.21, where a promoting effect is detected. The effect is lost for long term (fig. 4.20) and for increasing in Pd loading (fig. 4.21):

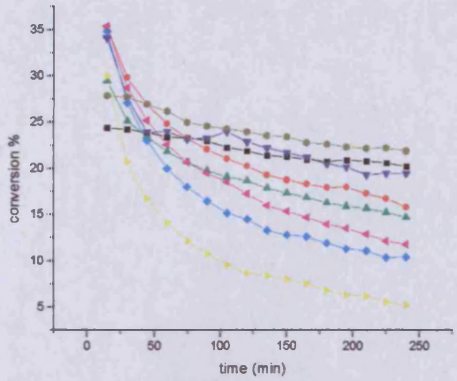

Fig 4.20: Acetylene conversion for Au and Au/Pd catalysts on carbon for low palladium loading and different batches. (■) Au batch 1, (●) Au batch 2, (▲) Au/Pd 99/1 batch1, (▼) Au/Pd 99/1 batch 2, (◀) Au/Pd 99/1 batch 3, (●) Au/Pd 99/5 batch 1, (◆) Au/Pd 95/5 batch 2 and (▶) Au/Pd 90/10

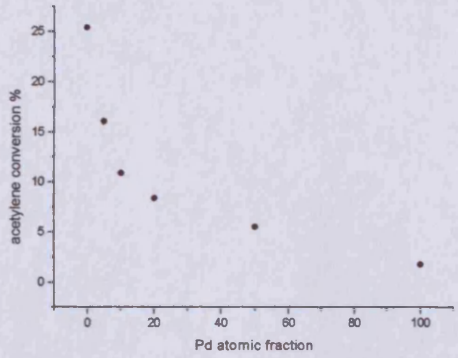

Fig 4.21: Conversion trend for Au/Pd catalysts after 2 h, for all the palladium loadings from 0 to 100%

It is possible to observe that the effect of palladium in the long term it is always negative, but a promoting effect is present at the beginning of the reaction, up to a maximum relative Pd loading of 10 % atomic fraction.

The conversion trend reported in figure 4.20 is significant because it is an indication of an alloy system or at least it is not consistent with independent Au and Pd clusters.
A priori three different possibilities are available as indicated in figure 4.22. The diagram in figure 4.20 is consistent since different catalyst batches have been tested.

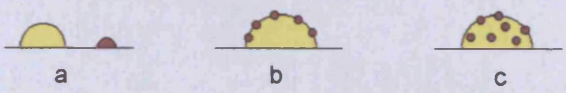

Fig. 4.22: Possible catalyst strucure: **a)** independent Au and Pd clusters, **b)** Au core structure with Pd particles on surface, **c)** alloy system with Au and Pd mixed together

The hypothesis of segregated Au and Pd dominions is not consistent, because Pd alone always displays an activity worse than gold, and because in the Au/Pd catalyst Au is diluted. If only independent clusters were present we should observe at the beginning of reaction, for all Au/Pd catalysts, activity lower than gold, but this does not happen.

A more likely hypothesis could be the presence of metal clusters with gold and palladium intimately mixed together with the palladium dispersed primarily on the surface of gold cluster, and this assumption has been confirmed using Scanning Transmission Electron Microscopy STEM (paragraph 4.5.2)

4.5.2 Au/Pd on carbon catalyst structure

In order to obtain more detailed structural information on the different behaviour of gold and palladium, TPR measurements have been carried out.

With the use of Temperature Programmed Reduction (TPR), it is possible to identify if a metal can be reduced at a given temperature. The experiment has been performed using the reducing agent 10% H_2 in Argon and a ramp rate in temperature from 50 to 300 °C (ramp rate 10°C min^{-1}, flow 50 mL min^{-1}, final temperature 300 °C held for 1 hour). All the gold-palladium catalysts prepared were subjected to TPR. The results obtained are for fresh catalysts (figure 4.23):

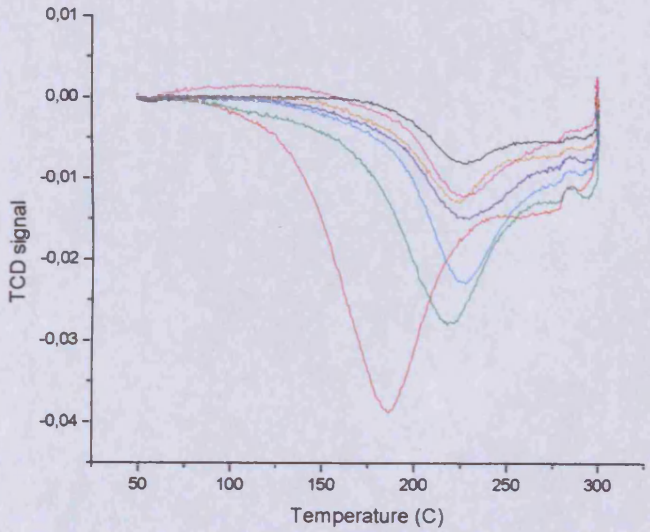

Fig. 4.23: TPR profile for Au, Pd and Au/Pd on carbon catalysts from 50 to 300°C: (—) Pd, (—) Au/Pd 50/50, (—) Au/Pd 80/20, (—) Au/Pd 90/10, (—) Au/Pd 95/5, (—)Au/Pd 99/1 and (—)Au. Only one peak was detected, supporting the proposed of a final homogenous structure.

Some important considerations can be developed from this plot.

The first is that the reduction temperature for palladium was 186 °C, which is almost the reaction temperature for hydrochlorination 180 °C, and this could be a partial explanation for the low activity of the palladium catalyst.

A second aspect is that for the Au-Pd catalyst two peaks were never observed one for gold and one for palladium, but always only one well defined peak. This is important, because it means that the two metals are mixed together well, and even if these measurements are not conclusive proof, it can be said that no metal segregation is present. Moreover, this is in agreement with the explanation of the relative activities discussed above.

Finally we can observe a temperature shift, even thought it is small, from the temperature for reduction of palladium, to the temperature reduction for of gold, as reported in table 4.2

Table 4.2 Reduction temperature for Au/Pd bimetallic catalysts

Catalyst	Reduction temperature (°C)
Au	228
Au/Pd 99/1	226
Au/Pd 95/5	226
Au/Pd 90/10	226
Au/Pd 80/20	226
Au/Pd 50/50	219
Pd	186

All these data are consistent with a homogenous final product, and these indirect experimental observations have been directly confirmed using STEM.

Using STEM it is possible not only to have information on the sizes of the metal clusters, but also about the chemical distributions of the species contributing to form the cluster which can be used to form a map. They are reported below, metal clusters and STEM maps for gold, palladium and chloride (figures 4.24, 4.25, 4.26, 4.27) using a dedicated STEM-XEDS scanning transmission electron microscope equipped with a Vacuum Generators (VG) HB 603 and a field-emission gun (FEG) operating at 300 keV. In order to correct the electronic aberration a Nion spherical aberration corrector was used, to

form a final probe size that is less than one angstrom. For the data analysis, and chemical map composition, Oxford Inca 300 program was used.

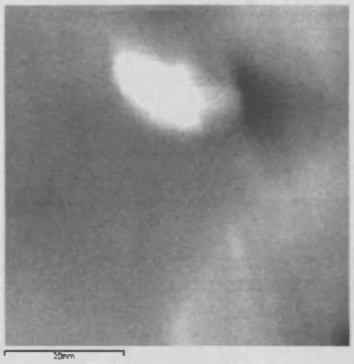

Fig. 4.24: TEM of Au/Pd 95/5 catalyst on carbon Darco 12-20

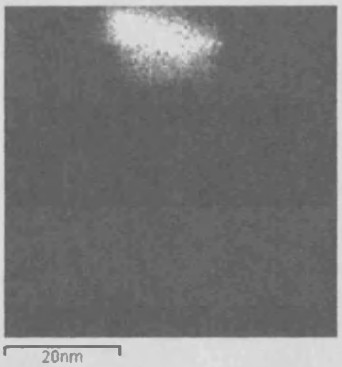

Fig. 4.25: STEM of Au/Pd 95/5 catalyst, Au map

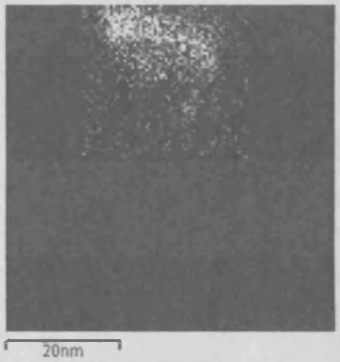

Fig. 4.26: STEM of Au/Pd 95/5 catalyst, Pd map

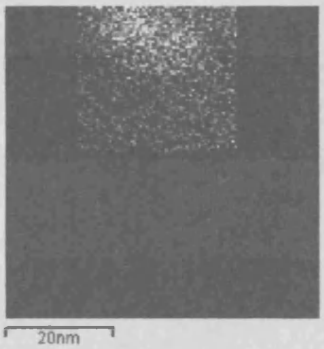

Fig. 4.27: STEM of Au/Pd 95/5 catalyst Cl map

The results show gold particle size is in the range of 10-20 nm, with very small Pd particles detected, but only on the Au surface. It is important to note that palladium can be detected only where gold is present. This is quite significant, because only the wetness impregnation technique has been used to prepare the catalyst.

4.5.3 Deactivation processes for Au/Pd on carbon catalysts

As mentioned above the selectivity of the Au/C catalyst for vinyl chloride monomer can be taken to be virtually 100%, since no secondary products were detected, whereas for the Au/Pd catalysts this is not the case obtaining as secondary products vinyl chloride

oligomers. For the Au/Pd 95/5 catalyst a significant loss of activity was observed after 45 minutes, while for the palladium only catalyst the selectivity was in the range of 30-40% from the start of the reaction.

The trend is reported in the diagram below (Fig. 4.28):

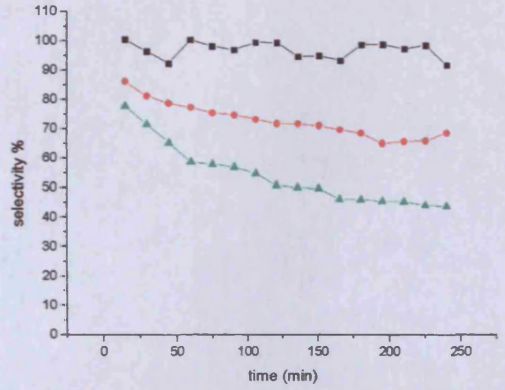

Fig. 4.28 Selectivity trend for the hydrochlorination reaction for the catalysts: (■)Au, (●)Au/Pd 99/1 and (▲) Au/Pd 95/5.

In order to identify an explanation for this behaviour, BET surface area measurements have been carried out before and after reaction. For the most important catalysts, the values obtained are reported in the table below (table 4.3).

Table 4.3 surface area before and after reaction for Au/Pd catalysts

Catalyst	Surface area before reaction ($m^2 g^{-1}$)	Surface area after reaction ($m^2 g^{-1}$)	Area loss (%)
Au	512	464	9.5
Au/Pd 95/5	429	271	37
Pd	554	75	86

The area loss for the palladium catalyst is very large, but also for the Au/Pd 95/5 catalyst the addition of a 5% relative molar fraction of palladium led to an area loss of almost 40%, while for the catalyst containing only gold the area loss can be considered to be quite low by comparison.

This loss in surface area can be attributed to oligomer formation. The possibility of the formation of oligomers during the hydrochlorination reaction has been reported in

paragraph 4.3, and this can be confirmed for the Au/Pd catalyst, since green products were obtained which are likely to be vinyl chloride oligomers. From the data described, palladium in small amounts is able to act like a promoter, but a competitive effect is the formation of carbonaceous product, reducing the surface area by occluding the catalyst pores with subsequent catalyst deactivation.

Attempts to characterize these undesired products more rigorously have been made such as dissolving them in a suitable solvent and carrying out NMR spectroscopy. However, these characterizations revealed little information, a part from the distinct presence of conjugated double bonds.

However, carbonaceous product formation is not the only reason for the observed trend. In order to obtain more information concerning the oxidation state of the two metals and possible changes during the reaction, XPS has been carried out.

The XPS spectra, Au 4f, for Au/Pd 95/5 catalyst before and after hydrochlorination reaction, are shown in Figs: 4.29, 4.30

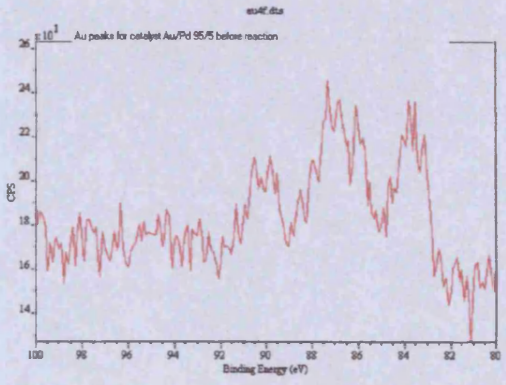

Fig. 4.29 Au 4f peaks for Au/Pd 95/5 on carbon catalyst before reaction

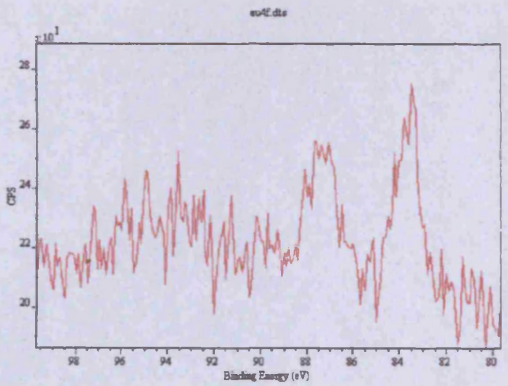

Fig 4.30 Au 4f peaks for Au/Pd 95/5 on carbon catalyst after reaction

It is interesting to observe that for the Au/Pd system a triplet is clearly detected. More precisely this is only an apparent triplet, because it is due to two doublets: one is Au(0), range 84-88 eV, while the other is Au(III), range 86-90 eV. This is a clear evidence of gold present in two different oxidation states. The presence of Au(III) has already been

indicated for the catalyst containing gold only (paragraph 4.3.4 figure 4.13), but here it is enhanced (Fig. 4.29). Nevertheless, Au(III) is not present after reaction (fig 4.30) and this is another reason for catalyst deactivation. This provides a useful insight and a more detailed investigation afterwards reported (chapter 5) concerning the effect of Au(III) on catalyst activity.

From the spectra shown in figures 4.29 and 4.30, arises the question as to whether the loss of the triplet, i.e. gold reduction, is due to the reaction, or to the temperature. For this reason, XPS analysis was carried out for Au and Au/Pd catalysts that had been heated at 180 °C in the absence of reaction mixture for 4.5 h. The spectrum of Au catalyst stays unmodified (Fig. 4.31), while for the Au/Pd catalyst the two doublets system is lost (Fig. 4.32), but is highly distorted.

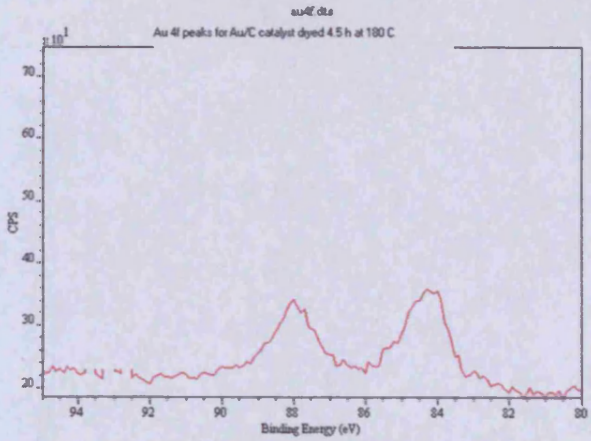

Fig. 4.31: Au 4f peaks for Au on carbon catalyst dried 4.5 h at 180 ° C. (note: the different scale of this spectra if compared with fig 4.32 is due to spikes during the acquisition of this spectra)

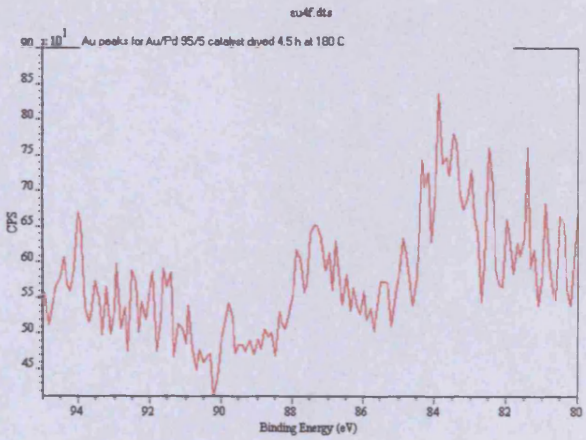

Fig. 4.32: Au 4f peaks for Au/Pd 95/5 on carbon catalyst dried 4.5 h at 180 °C.

There is also a possibility that loss of palladium occurs. To explore this, atomic absorption measurements have been carried out. Although, as indicated in paragraph 4.2.4, these measurements are not accurate if made on carbon samples, they indicate a loss of palladium, of at least 30-50%. Thermal gravimetric analysis, has been carried out, but again, due to the properties of carbon, this provided little information.

In conclusion, the deactivation process can be attributed to three factors:

a) Formation of oligomers on the surface of the Au/Pd catalyst, since it is likely that desorption of the product (vinyl chloride monomer) from the catalyst surface is difficult when Pd is present.
b) Loss of palladium. It is important to note distortion of the XPS peaks and loss of the two doublets after reaction and following thermal treatment. In addition, the STEM results (paragraph 4.5.2) show the metals are fully surrounded by a chloride environment, and $PdCl_2$ desorption could be involved and not Pd only. A sublimation process is not a surprise, as the industrial hydrochlorination catalyst ($HgCl_2$), loses activity by sublimation of $HgCl_2$ during the reaction [9, 10], and $PdCl_2$ can be affected by decomposition phenomena [40].
c) Reduction of the gold, which can affect the catalyst whether palladium is present or not.

Nevertheless an initial promotional effect has been observed. It is likely that the reaction initially takes place on the Au/Pd interphase, but as the reaction products are not able to desorb efficiently from Pd, the catalyst activity is quickly lost.

4.6 Hydrochlorination of acetylene over Au/Rh on carbon catalysts

4.6.1 Activity of Au/Rh catalysts

A similar treatment described previously for Au/Pd catalysts, has been followed for Au/Rh catalysts. Catalysts containing gold and rhodium on carbon were prepared at a nominal loading of 1% gold, with $HAuCl_4 \cdot xH_2O$ as precursor for gold, and $RhCl_3 \cdot 3H_2O$ for rhodium. The salts were dissolved in *aqua regia*, and the resulting solution used to impregnate the carbon. The solid was dried at 140° C for 18 h.
It worth noting that for rhodium, *aqua regia* it is not an optimal solvent to dissolve the precursor, hence it is necessary to boil the sample to obtain a homogeneous salt precursor solution. This is considered to be a factor that could affect the catalyst drying procedure

with the eventual formation of $RhCl_3$ crystallites, and this influence the catalytic performance.

Evaluation of the catalytic activity, in terms of acetylene conversion for Au/Rh on carbon catalysts with rhodium loading equal to 0, 5, 10, 20, 50, 80, 100 relative atomic fraction is reported below in figure 4.33

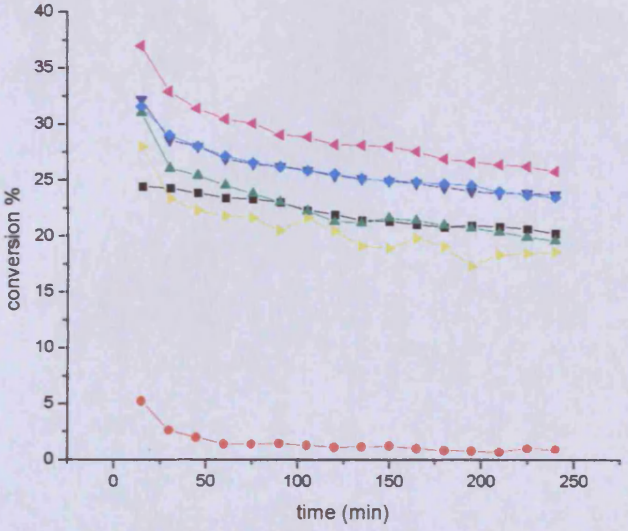

Fig. 4.33: % Acetylene conversion for Au/Rh catalysts on carbon (Darco 12-20) : (●) Rh, (▶) Au/Rh 20/80, (◀) Au/Rh 50/50, (♦) Au/Rh 80/20, (▼) Au/Rh 90/10, (▲) Au/Rh 95/5 and (■) Au

It is immediately evident that the general trend is quite different from Au/Pd. The first observation is that a higher conversion for Au/Rh catalysts is detected for Rh contents up to 50%, and this enhanced activity is displayed not only at the beginning, but for the whole reaction time. This is also reflected in the selectivity, which is always above 95-98% as for gold.

This is quite significant, since when Rh is used alone, it is not a good catalyst, and is actually the worst of the metals when used alone (Fig 4.18). Consequently the plot reported in figure 4.33 is evidence of a synergistic effect between Au and Rh.

4.6.2 Characterizations of Au/Rh catalysts

In order to identify differences and similarities with the Au and Au/Pd catalysts, XPS and TPR measurements have been carried out.

Taking into account the results in figure 4.33, XPS has been carried out on the catalyst with relative ratio Au/Rh 50/50 as this catalyst displayed the best performance.

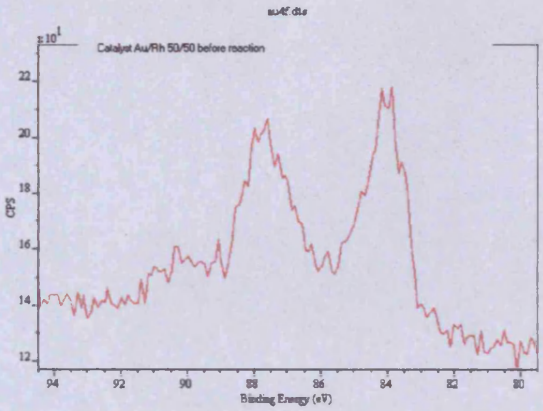

Fig. 4.34: Au 4f peaks for Au/Rh 50/50 on carbon before reaction

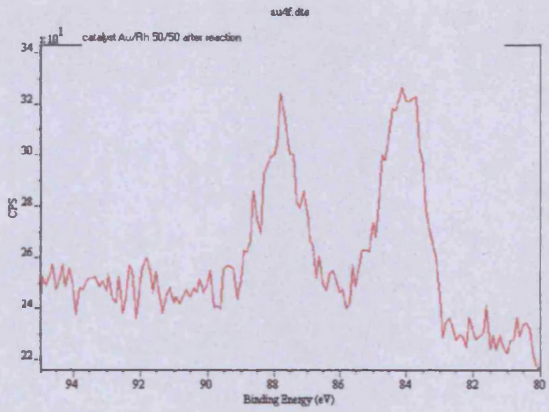

Fig. 4.35: Au 4f peaks for Au/Rh 50/50 on carbon after reaction

These data show some similarities with Au/Pd, indeed in the fresh catalyst two peaks have been identified, but the peak at 88 eV is broad, and at 90 eV another peak is present, attributed to Au(III). This signal is an apparent triplet due to overlap of Au(0) and Au(III) components. Again, after reaction the Au(III) has been reduced.

It is possible to identify a correlation between the presence of the Au(III) component and enhanced activity, which the second metal seems to influence, although it can be stated that gold catalysts can contain significant amounts of Au(III) when no other metal is added (chapter 5).

The second important method of analysis has been temperature programmed reduction (TPR) which was carried out using the same conditions as for the Au/Pd catalysts, that is 10 % H_2 in Argon as reducing reactant gas with a ramp temperature of 10 °C min^{-1} from 50 to 300 °C with a gas flow of 50 mL min^{-1}.

The results obtained for Au/Rh are shown in fig.4.36

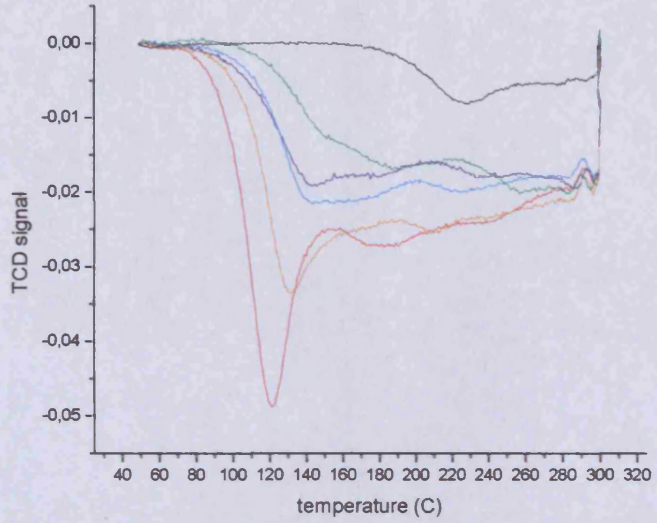

Fig. 4.36: TPR of Au/Rh catalysts on carbon Darco 12-20 (—) Rh, (—) Au/Rh 50/50, (—) Au/Rh 80/20, (—) Au/Rh 90/10, (—) Au/Rh 95/5 and (—) Au

For this analysis, significant differences are present when compared with Au/Pd. The first is that all rhodium containing catalysts display three reduction peaks, corresponding to three different reducible species, and consequently possible reaction sites. It is possible to detect the lower temperature peak at 120 °C and this moves continuously to higher temperature form the catalyst containing only rhodium to the catalyst containing only gold. But, in this case a relative fraction of only 5% Rh is able to change the TPR profile considerably, while with the corresponding Au/Pd 95/5 this does not occur (fig 4.36 and 4.23).

Observing the relative peaks positions it is possible to conclude that the peaks for the catalyst containing Rh only at the lower temperature (120 °C) can be attributed to the Au/Rh clusters, since its nature is preserved, i.e. it decreases in intensity continuously and moves to a higher temperature. The others peaks are probably due to crystallites.

This means that the catalyst is actually quite different from Au/Pd. As a consequence of the trend displayed in figure 4.34 similar considerations to those developed for Au/Pd are

possible, that is, Rh alone is a worse catalyst than gold, and when gold is diluted metals interact to form alloys system or gold with higher dispersion. Moreover, other structures are possible. The identification of the nature of these sites is difficult, but it could be an indication of the presence of $RhCl_3$ crystallites or rhodium in different oxidation states.

4.6.3 Reproducibility tests for Au/Rh catalysts

For the Au/Rh catalysts, repeated measurements have been carried out. Experiments using the first batch of catalysts prepared were repeated after about 5 months in order to evaluate possible aging effects on the activity. Moreover, another batch of catalysts were prepared and tested using carbon Darco-12 as support (and carbon from a different batch).

The trends observed can be summarized in the following figures (fig 4.37, 4.28)

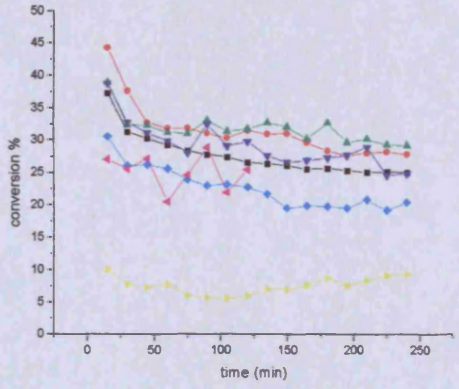

Fig 4.37: acetylene conversion over Au/Rh catalysts. First batch, measurements repeated after 5 months for evaluation of aging effects. (►) Rh, (◄) Au/Rh 20/80, (♦) Au/Rh 50/50, (▼) Au/Rh 80/20, (▲) Au/Rh 90/10, (●) Au/Rh 95/5 and (■) Au.

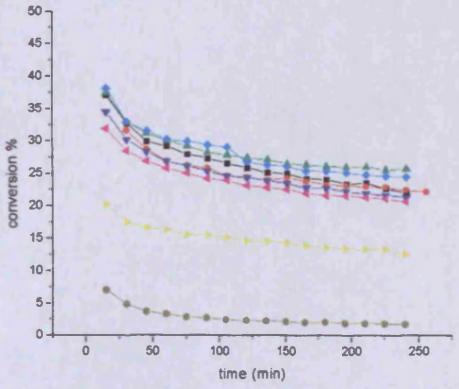

Fig 4.38: Acetylene conversion Au/Rh catalysts. Second batch, on second carbon batch Darco 12-20 mesh. (●) Rh, (►) Au/Rh 20/80, (♦) Au/Rh 50/50 test 1, (◄) Au/Rh 50/50 test 2, (▼) Au/Rh 80/20, (▲) Au/Rh 90/10, (●) Au/Rh 95/5 and (■) Au

A comparison is not simple, but some considerations can be put forward. The first is that although variations in catalytic activity are observed, these are in the range of 10%, when compared with the first series reported in figure 4.3.4. The second, and more significant, is that the catalysts more affected by aging and preparation procedure are the catalysts

with the higher Rh loadings Au/Rh 50/50 and 20/80, possibly due to segregation effects or contamination.

In order to better compare the three sets of data a comparison of the of the catalysts versus Rh loading after a reaction time of 2 h is reported below (figure 4.39)

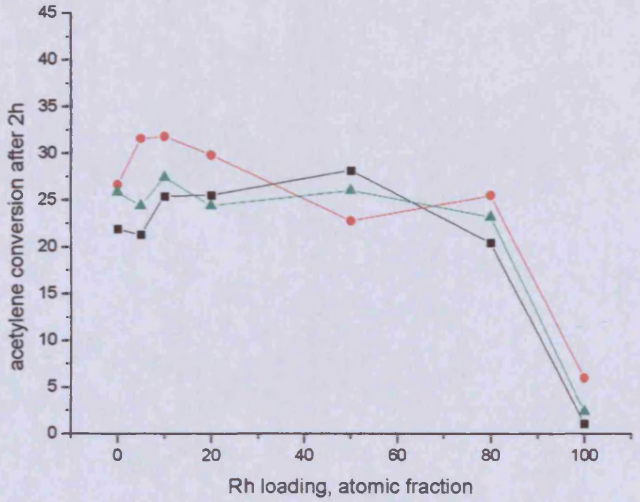

Fig. 4.39: comparison between the different Au/Rh catalysts, on different support and using time, after 2 h of reaction (■) batch 1 test 1, (●) batch 1 test 2 and (▲) batch 2 test 1

On inspecting the data, the catalyst that gives to a promotional effect in the reaction is Au/Rh 90/10. A significant decrease in conversion is observed only with a relative loading higher than 80%, seemingly as if Rh was in some way able to replace gold completely, even though Rh alone as a catalyst is not efficient for the hydrochlorination reaction of acetylene. However, to better rationalise this trend it is necessary to take into account the miscibility of Au with Rh; in fact Au/Rh solubility studies [41] indicate that at the peritectic temperature of 1068°C saturation concentrations of the terminal solid solutions were found to be 1.5 atomic per cent of rhodium and 0.3 atomic per cent of gold. As a consequence it is possible to imagine the catalyst as made of Au clusters, Rh clusters and Au/Rh aggregates but with Au and Rh not mixed. In this case the role of Rh is to increase the dispersion of Au, and this can explain why the activity trends show a change in conversion values only but not on the deactivation slope which is almost the same than the catalysts made by Au only.

4.7 Au/Ir on carbon for the hydrochlorination of acetylene

The procedure followed for palladium and rhodium catalysts has been repeated with Iridium. Au/Ir catalysts were prepared using the wetness impregnation method in *aqua regia*, and using the iridium precursor $IrCl_3 \cdot 3H_2O$.

The plots show below (fig 4.40 and fig 4.41) indicate the behaviour of catalysts containing gold and iridium only and two bimetallic catalysts containing 1 and 5% atomic fraction of iridium, with a total metal loading of 1 wt%.

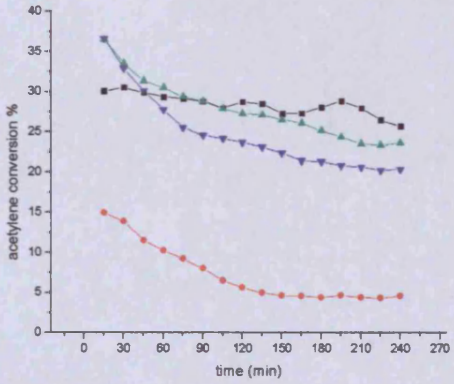

Fig 4.40: conversion trend for (■) Au, (●) Ir, (▲) Au/Ir 99/1 and (▼) Au/Ir 95/5 on carbon for hydrochlorination reaction of acetylene

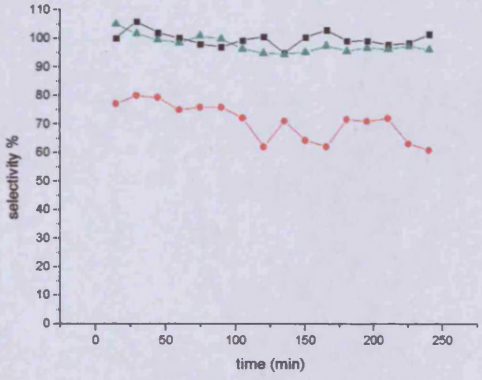

Fig. 4.41: selectivity trend for (■) Au, (●) Au/Ir 99/1 and (▲) Au/Ir 95/5 on carbon for hydrochlorination reaction of acetylene

The trend observed is quite similar to what observed for Au/Pd, with an initial promoting effect, and a fast deactivation. However, in contrast to Pd, Ir is able to preserve a selectivity similar to gold, at least for the catalyst Au/Ir 95/5. Selectivity is lower for the Au/Ir 99/1 catalyst. Again, mass balance is less than 100%, although better than for Au/Pd. It is likely Ir is able to lead to a promoting effect, but the desorption step is difficult and oligomers are formed.

TPR and XPS analysis have also been carried out, focusing on the sample with a low Ir loading. The results can be considered as an intermediate situation between Au/Pd and Au/Rh.

TPR plots versus time and temperature are reported in figures 4.42 and 4.43 where two or three peaks can be identified.

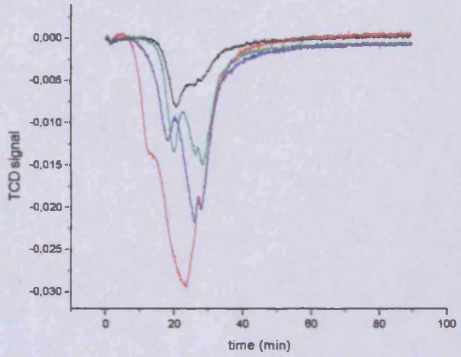

Fig. 4.42: TPR profile for (—) Ir, (—) Au/Ir 95/5, (—) Au/Ir 99/1 and (—) Au on carbon from 50 to 300°C, time measurement scale.

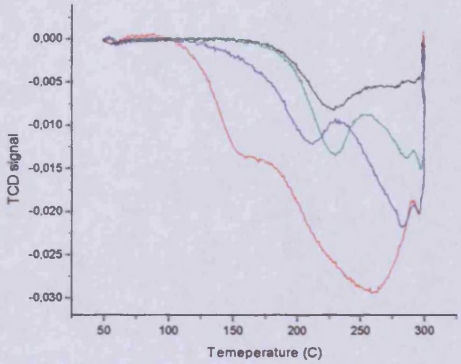

Fig. 4.43: TPR profile for (—) Ir, (—) Au/Ir 95/5, (—) Au/Ir 99/1 and (—) Au on carbon from 50 to 300°C, temperature measurement scale.

Consideration of the structure of the catalyst can be undertaken, taking into account the conversion trends, i.e. interaction between Au and Ir metal cluster, as in the case of Au/Rh. The TPR profiles indicate that more active sites are present, possibly due to $IrCl_3$ crystallites. However, it is worth noting that a small amount of Ir can significantly modify the reduction profile even with a relative 1% atomic fraction. This does not happen for Au/Pd, but is similar to Au/Rh. Developing the arguments proposed for Au/Rh it seems possible to conclude that the peak for Ir at lower temperature (150 °C) is the site modified by the alloy, while the other one could be due to a crystallite.

An XPS spectrum for a Au/Ir catalyst 95/5 is reported in figure 4.44

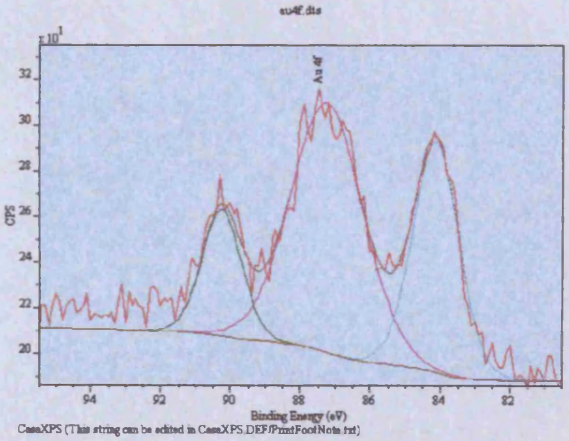

Fig 4.44: XPS Au 4f peaks of Au/Ir 95/5 on carbon catalyst

For this catalyst a triplet, i.e. overlap of the two Au doublets is very well defined, better than for Au/Rh and similar to Au/Pd.

Investigations of catalysts containing higher Ir loadings have been performed and are reported below (Fig. 4.45)

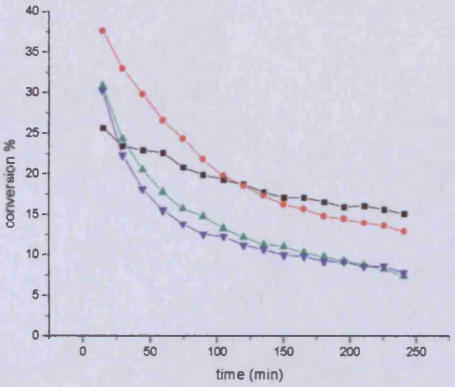

Fig. 4.45: Au/Ir catalysts on carbon with high Ir loading for the hydrochlorination reaction of acetylene on carbon: (▼) Au/Ir 20/80, (▲) Au/Ir 50/50, (●) Au/Ir 80/20 and (■) Au

In contrast to Pd, Ir is able to give a promotional effect for high Ir loadings although the deactivation rate is higher than for low Ir loadings.

For a better comparison of the results shown above, obtained from different batches, a normalized conversion relative to gold has been used, with a conversion value equal to 1 for gold, and relative values for the other Au/Ir catalysts. The plot for the initial activity, after 15 minutes of reaction, is reported in figure 4.46:

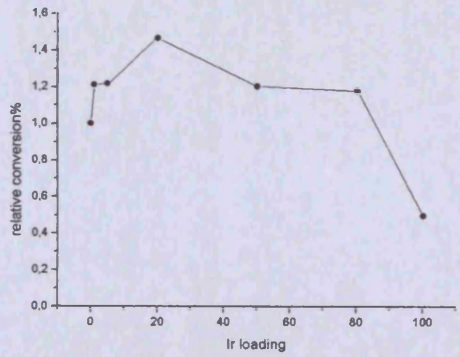

Fig. 4.46: Normalized initial conversion for Au/Ir catalysts for the hydrochlorination reaction of acetylene

In conclusion, similarities with Au/Pd in terms of initial enhanced activity are present, but also with the Au/Rh system, where a decrease in catalyst performance when the second metal added is in high concentration i.e. over 80% of relative atomic fraction. For Au/Pd this phenomenon is observed for the catalyst with a Pd loading of 10% atomic fraction.

However, also in this case it is useful to take into account the Au and Ir miscibility; it is usually accepted that Ir does not dissolve in liquid gold [42] and the primary solid solubility are approximately 0.1 atomic per cent of Ir in Au, and less than 2 atomic per cent of Au in Ir [43]. However, it has been reported the preparation of alloys with up to 2.76 atomic fraction of Ir in Au [44]. In this last case the final catalyst could be made by Au clusters, Ir clusters and Au/Ir clusters with the two metals partially together, which is a different condition if compared with Au/Rh catalysts; in fact for Au/Ir clusters no increased dispersion of gold could be obtained, and this could explain the high activity but also the high deactivation rate observed in contrast with Au/Rh catalysts.

4.8 Au/Pt on carbon for the hydrochlorination of acetylene

The same procedures described have been followed for Au/Pt catalysts. A platinum atomic fraction in the range 0, 5, 10, 20, 50, 80, 100 has been explored. Two activity data sets are reported, the first (Fig. 4.47) for fresh catalysts, while the others after beings stored four months in order to evaluate possible aging effects (Fig. 4.48). It is important to note that for platinum H_2PtCl_6 has been used as precursor and in this salt the platinum oxidation state is IV; a fact that can influence the final catalytic activity.

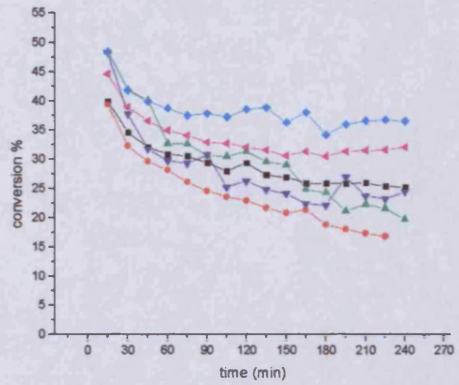

Fig. 4.47: Acetylene conversion for different Au/Pt catalysts on carbon Darco 12-20. Tests for fresh catalysts: (●) Au/Pt 50/50, (▲) Au/Pt 80/20, (▼) Au/Pt 90/10, (♦)Au/Pt 95/5, and (■) Au test 1, (◄) Au test 2.

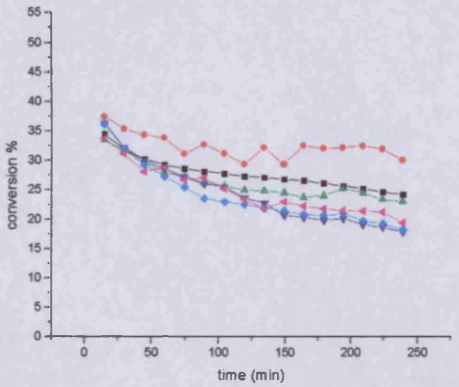

Fig. 4.48: Acetylene conversion for different Au/Pt catalysts on carbon Darco 12-20. Tests for catalysts 4 months old (♦) Au/Pt 50/50, (▼) Au/Pt 80/20 test 1, (◄) Au/Pt 80/20 test 2, (▲) Au/Pt 90/10, (●) Au/Pt 95/5, and (■) Au.

The two data sets appear quite difficult to compare, especially in terms of an order of activity versus Pt loading. The catalyst with composition Au/Pt 95/5 is the only one to have a distinct behaviour compared with the others, always having greater activity than the catalyst containing by gold only and the other Au/Pt catalysts.

It the two sets of data are compared in terms of initial activity (15 min) for the fresh and aged catalyst the following plot is obtained (Fig. 4.49):

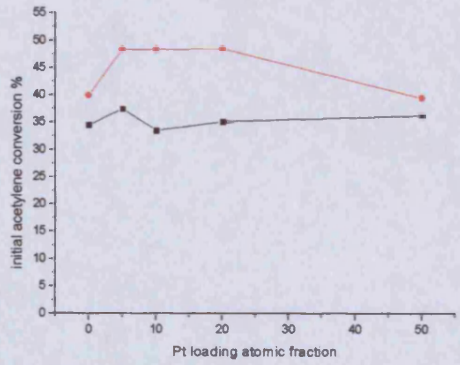

Fig. 4.49 (left): initial activity (15 min) for Au/Pt catalysts with different Pt loading and aging, comparison between (●) fresh catalysts, and (■) catalysts 4 months old

Although the activity trend is the same, an aging effect is present with lower activity for the aged catalysts.

In order to identify similarities or differences between the Au/Pt 95/5 catalysts and the catalysts with lower activity, XPS of Au/Pt 95/5 and Au/Pt 50/50 has been carried out. The spectra are reported in figs 4.51 and 4.51

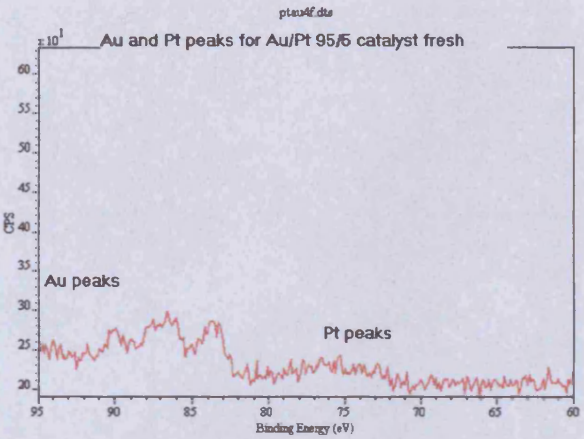

Fig. 4.50 Au 4f peaks for the catalyst Au/Pt 95/5 before reaction

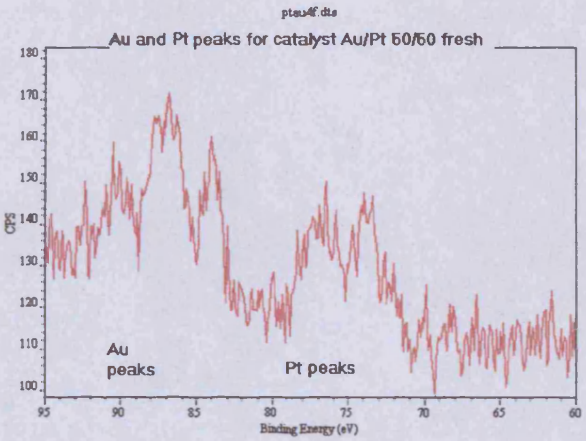

Fig. 4.51 Au 4f peaks for the catalyst Au/Pt 50/50 before reaction

In both cases the Au 4f peaks indicate the presence of Au(0) and Au(III), phenomena which have been seen when a second metal is added. This could explain the enhanced activity for Au/Pt 95/5 while for Au/Pt 50/50 the large amount of Pt may have a dominant deleterious effect on the final activity.

It worth noting, that the expected binding energies for Pt are 71.2 eV for the Pt $4f_{7/2}$ component and 74.5 eV for the Pt $4f_{5/2}$ component in the case of Pt (0). The XPS spectrum displayed in figure 4.51, shows a shift to higher binding energy, with the component Pt $4f_{7/2}$ component in the range 73-74 eV, which is consistent with $PtCl_2$ species [30]. Consequently the oxidation state of Pt changes from the precursor value of IV to II. It is likely to think that this is again due to the ability of carbon to reduce the metal deposited on it during the preparation process.

4.9 Au/Ru on carbon for the hydrochlorination of acetylene

A similar approach to those described earlier has been followed for gold/ruthenium catalysts. For this metal $RuCl_3 \cdot H_2O$ has been used as a precursor and catalysts here prepared using the wetness impregnation technique with *aqua regia* as solvent like for the other catalysts.

The catalysts prepared using this metal displayed the poorest reproducibility of all the bimetallic catalysts tested. It was very difficult to compare them. The behaviour of different catalyst batches is shown in figures 4.52, 4.53 and 4.54

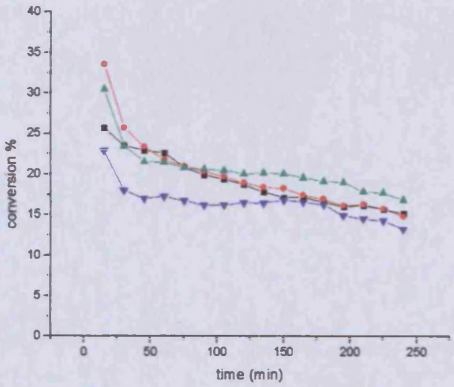

Fig. 4.52: Au/Ru on carbon, high Ru loading, for the hydrochlorination reaction of acetylene. (▼) Au/Ru 20/80, (▲) Au/Ru 50/50, (●) Au/Ru 80/20, and (■) Au

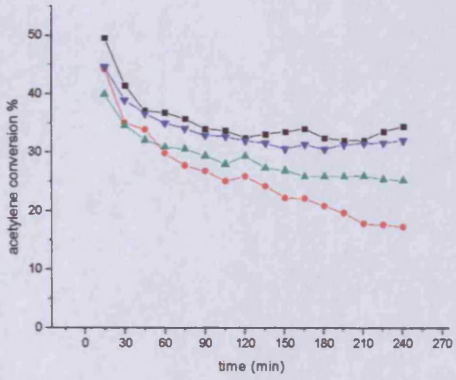

Fig. 4.53: Repeat tests on different batches on Au and Au/Ru catalysts for the hydrochlorination reaction of acetylene. (■) Au/Ru 80/20, (●) Au/Ru 90/10, (▲) Au test 1 and (▼) Au test 2.

The most tested catalyst was the Au/Ru 80/20 and as is possible to see one batch display an activity similar to gold (Fig 4.52) in another batch higher activity (Fig 4.53) and in another batch lower activity (Fig. 4.54) making it impossible to undertake systematic studies, possible explanation for this lack of reproducibility could lie in the complex chemistry of ruthenium.

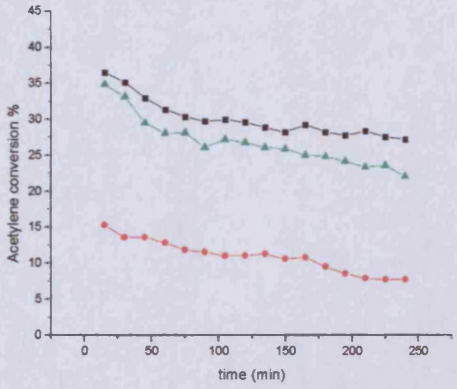

Fig. 4.54: Further tests on (■) Au, (▲) Au/Ru 80/20 and (●) Ru catalysts for the hydrochlorination reaction of acetylene.

Firstly, the precursor $RuCl_3$ is quite difficult to obtain independently whether it is hydrated or not, and this can lead to a starting material which is actually a mixture of different oxidation states [40], moreover the chloride can exist in two different crystal forms, named respectively α and β, which can lead to a different reactivity [45]. Although the method used to prepare the catalyst is relatively straight forward, complicated recrystallisation can occur during drying and this could explain the difficulty in obtaining a final product with the desired characteristics, and for this reason ruthenium has not been deeply investigated.

4.10 Effect of support on the hydrochlorination of acetylene and further sources of variability

4.10.1 Effect of the support

Some different supports or catalyst treatments have been tested in order to evaluate the effect on final performances.

Tests have been carried out using a Au/TiO_2 catalyst (as used for the low temperature CO

oxidation studies) and a calcined gold on carbon catalyst. The results are reported below (Fig. 4.55)

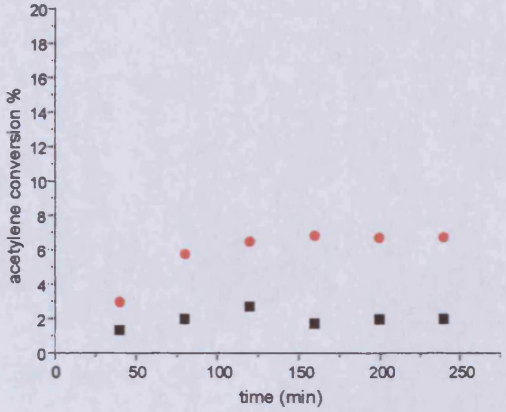

Fig 4.55: Conversion comparison, for the hydrochlorination reaction of acetylene between (■) Au/TiO_2 and (●) Au/C calcined catalyst.

In both cases activity was low, with Au/TiO_2 almost inactive. Au/TiO_2 has been tested for other hydrochlorination reactions (chapter 6), and in no case does it display significant activity, leading to the conclusion that this support, or the metal particle size is not suitable for the hydrochlorination reaction.

The poor activity of the calcined gold on carbon catalyst is also an important observation. Calcination was carried out in static air at 300 °C for 4 h. This could result in an increase in particle size, but also, as will be demonstrated, an increased amount of reduced gold.

Considering the significant differences between carbon and graphite, not only in terms of acid-base property, but also in terms of structure and surface area, a gold on graphite catalyst has been prepared, using the same conditions as for the charcoal catalyst. This catalyst did not show any activity. A possible explanation for this lack of activity could be that the surface area of graphite is too low (experimental value 82 $m^2\ g^{-1}$), leading to the formation of large gold particles, which are inactive in the hydrochlorination reaction. Alternatively, a different metal nucleation process may occur due to the different properties of this material.

All these tests were performed using the usual reaction conditions of 180 °C as reaction temperature and reactant flow of 5 mL min^{-1} for both acetylene and hydrochloric acid.

Additional tests using the catalysts: Au, Au/Pd 95/5 and Au/Rh 90/10 on carbon Darco 12-20 at a reaction temperature of 120°C have been performed. The results, in terms of VCM/C_2H_2 ratio, are reported in figure 4.56

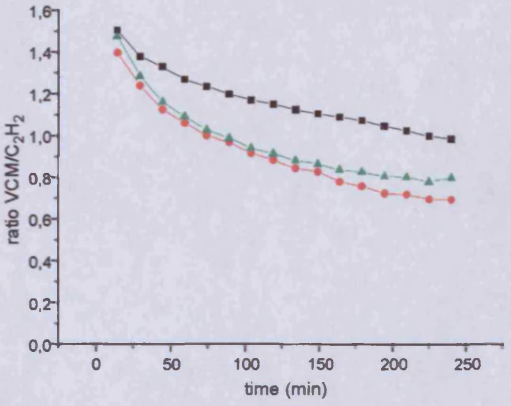

Fig. 4.56: Ratio VCM/C_2H_2 for hydrochlorination reaction of acetylene at 120 °C on carbon Darco 12-20 for (■) Au, (●) Au/Pd 95/5 and (▲) Au/Rh 90/10

As previously discussed (paragraphs 4.5.1 and 4.6.1) for the catalysts Au/Pd 95/5 and Au/Rh 90/10, if a reaction temperature of 180 °C is used, an improvement in activity is apparent when compared with gold alone. At 120 °C this effect is lost.
As previously mentioned for the hydrochlorination of acetylene a reaction temperature of 120 °C for gold on carbon catalysts is better in terms of acetylene conversion, but worse in terms of possible oligomer and polymer formation [13]. A possible explanation for the loss of a promoting effect for Au/Pd and Au/Rh could be the immediate formation of these high molecular weight species on the catalyst surface, processes which are reduced at high temperature.

For this reason, another set of catalysts of Au, Au/Pd 99/1 and Au/Pd 95/5 has been prepared on a different carbon, Aldrich G-60, in order to verify possible effects on the bimetallic catalysts. This carbon is characterized as having a high surface area in the range of 700 $m^2 g^{-1}$, while Darco12 is in the range of 500 $m^2 g^{-1}$. Also the mesh number is different, for G-60 it is about in the range of 100, while for Darco 12 it is in the range 12-20.

Acetylene conversion for this new set of catalysts at a reaction temperature of 180 °C is reported in figure 4.57

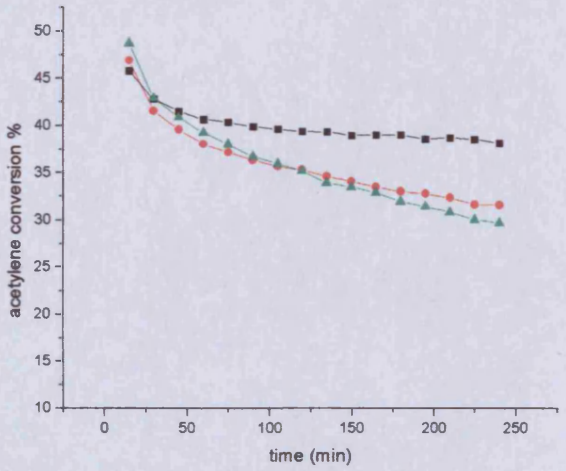

Fig. 4.57 Acetylene conversion over Au/Pd on carbon G-60.
(■) Au, (●) Au/Pd 99/1 and (▲) Au/Pd 95/5.

Again there is a promoting effect for Pd at the beginning of the reaction, but this promotion is very small. Nevertheless, the overall activity is higher than for Darco 12 carbon when compared with fig 4.20. It is likely that these different results are due to a different nucleation process relating to the different acid-base properties of the carbon with consequently different gold particle sizes. The average activity is higher, but the promotional effect is lost.

It is also useful to note how the surface area changed after reaction: see table 4.4 and compare with the table 4.3 where Darco-12 carbon was used.

Table 4.4: Comparison of surface area before and after reaction for Au and Au/Pd 95/5 catalysts on carbon G-60

	Surface area ($m^2 g^{-1}$)		Surface area ($m^2 g^{-1}$)	Area loss%
G-60 fresh	728			
Au1% on G60 before reaction	695	Au1% on G-60 after reaction	535	23%
Au/Pd 95/5 on G60 before reaction	678	Au/Pd 95/5 on G-60 after reaction	412	39%

Surface areas of fresh carbon and fresh catalyst do not display large differences. Moreover, the loss of area for Au/Pd 95/5 is similar for the two different carbons, while the gold only catalyst is more affected, having lost 23% of its surface area after reaction,

while for the previous carbon this was around 9%. In conclusion, even using support with similar natures, simply moving from one carbon type to another can lead to quite different results with effects difficult to predict; although, different porosity between the two carbons and different diffusion limitations effects should be considered as affecting the observed results.

In order to collect further information on the effect of catalyst activity on changing carbon, a complete series of Au/Rh catalyst has been prepared and tested. The results are reported in figure 4.58

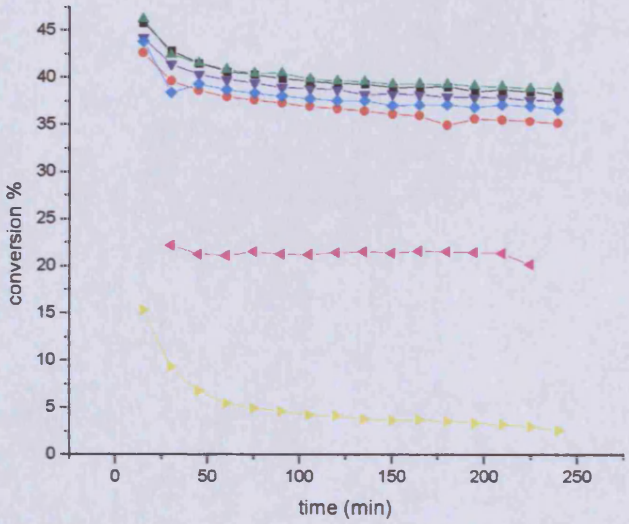

Fig. 4.58 acetylene conversion trend for Au and Au/Rh catalysts on carbon G-60. (■) Au, (●) Au/Rh 95/5, (▲) Au/Rh 90/10, (▼) Au/Rh 80/20, (♦) Au/Rh 50/50, (◀) Au/Rh 20/80, and (▶) Rh

In this case, no significant differences are apparent if this set is compared with the results previously described in paragraph 4.6.1. All the bimetallic catalysts display a similar activity to the Au catalyst and it is only for high rhodium content that the activity is lost. However, for this carbon catalysts with low rhodium loading, have similar activities and the considerations made for Au/Pd can again be applied, activity is higher but the relative differences in activity among the bimetallic catalysts are reduced.

4.10.2 Variability of the performance of gold on carbon catalysts

An important rule in the comparison of all the catalysts described up to now, has been to prepare all the catalysts in the same series, at the same time, using the same carbon batch, the same washed carbon, the same *aqua regia* solution and comparable drying procedure. This is to minimize the source of variability associated with the final product. It is evident that a comparison of all the gold on carbon catalysts prepared leads to conversion values in the range from 25 to 50%. It has been stated at the beginning of this chapter that variability of gold catalyst performance it is well known [15, 16, 32], and gold it is likely to be the metal more affected by this variation.

Taking into account the procedure used to prepare the catalyst, is reasonable to think that the biggest source of variation could be due to the concentration gradient effect when the gold precursor solution is impregnated on a carbon matrix, and this effect has been reported in literature [46]. In addition, although *aqua regia* is the best solvent to impregnate gold, because it leads to the lower leaching phenomena [13], the nitric acid contained in *aqua regia* could modify during the impregnation some functional carbon group [47] and so the cluster formation process described in paragraph 4.3.3.

Moreover it has been seen that gold is distinctly present in two different oxidation states. For this reason TEM analysis and high resolution XPS has been carried out. TEM analysis on the same carbon batch, but exploring different regions gave the following bright-field images (Fig 4.59 and 4.60), using a JEOL 2000FX TEM equipped with a lanthanum hexaboride thermoionic emission gun (TEG) operating at 200 keV.

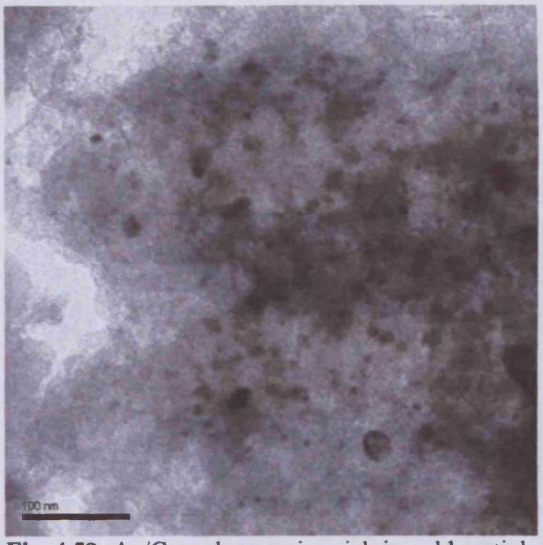

Fig. 4.59: Au/C catalyst, region rich in gold particles of different sizes

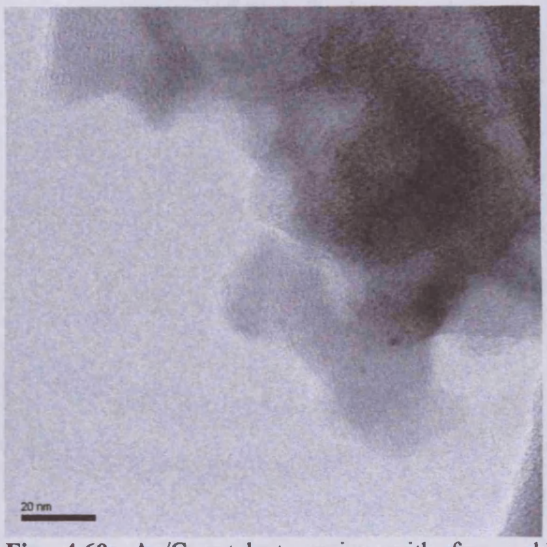

Fig. 4.60: Au/C catalyst, region with few gold particles

The analysis leads to an average particle size of 10.9 nm, but with a particle size distribution from 1.9 to 26 nm, which is quite wide. However, even more important is the observation that it is possible to observe regions quite rich in gold particles (fig. 4.59), and regions where gold is almost absent (fig. 4.60). The absence of a final homogenous product has also been confirmed using high resolution XPS; see the two spectra reported below (Fig. 4.61 and 4.62). The spectra has been collected using a Kratos AXIS-Ultra spectrometer, using a Al-K_α X-ray source (75-150 W) and an analyser pass energy of 160 eV (survey scans) or 20 eV (detailed scans).

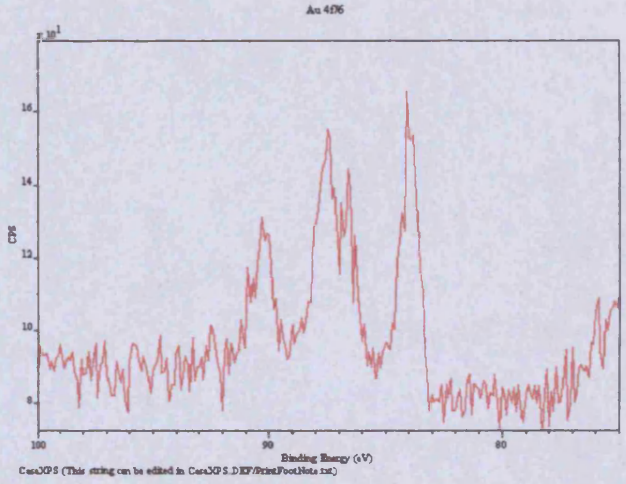

Fig. 4.61: Au 4f peaks for gold on carbon, specimen 1

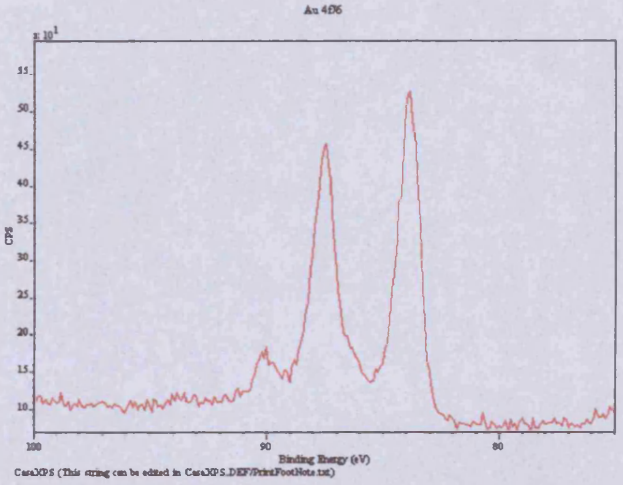

Fig. 4.62: Au 4f peaks for gold on carbon, specimen 2

The catalyst batch is the same in this case, but the two spectra are quite different. The first difference is the different surface gold content, and the second is that in figure 4.61 the two doublets system is very evident although no second metal is added. Consequently, it is not possible to state that the doublet system is a result of adding a second metal, although it is matter of fact that this system has been observed systematically when a second metal was added. Nevertheless, the higher the amount of Au(III) detected and the higher is the catalytic activity.

In conclusion, even when great care is taken to prepare the catalyst in order to guarantee a homogenous final material, it is possible to conclude that a carbon matrix is not fully suited for this purpose, and this inhomogeneity could be due to intrinsic properties of the wetness impregnation technique for gold on carbon. Similar phenomena have been reported for impregnated solutions of platinum salts on carbon [48] and afterwards thermal treatment for impregnation. In addition, investigations on the chemistry of the impregnation of hexachloroplatinic acid on carbon as support, leads to conclude that the presence of Pt in two different oxidation states could be the consequence of two different ligand carbon sites. One type consisting of oxygen-containing functional groups on the basal plane edges, and the other consisting of π-complex structures in the carbon basal plane [49, 50]. Maybe similar phenomena could occur during gold impregnation.

4.11 Conclusions

The behaviour of the most active bimetallic catalysts relative to gold, are summarized in the following diagram (Fig. 4.63):

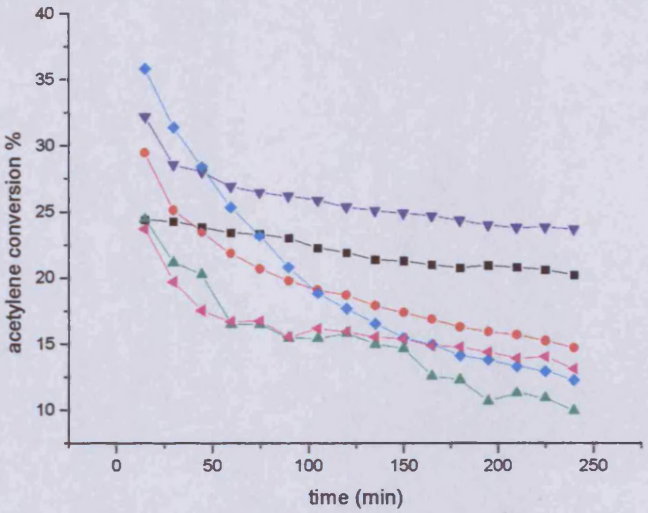

Fig 4.63: Acetylene hydrochlorination reaction, conversion trend for the most active bimetallic catalysts investigated: (■) Au, (●) Au/Pd 95/5, (♦) Au/Ir 80/20, (▼) Au/Rh 90/10, (▲) Au/Pt 80/20 and (◄)Au/Ru 80/20.

For each bimetallic catalyst a representative example has been chosen, and the conversion values have been scaled to gold in order to compare them. It is possible to classify the catalysts into three groups. The first group consist of Au/Pd and Au/Ir where the catalysts display an initial activity which is higher than gold, but they quickly loose their activity during the time on line. The second group where the activity is lower than gold comprises Au/Pt and Au/Ru, although there are reproducibility problems associated with Au/Ru. The final group contains Au/Rh catalysts where the conversion trend is similar to gold, and the effect of the second metal is to increase conversion, with little effect on catalyst deactivation.

In the case of the Au/Pd catalysts, a system with Pd selectively dispersed on Au is obtained even using a simple method such as incipient wetness impregnation, while for Au/Rh and Au/Ir although enhanced catalytic performance is obtained, the resulting systems also contains independent metallic clusters. Little information is available for Au/Ru and Au/Pt but it is evident that for them no synergistic effect is operating.
Moreover Au/Pd and Au/Ir are not able to maintain selectivity, while Au/Rh can, and this is probably related to carbonaceous product formation for Pd and Ir, while Rh does not appear to be affected in this way.

An important aspect is the relationship between the presence of Au(III) and the observed activity. With the presented data, it is possible to state that a correlation exists between the presence of Au(III) and enhanced activity. This conclusion is true both for catalysts containing gold only (for further details see chapter 5) and the bimetallic systems.

Finally, the use of carbon as support and the wetness impregnation preparation technique are able to lead to a final product suitable for the hydrochlorination of acetylene. However, the final product can be affected by variability in activity even if only to a small extent compared to the other common techniques used for catalyst preparation. It is possible to state that the lack of reproducibility for the cases presented here can be related to the inhomogeneous concentration gradient which leads to regions of support rich in metal, and others that are poorly covered.

The interaction of metal atoms with each other and with the support is also important, because by using carbon supports of a different nature, it is possible to obtain enhanced activity. However, interaction effects when bimetallic cluster are used may be lost, showing that the final effects of these parameters are difficult to predict a priori.

4.12 References

[1] J. G. Speight, *Chemical and Process Design Handbook*, McGraw-Hill, New York, 2002

[2] United Nation Environment Programme, International Labour Organization, and World Health Organization, International Programme on Chemical Safety (IPCS), Entry file EHC-215, WHO, Geneva, 1999

[3] G. J. Hutchings, *J. Catal.*, 292, **96**, 1985

[4] L. F. Albright, *Chem. Eng.*, 213, **10**, 1967

[5] J. Burks and M. William, United States Patent 4665243, AN447869, FD1982, 1987

[6] I. M. Clegg and R. Hardman, United States Patent 5763710, AN797841, FD1997, 1998

[7] C. E. Wilkes, J. W. Summers and C. A. Daniels (Eds.) *PVC Handbook*, Carl Hanser Verlag, München 2006

[8] United States Environmental Protection Agency, Entry file EPA/600/X-84/178, Washington D.C., 1988

[9] G. J. Hutchings and D.T. Grady, *Appl. Catal.*, 441, **16**, 1985

[10] G. J. Hutchings and D.T. Grady, *Appl. Catal.*, 155, **17**, 1985

[11] K. Saito and C Fujii, Japan Patent 52136104, AN51349, FD1976, 1977

[12] J. McKetta, *Chemical Processing Handbook*, Marcel Dekker ed., New York, 1994

[13] B. Nkosi, N. J. Coville, G. J. Hutchings, M. D. Adams, J. Friedl and F. E. Wagner, *J. Catal.*, 366, **128**, 1991

[14] V. E. Popov, V. I. Lazukin, T. Skaya, I. N. Novikov, M. N. Yakumova and A. Yu, *Kinet. Katal.*, 60, **17**, 1979

[15] F. E. Wagner, S. Galvagno, C. Milone, A. M. Visco, L. Stievano and S. Calogero, *J. Chem. Soc., Faraday Trans.*, 3403, **93**(18), 1997

[16] A. Wolf and F. Schueth, *Appl. Catal. A*, 1, **226**, 2002

[17] United States Environmental Protection Agency, Entry file EPA-560/13-80-002, Washington D.C., 1980

[18] R. J. Irwin, M. van Mouverick, L. Stevens, M.D. Dubler-Seese and W. Basham, *Environmental Contaminants Encyclopaedia*, National Park Service, Water Resources

Division, Fort Collins CO, 1997

[19] W. Jennings, E. Mittlefehldt and P. Stremple, *Analytical Gas Chromatography* (II Ed.), Academic Press, San Diego CA, 1997

[20] B. Nkosi, M. D. Adams, N. J. Coville and G. J. Hutchings, *J. Catal.*, 378, **128**, 1991

[21] J. K. Brennan, T. J. Bandosz, K. T. Thomson and K. E. Gubbins, *Coll. and Surf. A* 539, **187**, 2001

[22] F. Stoeckli and T.A. Centeno, *Carbon*, 1184, **43**, 2005

[23] M.M. Dubinin, *Carbon*, 355, **18**, 1980

[24] D.S. Cameron, S.J. Cooper, I.L. Dodgson, B. Harrison and J.W. Jenkins, *Catal. Today*, 113, **7**, 1990

[25] H. P. Boehm, *Adv. Catal.* 137, **13**, 1962

[26] A. Contescu, C. Contescu, K. Putyera and J.A. Schwarz, *Carbon* 83, **35**(1), 1997

[27] K. Lászlò, K. Josepovits and E. Tombácz, *Anal. Sci.* 1741, **17**, 2001

[28] L. B. Okhlopkova, A. S. Lisitsyn, V. A. Likholobov, M. Gurrath and H. P. Boehm, *Appl. Catal. A*, 229, **204**, 2000

[29] D. M. Hercules, *Anal. Chem.*, 1177, **58**, 1986

[30] C. D. Wagner, W. M. Riggs, L. E. Davis, and J. F. Moulder, *Handbook of X-ray Photoelectron Spectroscopy*, Perkin-Elmer Corporation (Physical Electronics), G.E. Muilenberg, ed., 1979

[31] T. Ohgi and D. Fujita, *Phys. Rev. B*, 115410-1, **66**, 2002

[32] C. L. Bianchi, S. Biella, A. Gervasini, L. Prati and M. Rossi, *Catal. Lett.*, 91, **85**(1), 2003

[33] L. Prati and M. Rossi, *J. Catal.*, 552, **176**, 1998

[34] D. A. Skoog, J. L. Leary, *Principles of Instrumental Analysis* (IV Ed.), Sanders College Publisching, Orlando FL, 1992

[35] B. D. Cullity, *Elements of X-ray Diffraction (II Ed.)*, Addison-Wesley, Reading MA, 1978

[36] V. Rößiger and B. Nensel, *Gold Bull.*, 125, **36**(4), 2003

[37] E. W. Abel, F. G. A. Stone and G. Wilkinson, *Comprehensive Organometallic Chemistry*, vol. 9, Elsevier, Oxford, 1995

[38] S. A. Mitchenko, V. V. Zamashchikov, A. A. Shubin, *Kinet. Katal.*, 421, **34**(3), 1993

[39] S. A. Mitchenko, E. V. Khomutov, A. A. Shubin and Y. M. Shul'ga, *J. Mol. Catal., A*, 345, **212**, 2004

[40] S. A. Cotton, *Chemistry of Precious Metals*, Chapman & Hall, London, 1997

[41] Third International Congress on Catalysis, *The role of the platinum metals in heterogeneous catalysis*, Amsterdam 1964, Platinum Metals Rev., 133, **8**(4), 1964

[42] H. Rossler, *Chem. Ztg.*, 733, **24**, 1900

[43] H. Okamoto and T. B. Massalski, *Bull. Alloy Phase Diagrams*, 381, **5**(4), 1984

[44] J. O. Linde, *Ann. Physik*, 69, **10**, 1931

[45] Y. Kobayashi, T. Okada, K. Asai, M. Katada, H. Sano and F. Ambe, *Inorg. Chem.*, 4570, **31**, 1992

[46] Y. F. Jia, C. J. Steele, I. P. Hayward and K. M. Thomas, *Carbon*, 1299, **36**(9), 1998

[47] E. Papirer, A Polania-Leon, J. B.Donnet, and P. Montagnon, *Carbon*, 1131, **33**, 1995

[48] M. Kang, Y-S. Bae, C-H. Lee, *Carbon*, 1512, **43**, 2005

[49] F. Coloma, A. Sepulveda-Escribano, J. L. G. Fierro and F. Rodriguez-Reinoso, *Langmuir* 750, **10**, 1994

[50] D. E. van Dam and H. van Bekkum, *J. Catal.*, 335, **131**, 1991

CHAPTER 5: GOLD ON CARBON CATALYSTS FOR THE HYDRO-CHLORINATION OF ALKYNES INCLUDING PROPOSALS FOR THE REACTION MECHANISM

5.0 Regeneration and role of the reagents over Au/C catalyst

Taking into account the results and the considerations described in the previous chapter, a more detailed study of catalyst properties and catalytic activity towards other substrates containing triple C-C bond has been carried out.

5.1 Regeneration of Au/C catalyst

In paragraph 4.5.3 it has been stated that different processes can participate to deactivate Au/Pd catalyst, and one of these involved Au reduction (figs 4.29 and 4.30). More detailed investigations are reported here of the role of Au (III) in monometallic catalysts containing gold only.

The first study involved regeneration of the catalyst with aqua regia. It has already been stated (paragraph 4.3.2) that treatment of the catalyst with aqua regia is not able to remove gold from carbon. In particular, a 24 h treatment of the fresh catalyst with such solvent leads to a relative removal of gold of less than 3% when a total 1% wt gold loading was used. In addition, even after treating the catalyst with aqua regia under reflux for 4 h, such treatment was able to remove around 60% of gold, with the remainder is still on the carbon. For this reason it was decided to take a sample of 300 mg of gold, carry out a hydrochlorination reaction of acetylene, and then to treat an aliquot by boiling the catalyst with aqua regia for 20 minutes. This kind of treatment leads to less than 1% relative amount of gold in the aqua regia, so it is possible to assume that the sample used for the second test has the same total, 1% wt gold, loading as the original catalyst.

The catalytic activity tests, using the usual reactant flows of C_2H_2 and HCl of 5 mL min^{-1} and a reaction temperature of 180 °C, are displayed in figure 5.1 below for the fresh and the regenerated catalyst.

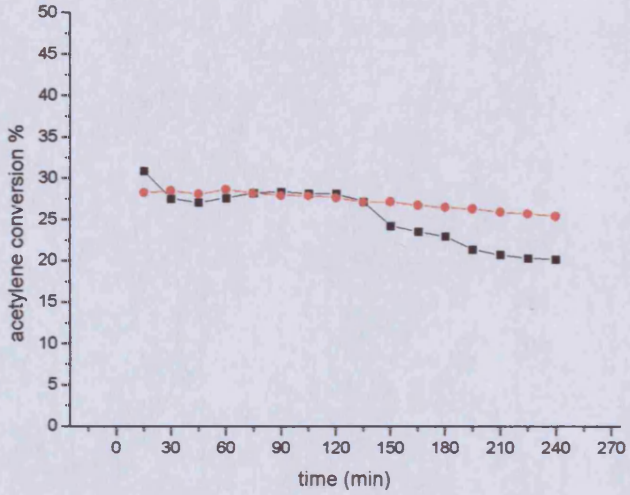

Fig. 5.1; Activity trend for the hydrochlorination reaction, over Au/C, (■) fresh catalyst and (●) regenerated catalyst using a short treatment with aqua regia.

It is possible to observe that, after regeneration, the activity is fully recovered, and both fresh and regenerated catalysts display quite similar activity. It is also worth mentioning that in order to always use the same portion of catalyst to carry out rigorous characterization on the Au/C catalyst in the various steps of the procedure, 300 mg of catalyst has been used for the test using fresh catalyst, and 200 mg for the test using the regenerated catalyst. This to reduce the effect of sample inhomogeneity (chapter 4). The fact that in both cases the activity is recovered, with similar conversion values using different amount of catalyst, is also suggestive that the reaction, using the specified reaction conditions, is under diffusion control.

In order to detect the presence and role of Au(III), XPS spectra have been collected for the fresh catalyst (fig 5.2), for the catalyst after reaction (fig. 5.3), for the regenerated catalyst (fig 5.4) and for the regenerated after reaction (fig 5.5).

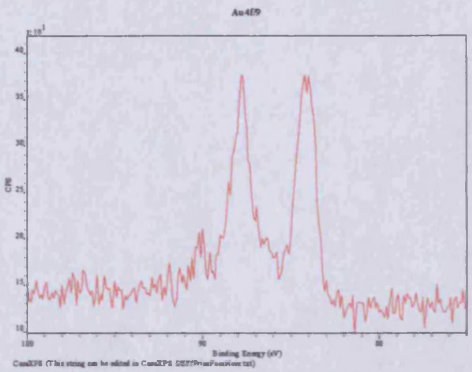

Fig 5.2: Au 4f XPS spectrum of Au/C catalyst before reaction. It is possible to detect the presence of Au(III)

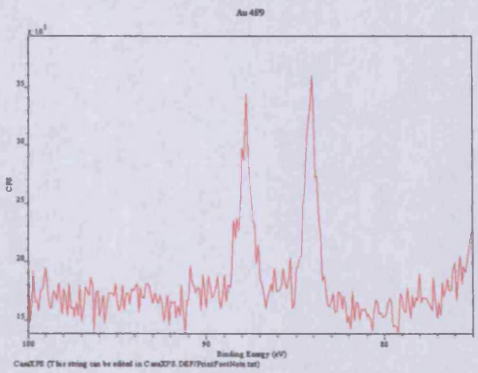

Fig 5.3: Au 4f XPS spectrum of Au/C catalyst after reaction. Au(III) is reduced.

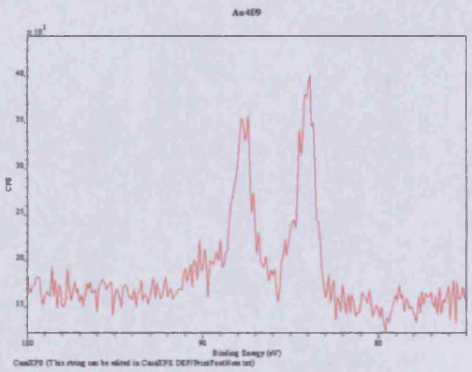

Fig 5.4: Au 4f XPS spectrum of Au/C catalyst after regeneration. It is possible to detect again the presence of Au(III)

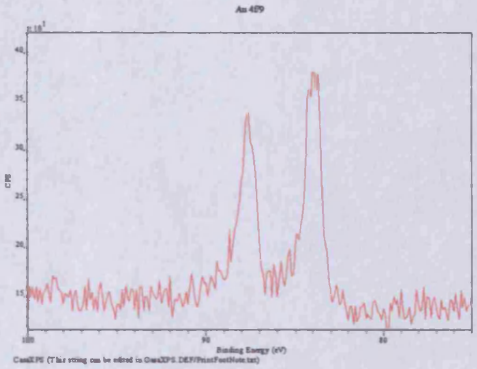

Fig 5.5: Au 4f XPS spectrum of Au/C catalyst after regeneration and after the second reaction. Au(III) is reduced.

It is possible to observe the presence of the Au(III) component at 90 eV, which is clearly evident in the fresh catalyst, but this component is not present after reaction. Au(III) is recovered after regeneration, but it is reduced again after the second reaction.

These results are quite important because they directly correlate gold oxidation state with catalytic activity, and it is possible to state that the reduction of gold is definitely involved in the catalyst deactivation process, or in another way, that its presence leads to a catalyst with enhanced performance. It has to be remembered, that all the bimetallic catalysts shown in chapter 4, which displayed an activity higher than gold, contained more Au(III).

5.1.1 Reactant effects over Au/C catalyst

The results described in the previous paragraph, prompt the question of which factor is responsible for Au(III) reduction. Indeed, the reactant C_2H_2 is a well known reducing agent, and it is important to determine if the gold reduction is an effect of the reaction or of acetylene only, and more generally to identify also the role played by HCl during reaction. In order to achieve this, a series of experiments using an inert gas have been carried out, and they are schematically reported here:

C_2H_2/HCl (2h) → **He**/HCl (2h) → C_2H_2/HCl (2h) (test 5.1)

He/HCl (2h) → C_2H_2/HCl (2h) → **He**/HCl (2h) (test 5.2)

C_2H_2/HCl (2h) → C_2H_2/**He** (2h) → C_2H_2/HCl (2h) (test 5.3)

C_2H_2/**He** (2h) → C_2H_2/HCl (2h) → C_2H_2/**He** (2h) (test 5.4)

In all cases, the flow was kept constant and helium was introduced on line immediately after closing the other reactant, with a flow of 5 mL min^{-1} for each gas, and a reaction time for each step of 2h.

The effects of these treatments on the conversion for hydrochlorination of acetylene are reported in figure 5.6 below:

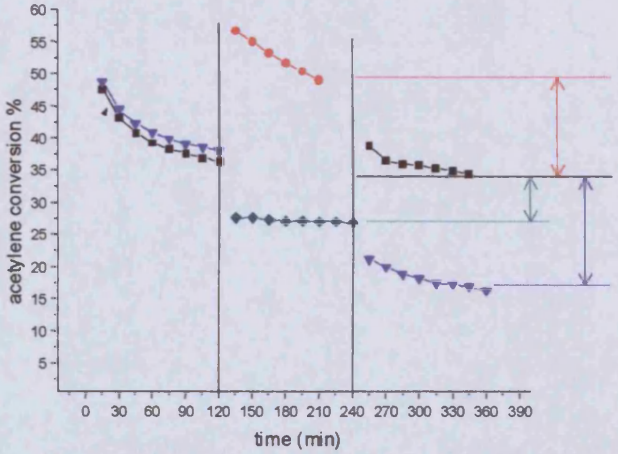

Fig. 5.6: crossed experiment with inert gas to evaluate the effect of each reactant for the hydrochlorination reaction of acetylene over Au/C catalyst. (■) C_2H_2/HCl (2h) → **He**/HCl (2h) → C_2H_2/HCl (2h); (●) **He**/HCl (2h) → C_2H_2/HCl (2h) → **He**/HCl (2h) (▼)C_2H_2/HCl (2h) → C_2H_2/**He** (2h) → C_2H_2/HCl (2h) and (♦) C_2H_2/**He** (2h) → C_2H_2/HCl (2h) → C_2H_2/**He** (2h)

The results of these experiments are quite important. The role of HCl is well evidenced in test 5.1 and test 5.2. Indeed, in test 5.1 where the intermediate step is He/HCl, this step acts like a regeneration treatment and the catalytic activity is completely recovered. However, also the possibility of an increasing in surface population of HCl on the catalyst surface should be taken into account to explain the phenomenon observed. This result is not new for this kind of reaction as regenerating agent NO has been used [1] but here it is confirmed for the use of HCl. In test 5.2 a pretreatment with He/HCl, led to a very active catalyst, even if this activity decreased quite quickly.
The role of C_2H_2 is well described from test 5.3 and test 5.4. In test 5.3 it is clear that, even if no reaction occurred, the catalyst deactivated, and when the reaction was brought online again, its performance was worse when compared to a reaction without interruption. The same conclusion applies for the test 5.4, where at the beginning only C_2H_2/He was used.

In conclusion, both reactants are able to modify the final performance of the catalyst, but in opposite directions: a regeneration and an activation role for HCl, while C_2H_2 acts to decrease the activity of the catalyst, independent of whether if the reaction is taking place or not.
In order to evaluate further the effects of the reactants, two additional tests with variable amounts of HCl have been carried out. The tests were:

C_2H_2/HCl (2h) 1:1 → C_2H_2/HCl (2h) 1:1.5 → C_2H_2/HCl (2h) 1:1 (test 5.5)
C_2H_2/HCl (2h) 1:1 → C_2H_2/HCl (2h) 1:0.5 → C_2H_2/HCl (2h) 1:1 (test 5.6)

Where a 1:1 ratio, means a flow of 5 mL min^{-1} for each reactant, and the usual reaction temperature of 180 °C was used.

The results obtained are displayed in figure 5.7:

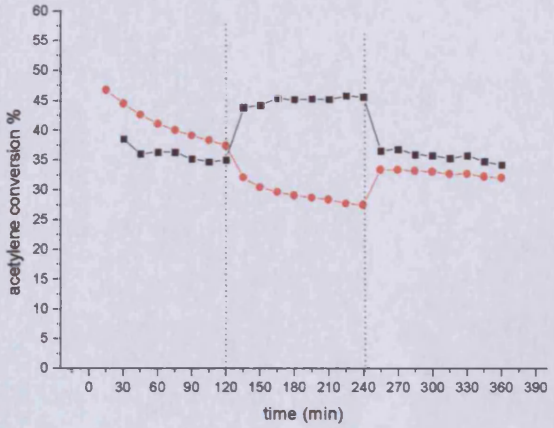

Fig 5.7: hydrochlorination reaction of acetylene, conversion towards different amount of HCl on line over Au/C catalyst
(■) C_2H_2/HCl (2h) 1:1 → C_2H_2/HCl (2h) 1:1.5 → C_2H_2/HCl (2h) 1:1 and
(●) C_2H_2/HCl (2h) 1:1 → C_2H_2/HCl (2h) 1:0.5 → C_2H_2/HCl (2h) 1:1

For test 5.5 with an intermediate step using excess HCl, the results are similar to test 5.2 in figure 5.6, where there was a pretreatment step with the gas mixture He/HCl. In both cases the catalyst was able to recover its activity. While for the test where the acid was deficient, this did not happen, although the activity loss was quite less marked in comparison with the test where the intermediate step was C_2H_2/He (test 5.3, figure 5.6)

Moreover, considering the results of these experiments and the XPS spectra previously described, it is possible to state that a gold reduction process is involved in the deactivation of the catalyst, and that Au(III) is one of the active gold species, supporting the existence of a redox cycle for the catalyst, as reported in scheme 5.1.

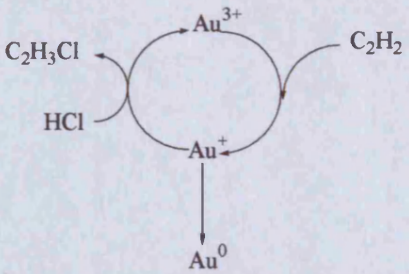

Scheme 5.1: Proposed redox cycle for the hydrochlorination reaction of acetylene over Au/C catalyst.

In this redox cycle, HCl plays the double role of reactant and catalyst regenerating species. As indicated in scheme 5.1, the existence of Au(I) as an intermediate is assumed. If the combination of HCl and the reaction conditions are able to keep the cycle Au(III) ↔ Au(I) going, the catalyst preserves high activity. Nevertheless, Au(I) is well known to be an instable gold species, and if disproportionation occurs, an increase in the amount of Au(0) is observed, in agreement with the reaction: $3Au^{+} \rightarrow Au^{3+} + 2Au^{0}$. This process could be responsible for catalyst deactivation.

5.2 Proposals for the reaction mechanism of acetylene hydrochlorination over Au/C

All the information collected on the behaviour of Au/C catalyst towards hydrochlorination of acetylene can be brought together and, a reaction mechanism proposed.

Firstly, two possible mechanisms will be discussed. Even if they will eventually be rejected on the grounds of the experimental observations, they will be a useful introduction to a third mechanism, which is considered to be operating in this reaction.

The first proposal is an Eley-Rideal mechanism, with C_2H_2 on the metal surface and HCl approaching above the organic species, as depicted in figure 5.8

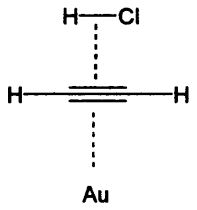

Fig. 5.8: Eley-Rideal mechanism with acetylene on the metal surface

It is known that this kind of mechanism is true using $HgCl_2$ as a catalyst for the hydrochlorination of acetylene [2]. In that case, a carbocation mechanism has been identified, and this is consistent with the experimental observation that if the amount of HCl increases the conversion also increases, but the selectivity decreases. But when gold

is used the selectivity is always preserved, even using a large excess of HCl, and vinyl chloride monomer is always obtained with selectivity above 95-98%. Consequently, this mechanism has to be considered as not being correct for gold. Even using reaction conditions with lower GHSV and a reactant ratio C_2H_2 : HCl 1:3 with a C_2H_2 flow of 1.5 mL min^{-1}, a conversion value around 95% was obtained, but a negligible decrease of selectivity was detected, with values always virtually equal to 100%.

In order to explain this high selectivity, the second option could involve HCl on the metal surface, as shown in figure 5.9.

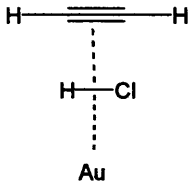

Fig. 5.9: Eley-Rideal mechanism with HCl on the metal surface

A mechanism like this could be in agreement with the activation role of HCl on the Au/C catalyst as described in fig 5.6 and for the high selectivity detected. However, it should not be forgotten that a reason for deactivation, true for any kind of catalyst for hydrochlorination, including gold, is the formation of oligomers on the catalyst surface. As mentioned in chapter 4, the reaction temperature of 180 °C is not the optimal temperature in terms of conversion, which is around 100-120 °C [3], but is a compromise to discourage oligomer formation and quick catalyst deactivation. Because of this experimental evidence, the second option has to be rejected as well, as the growth of oligomer species on a metal surface already covered by HCl is difficult.

The third hypothesis is the formation of a C_2H_2/Au/HCl complex as shown in figure 5.10:

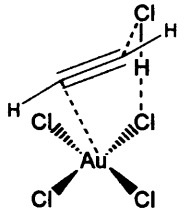

Fig. 5.10: Gold-acetylene-HCl complex, formation of a six membered ring is assumed.

It worth mentioning that the hypothesis of the formation of a complex is not new for this reaction [4]. Moreover, previous kinetic studies have identified a kinetic law that is first order in C_2H_2 and first order in HCl [5] when gold is used. However, no strongly supportive experimental evidence has been provided for gold up to now. The only example reported in the literature with data directly supporting complex formation for the hydrochlorination reaction is for a non-supported K_2PtCl_6 salt mechanically activated [6].

For the proposed model it was assumed that Au(III) is the most active species for the process, and the Au environment is fully surrounded by chloride (see paragraph 4.5.2). For this reason, a simpler model is proposed with gold tetrachloroaurate as the active species.

The hypothesis of C_2H_2/Au/HCl complex is consistent with the high selectivity; the regeneration effect of HCl and the deleterious effect of C_2H_2, and can explain polymerisation. The model is reported below in scheme 5.2

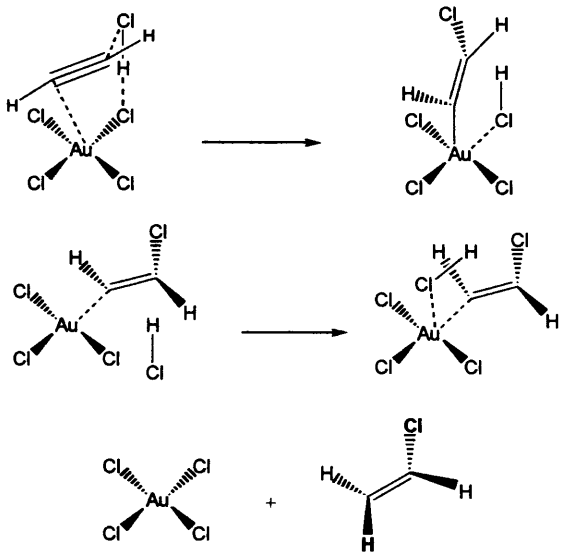

Scheme 5.2: Proposed model for the hydrochlorination of acetylene over Au/C

This model requires the presence of both reactants to give an initial six member ring and subsequent cleavage of HCl, with H transfer to an adjacent chloride. The resulting penta-

coordinated complex can be assumed as quite unstable, and to reobtain a saturation level of four, removal of HCl is required. The third step is necessary to give the final product and to regenerate the catalyst. This is obtained *via* addition of HCl, with H that gives the final organic substrate, and Cl that regenerates the catalyst. It worth noting, that if C_2H_2 is present instead of HCl on the regeneration step, it is possible to obtain a conjugate polymer with an even number of carbon atoms.

It is important to note that in the proposed model, the final product has H and Cl with *trans* isomerism, and a HCl-*trans* isomerism can be obtained only *via* the complex although, as described in the following paragraphs, the use of higher alkynes as substrates do not exclude the formation of a carbocation intermediate

5.3 Verification of the hypothesis of C_2H_2/Au/HCl complex formation for the hydrochlorination of acetylene

In order to verify the consistency of the model, the possibility of gold to be active for different alkynes and to test the Markovnikov or anti-Markovnikov nature of this reaction, the reagent 1-hexyne has been chosen. Also, the final products are easier to handle, for safety reasons, than vinyl chloride monomer. The reactant 1-hexyne is a liquid at room temperature, but it is possible use its vapour by incorporating a saturator under He flow to obtain gas-phase reaction conditions close to those used for acetylene.

5.3.1 Hydrochlorination of 1-hexyne over Au/C catalyst

The reaction has been carried out using Au/C catalyst and a reaction temperature of 180 °C. Using the specified reaction conditions, with 1-hexyne it is possible to obtain information from gas chromatography only for the initial activity i.e. in the first hour, with a conversion value around 10%. An accurate determination of the nature of the product is instead possible using NMR by collecting the reaction products in a

chloroform trap at the outlet of the reactor for a time on line of 3 h.

Taking into account all the possible isomers, i.e. the Markovnikov and anti-Markovnikov and the *sin* or *anti* addition of HCl to the triple bond, the number of possible products that can be obtained is four, and they are reported in scheme 5.3 below:

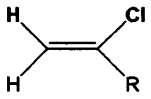

Markovnikov – **HCl** *cis*

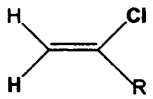

Markovnikov –**HCl** *trans*

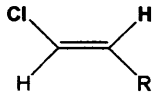

Anti-Markovnikov – **HCl** *cis*

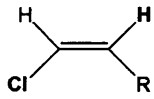

Anti-Markovnikov – **HCl** *trans*

Scheme 5.3 Hydrochlorination products of 1-hexyne, involving Markovnikov and HCl-*cis/trans* isomers

The reaction displays very high selectivity towards the Markovnikov products (which are NMR equivalent) and only traces of the anti-Markovnikov product have been detected.

In scheme 5.4 the expected chemical shift values in ppm and hydrogen coupling constant J_{AB} in Hz are reported [7]

Scheme 5.4: Expected chemical shifts and coupling constants for the indicated products

1-Hexyne

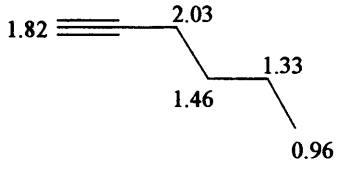

Markovnikov
(HCl *cis* and *trans*)

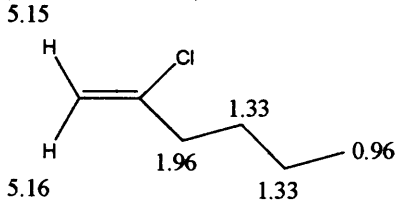

J_{AB} 0-2 Hz

Anti-Markovnikov
(HCl *cis*)

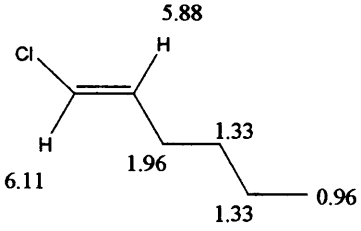

J_{AB} 12-18 Hz

Anti-Markovnikov
(HCl *trans*)

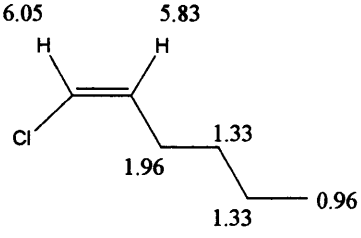

J_{AB} 6-12 Hz

The presence of the Markovnikov product is evident from an NMR doublet at 5.14 ppm, as reported in figure 5.11

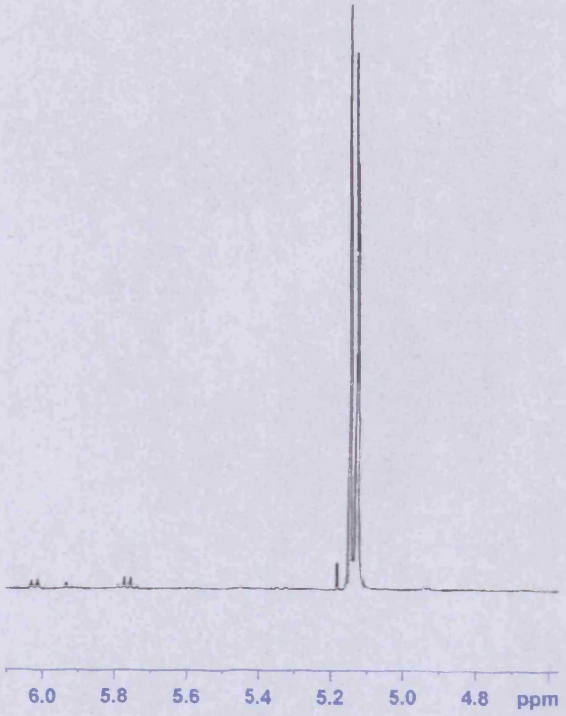

Fig. 5.11: Identification of the product for the hydrochlorination reaction of 1-hexyne using ^{1}H-NMR at 400 MHz. At 5.15 ppm it is possible to detect the Markovnikov product, and traces of the anti-Markovnikov which displays two distinct signals at 5.76 and 6.03 ppm

Concerning the anti-Markovnikov products, the difference in terms of chemical shift between the *cis* and *trans* is not significant for unambiguous characterization. However, in the region 5.76-6.03 ppm it is possible to observe a doublet of triplets, with a coupling constant J_{AB} equal to 6.7 Hz, which is a numerical value consistent with the HCl-*trans* isomer, expected to have a value in the range of 6-12 Hz.

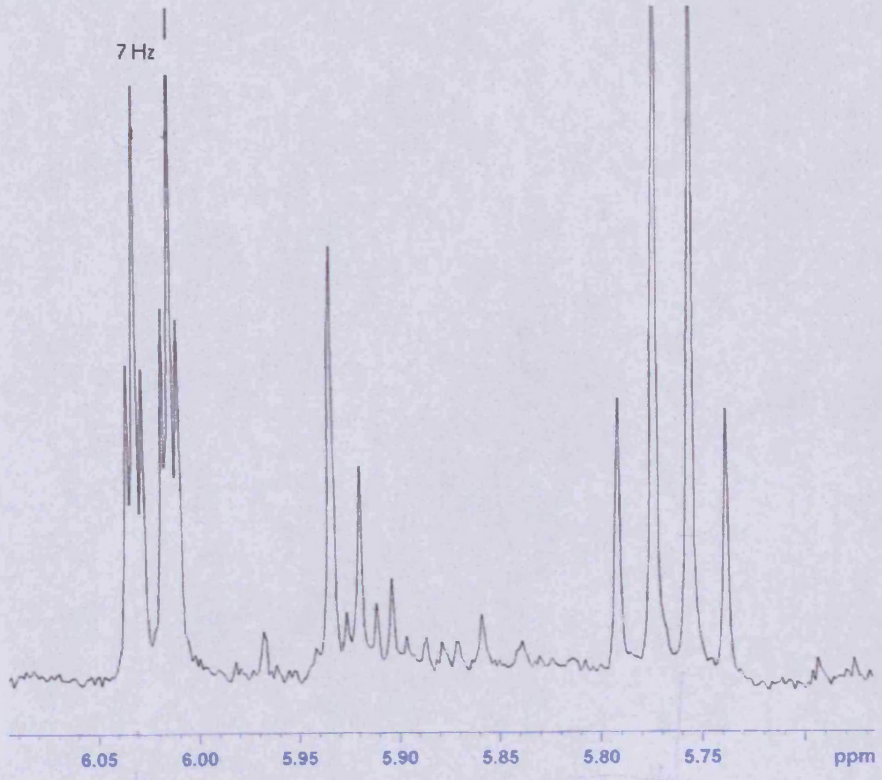

Fig 5.12: Identification of the anti-Markovnikov product for the hydrochlorination reaction of 1-hexyne, using ^{1}H-NMR at 400 MHz. Details of the splitting at 6.03 and 5.76 ppm. The coupling constant consistent with the *trans* isomer

In conclusion, it is possible to state that if 1-hexyne is used as reactant, a product derived from HCl *trans* isomerism can be detected, and this supports the hypothesis of complex formation.

5.3.2 Hydrochlorination of phenyl-acetylene over Au/C catalyst

In order to collect further information on the reactivity towards different substrates, hydrochlorination of phenyl acetylene has been carried out. The reaction condition were the same as those used for 1-hexyne, i.e. a reaction temperature of 180 °C, a flow of HCl of 5 mL min^{-1} and phenyl acetylene introduced *via* a saturator with an He flow of 20 mL min^{-1}.

Also this time it is possible to obtain conversion at the beginning of the reaction, while the identification of the product has been done using NMR, collecting the products in a chloroform trap.

Scheme 5.8 Expected chemical shifts and coupling constants for the products indicated

Phenyl-acetylene

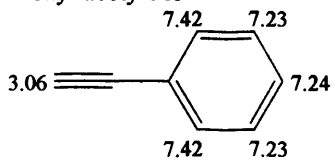

Markovnikov
(HCl *cis* and *trans*)

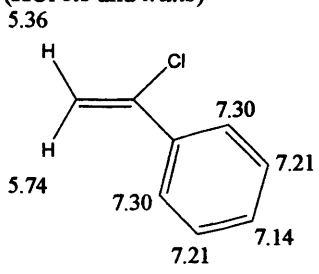

J_{AB} 0-2
Main product

Anti-Markovnikov
(HCl *cis*)

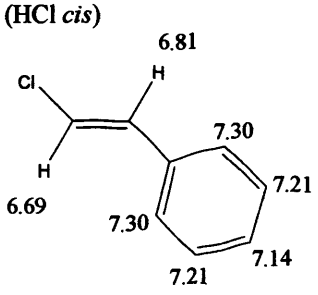

J_{AB} 12-18
Absent

Anti-Markovnikov
(HCl *trans*)

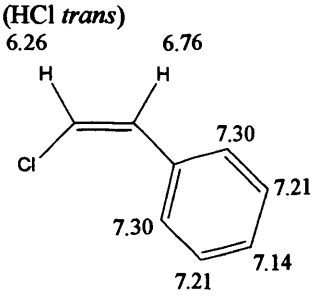

J_{AB} 6-12
Traces

The Markovnikov product can easily be distinguished from the other two products, due to the different chemical shift of the protons (Fig. 5.13). For the other products the assignment is more difficult.

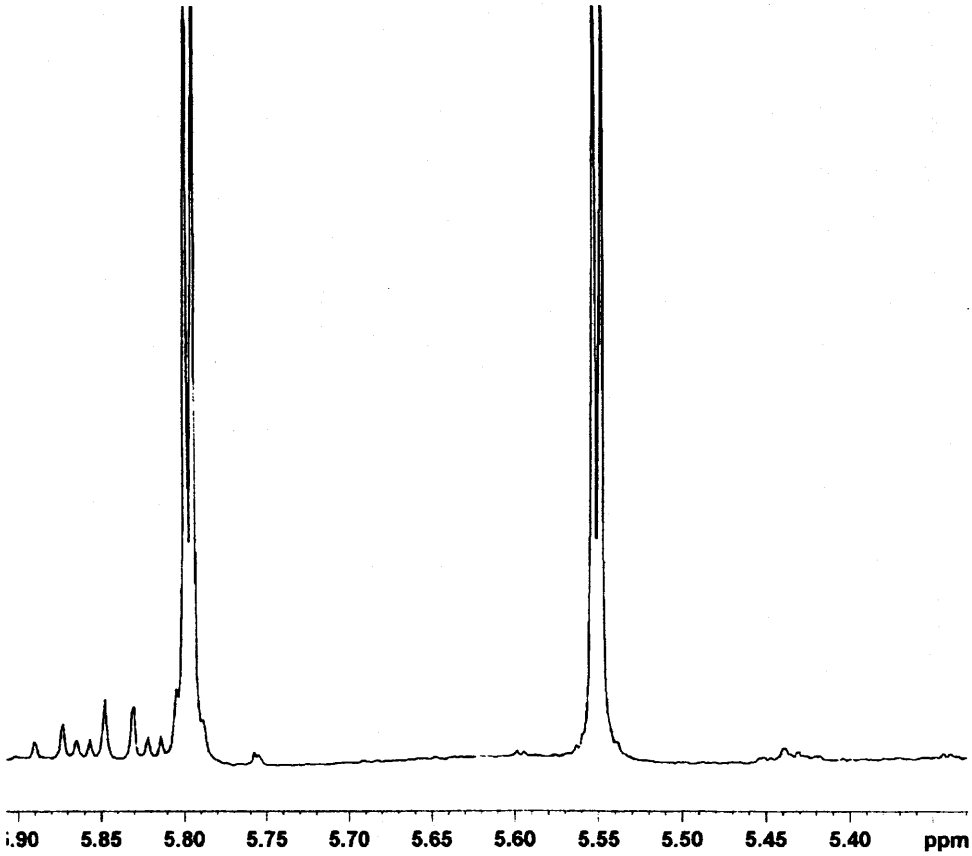

Fig. 5.13: Identification of the Markovnikov product for the hydrochlorination reaction of phenyl acetylene, using ^{1}H-NMR at 400 MHz. Detail of the region at 5.79 ppm (H_A) and 5.55 ppm (H_B).

However, for the anti-Markovnikov (HCl *cis*) the expected coupling constant should be in the range 12-20 Hz, while for the anti-Markovnikov (HCl *trans*) the expected coupling constant should be in the range of 0-10 Hz and a value of 8 Hz has been detected, as indicated in figure 5.14

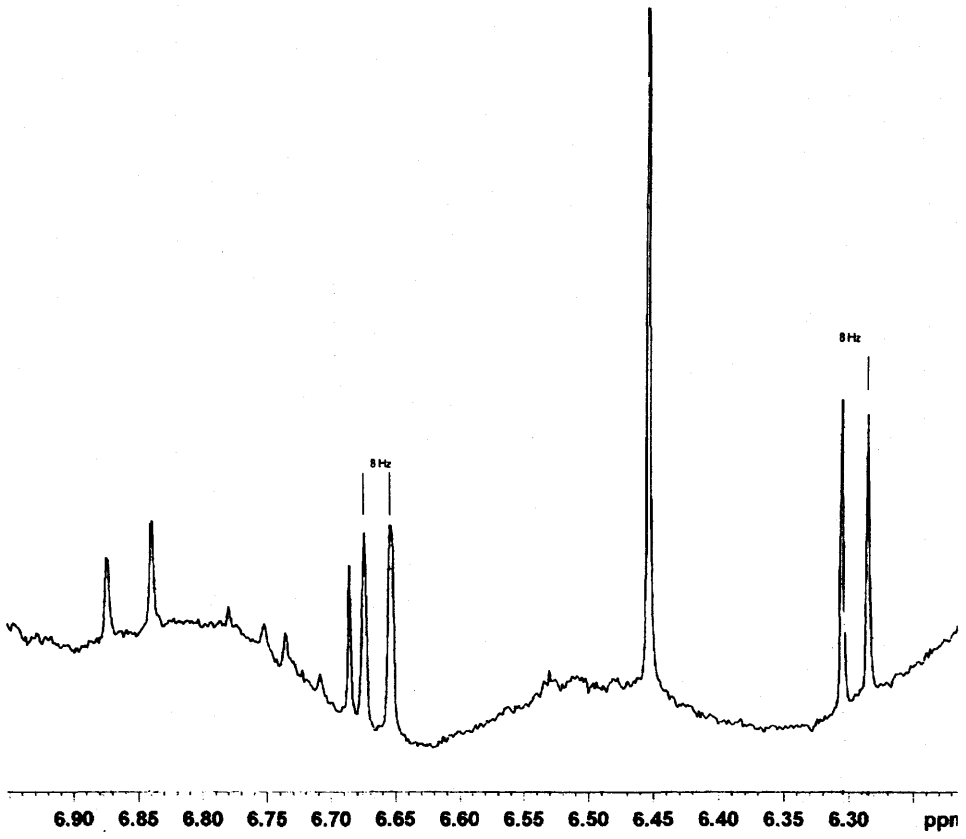

Fig. 5.14 Identification of the anti-Markovnikov product for the hydrochlorination reaction of phenyl acetylene, using ^{1}H-NMR at 400 MHz. Detail of the region at 6.68 ppm (H_A), and 6.29 (H_B). Coupling constant consistent with the *trans* isomer.

The difference in reactivity if compared with 1-hexyne, it could be explained with the fact that in phenyl-acetylene the triple bond is conjugated with the aromatic ring.

5.3.3 Hydrochlorination of 2-hexyne over Au/C catalyst and effects of terminal alkynes

In a catalytic test using 2-hexyne as substrate under the same experimental conditions described above, very little conversion, below 2% was detected. In addition, in this case it was not possible to carry out assignments for regioisomerism of the final products

obtained. This is because the difference in coupling constants between the two HCl *cis* and *trans* isomers, (7.2 and 6.7 Hz respectively for the similar 2-chloro-2-butene molucule), is too small for an unambiguous determination, and this test can be considered useful only in terms of conversion values.

In conclusion, for the alkynes tested the reactivity order can be summarized in scheme 5.6

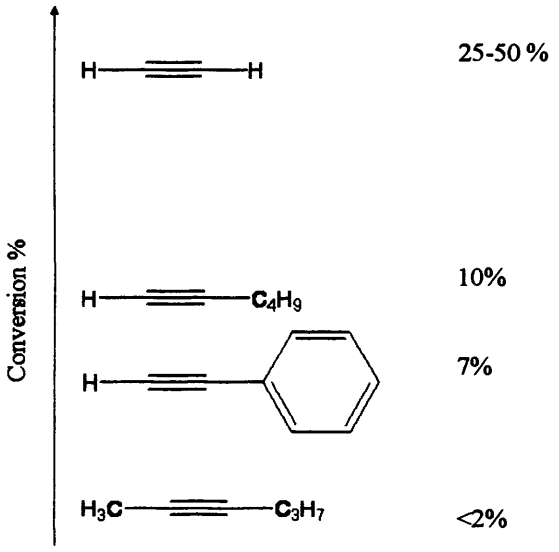

Scheme 5.6: Average hydrochlorination conversion for different alkynes (for acetylene the range 25-50% is function of the support used and final catalyst inhomogeneous)

Acetylene is the substrate that displayed the highest conversion, and the presence of an alkyl or aryl group leads to a loss of conversion, while in the case of 2-hexyne specific considerations are needed. It could be possible to explain the low activity of 2-hexyne in terms of a steric factor on the catalyst surface, but another difference to take into account is that this reagent it is not a terminal alkyne, and so acidic protons are absent, while in the other substrates they are present.

The reactivity of gold, especially Au(III) towards alkynes is usually explained in two ways: one is a nucleophilic-electrophilic interaction between the Au(III) centre and the

triple bond (scheme 5.7) *via* π-coordination [8].

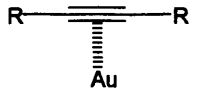

Scheme 5.7: Nucleophilic-electrophilic interaction between Au(III) and triple C-C bond

The second option, observed for gold(I)-alkynyl complexes [9] use the acidity of the acid protons of the terminal alkyne to give a σ-coordination, as indicated in scheme 5.8 *via* exchange reaction

Scheme 5.8: σ-coordination between Au(I) and terminal alkynes *via* exchange reaction

In addition, sometimes both π- and σ- coordination can also be observed [10] (scheme 5.9)

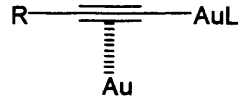

Scheme 5.9: Contemporaneous presence of π- and σ- coordination of a terminal alkyne on two different Au centres.

It should be stated that schemes 5.8 and 5.9 have been observed for homogenous catalysis reactions, but they show a possible pathway that could explain the observed reactivity for primary alkynes and the absence towards secondary alkynes that could be operating for the systems studied in this work. This could indirectly support the proposed mechanism involving a C_2H_2/Au/HCl complex, with a non-symmetrical orientation of the alkyne above the metal centre.

5.3.4 Reaction mechanism *via* oxidative addition

As well as to the reaction pathway described above, another pathway involving oxidative addition could be proposed to explain the observed trend and reactivity. In fact, the predominant presence of Markovnikov products is supporting the formation of a

carbocation intermediate, rather than a six membered ring complex. For this reason an alternative reaction pathway is indicated in the scheme 5.10 below:

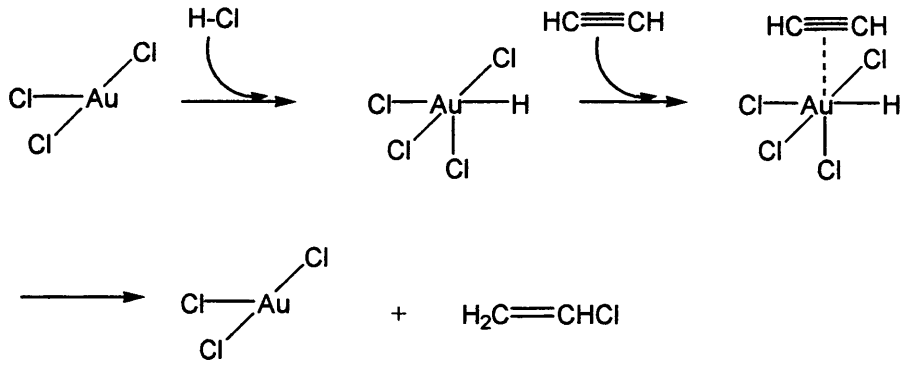

Scheme 5.10: oxidative addition reaction pathway involving the use of $AuCl_3$ as precursor and formation of octahedral complex as intermediate

This mechanism uses $AuCl_3$ as precursor with an oxidative addition of HCl followed by electrophilic addition of this intermediate to acetylene and final reductive elimination to give the product and reform the active catalyst specie. It should be noted that up to now oxidative addition has been observed for Au(I) complexes [11] only, and not for Au(III) complexes as proposed in the scheme above. However, this pathway could explain the activation role of HCl, which in this case is needed to generate an active intermediate, and the predominance of Markovnikov products, in fact the octahedral complex obtained after addition of C_2H_2 is a carbocation intermediate. Moreover, the decreasing in reactivity of higher alkynes and the negligible reactivity of 2-hexyne could be due to steric factor of the organic substrate on the formation of the octahedral complex.

5.4 Hydrochlorination using deuterated reactants

The data provided up to now give, clear indications about the regioselectivity in terms of whether Markovnikov or anti-Markovnikov are present. Distinguishing between the *cis* / *trans* isomers is more difficult. In fact, having directly observed the HCl-*trans* isomer on the minor product, and not on the main one, this experimental evidence cannot be

considered as conclusive to claim that this also occurs for the main Markovnikov product. Moreover, anti-Markovnikov products could be obtained as results of a non-carbocationic pathway rather than a six membered ring formation. For this reason tests with deuterated substrates have been carried out.

5.4.1 Hydrochlorination of 1-hexyne using deuterated hydrochloric acid

The tests have been carried out with 1-hexyne and DCl. DCl was used in ether solution, 1 mol L^{-1} and placed in a saturator. The effect of the presence of ether was tested separately and no reaction occurred.

As usual the reaction products were collected in a chloroform trap and using deuterated chloroform as NMR solvent. This procedure has been used for all the NMR described in this chapter. NMR (figure 5.15) revealed the presence of only one deuterated product. Taking into account the effect induced on the chemical shift by deuterium [12], it is possible to conclude that deuterium occupied the terminal position, leading to the conclusion that DCl attacks with symmetry of the *anti* type and so the product is the DCl *trans* isomer.

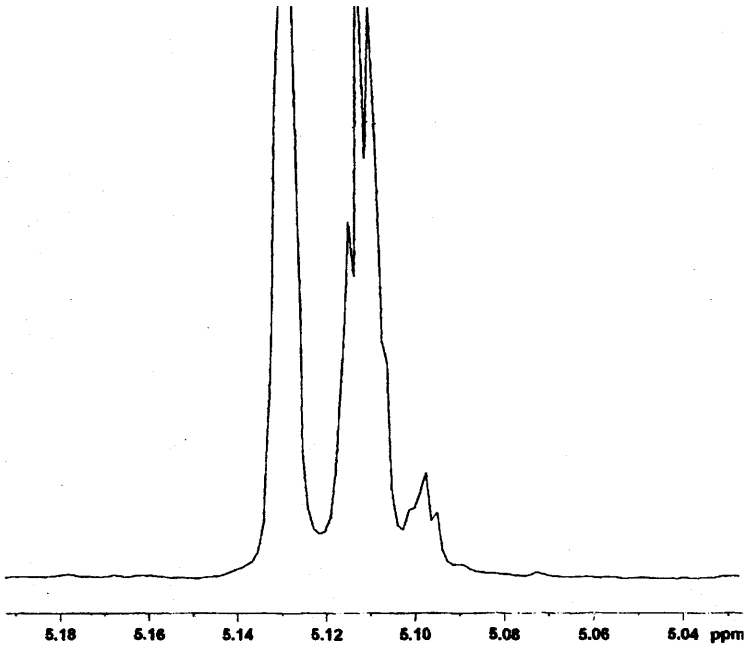

Fig. 5.15: ^{1}H-NMR detail of reaction products of 1-hexyne and DCl. Both deuterated (5.9 ppm) and non-deuterated (5.11 and 5.13 ppm) products are present. The deuterated chemical shift is consistent with *anti* attack of DCl to triple C-C bond.

However, further explanation is necessary. In figure 5.15 a small triplet is present at 5.97 ppm, which originates from a H-D coupling, but also present are the characteristic peaks for the not deuterated product at 5.11 and 5.13 ppm. Water was used in this experiment. The only source of water can be traces in the helium, which is used as a carrier gas through the saturator. From the peak intensities (and also taking into account the minor response factor for the H-D coupling) it is evident that, although water is presence in traces, it is able to lead to a higher amount of product. Further tests using a silica gel cartridge were carried out, but were unsuccessful; as a consequence, trace of HCl could be present in the starting DCl material. A result like this can be explained only in term of an isotope effect, with a slower cleavage of the D-Cl bond in comparison with H-Cl. Nevertheless, this experimental evidence indirectly supports the proposed mechanism in scheme 5.2. Indeed, the first step involving H-Cl cleavage, and the results obtained here suggest that the first step could be the rate-determining step of the reaction.

5.4.2 Hydrochlorination using deuterated 1-D-hexyne

In order to collect further mechanistic information, a catalytic test using deuterated 1-D-hexyne has been performed using the same experimental conditions described for the other tests involving hexyne. It has to be taken into account that if the proposed mechanism is true, no cleavage of C-H bond is involved, and so, no isotope effect should be observed.

NMR spectra of the products are reported in figure 5.16 and some important considerations can be made.

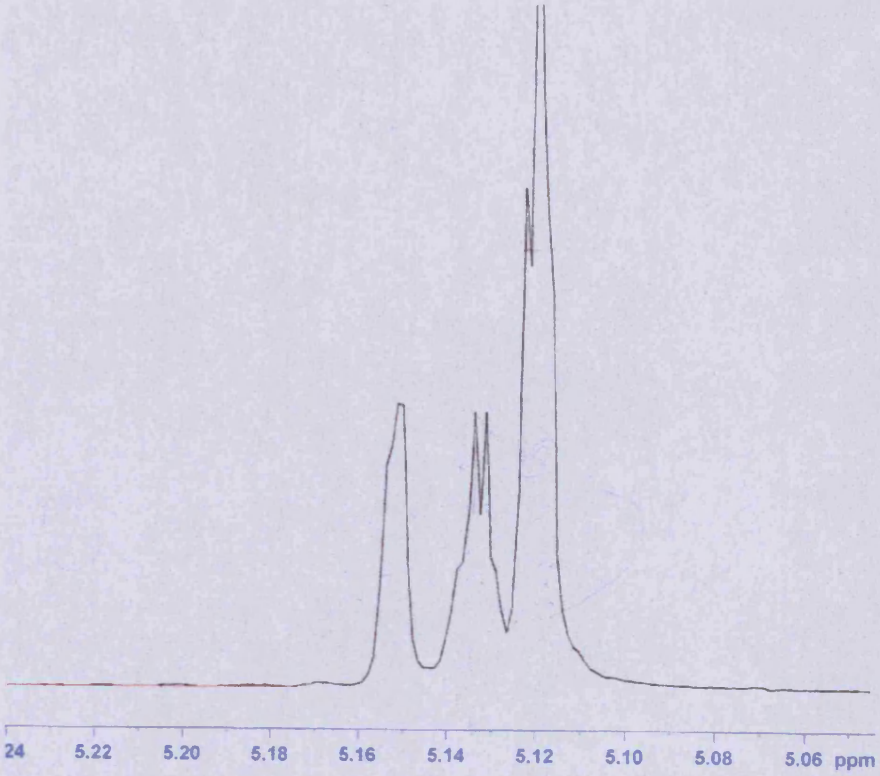

Fig 5.16: ^{1}H-NMR detail of reaction products of 1-D-hexyne and DCl. Higher conversion is detected for the deuterated product in comparison with fig 5.15

In contrast with the experiment where DCl was used, here it is possible to observe that the deuterated product is the major one, and this is in agreement with the assumption of isotope effect on DCl that in this test is absent.

However, a more detailed analysis of the reaction product obtained, lead surprising to observe that the deuterated species detected when D-Hexyne is used is the same when DCl was used (^{1}H-NMR spectra in figures 5.17 and 5.18) using a 500 MHz frequencies.

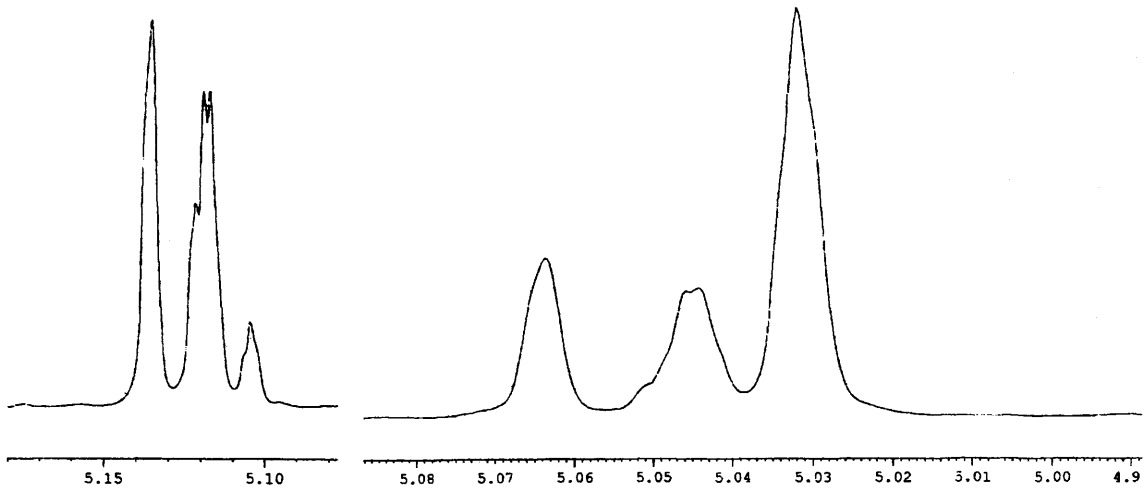

Fig 5.17: ^{1}H-NMR 500 MHz detail of the Markovnikov product for the reaction of 1-hexyne/DCl

Fig 5.18: ^{1}H-NMR 500 MHz detail of the Markovnikov product for the reaction 1-D-hexyne/HCl. Apart from a higher amount of deuterated product, this reaction led to the same products shown in fig 5.17

This is quite surprising because, if pure *anti*-attack of HCl/DCl was involved, it should be expected that different isomers should be obtained using DCl or D-hexyne, as reported in scheme 5.11.

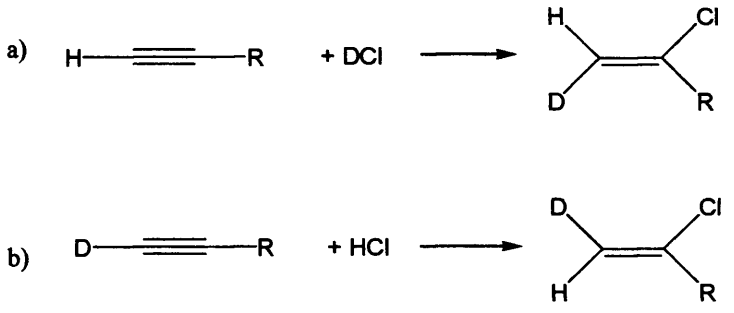

Scheme 5.11: Expected isomer for the Markovnikov product using a) hexyne/DCl and b) D-hexyne/HCl. If *anti* addition is operating deuterium in the two different positions should be obtained.

While the product obtained is in both cases a) with D and Cl in *trans* position. In order to explain this unexpected result, it has to be assumed the existence of a H/D exchange equilibrium, as shown in scheme 5.12:

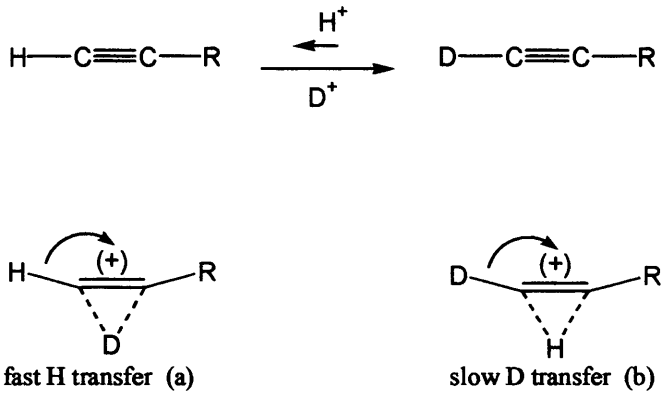

Scheme 5.12: Hypothesis of exchange equilibrium between H and D on triple bond. If D is already present on the substrate it could be possible to propose a slow transfer process for H exchange.

With a fast H transfer, and a slow D transfer, if H and D are already initially present on the substrates, this could be an alternative explanation because when D-Hexyne is used the deuterated product is the major one. In addition for this kind of equilibria the role of the terminal alkyne is fully evident, and no or negligible reaction can take place if a secondary hexyne is present.

5.4.3 Hydrochlorination of phenyl-acetylene using deuterated hydrochloric acid

An attempted hydrochlorination of phenyl acetylene using DCl/ether has been carried out, but the reaction did not occur. This can be assumed as additional evidence of an isotope effect operating, suggesting that the rate-determining step of the reaction is cleavage of the H-Cl bond. However, further considerations can be done. If the mechanism involves an asymmetric orientation of the triple bond using the acidity of the terminal proton, the reaction should be favoured by the presence of a phenyl group, which is an electron-withdrawing group. Nevertheless, there are likely to be two different effects operating, maybe the initial approaching step is favoured, but the exchange reaction when deuterium is present could be slower in comparison with 1-hexyne, so at the end no reaction occurs.

However, independent from the real sequence of molecular steps, all these data are in agreement with a cooperative effect of the organic substrate, and hydrochloric acid.

In conclusion, due to the presence of traces of water, information on the *cis/trans* isomerism is partially lost; on the other hand, the presence of the equilibrium with a H/D exchange is possible only with the presence of a terminal alkyne. And it has been shown that: i) interaction with the metal substrate cannot be a pure π-coordination and ii) σ-coordination has been observed for Au(I) species, and this could be indirect evidence for the presence of this gold species in the catalytic cycle, as assumed in scheme 5.1. Nevertheless, all the data reported are consistent with a reaction that occurs *via* complex formation.

5.5 Molecular modelling investigations on formation of C_2H_2/Au/HCl complex

In order to have more detailed information on a possible mechanism operating at the molecular level on Au surface, a molecular modelling study has been carried out.

In the mechanism proposed in paragraph 5.2 $AuCl_4^-$ has been considered as the active species i.e. a species that can be directly obtained from the precursor $HAuCl_4$. Although the proposed mechanism is possible, molecular modelling investigations using $AuCl_4^-$ could lead to some complications due to the presence of a negative charge. Moreover, we were also interested to take into account the effect of the support. For this reason the molecular geometry studies have been performed assuming $AuCl_3$ as active species. The presence of this species is not excluded by the XPS data described in this chapter and in chapter 4. In addition, if a supported species is taken into account it is more reliable to propose the existence of $AuCl_3$ rather than $AuCl_4^-$, in other words for the effect of the support it is assumed that there is a neutral charged gold species on the support surface. Nevertheless, attention to the geometry and proton exchange of $HAuCl_4$ has also been taken into account, due to the possibility of proton transfer operating at a molecular level and proton transfer is present in scheme 5.2.

5.5.1 Geometry and formation of Au/C_2H_2 complex

The first step was the calculation of the energy levels of the reacting species, which are: $AuCl_3$, C_2H_2 and HCl taken separately. Density functional theory calculations was applied to determine geometries and energy levels. Using a 6-31G data set base the following energies values in Hartees have been obtained: $AuCl_3$: -1516,36; C_2H_2: -77,33 and HCl: -460,8 (1kJ mol^{-1}=2625.5 Ha)

Using this starting point, the first step was to calculate the energies and the geometry of a gold acetylene complex and the result is reported in figure 5.19

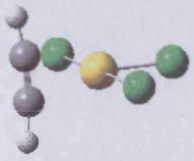

Fig 5.19: Initial Au/C_2H_2 complex formation.
Yellow=Au; green= Cl; grey=C; white=H

It is quite evident distortion of the C-H angle is an effect of π-interaction between Au(III) and the triple bond, in addition it is worth noting that acetylene does not stay in a position perpendicular to the plane identified by $AuCl_3$. This is not an artefact of the calculation, but is a consequence of the lower high-field energy of gold when compared with platinum metal group metals [13]. For this complex an energy level of –1593.73 Ha has been calculated which leads to a stabilization of –100.02 kJ mol^{-1} when compared with the energy level of $AuCl_3$ and C_2H_2.

However, if the distance Au-C is slightly decreased, as assumed for a reaction, this is not the most stable geometry and a twisting motion is observed leading to a metallacycle unit as shown in figure 5.20 below.

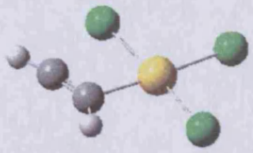

Fig 5.20: Metallacycle complex after approaching and twisting of the initial complex in fig 5.19

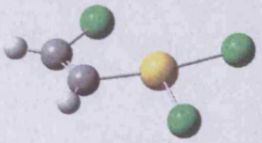

Fig 5.21 Metallacycle complex and VCM precursor formation from the metal-cycle unit in fig 5.20

In addition, it is possible to observe a Cl transfer from Au to C, leading to a precursor of vinyl chloride monomer (fig 5.21). A pathway like this is not able to lead to the final product, however it is important because it shows the possibility of Au(III) activating the triple bond, moreover it does not exclude the possibility that this pathway could be operating as well, especially when DCl is used.

5.5.2 Geometry and formation of Au/HCl complex

The second step to consider is the $AuCl_3$/HCl interaction. It is evident that the immediate interaction leads to $HAuCl_4$. However, the geometrical considerations are not trivial.

H and Cl have not a linear geometry along the H—Cl—Au axis but hydrogen is almost orthogonal, as displayed in the figure 5.22 below:

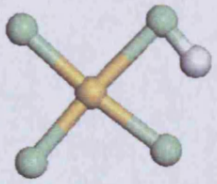

Fig. 5.22 Geometry of $HAuCl_4$, distortion of Au-Cl-H is present

In this case the phenomenon is not an artefact, but is due to two effects. The first is the low high-field energy of gold as noted for the Au/acetylene complex, the second is the

hydrogen bond interaction of the H between the two chlorides, and in this case this is the dominant effect, leading also to a distortion of the Au-Cl bond. This effect has been examined because it could be involved in product formation (see next paragraph), and the energy barrier of H transfer among chlorides has been determined to be around 10 kJ mol $^{-1}$. An energy level diagram is shown in scheme 5.14.

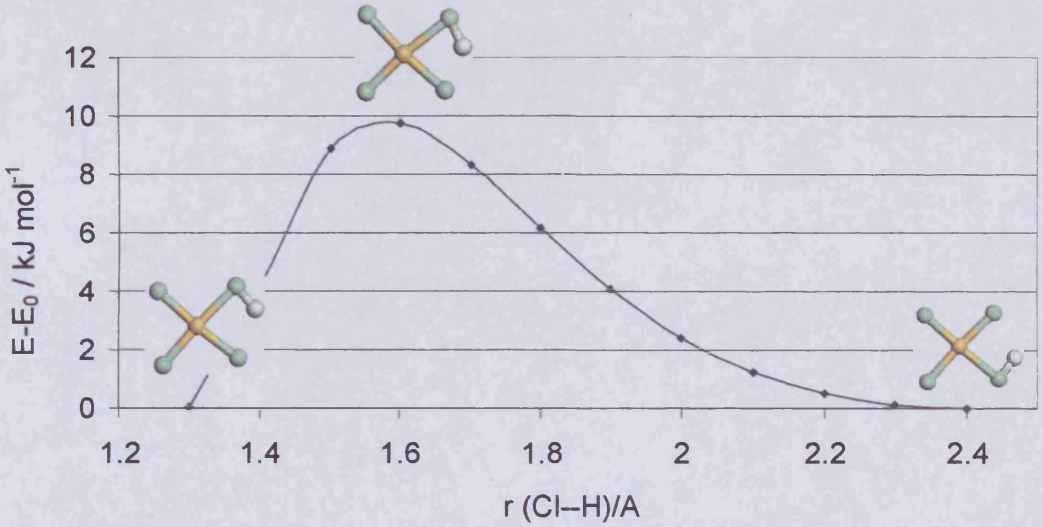

Scheme 5.14: Energy barrier of the proton transfer among chlorides in $HAuCl_4$

5.5.3 Formation of C_2H_2/Au/HCl and proposal of reaction pathway

Taking into account these results, the effect of HCl has been considered separately and interesting results obtained. Assuming a coordinate action of both HCl and C_2H_2, the effect of the approaching of HCl to the π-Au/Acetylene complex has been considered. The initial geometry is shown in figure 5.23.

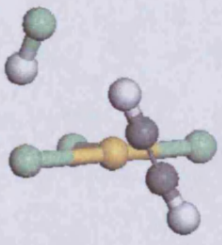

Fig. 5.23 Initial geometry of the C_2H_2/Au/HCl complex

It is possible to observe that HCl is quite far from the π-Au/C_2H_2 complex, with a Cl—C distance over 3.5 Å. Consequently, it could be more appropriate for this initial step to talk about an approach of HCl to a pre-formed Au/C_2H_2 complex. However, if this distance is used it is possible to calculate an energy of –2054.54 Ha, which, when compared with the energy level of the reagents, leads to a stabilization of 40 kJ mol^{-1}. In other words, the proximity effect of HCl is stabilizing the preformed Au/acetylene complex. This result is quite important and can explain, in a completely different way, the observed activation effect of HCl on Au/C catalysts. In paragraph 5.1 and 5.2 the effect of HCl can be explained by a species able to induce more Au(III), which has higher reactivity. While in this case the role of HCl is to stabilize the initial complex formation, and this could explain the effect observed in figure 5.6.

In order to simulate the reaction, the Cl—C distance was reduced, a destabilization was observed, with a transition state that consist of closer HCl. However, if cleavage of HCl is induced it is possible to observe the formation of a metallacycle unit, which is more stable than the initial complex, suggesting a possible pathway reaction, as shown in scheme 5.15.

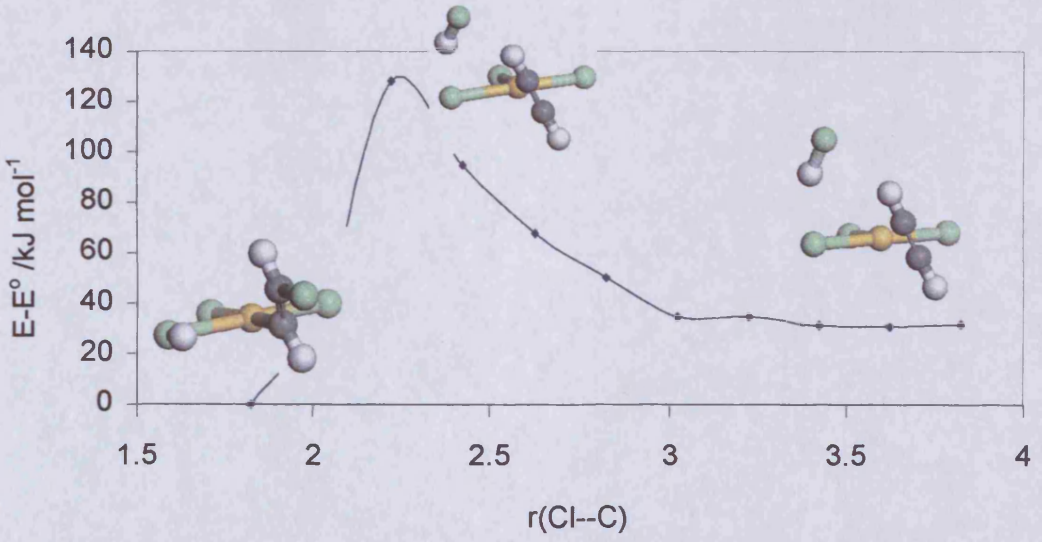

Scheme 5.15: Energy barrier to the approach of HCl to Au/C_2H_2 π- system and intermediate formation.

It is significant that the final intermediate obtained is a *trans* isomer, and this is consistent with the proposed mechanism and the experimental observations. The metal-cycle species obtained at the end of these steps requires proton transfer. Investigations in this area have been carried out, however, it has not been possible so far to identify a steady state, as reported in scheme 5.16 where proton transfer among chlorides on the metallacycle unit is investigated for the *cis* isomer.

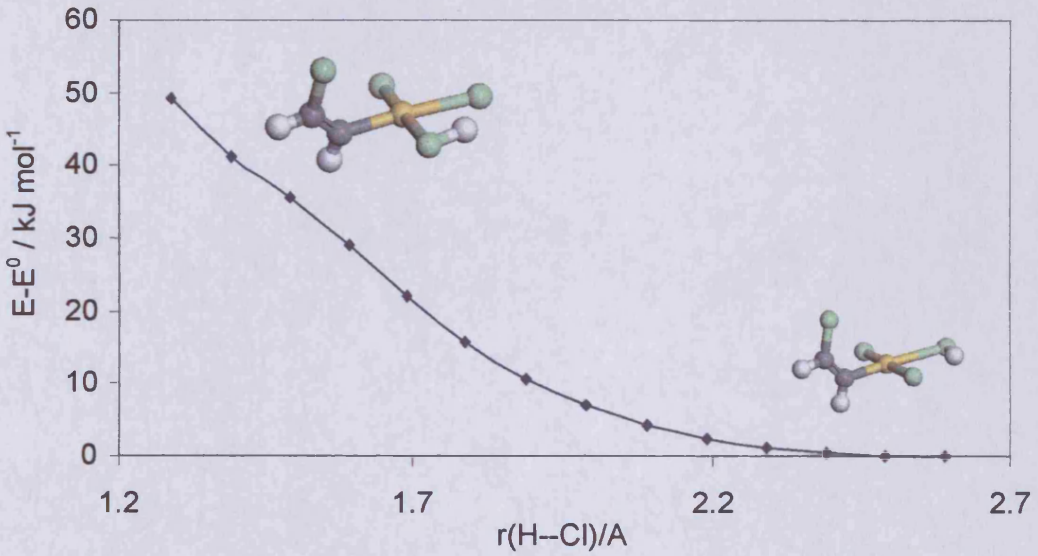

Scheme 5.16: Potential energy of states (PES) for the proton transfer among chlorides on the planar gold metallacycle intermediate $AuCl_3H\text{-}C_2H_2Cl$

This molecular modelling investigation, does not sufficiently explain the last step of the reaction and consequent desorption. Nevertheless, it is quite helpful because it clarifies the possible nature of the proposed complex, and it shows clearly the effect of HCl on activation and regeneration of the catalyst, although in a different way when compared with the other model proposed (paragraph 5.2) where $AuCl_4^-$ is used instead of $AuCl_3$.

5.6 Conclusions

The investigations carried out on the nature and performance of Au/C catalyst towards the hydrochlorination reaction of acetylene lead to the conclusion that the Au(III) species is very likely to be the one responsible for the catalytic activity. It should be noted that a short treatment of the catalyst with aqua regia is not able to dissolve the gold, but regenerates the catalyst. A regeneration effect can also be obtained *in situ*, using HCl. The catalyst behaviour and the activation role of HCl and the deleterious effect of C_2H_2 on catalytic performance lead to the conclusion that a redox cycle Au(III) ↔ Au(I) could be operating, involving the formation of a gold complex.

The work discussed can be considered as the first example of a detailed study of acetylene gold complexes on heterogeneous gold catalysts.
When gold is used with substrates containing triple C-C bond it can be considered as a catalyst of exceptional selectivity, having observed for all the substrates investigated selectivity of almost 100% towards the mono-chlorinated product and always greater than 95% towards the Markovnikov products when different organic substrates have been used.
Experiments using deuterated substrates have clearly displayed the presence of an isotope effect involving the cleavage of H-Cl bond, which can be considered as the rate-determining step of the reaction

The experimental evidence, the role of the reagents and the observed exchange reactions when deuterated substrates are used, do not provide final proof for this pathway, although they are all strongly support it.

Molecular modelling investigations are also supportive of the hypothesis of complex formation, even if a different route involving $AuCl_3$ is used in order to simulate the effect of the support. Although the mathematical model is not able to provide an efficient desorption process, which on the other hand could be in agreement with the formation of oligomers on the catalyst surface, it can explain the role of HCl in terms of stabilization

of an initial Au/acetylene complex, as well as the reaction, and the catalyst regeneration.

However, it should be remarked that the formation of a carbocation intermediate cannot be excluded with the data up to now available. In fact, an oxidative addition pathway leading to an octahedral complex could also explain the regenerating effect of HCl, the predominance of Markovnikov products as well as the lower activity to higher alkynes.

5.7 References

[1] G. J. Hutchings, *Catal. Today,* 11, **72**, 2002

[2] A. I. Gel'bshtein, G. G. Shcheglova and A. A. Homenko, *J. Catal.*, 110, **3**(1), 1964

[3] B. Nkosi, N.J. Coville, G.J. Hutchings, M.D. Adams, J. Friedl and F.E. Wagner, *J. Catal.*, 366, **128**, 1991

[4] A.I. Gel'bshtein, G.G. Shceglova and A.A. Khomenko, *Kinetic. Catal.*, 543, **4**, 1964

[5] B. Nkosi, M. D. Adams, N. J. Coville and G. J. Hutchings, *J. Catal.*, 378, **128**, 1991

[6] S. A. Mitchenko, E. V. Khomutov, A. A. Shubin and Y. M. Shul'ga, *J. Mol. Catal. A*, 345, **212**, 2004

[7] R. M. Silverstein and F. X. Webster, *Spectrometric Identification of Organic Compounds* (VI Ed.), John Wiley and Sons, Inc., New York 1998

[8] A. S. K. Hashmi, *Gold Bull.*, 3, **36**(1), 2003

[9] H. Schmidbaur, A. Grohmann and M.E. Olmos, *Gold: Progress in Chemistry, Biochemistry and Technology* (Ed. H. Schmidbaur), Wiley, 1999

[10] D. M. P. Mingos, J. Yan, S. Menor and D. J. Williams, *Angew. Chem. Int. Ed.*,1894, **34**, 1995

[11] D. Schneider, A. Schier and H. Schmidbaur, *J Chem. Soc., Dalton Trans.*, 1995, 2004

[12] S. Bolvig, P. E. Hansen, H. Morimoto, D. Wemmer and P. Williams, *Magn. Reson. Chem.*, 525, **38**, 2000

[13] S. Al-Jibori, C. Crocker, W. S. McDonald and B.L. Shaw, *J. Chem. Soc., Dalton Trans.*, 1572, 1981

CHAPTER 6: OXY- AND HYDRO- CHLORINATION REACTIONS OF DOUBLE C-C BONDS CONTAINING SUBSTRATES

6.1 Introduction

The most promising catalysts for hydrochlorination of molecules containing triple bonds have been tested towards the hydrochlorination of ethylene, and subsequently tested for the oxychlorination reaction. Gold supported on metal oxides have been investigated for the oxychlorination reaction and finally identification of the active chemical species involved and the real nature of this reaction has been elucidated.

Indeed, it has been possible to observe that even over metal oxide catalysts oxychlorination does not occur, but hydrochlorination does. Moreover, although Au is able to affect the final performance in terms of selectivity, the active species responsible for the activity has been identified as $ZnCl_2$ from the support.

6.1.1 Industrial manufacture and uses of chloroethane

When this reaction is carried out in one pot it involves the direct reaction of ethylene and hydrochloric acid in a temperature range 130 ° – 250 °C, at a pressure around 1 bar, and the use of $AlCl_3$ as catalyst [1]. Industrially the process has a good efficiency, however safety related problems can be encountered due to the properties of $AlCl_3$. In fact, if traces of water are present, $AlCl_3$ can easily hydrolyse, and if this parallel reaction goes out of control, it can be potentially explosive [2]. This has stimulated the interest to look for other catalysts that are able to carry out the reaction under safer conditions, as well as using a smaller amount of active species. Indeed the role of $AlCl_3$ is to act as a Lewis acid, but the amount required to carry out the reaction is close to stoichiometric [3].

Further industrial routes used to manufacture chloroethane are:

a) pyrolysis of ethanol (in the presence of HCl)
b) addition reaction between CH_2=CH_2 and Cl_2
c) byproduct of polyvinylchloride manufacture

However, it worth mentioning that pyrolysis and chlorination reactions are nowadays no longer economical [4].

Chloroethane has a wide range of applications; nowadays the most important is as a treatment agent of cellulose to manufacture ethyl-cellulose, with an annual production of some thousands of tons per year [5]. It has to be remembered that chloroethane has been used for years, for the manufacture of tetraethyl-lead, the most used anti-knock additive for gasoline with an average production around 10 millions of tons per year [5]; it has been replaced by methyl ter-butil ester [6].

6.1.2 Industrial manufacture and uses of 1,2-dichloroethane

1,2 dichloroethane is a chemical that finds applications such as: additive for paints, coatings and adhesives, extraction of oil from seeds, treating animal fats and processing of pharmaceutical products as well as in the manufacture of grain fumigants [7]. However, nowadays around 60% of 1,2-dichloroethane is used as the precursor for the manufacture of vinyl chloride monomer using the balance process mentioned in chapter 4 (paragraph 4.1.2) [8].

Industrial routes for the manufacture of 1,2-dichloroethane are:
a) direct ethylene chlorination:

$$CH_2=CH_2 + Cl_2 \rightarrow C_2H_4Cl_2 \qquad \text{(eq. 6.1)}$$

b) the oxychlorination reaction:

$$CH_2=CH_2 + 2\ HCl + 1/2\ O_2 \rightarrow C_2H_4Cl_2 + H_2O \qquad \text{(eq. 6.2)}$$

The route shown in eq. 6.2 is the most used industrial process. Industrially it is carried out using pressure and temperature in the range of 1.5 to 4.5 bar and 200°C to 315°C, respectively, and with catalysts including ferric, aluminium, cupric, and antimony chlorides, with a reactant ratio C_2H_4 : HCl : O_2 in the range 1 : 2 : 1 [7]. One the most recent patents for this reaction (2005) involves the use of a Cu/Mg catalyst supported on alumina with a reactant ratio of C_2H_4 : HCl : O_2 = 1.07 : 2 : 0.7 and reaction temperature of 220 °C. [9]

Concerning the nature of the reaction product, 1,2-dichloroethane, it is worth mentioning that it decomposes slowly when exposed to air, moisture and light, forming hydrochloric acid and other corrosive products [7]. The decomposing liquid becomes darker in colour and progressively acidic, leading to the production of 2,2,2-trichloroaldehyde (commercially known as chloral). These properties are reported here because they have been useful in order to identify the real reaction products from the tests carried out.
The reactivity of 1,2-dichloroethane can be explained by the ease with which hydrogen chloride can be removed to form vinyl chloride with the application of heat, a property which is indeed the principle of the balance process.

6.2 Experimental for hydro- and oxy- chlorination reactions of ethylene

6.2.1 Catalyst preparation

A wide number of catalysts has been prepared and investigated for different oxy- and hydro-chlorination reactions.

The catalysts investigated first, were gold on carbon previously used in hydrochlorination of acetylene (for the preparation see paragraph 4.2.2) and the Au/TiO_2 catalyst described in chapter 3.

6.2.1.1 Preparation of Au/MO_x *via* deposition precipitation

ZnO (Aldrich, 3.0 g) was stirred in distilled water (150 mL), and $HAuCl_4 \cdot xH_2O$ (Strem 62 mg, assay 50.14% in 10 mL water) was added dropwise over 2min, in order to have a final Au loading of 1% wt. The slurry was then heated to 80 °C and the pH adjusted with the addition of a saturated Na_2CO_3 solution in order to reach a final pH 9 value, and stirred for a further 1 h. After cooling, the slurry was filtered using approximately 4L of distilled water. The solid was then dried at 120 °C for 16 h.

The same sequence of operation, and amount of reagents, was followed for the preparation of the catalysts: Au/CeO_2, Au/La_2O_3, Au/Al_2O_3, Au/SiO_2, and Au/MgO. For this last catalyst the Au loading was 3%.

All catalysts were prepared also calcined, in these cases, the solid was heated in static air at 400 °C for 4 h.

6.2.1.2 Au/ZnO and Au/MgO *via* co-precipitation

The precursor $Zn(NO_3)_2 \cdot 6H_2O$ (Aldrich, 7.3 g) was dissolved in distilled water (150 mL), and $HAuCl_4 \cdot xH_2O$ (Strem 41 mg, assay 50.14%, in 10 mL water) were added dropwise over 2 min, in order to have a final Au loading of 1% wt. The solution was then heated to 80 °C and the pH adjusted with the addition of a saturated Na_2CO_3 solution in order to reach a final pH 9 value, and stirred for 3 hours. The resulting precipitate was then filtered and dried 16 h at 120 °C.

The same procedure to prepare co-precipitated Au/MgO, but using $Mg(NO_3)_2 \cdot H_2O$ as precursor. Both catalysts were also calcined, the solids have been heated in static air at 400 °C for 4 h.

6.2.1.3 Au/ZnO/SiO_2 *via* co-precipitation and deposition precipitation

To prepare this catalyst, the co-precipitation technique has been used to obtain ZnO/SiO_2. On this support, and after calcination, the deposition-precipitation technique has been used in order to obtain the final product.

The precursor $Zn(NO_3)_2 \cdot 6H_2O$ (Aldrich, 14.6 g) was dissolved in a slurry containing distilled water (250 mL) and SiO_2 (Aldrich, 4 g). The amount of precursor was calculated in order to have a final ratio ZnO/SiO_2 1:1 wt. The slurry was then heated to 80 °C and maintained at this temperature for 5 h. The obtained solid was then dried for 16 hours at 120 °C and afterwards calcined in static air using a calcination temperature of 500 °C for 5 h.

From the support ZnO/SiO_2 so prepared, a portion was used to prepare Au/ZnO/SiO_2 using the deposition precipitation technique. ZnO/SiO_2 (2 g) was stirred in distilled water (150 mL), $HAuCl_4 \cdot xH_2O$ (Strem 41 mg, assay 50.14%, in 10 mL water) were added dropwise over 2min, in order to have a final Au loading of 1% wt. The slurry was then heated to 80 °C and the pH adjusted with the addition of a saturated Na_2CO_3 solution in order to reach a final pH 9 value, and stirred for a further 1 h.

6.2.1.4 $ZnCl_2/SiO_2$ and $ZnCl_2/Al_2O_3$ *via* impregnation

Two catalysts have been prepared using wetness impregnation technique using water as a solvent. The precursor $ZnCl_2$ was previously dried overnight; afterwards a solution containing an amount of salt to give a final catalyst containing around 15 % wt of Zn was prepared (BDH, $ZnCl_2$, 265 mg per gram of silica). The solution was added to the support (7 mL of solution per gram of silica), and the product obtained was dried for16 h at 80 °C.

The drying temperature can appear to be quite low, however it has been preferred to use this value to dry the catalyst slowly, taking into account the properties of $ZnCl_2$ (which has a melting point of 272 °C) [10] and to ensure a relatively slow evaporation of the

solvent.

An identical procedure was used to prepare $ZnCl_2/Al_2O_3$.

6.3 Hydro- and oxychlorination of ethylene

6.3.1 Hydrochlorination reaction of ethylene over Au/C and Au/TiO_2 catalysts

The most promising catalysts previously investigated for the hydrochlorination reaction: Au/C, Au/Pd 95/5, Au/Rh 90/10 and Au/Ir80/20 have been used to carry out the hydrochlorination reaction of ethylene. However, using reaction temperatures of 180 °C or 250 °C negligible or no reaction products have been observed.

Although the conclusion is that these catalysts are not active for the hydrochlorination of ethylene, on the other hand this fact can be seen as an evidence of the selectivity of gold on carbon towards molecules containing carbon-carbon triple bond only.

Further catalytic tests have been carried out using Au/TiO_2 catalysts with different metal loading (1 and 5% wt) using calcined and uncalcined samples and reaction temperatures between 180 and 250 °C. Also in this case, as for the hydrochlorination reaction of acetylene, no reaction occurs, leading to the conclusion that this catalyst is not suitable when HCl is involved, independent of the substrate used.

6.3.2 Oxychlorination over Au/C and Au/TiO_2 catalysts

The synthesis of vinyl chloride monomer (VCM) was one of the aims of the project, and taking into account that thermal cracking of 1,2-dichloroethane can lead to VCM, attempts at oxychlorination of ethylene were made using the same catalyst tested for hydrochlorination.

Reaction conditions used were temperatures between 180 and 250 °C, a reactant ratio $C_2H_4 : HCl : O_2 = 1 : 2 : 0.7$ using air as the source of oxygen and reactant flows of C_2H_4

and HCl of 5 and 10 mL min^{-1} respectively. However, also in this case negligible activity has been observed, leading to the following summary scheme 6.1 for the $Au/MO_x/C$ catalysts:

Scheme 6.1: Activity summary of Au and Au bimetallic catalysts ($Au/MO_x/C$) towards hydrochlorination and oxychlorination reaction

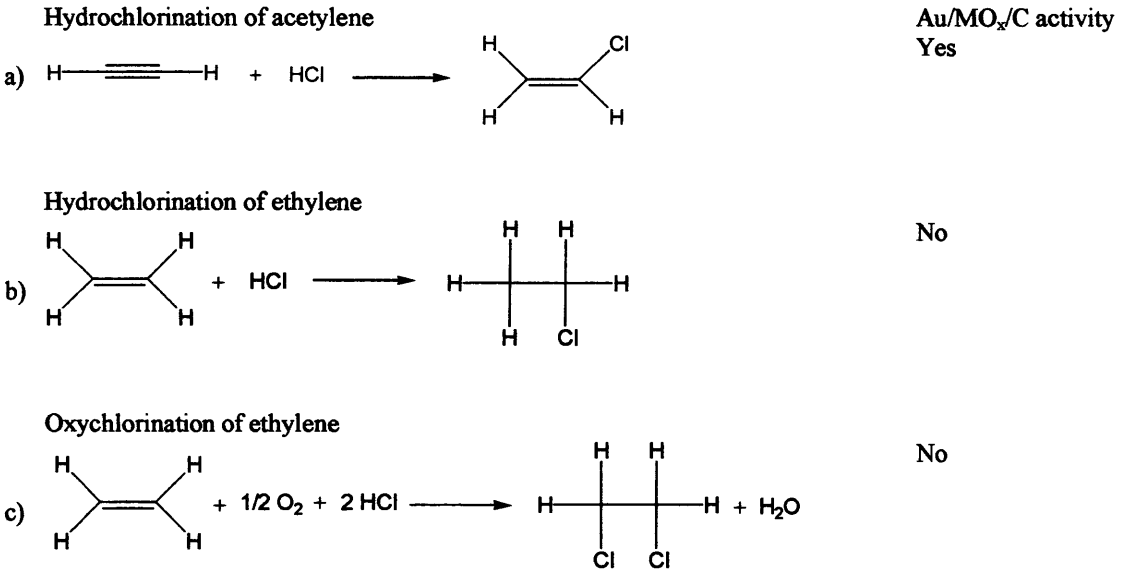

6.3.3 Oxychlorination reaction over Au supported on metal oxides catalysts

In consideration of the industrial importance of the oxychlorination reaction, and its link with VCM manufacture, further investigation using Au supported on metal oxide has been carried out, having previously found that carbon was a not suitable support for this reaction.

For this reason catalysts such as Au/MgO (3% wt), and Au/ZnO (1% wt), known to be good oxidation catalysts [11, 12], have been prepared and tested. Both catalysts were prepared using deposition precipitation techniques, as described in paragraph 6.2.1.1

Using the experimental conditions specified in paragraph 6.3.2 the catalytic test gave the results displayed in figure 6.1:

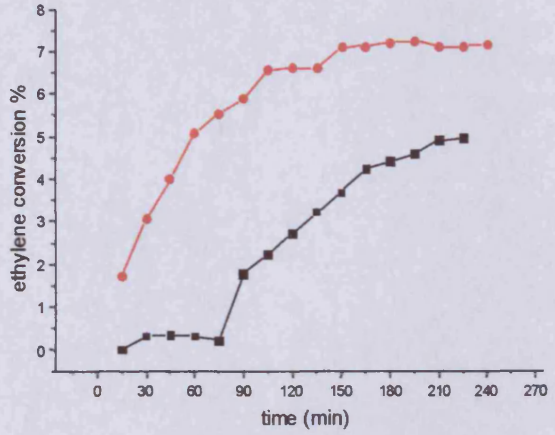

Fig. 6.1: Oxychlorination reaction of ethylene, conversion trend over (•) Au/ZnO and (■) Au/MgO

An appreciable activity was detected, moreover the conversion trend observed is quite important: low at the beginning, subsequently increasing to a steady state. A trend like this can be explained by the basic properties of the supports. In addition, MgO, which is the more basic support, initially does not display any activity. It is reasonable to postulate the presence of an activation step by HCl, which reacts with the oxide to give a metal chloride species on the surface, and afterwards reaction takes place. It seems significant to note that both catalysts, after reaction, appear quite different in colour and mechanical consistency, leading to the formation of $ZnCl_2$ and $MgCl_2$. Experimental evidence will be shown later for Zn (paragraph 6.4).

As a consequence of the trend observed in figure 6.1, a more systematic study of the effect of basic supports on the reaction has been undertaken. Gold catalysts over different supports have been prepared and they are summarized in the table 6.1.

Table 6.1: Summary of Au on metal oxides catalysts tested for oxychlorination reaction of ethylene

Catalysts	Catalysts	Support or precursor
Au/Al_2O_3 D.P.	Au/Al_2O_3 D.P. calcined	Al_2O_3
Au/CeO_2 D.P.	Au/CeO_2 D.P. calcined	CeO_2
Au/MgO C.P.	Au/MgO C.P. calcined	$Mg(NO_3)_2{\cdot}6H_2O$
Au/La_2O_3 D.P.	Au/La_2O_3 D.P. calcined	La_2O_3
Au/ZnO C.P.	Au/ZnO C.P. calcined	$Zn(NO_3)_2{\cdot}6H_2O$

The results of the catalytic tests carried out are reported below in figure 6.2. The reaction conditions used were: a temperature of 250 °C, a reactant ratio of O_2 : C_2H_4 : HCl = 0.7 : 1 : 2 and a HCl flow of 10 mL min^{-1}

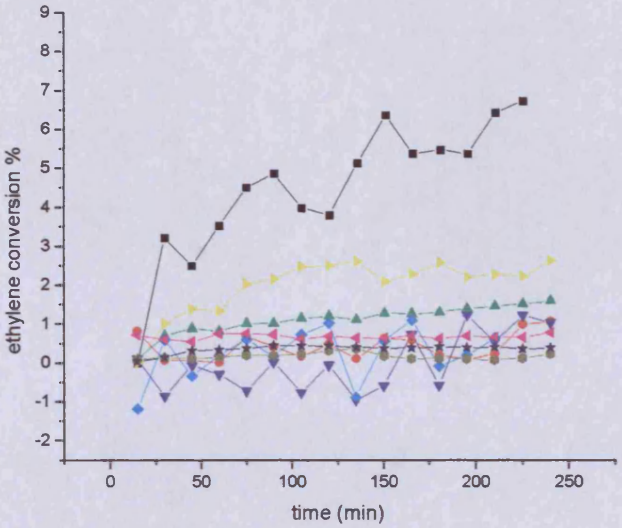

Fig. 6.2 : Oxychlorination of ethylene and ethylene conversion over Au/MO_x catalysts. (■) Au/ZnO DP, (●) Au/CeO_2 DP, (▲) Au/La_2O_3, (▼) Au/MgO CP, (♦) Au/MgO CP clc, (◀) Au/ZnO CP clc, (▶) Au/Al_2O_3 DP clc, (●) Au/CeO_2 CP clc, (*) Au/ZnO CP
Where: DP= deposition precipitation; CP= co precipitation; clc= calcined; all catalysts have a gold loading of 1%

In this series, the catalyst Au/ZnO obtained using deposition-precipitation (DP) was used as a reference catalyst to compare with the other catalysts. The catalysts Au/MgO co-precipitated (CP), Au/MgO CP calcined, Au/ZnO CP and Au/CeO_2 DP calcined, do not display any activity and conversion over Au/La_2O_3 DP was negligible.

Au/ZnO DP and Au/Al_2O_3 displayed similar behaviour, with low conversion, while for all the other catalysts tested, massive formation of polymerisation products was observed. However, although a conversion trend is clearly observed, at least for the Au/ZnO catalyst, it raised the problem that identification of the expected product 1,2-dichloroethane, was ambiguous. In fact, 1,2-dichloroethane was not directly identified from the chromatograms. Initially, this lack of identification has been ascribed to an *in situ* consecutive reaction on the catalyst surface. Industrially this is a known problem, like the formation of the byproduct 2,2,2-trichloroaldehyde (commercially known as chloral)

[13]. The by-product chloral is always present if oxychlorination occurs, and it is possible to find patents focused on how to remove it from the reaction environment to increase the catalytic efficiency. Due to its corrosive nature, and the possibility of subsequent reactions, the process is industrially carried out at the exit of the reactor, which is connected to a distillation column [14] in order to separate the products immediately. Several attempts have been made to identify the presence of this byproduct which led to the conclusion that chloral is absent. (for a complete description of characterization tests, see appendix B).

This experimental evidence raises the question as to whether the catalyst is able to perform oxidation reactions when ethylene is used as substrate. For this reason, a catalytic test with a C_2H_4/Air mixture (C_2H_4 : O_2 ratio 1:1) has been performed using a C_2H_4 flow of 5 mL min^{-1}. The results obtained are reported in figures 6.3 and 6.4.

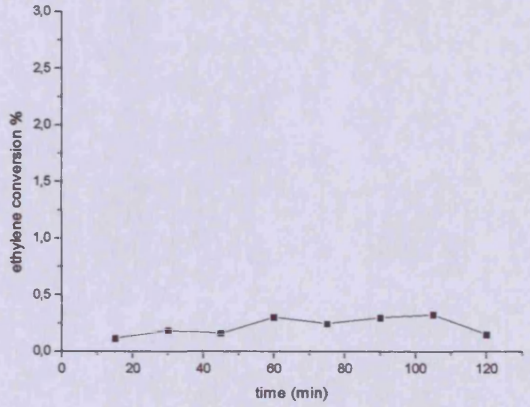

Fig. 6.3: Ethylene conversion toward ethylene oxidation over Au/ZnO catalyst

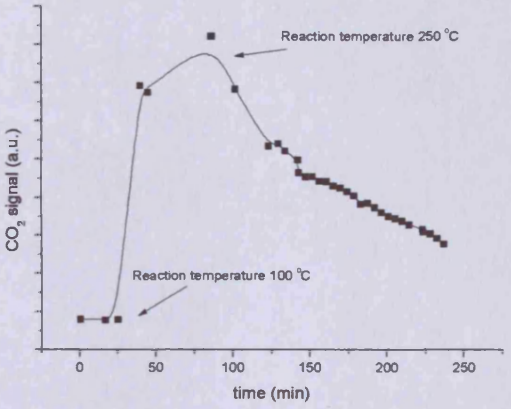

Fig. 6.4: CO_2 production trend with temperature and time on line for the ethylene oxidation reaction over Au/ZnO catalyst.

An almost negligible conversion was detected (fig. 6.3) with CO_2 and H_2O as reaction products. The aspect of interest is the CO_2 produced with time and temperature (fig. 6.4), which evidences an optimal temperature range around 250 °C, which is the same range used to trigger the reaction.

Further oxychlorination tests have been carried out using Au/ZnO/SiO_2 (fig. 6.5) catalyst,

which is known to be a good oxidation catalyst, but also in this case the conversion was poor and 1,2-dichloroethane was not detected.

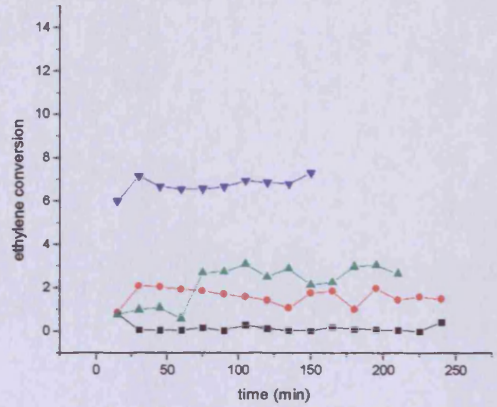

Fig. 6.5 : Activity towards oxychlorination reaction for additional catalysts (■) Au/Al_2O_3 DP, (●) Au/La_2O_3 DP clc, (▲) Au/CeO_2 DP clc and (▼) $Au/ZnO/SiO_2$.

As a consequence of these results, it was decided to do a test in absence of oxygen but with C_2H_4 and HCl in 1:1 ratio, and the results are reported in figures 6.6 and 6.7.

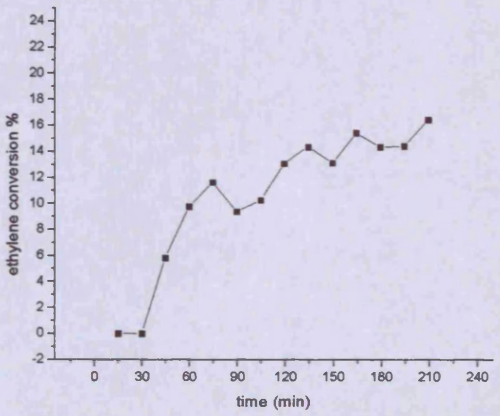

Fig. 6.6: Conversion trend for the $Au/ZnO/SiO_2$ catalyst, hydrochlorination reaction of ethylene; oxygen has been removed

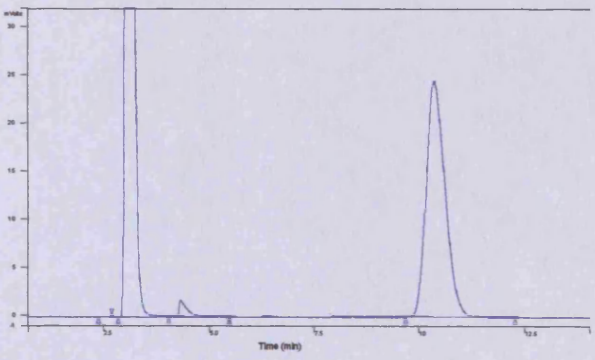

Fig. 6.7: Chromatographic assignment of the products for the test in fig 6.6. C_2H_4 2.1 min, C_2H_4 impurity likely ethane at 3.4 min and chloroethane at 9.4 min

The removal of oxygen from the reaction mixture, led an enhanced activity, which after two hours was about 15%, and this allowed sufficient reaction product to be collected in a chloroform trap to enable an unambiguous characterization. The product was identified as chloroethane and is shown in figure 6.7 (appendix B).

In conclusion, the reaction that actually occurs is not oxychlorination, but hydrochlorination.

$CH_2=CH_2 + HCl \rightarrow CH_3\text{-}CH_2\text{-}Cl$ (eq. 6.3)

A similar result is also obtained using Au/ZnO in the absence of oxygen, as displayed in figure 6.8.

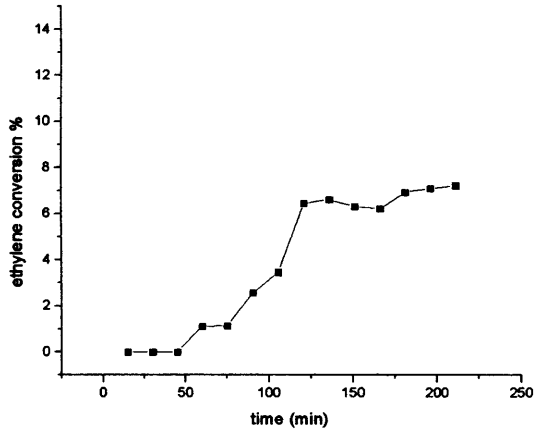

Fig. 6.8: Hydrochlorination reaction of ethylene over Au/ZnO catalyst in absence of oxygen. An increase in activity is observed also for this catalyst

It is significant to note that in both cases, the selectivity can be considered to be virtually 100 % since chloroethane was the only product detected.

However, it is worth mentioning that if the Au/ZnO catalyst is calcined, negligible activity is detected. Although an effect due to different particle size is present, the main effect is due to modification of the support. (For a detailed structure comparison between the calcined and the uncalcined catalyst, see paragraph 6.4.4)

6.4 Chemical behaviour of Au/ZnO catalysts

Since the reaction over Au/ZnO has been identified as hydrochlorination, a more systematic study of this catalyst has been carried out, focusing especially on reactivity and afterwards on its structure.

Also in this case, there has been interest in the study of substrates containing secondary

and ternary carbons atom in order to obtain information on the regioselectivity of the reaction and to propose possible reaction mechanisms.

6.4.1 Hydrochlorination of ethylene and homologues over Au/ZnO

Further substrates investigated include propene and isobutylene. Both these reactants are gases and the reaction was carried out in the usual conditions using a reaction temperature of 250 °C, a reactant flow ratio of 1:1 and a relative inlet pressure of 1.1 bar. It is worth mentioning that in these cases only approximate information has been obtained concerning conversion versus time on line, indicating the catalyst underwent coking. However, the lifetime of the catalyst can be assumed to be at least one hour and in both cases conversion values were observed in the range of 5-7%.
Collecting the reaction products in a chloroform trap for 3 hours, and carrying out GC-MS and NMR analysis (appendix B), it has been possible to obtain detailed information on selectivity. In both cases the Markovnikov products was preferred, leading to traces of 1-chloropropane, the anti-Markovnikov product for propene, and the complete absence of 1-chloro-2-methyl propane when isobutylene was used.

The reactivity of Au/ZnO towards different alkenes can be summarized in scheme 6.2.

Scheme 6.2: Au/ZnO activity versus different alkenes; a) ethylene, b) propene and c) isobutylene. The Markovnikov product is always observed, consistent with the Zn(II) chemistry

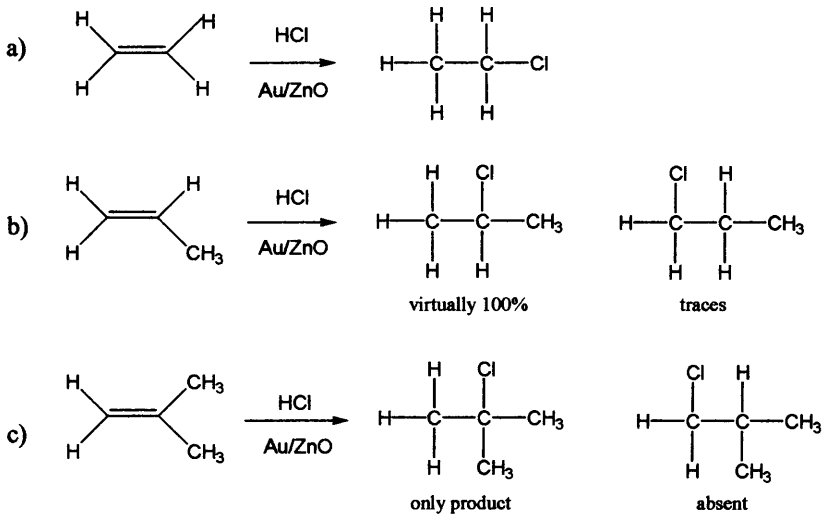

A selectivity trend like this is consistent with the hypothesis of a carbocation intermediate with the organic species previously bonded to a chemical surface and subsequent attack of HCl. However, it should be considered that a chemistry like this is consistent not only with the chemical behaviour of Au(III) but also with Zn(II) [15]. For this reason, further investigation of the reactivity of Au/ZnO has been carried out.

6.4.2 Effect of C_2H_2 and HCl over Au/ZnO towards hydrochlorination reaction of ethylene

In order to identify the effect of each reactant on activity, a series of experiments with inert gas, analogous to that described in chapter 5 on the reactivity of Au/C towards hydrochlorination of acetylene, has been performed with Au/ZnO for the hydrochlorination of ethylene.

The tests carried out using inert gas are shown in the following:

C_2H_4/HCl (2 h) → **He**/HCl (2 h) → C_2H_4/HCl (2 h) (test 6.1)

He/HCl (2 h) → C_2H_4/HCl (2 h) → **He**/HCl (2 h) (test 6.2)

C_2H_4/HCl (2 h) → **He**/C_2H_4 (2 h) → C_2H_4/HCl (2 h) (test 6.3)

He/C_2H_4 (2 h) → HCl/C_2H_4 (2 h) → **He**/C_2H_4 (2 h) (test 6.4)

And the results are reported in figure 6.9:

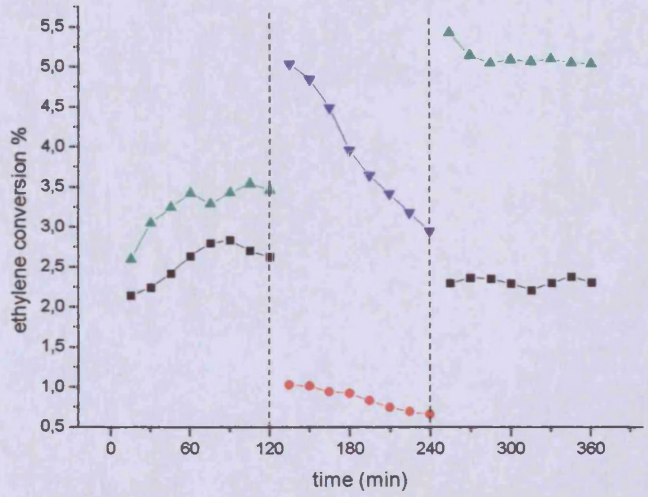

Fig. 6.9: Hydrochlorination of ethylene over Au/ZnO catalyst for each test.
(■) C_2H_4/HCl (2 h) → **He**/HCl (2 h) → C_2H_4/HCl (2 h)
(●) **He**/HCl (2 h) → C_2H_4/HCl (2 h) → **He**/HCl (2 h)
(▲)C_2H_4/HCl (2 h) → **He**/C_2H_4 (2 h) → C_2H_4/HCl (2 h)
(▼) **He**/C_2H_4 (2 h) → HCl/C_2H_4 (2 h) → **He**/C_2H_4 (2 h)

The first observation is that, these trends are almost the opposite for the same series collected for the hydrochlorination reaction of acetylene over gold on carbon catalyst (paragraph 5.1.1).

The most significant test seems to be test 6.3: C_2H_4/HCl→ **He**/C_2H_4→ C_2H_4/HCl. After the step with inert gas and ethylene, the chloroethane formation is improved (whereas for the acetylene reaction this was observed when the intermediate step was He/HCl.

For the similar test 6.1: C_2H_4/HCl→ **He**/HCl→ C_2H_4/HCl), with the intermediate step He/HCl, no significant changes were present.

From the test 6.2: **He**/HCl→ C_2H_4/HCl→ **He**/HCl conversion is obtained, but this is quite poor. This test is useful, if it is true that the conversion trend observed up to now for this catalyst, poor conversion at the beginning and then a steady state, due to modification of HCl to the support, it is also true that HCl alone it is not responsible for this trend.

Finally test 6.4 **He**/C_2H_4→ HCl/C_2H_4→ **He**/C_2H_4 where the pretreatment is He/C_2H_4, the conversion is quite good at the beginning, but decreases with time.

From these experiments, the conclusions are that HCl is responsible for catalyst modification, while C_2H_4 is the chemical species responsible for the activity.

6.4.3 Activity for low temperature CO oxidation of Au/MO_x

In order to find a correlation between the hydrochlorination reaction of C≡C, C=C together with CO oxidation, and to explain the described activity of Au/ZnO and other Au/MO_x catalysts previous prepared these materials have been tested towards low temperature CO oxidation. The results are reported in figure 6.10.

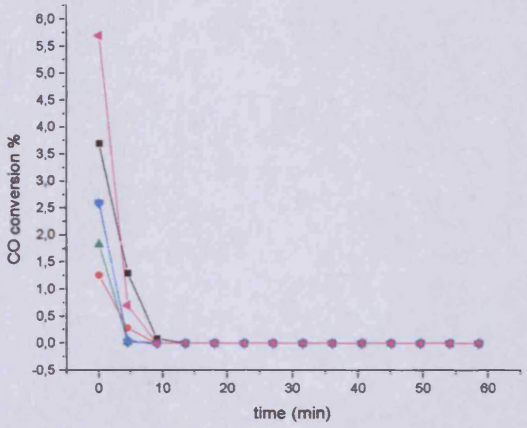

Fig. 6.10: Activity versus time for low temperature CO oxidation over the catalysts: (■) Au/ZnO, (●) Au/ZnO/SiO_2, (▲) Au/ZnO calcined, (▼) Au/MgO, (♦) Au/La_2O_3 and (◄) Au/Al_2O_3

The most important tests were for the Au/ZnO and Au/ZnO/SiO_2 catalysts where it is possible to see they do not display catalytic activity (apart from at the beginning). Taking also into account the activity of Au/C catalyst for hydrochlorination reaction of acetylene and the activity of Au/TiO2 catalysts for CO oxidation, it is possible to write the following table (where 'yes' and 'no' mean activity) in table 6.2.

Table 6.2: Activity of gold catalysts towards hydrochlorination and CO oxidation reactions

Reaction → Catalyst ↓	Hydrochlorination C≡C	Hydrochlorination C=C	Low T CO oxidation
Au/C	Yes	No	No
Au/ZnO	No	Yes	No
Au/TiO_2	No	No	Yes

The reaction trend shown in table 6.2 is quite interesting but if it is assumed that the reactivity is due to gold only, can be considered to be of limited use. Assuming a particle size correlation for the three classes of reaction, with highest Au particle size for hydrochlorination reaction of C≡C and lowest for CO, it is difficult to explain why Au/ZnO, which should be in the middle, is not able to perform the other two reactions, if the activity is due to Au particle size only.

Moreover, if a Au/ZnO catalyst obtained using co-precipitation, instead of deposition precipitation is used, which was not active for ethylene hydrochlorination, it is active towards CO oxidation (fig 6.11).

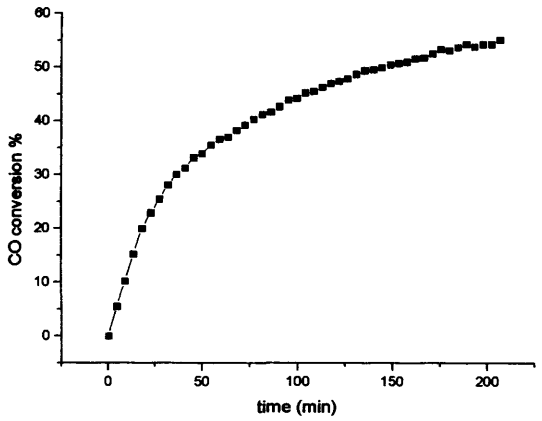

Fig 6.11: Low temperature CO oxidation over Au/ZnO catalyst obtained *via* co-precipitation technique.

Which leads to a further correlation between Au/ZnO catalysts shown in table 6.3:

Table 6.3: Activity of Au/ZnO catalysts towards low temperature CO oxidation as function of the preparation method

Reaction → Catalyst ↓	Hydrochlorination C=C	Low T CO oxidation
Au/ZnO D.P.	Yes	No
Au/ZnO C.P	No	Yes

These tests lead to the conclusion that Au cannot be the responsible for the observed activity, or at least it is not the only active species. In fact, deposition precipitation is not the usual method to prepare gold supported catalysts on ZnO, and taking into account the basic properties of this oxide a hydroxyl containing phase could be obtained.

For this reason a more detailed study of the catalysts used for the hydrochlorination of ethylene has been carried out using XRPD and TEM.

6.4.4 XRPD of Au/MO_x catalysts used for hydrochlorination reactions

XRPD of Au/CeO_2, Au/La_2O_3, Au/MgO and Au/Al_2O_3 compared with the fresh support and calcined samples are reported in figures 6.12, 6.13, 6.14 and 6.15 respectively.

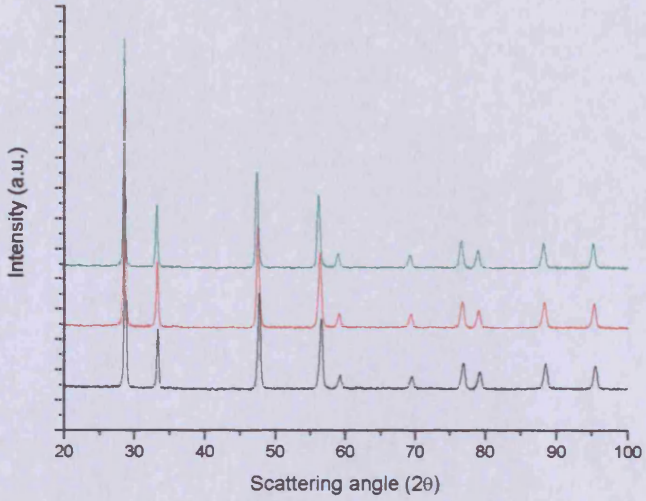

Fig. 6.12: XRPD pattern of (—) CeO_2, (—) Au/CeO_2 DP and (—) Au/CeO_2 DP calcined. Au/CeO_2 No apparent changes in structure were detected.

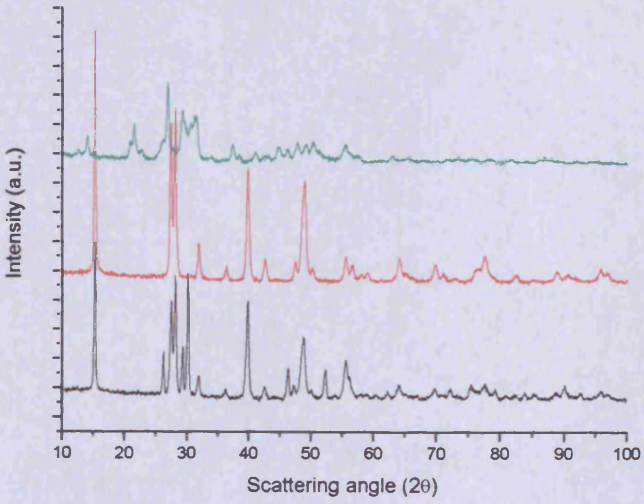

Fig. 6.13: XRPD pattern of (—) La_2O_3, (—) Au/La_2O_3 DP and (—) Au/La_2O_3 DP calcined. Slight modification of the structure of the support after deposition precipitation, but significant loss of crystallinity after calcination.

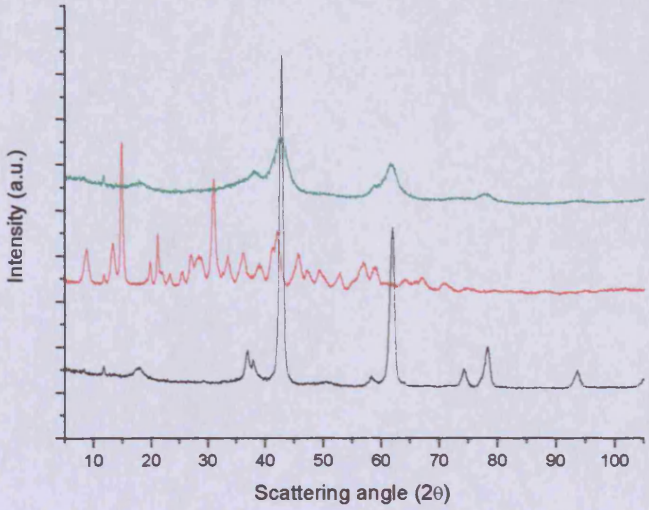

Fig. 6.14: XRPD pattern of (—) MgO, (—) Au/MgO CP and (—) Au/MgO CP calcined. Significant loss of crystallinity after calcination.

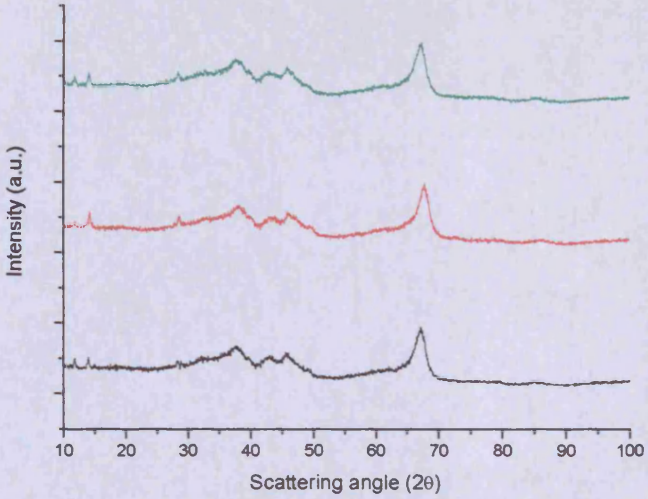

Fig. 6.15: XRPD pattern of (—) Al_2O_3, (—) Au/Al_2O_3 DP and (—) Au/Al_2O_3 DP calcined. An almost amorphous material was always present.

It is not possible to obtain any particular information from these comparisons. Indeed, it is not possible to detect Au peaks (for the positions and intensity of Au reflections see paragraph 3.4), and the thermal treatment leads to modification of the XRPD pattern only for Au/La_2O_3 and Au/MgO catalysts, with a less crystalline final product, but this does not have any influence on final activity. The XRPD of Au/Al_2O_3 remained unchanged but the catalytic activity of it was very low.

The case of Au/ZnO is rather different, and it required a more detailed analysis. In figure 6.16 are reported the XRPD patterns for co-precipitated samples, while in fig 6.17 the XRPD patterns for the deposition-precipitated sample are presented.

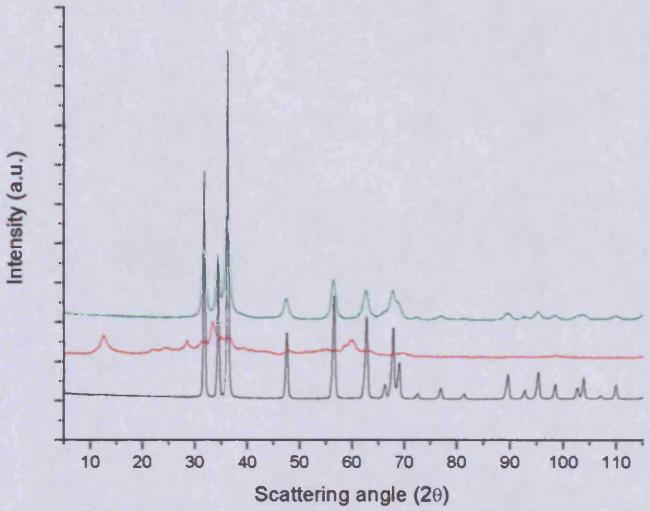

Fig 6.16: XRPD pattern of (—) ZnO, (—) Au/ZnO CP and (—) Au/ZnO CP calcined. A less crystalline final product was obtained.

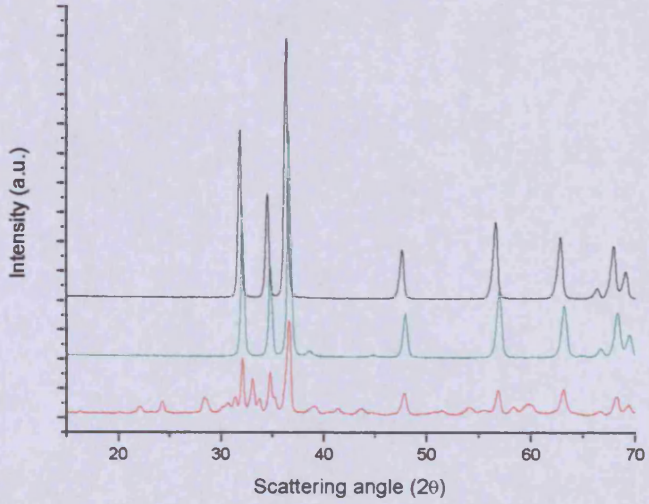

Fig. 6.17: XRPD pattern of (—) ZnO, (—) Au/ZnO DP and (—) Au/ZnO DP calcined. A subset of peaks is present for Au/ZnO before calcination in the region 20-35° 2θ

For the co-precipitated sample a product with a low level of crystallinity was detected, whereas with deposition-precipitated the calcined sample reflected the ZnO structure. For the uncalcined it is possible to observe a subset of peaks in the region 20-35° 2θ, indicating the presence of two different phases.

A comparison with tabulated data [16, 17], led to an assignment of zincite ZnO phase, which is the same for all the samples, while for the subset of peaks in the uncalcined sample these have been identified as the wulfingite phase, which is made by $Zn(OH)_2$.

The presence of two phases in the uncalcined sample and one phase in the calcined is fully evident using TEM diffraction fig 6.18, 6.19 and 6.20

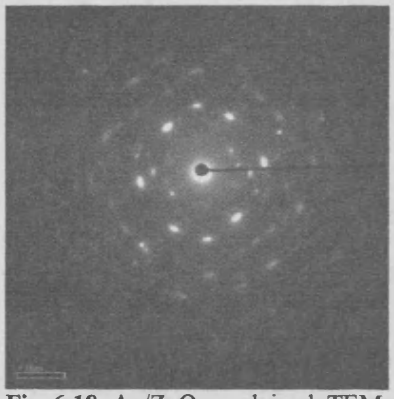

Fig. 6.18: Au/ZnO uncalcined, TEM diffraction pattern phase 1 (zincite)

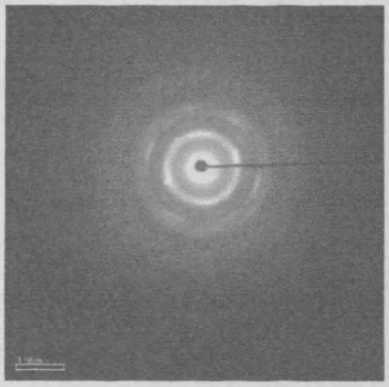

Fig. 6.19: Au/ZnO uncalcined, TEM diffraction pattern phase 2 (wulfingite)

And

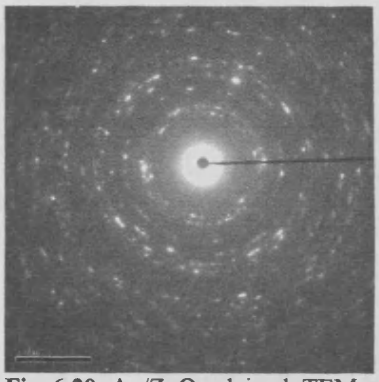

Fig. 6.20: Au/ZnO calcined, TEM diffraction pattern; only phase 1 zincite is present.

Initially the absence of activity for the calcined sample was ascribed to the well known sintering of gold particles at high temperature, but actually the main difference is the absence of $Zn(OH)_2$ for the calcined sample, as evident in the TEM images of figs. 6.21 and 6.22

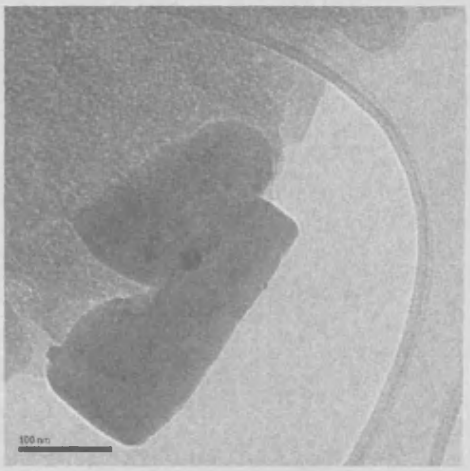

Fig. 6.21: TEM of Au/ZnO uncalcined sample. Two phases present, one is zincite which consists of big particles, while the other, wulfingite consists of very fine material.

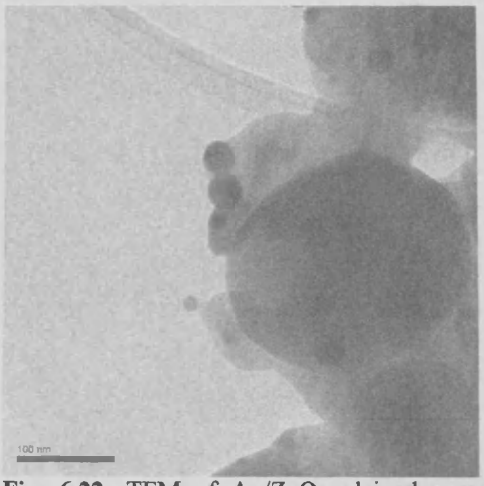

Fig. 6.22: TEM of Au/ZnO calcined sample. Only zincite is present.

The "spotty" TEM diffraction pattern in figure 6.18 and 6.20 is generated from the large crystal of zincite, while the very fine wulfingite is responsible for the circular pattern in figure 6.19 and for the subset of reflections in the XRPD shown in figure 6.17.

The contemporaneous presence of two different phases is also apparent for the $Au/ZnO/SiO_2$ catalyst:

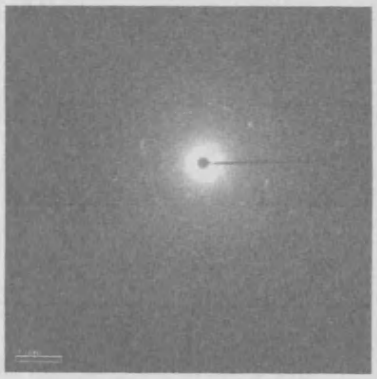

Fig. 6.23: TEM diffraction of $Au/ZnO/SiO_2$. Presence of wulfingite detected.

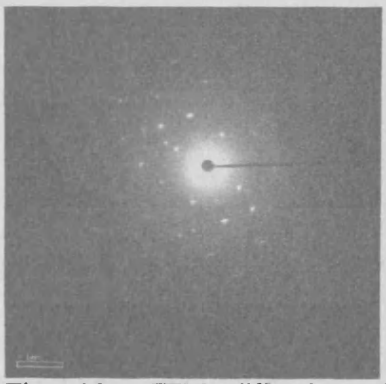

Fig. 6.24: TEM diffraction of $Au/ZnO/SiO_2$. Presence of zincite detected.

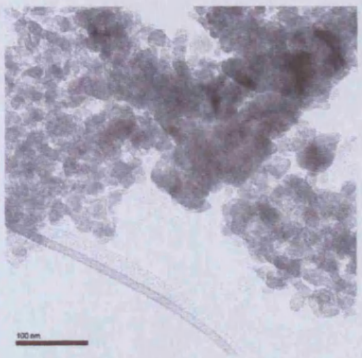

Fig. 6.25: TEM imaging - $Au/ZnO/SiO_2$.

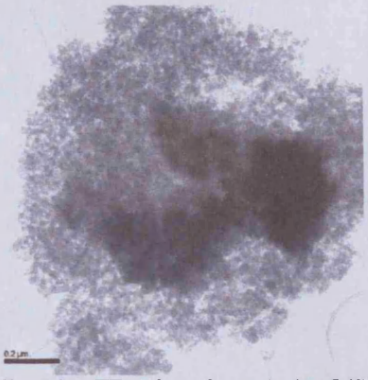

Fig 6.26: TEM imaging - $Au/ZnO/SiO_2$ detail.

If it is assumed that supported $Zn(OH)_2$ is responsible for the activity, this can also explain the conversion trend initially described, where HCl leads to the formation of $ZnCl_2$, and with Zn(II) species like catalytically active centre.

In order to test this hypothesis a catalyst comprising $ZnCl_2$ (15% Zn wt) supported on SiO_2 was prepared and tested. Supported ZnO/SiO_2 was also tested.

The results are reported in fig 6.27. Both catalysts were active and they give chloroethane as the only product.

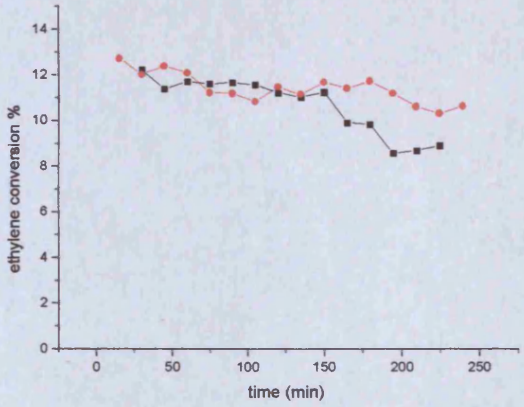

Fig. 6.27: Hydrochlorination reaction of ethylene over (■) ZnO/SiO_2 and (●) $ZnCl_2/SiO_2$

It worth mentioning that tests carried out using ZnO, $ZnCl_2$, and $Zn(OH)_2$ in the bulk state do not lead to any kind of activity, demonstrating that only supported $ZnCl_2$ is

active. It is reasonable to think that as the catalyst is active at a reaction temperature of 250 °C, and the melting point of bulk $ZnCl_2$ is 272 °C, the formation of a supported, almost liquid like layer is responsible for the activity. This can also explain why supported ZnO is active, but not the bulk material. However, the low activity of the bulk materials could also be ascribed to their low surface area if compared with $ZnCl_2$ prepared as dispersed species.

Moreover, in order to test that $ZnCl_2$ is the real species responsible for the activity, a supported Al_2O_3 catalyst has also been prepared, and it displays an activity similar to $ZnCl_2/SiO_2$; see figure 6.28

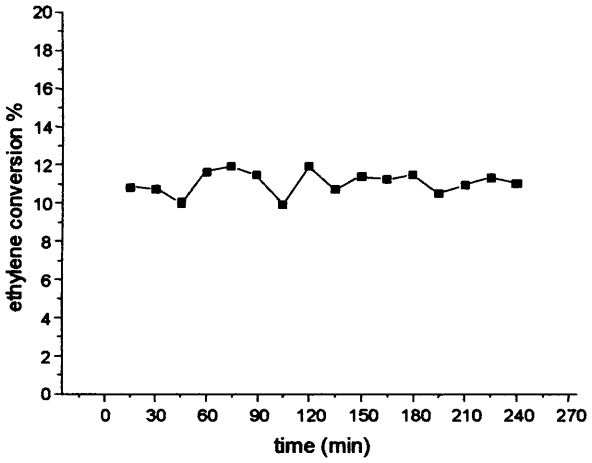

Fig 6.28: Hydrochlorination reaction of ethylene over $ZnCl_2/Al_2O_3$

This is a significant result, because no literature information is available for the use of Zn as heterogeneous catalyst for hydrochlorination reactions. Moreover, the described chemistry is consistent with a Zn(II) species as a Lewis acid. If this is assumed to be the driving force of the process, it is easier to explain the results described in the sections where gold was used on different substrates oxides. Indeed the activity is not due to Au, but to the Lewis acid properties of the support.

In addition it is worth mentioning that all catalysts seem to have an activity limit around 12-14%, but this is probably related to the coking phenomena.

6.5 Reactivity of $ZnCl_2/SiO_2$ towards different substrates and experiments with inert gas

Having established the nature of $ZnCl_2$ like active species for the hydrochlorination reaction, a test similar to the test reported in paragraph 6.4.2 using inert gas has been carried out, in order to identify possible correlations and influences on final activity.

6.5.1 Effect of C_2H_2 and HCl over $ZnCl_2/SiO_2$ catalyst for hydrochlorination of ethylene

The sequence of experiment carried out was the same as described in paragraph 6.4.2

C_2H_4/HCl (2 h) → **He**/HCl (2 h) → C_2H_4/HCl (2 h) (test 6.5)

He/HCl (2 h) → C_2H_4/HCl (2 h) → **He**/HCl (2 h) (test 6.6)

C_2H_4/HCl (2 h) → **He**/C_2H_4 (2 h) → C_2H_4/HCl (2 h) (test 6.7)

He/C_2H_4 (2 h) → HCl/C_2H_4 (2 h) → **He**/C_2H_4 (2 h) (test 6.8)

The results are displayed below in figure 6.29:

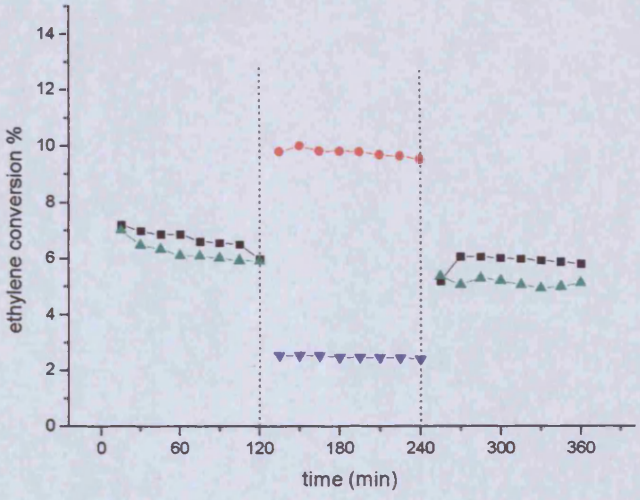

Fig. 6.29: Hydrochlorination reaction of ethylene. Effect of each reactant on conversion trend over $ZnCl_2/SiO_2$ catalyst.
(■) C_2H_4/HCl (2 h) → **He**/HCl (2 h) → C_2H_4/HCl (2 h)
(●)**He**/HCl (2 h) → C_2H_4/HCl (2 h) → **He**/HCl (2 h)
(▲)C_2H_4/HCl (2 h) → **He**/C_2H_4 (2 h) → C_2H_4/HCl (2 h)
(▼) **He**/C_2H_4 (2 h) → HCl/C_2H_4 (2 h) → **He**/C_2H_4 (2 h)

The first experimental evidence is that the plot reported (fig 6.29) is almost the opposite compared to when gold is present, (fig 6.9), and it has similarities with the Au/C catalyst for the hydrochlorination of acetylene (figure 5.6 paragraph 5.1.1).
In addition, the effect of gold over ZnO seems like a poison. Indeed when Au/ZnO is used the average activity is in the range of 3-4%, while for $ZnCl_2/SiO_2$ it is in the range of 7-8%; but with an opposite effect of the reactants to the catalyst. Although gold is not able to facilitate the reaction, it could be the preparation procedure is responsible for these kinds of phenomena. In the case of $ZnCl_2$ the active species is already present, while in Au/ZnO the active species is created *in situ*. This could be also deduced from the conversion trend, which increased to a steady state for Au/ZnO, while for $ZnCl_2/SiO_2$ it remained steady throughout. However, also in this case the observed effect could be indicative of population of catalyst surface with precursor as for the Au/C catalyst for the hydrochlorination of acetylene.

6.5.2 Hydrochlorination reactions using $ZnCl_2/SiO_2$ and reactivity towards different substrates

Further substrates containing double carbon-carbon bonds have been tested in order to evaluate the catalytic activity on Zn(II) like active species and enable further comparison with Au/ZnO in order to evaluate the effect of the catalyst preparation method.

6.5.2.1 Hydrochlorination of propene over $ZnCl_2/SiO_2$

The first test was to compare the activity towards propene. The reaction was carried out using a reactant flow ratio propene: HCl of 1:1 using 5 mL min^{-1} for each reactant, a relative inlet pressure of 1.1 bar and a reaction temperature of 250 °C. Products were directly collected in a chloroform trap for NMR characterization.
Using NMR data it is possible to estimate a conversion around 20% (appendix B), which is quite high compared with the 4-7% conversion that was obtained using the Au/ZnO

catalyst. Moreover it is quite important to note that, whereas using Au/ZnO the Markovnikov product 2-chloropopane is the only one obtained, with only traces of the secondary product 1-chloroethane, in this case of $ZnCl_2/SiO_2$ a significant amount of anti-Markovnikov product resulted, with an approximate ratio between main and secondary product around 5:1 (appendix B)

It is important to underline that major coking phenomena were present, the catalyst was fully covered by black carbonaceous products after reaction (4 h).

For this reason, in order to determine if the two products can be directly obtained over the catalyst surface, or whereas an isomerisation mechanism may be operating, a test using 1-chloropropane has been performed.
This reactant is a liquid, and the reaction has been carried out using a saturator containing 1-chloropropane and using a flow of helium of 15 mL min^{-1}.

A relative amount of 10% of 2-chloropropane (appendix B) was obtained, and quite importantly also traces of propane were also detected. However, the catalyst was still seriously affected by coking. Consequently, a test using SiC was carried out, and no 2-chloropropane was detected, proving that Zn(II) is able to perform the reaction, and this is not simply due to the high temperatures used. In fact, two possible routes can be proposed for the isomerisation product using the Lewis acid properties of Zn.

The first, direct route, is reported in scheme 6.3 below:

Scheme 6.3: Isomerisation of chloropropane and 2-chloropropane formation.

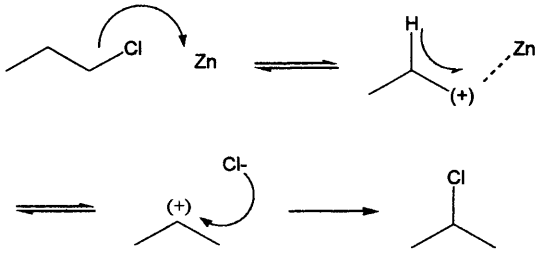

Which leads to 2-chloropropane. The first step involves interaction between Zn and Cl. The second route involves the elimination product in scheme 6.4:

Scheme 6.4: Elimination product of chloropropane and consequent formation of propene.

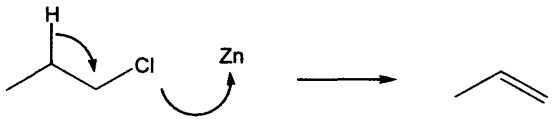

The elimination product is propene, which can react again, *via* H^+, to give further 2-chloropropane.

The coking products can be explained (for this and the other reactions) in terms of cationic polymerisation products, starting from the carbocation shown in scheme 6.5

Scheme 6.5: Coking products can be explained as a consequence of cationic polymerisation products

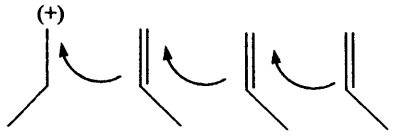

6.5.2.2 Hydrochlorination of isobutylene over $ZnCl_2/SiO_2$

Reaction over $ZnCl_2/SiO_2$ leads to a relative conversion around 15% of 2-chloro-2-methylpropane (appendix B) with traces of 1-chloro-2-methylpropane. In comparison with Au/ZnO, the $ZnCl_2$ catalyst gives higher conversion, but with lower selectivity. The main double bond containing substrates are summarized in scheme 6.6, which is useful to compare with the corresponding scheme 6.2, where Au/ZnO was used.

Scheme 6.6: Selectivity trend for a) ethylene, b) propene and c) isobutylene for hydrochlorination over $ZnCl_2/SiO_2$ catalysts.

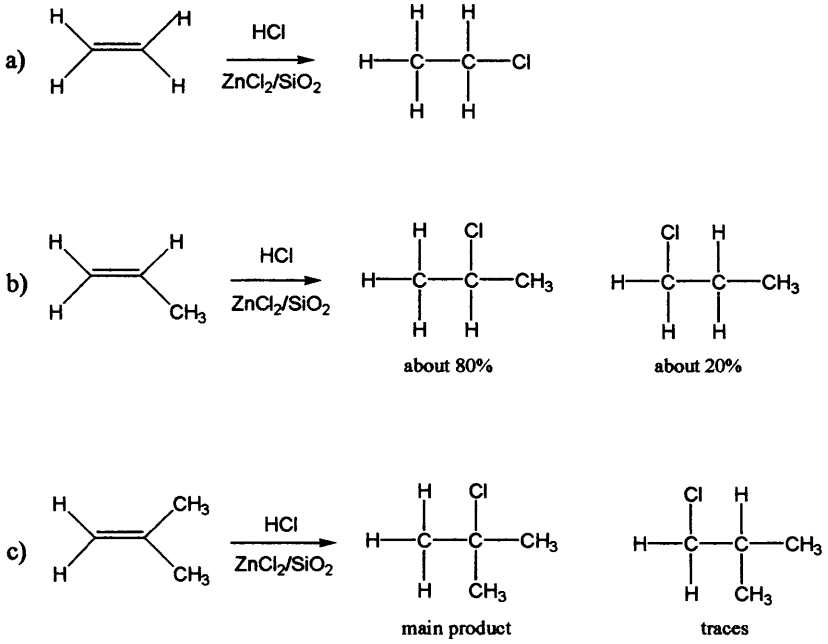

Comparing the same series when gold is present in the catalyst, it is possible to state that Au acts like a poison, but it can also lead to higher selectivity. $ZnCl_2$ is a most efficient catalyst but it must be underlined that is affected by coking.

6.5.2.3 Hydrochlorination of vinyl acetate and isoprene over $ZnCl_2/SiO_2$

Due to the industrial importance of products derived from vinyl acetate and isoprene, an attempted hydrochlorination reaction has carried out, in order to collect qualitative information on $ZnCl_2$ reactivity, using the same experimental conditions described for the reaction with 1-chloropopane.

Concerning vinyl acetate, a comparison between NMR spectra (appendix B) for fresh vinyl acetate, and reaction products collected in a chloroform trap show that no significant reaction occurs, apart from traces of rearrangement products like aldehyde, and a ternary carbon. However, these are considered to be products formed subsequent to catalyst coking.

When isoprene is used as substrate, two well defined chlorinated products are obtained (1) 2-methyl-4-chloro-2-butene and (2) 2-methyl-2-chloro-3-butane (scheme 6.7) with a conversion in the range of 7-8%. However, complicated phenomena of π-interactions occur.

The reaction products were collected in a chloroform trap. After 1 h collection time, it was possible to observe the solution had a pale pink colour. Reaction products were collected for two hours and then immediately stored in a fridge due to the very low boiling point of isoprene (37 °C). After storage, the solution appeared to be dark purple. After NMR measurements and solution storage at room temperature it became pale yellow.

Scheme 6.7: Hydrochlorination products using isoprene as substrate over $ZnCl_2/SiO_2$ catalyst

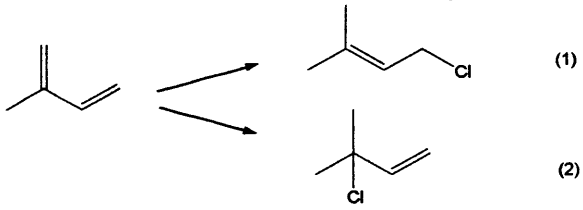

(1)

(2)

Although no metal centre is present to lead to coordinated products the phenomena observed are clear evidence of intra-molecular interaction *via* π stacking [18] and changing colour of the solution. Nevertheless, product characterization identified the two chlorinated products shown in scheme 6.7. They were obtained in low conversion and high purity (appendix B), and the route to obtain them can be assumed as the same as that described for the chloropropane reaction. This can be considered a significant result, because no literature is present for the use of $ZnCl_2$ to synthesise these chlorinated products.

6.6 Further hydrochlorination tests and crossed experiment with acetylene

6.6.1 Reactivity of the supports CeO_2 and La_2O_3 towards hydrochlorination of ethylene

Finally reported here are two tests in order to verify if the observed behaviour towards hydrochlorination of acetylene is specific to ZnO only, and a crossed experiment with acetylene using a physical mixture of Au/C and $ZnCl_2/SiO_2$ catalyst.

Among the metal oxides tested, repeated measurements for the hydrochlorination reaction using Au/CeO_2, Au/La_2O_3, CeO_2 and La_2O_3 have been carried out. Both supports have been tested with and without gold using a reaction temperature of 250 °C. Only traces of product have been detected in all cases, but with negligible activity.
It is possible to observe the catalysts and the respective oxides are not able to perform oxychlorination (fig 6.2) or the hydrochlorination reaction (fig 6.30), and the activity seems to be peculiar to Zn only.

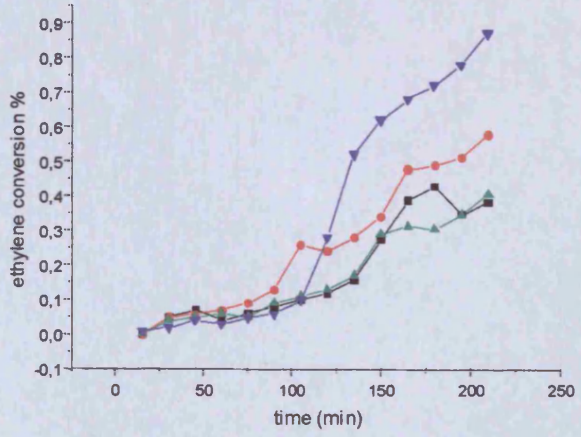

Fig 6.30: Hydrochlorination of ethylene over (■) CeO_2, (●) Au/CeO_2, (▲) La_2O_3 and (▼) Au/La_2O_3

The scale has been enlarged in order to appreciate differences among the different Au oxides catalysts and the supports. The catalysts all display the same behaviour with negligible activity.

6.6.2 Crossed test with acetylene and chloroethane

Because of the selectivity of Au/C catalyst towards hydrochlorination of acetylene, and $ZnCl_2$ catalyst towards hydrochlorination of ethylene, attempts to obtain di-chlorinated products have been carried out. For this purpose a test using a first catalytic bed of Au/C followed by a second bed of $ZnCl_2/SiO_2$ (200 mg each) has been done using both 180 °C and 250 °C as reaction temperature. A second test has been carried out using single bed containing a physical mixture of them.

No significant change in activity was observed in comparison with Au/C catalyst, for example the catalytic test for the physical mixture at 250 °C is reported in fig 6.31. The test was carried out at 250 °C, which is the minimum temperature for $ZnCl_2$ to be active.

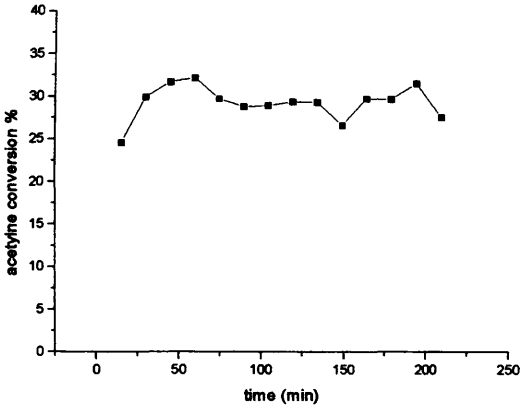

Fig. 6.31: Crossed test involving hydrochlorination of acetylene using a physical mixture of Au/C and $ZnCl_2/SiO_2$ acetylene conversion at 250 °C.

The assumption of this experiment was that subsequent reaction of vinyl chloride monomer on $ZnCl_2$ surface, in order to obtain 1,1- or 1,2 dichloroethane may occur. However, the experiment proved unsuccessful. This is probably because the Lewis acidity of $ZnCl_2$ is low and the vinyl chloride monomer is not sufficiently basic in terms of electronic donation to lead to a reaction.

6.7 Conclusions

It has been observed that Au/C catalysts are selective towards substrates containing carbon-carbon triple bond only, whereas Au/ZnO catalysts are selective to hydrochlorination of substrates containing carbon-carbon double bonds only. However, it is important to note that none of them is able to perform the oxychlorination reaction, and that the real active species for the hydrochlorination reaction of ethylene and homologues is not Au, but $ZnCl_2$ generated from the support ZnO.

This is a quite significant result, because although the Lewis acid nature of $ZnCl_2$ is known [15], no literature information is available for the use of this metal salt for hydrochlorination reactions.

In addition, this kind of study is a good example of a reaction that is not carried out by the metal species but is instead carried out by a modification of the support. Nevertheless, gold has a role, but its exact function remains unclear. It is evident that gold acts as a poison, but it can have an effect on selectivity and a tuning effect on the action of the single reactants on the final catalytic behaviour. This effect could be due to gold or modification of the ZnO surface due to the preparation technique with presence of $Zn(OH)_2$ poorly dispersed. Indeed, it has been possible to demonstrate that a particular phase, $Zn(OH)_2$ wulfingite, is necessary to generate *in situ* the active component $ZnCl_2$, while bulk ZnO zincite, bulk $Zn(OH)_2$ or bulk $ZnCl_2$ are not able to carry out the reaction.

$ZnCl_2$ can catalyse important reactions like the Fischer-Indole synthesis [19], and the important chlorination of alcohol using a mixture of $ZnCl_2$ and HCl, known as Luca's reagent [20]. Related to the Fischer-Indole synthesis there is also the preparation of fluorescein from phtalic anhydride and resorcinol [21], which involves a Friedel-Craft acylation using wet $ZnCl_2$. However, in all cases, the amount of $ZnCl_2$ required is almost stoichiometric and in none of these cases is $ZnCl_2$ used as a supported species, but is used directly as a salt in the reaction media.

One of the few roles of $ZnCl_2$ is the activation of benzylic and allylic halides towards substitution by weak nucleophiles such as alkenes [22], but again it is not used in catalytic amounts. An exception is represented by the benzylation of benzene by benzyl chloride, where a $ZnCl_2$ over Al_2O_3 catalyst can be used [23].

The only well defined study of supported $ZnCl_2$ has been carried out by Fu and co-workers using supported $ZnCl_2$ on Al_2O_3 for the vapour phase O-methylation of catechol [24]. Also, in this case the catalyst is able to display a good performance, but a relatively high loading of $ZnCl_2$ is required, similar to the present study at around 10-15% of Zn. In addition, the catalyst for this reaction is affected by coking and Zn desorption, which is the most limiting parameter to use the catalyst efficiently as described in the present work.

6.8 References

[1] J. March, *Advanced Organic Chemistry*, John Wiley & Sons Inc., New York, 1992

[2] F. G. Mann and B. C. Saunders, *Practical Organic Chemistry*, Longman Inc., New York 1978

[3] C. Chambers and A. K. Holliday, *Modern Inorganic Chemistry*, Butterworth & Co Ltd, London, 1975

[4] J. G. Speight, *Chemical and Process Design Handbook*, McGraw-Hill, New York, 2002

[5] National Safety Council, *Chloroethane*, Itasca IL, 2005

[6] United States Environmental Protection Agency, Entry file EPA420-R-99-021, Washington DC, 1999

[7] United States Environmental Protection Agency, Entry file EPA-450/4-84-007d, North Carolina, 1984

[8] P. Tao, US Patent 4302617, Appl. N. 856840, Publ. Date 1981-11-24

[9] C. Orsenigo and F. Casagrande, Sud-Chemie, US Patent 6872684, Appl. N. 791952, Publ. Date 2005-03-29

[10] N. N. Greenwood and A. Earnshaw, *Chemistry of the Elements* (II Ed.), Butterworth, UK, 1997.

[11] D. Syomin, and B.E. Koel, *Surf. Sci.*, 53, **498**, 2002

[12] Z. Yan, S. Chinta, A. A. Mohamed, J. P. Fackler, and D. W. Goodman, *J. Am. Chem. Soc.*, 1604, **127**, 2005

[13] H. Grumann, M. Stoger, J. Eichler, D. Jaculi, W. Lork, A. Greve, and J. Wilkens, US Application Patent 20030004380, Appl. N. 181185, Publ. Date 2003-01-02

[14] M. Clegg, R. Hardmann, US Patent 5763710, Appl. N. 797841, Publ. Date: 1998-06-09

[15] I. S. Butler and J. F. Harrod, *Inorganic Chemistry*, Benjamin/Cummings Inc., Redwood, 1989

[16] H. McMurdie *et. al.*, *Powder Diff.* 76, **1**, 1986, International Centre for Diffraction Data, Powder Diffraction File, Entry 36-1451 (1996)

[17] K. Schmetzer, G. Schnorrer-Kohler and O. Medenbach, Neues Jahrb. *Mineral.*,

Monatsh., 1985, **145**, 1985, International Centre for Diffraction Data, Powder Diffraction File, Entry 38-385 (1996)

[18] C. Glidewell, J. N. Low, J. M. S. Skakle and J. L. Wardell, *Acta Cryst. Sec. C*, 350, **60**, 2004

[19] R. C. Morales, V. Tambyrajah, P. R. Jenkins, D. L. Davies and A. P. Abbott, *Chem. Comm.*, 158, 2004

[20] R. T. Morrison and R. N. Boyd, *Organic Chemistry* (IV Ed.), Allyn and Bacon Inc., Newton, 1983

[21] B. S. Furniss, A. J. Hannaford, P. W. G. Smith and A. R. Tatchell, *Vogel's Textbook of Practical Organic Chemistry* (V Ed.), John Wiley and Sons, New York, 1989

[22] E. Bäuml, K. Tscheschlok, R. Pock, and H. Mayr, *Tetrahedron Lett.*, 6925, **29**(52), 1988

[23] M. Salavati-Niasari., J. Hasanalian, and H. Najafian, *J. Mol. Catal. A: Chem.*, 209, **209**, 2004

[24] Z. Fu, Y. Yu, D. Yin, Y. Xu, H. Liu, H. Liao, Q. Xu, F. Tan and J. Wang, *J. Mol. Catal. A: Chem.*, 69, **232**, 2005

Chapter 7: PHASE TRANSITIONS IN VANADIUM PHOSPHORUS OXIDES FOR n-BUTANE OXIDATION

7.1 Introduction

Vanadium phosphorus oxides are materials largely investigated in chemistry due to their magnetochemical properties [1] catalytic activity [2] and challenge in their crystal structure determination [3, 4].

Industrially, particular interest is focused on the vanadyl pyrophosphate $(VO)_2P_2O_7$ due to its efficiency in carrying out partial oxidation and ammoxidation of hydrocarbons [5], especially for the oxidation of *n*-butane to maleic anhydride (MA) [6]. The reaction is shown schematically below:

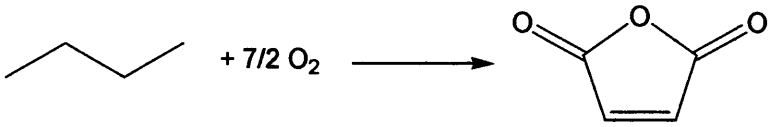

(eq. 7.1)

Maleic anhydride is used in the manufacture of unsaturated polyester resins, copolymers, food additives, agricultural chemicals, and lube oil additives [7]. Industrially the reaction is carried out using a temperature range of 380-430 °C and 3-4 bar of pressure with a limit of 2% of butane in air, due to the flammable limit of the hydrocarbon in air. The reaction is one pot and the final product is extracted with water with a total yield of 45-55% using a fixed bed reactor [7]

The interest in this reaction is not limited to industry and catalysis, but also in the science of materials and chemical kinetics. Indeed, the active catalyst form is obtained from a precursor that formally can be considered $VOHPO_4 \cdot 0.5H_2O$, which under reaction conditions [8, 9] leads to a complex solid mixture made of vanadyl pyrophosphate $(VO)_2P_2O_7$, in combination with vanadyl phosphates α_{II}-$VOPO_4$ and δ-$VOPO_4$ [10]. The real active species responsible for the reaction is still a matter of debate. Indeed the

accepted active species is considered to be $(VO)_2P_2O_7$, which is V(IV). However, Coulston and co-workers [11] have demonstrated that the presence of V(V) centres are essential to carry out the oxidation reaction of *n*-butane, and in fact the presence of α_{II} and δ phases although made by V(V) are considered essential for the industrial catalyst. In addition, many researchers have demonstrated that catalyst selectivity is dependent on the V(IV)/V(V) ratio [12] and a further peculiarity for this complex catalyst is that the activation process from $VOPO_4{\cdot}0.5H_2O$ to $(VO)_2P_2O_7$ is a topotactic process [13, 14] i.e. the final catalyst morphology and surface area are dictated by the precursor morphology.

7.1.1 Crystal structures of vanadyl ortho phosphates $VOPO_4$

Up to now seven different crystal structures of vanadyl ortho phosphates $VOPO_4$ are known, and they are named: α_I, α_{II}, β, γ, δ, ε, and ω. All these phases are polymorphs, i.e. they have the same stoichiometry but different orientation of their constituent units, which in this case can be assumed like VO_6 octahedra and strongly bonded PO_4 units to form the final network. A change in the conformation of individual units in the solid state is usually accompanied by a change in the crystalline structure itself, i.e. it defines a different polymorph [15].

It is worth mentioning that many authors prefer to identify the unit cell with VO_5 pyramids rather than VO_6 octahedra [16]. This is due to the longer V···O distance of an axial V—O bond, and it can have consequence on the final network of the vanadium oxides, leading to a 3D or 2D dimensionality of the structure network, which for omega can be assigned as 3D [17].

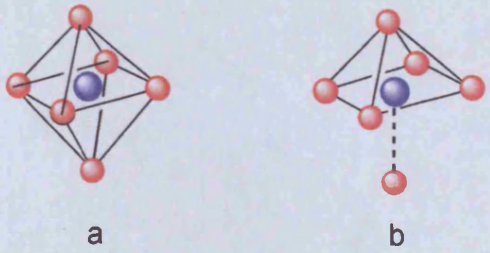

Fig 7.1 Typical geometry of V(V) in $VOPO_4$ structures, a) octahedral view and b) pyramidal view. The pyramidal view is characterized by a longer V···O distance. Colour code: red, oxygen atom; blue, vanadium atom.

However, these differences can have massive effects on the final properties of the polymorph phase, as well as the presence of amorphous material [18]. In fact only α_{II} and δ are predominant in catalyst composition for *n*-butane oxidation [19] and only β and ε can be considered stable phases to hydration, hence α_I, α_{II}, γ and δ all hydrate quite easily [20].

Among these phases, the case of ω-$VOPO_4$ can be considered to be particularly special, because the phase is well defined only at high temperature, usually above 350 °C, and it is quite difficult to obtain and to characterize [4]. Most of this chapter will be focused on characterization of the omega-phase and its reactivity towards reducing agents, focusing on the observed solid-state transition from omega to delta during reaction conditions.

The literature available on ω-$VOPO_4$ is up to now quite limited for several reasons: firstly the phase can exist only at high temperature, 400-600 °C, which requires appropriate apparatus to investigate it, secondly no specific and reproducible procedure has been established up to now by which it can be obtained without the use of oxovanadium hydrogen phosphates, and finally it is a metastable phase. In the present work, a reliable synthesis method will be proposed as well as an explanation for the observed metastability [21].

The first reported observation of the existence of the omega phase, i.e. the first attempt to index the unit cell was in 1985 by Wibbeke when he obtained omega after heating a powder consisting of vanadyl hydrogen phosphate at 480 °C for 72 hours. The sample was characterized at 480 °C and is the high temperature form of ω-$VOPO_4$ [22]. The high temperature form is stable up to 510 °C. The low temperature form rapidly adsorbs water and it is not stable under normal conditions [23]. Until 2001 and the indexing proposed by Amorós and co-workers [4], many authors did not even consider fully Wibbeke's observations to be fully reliable, and disagreement among investigators are still present.

7.2 Experimental

7.2.1 Synthesis of ω-$VOPO_4$

Amorós and co-workers, reported that it is possible to obtain ω-$VOPO_4$ by thermal decomposition of different oxovanadium hydrogen phosphates, namely: $VO(HPO_4)\cdot nH_2O$ and β-$NH_4(VO_2)(HPO_4)$ [24 – 26], which allowed a pure omega phase to be obtained suitable for indexing studies [4]. However, these routes do not take into account the possible role of the pyro phosphate $(VO)_2P_2O_7$. Indeed, it is possible to obtain ω-$VOPO_4$ from $(VO)_2P_2O_7$ in an oxidizing atmosphere under thermal treatment; and the pyro-phosphate can play a crucial role in the commercial catalysts [27]

This novel route has been previously investigated by Budroni and Hutchings [28] and in the present work it is optimised.

The first step consists of the preparation of suitable vanadium phosphates precursors like $VOHPO_4\cdot 0.5H_2O$ using two different routes [29]. In the first route – known as VPO method - $VOHPO_4\cdot 0.5H_2O$ was prepared by refluxing V_2O_5 (Strem, 11.8 g) with H_3PO_4 (Aldrich 16.49 g, 85%) in isobutanol (Fisher 250 mL) for 16 h. The light blue solid was recovered by vacuum filtration, washed with isobutanol (200 mL) and ethanol (150 mL, 100%), refluxed in water (9 mL H_2O/g solid) for 2 h; filtered hot, and dried in air (110°C, 16 h).

In the second route – known as VPD method - the $VOHPO_4\cdot 0.5H_2O$ was prepared from $VOPO_4\cdot 2H_2O$. V_2O_5 (5.0 g, Strem) and H_3PO_4 (30 mL, 85%, Aldrich) were refluxed in water (120 mL) for 24 h. The yellow solid (yield 50% based on V) was recovered by vacuum filtration, washed with cold water (100 mL) and acetone (100 mL) and dried in air (110°C, 24 h). Powder X-ray diffraction and laser Raman spectroscopy confirmed that this solid was the dihydrate, $VOHPO_4\cdot 2H_2O$. The dihydrate (4 g) was refluxed with isobutanol (80 mL) for 21 h, and the resulting $VOHPO_4\cdot 0.5H_2O$ was recovered by filtration, dried in air (110°C, 16 h), refluxed in water (9 mL H2O/g solid) for 2 h, filtered hot, and dried in air (110°C, 16 h).

Using this procedure is possible to obtain $VOHPO_4 \cdot 0.5H_2O$ at a high purity level. It is well known that $VOHPO_4 \cdot 0.5H_2O$ at temperature above 350 °C can dehydrate to give $(VO)_2P_2O_7$ as reported below in eq 7.2:

$$2\ VOHPO_4 \cdot 0.5H_2O \rightarrow (VO)_2P_2O_7 + 2\ H_2O \qquad \text{(eq. 7.2)}$$

The method previously developed [28] consisted of the *in situ* preparation of $(VO)_2P_2O_7$ from $VOHPO_4 \cdot 0.5H_2O$, in an inert atmosphere (table 7.1), and subsequent oxidation at high temperature to obtain the ω-$VOPO_4$ species (table 7.2). The process was carried out using an *in situ* powder X-ray diffraction cell Anton Parr XRK 900 controlling the reaction temperature using a thermocouple directly connected with to sample holder. Data were collected using an Enraf Nonius diffractometer, and using an FR 591 rotating anode to generate a Cu X-ray source and a Ge (111) single crystal monochromator to select the Cu K_α component. Diffraction data were collected using an INEL CPS-120 position sensitive detector using a mixture of 15% ethane in argon as a gas probe. Finally, the reactant flow was regulated using mass flow controllers.

Table 7.1
Preparation of $(VO)_2P_2O_7$ from $VOHPO_4 \cdot 0.5H_2O$ in flowing nitrogen 60 mL min^{-1}

Temperature step	Temperature (°C)	Time (seconds) to reach the assigned temperature	Stabilization time (seconds)	Acquisition time (seconds)
1	50	1800	300	900
2	100	1500	300	900
3	200	3000	300	900
4	300	3000	300	900
5	400	3000	300	900
6	500	3000	300	900
7	500	300	300	900
8	50	3600	300	900

Table 7.2
Preparation of ω-$VOPO_4$ from $(VO)_2P_2O_7$ in flowing air 60 mL min^{-1}, step 1

Temperature step	Temperature (°C)	Time (seconds) to reach the assigned temperature	Stabilization time (seconds)	Acquisition time (seconds)
1	50	1800	300	900
2	200	600	300	900
3	300	600	300	900
4	400	600	300	900
5	500	600	300	900
6	600	600	300	900
7	**625**	**600**	**300**	**900**
8	500	600	300	900
9	400	600	300	900
10	300	600	300	900
11	200	600	300	900
12	50	1200	300	900

The combination of the two processes is reported in figure 7.2, where the transformations from hemihydrate to pyrophosphate and from pyrophosphate to omega vanadyl phosphate are evident [21, 28].

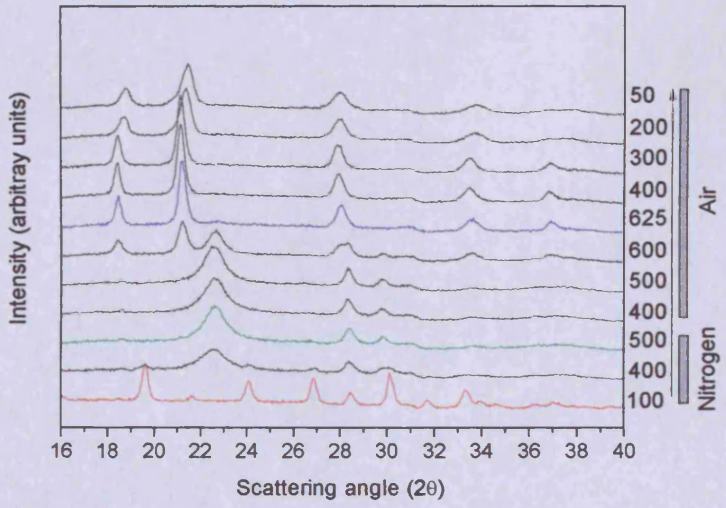

Fig. 7.2 *in situ* preparation of (—) $(VO)_2P_2O_7$ from (—) $VOHPO_4 \cdot 0.5H_2O$ in nitrogen, and afterwards preparation of (—) ω-$VOPO_4$ in air.

The intrinsic importance of this method is that the conditions used to obtain ω-$VOPO_4$

are quite close to the industrial conditions used for maleic anhydride manufacture using pyrophosphate as the active component [27, 31]. As a direct consequence, it is of interest to investigate the reactivity of the omega phase using a reducing agent under reaction condition. Indeed, the best catalytic performance of an industrial catalyst can be obtained if the procedure to activate the catalyst discourages the formation of the ω phase.

Later, it will be shown that the phase obtained, if treated with butane, leads to a phase transition from ω-$VOPO_4$ to δ-$VOPO_4$ (paragraph 7.3). However, it is important to note that the ω phase obtained using the data reported in table 7.1 and 7.2, can often also contain traces of pyrophosphate (fig 7.3), which could be responsible for the reactivity phenomena observed.

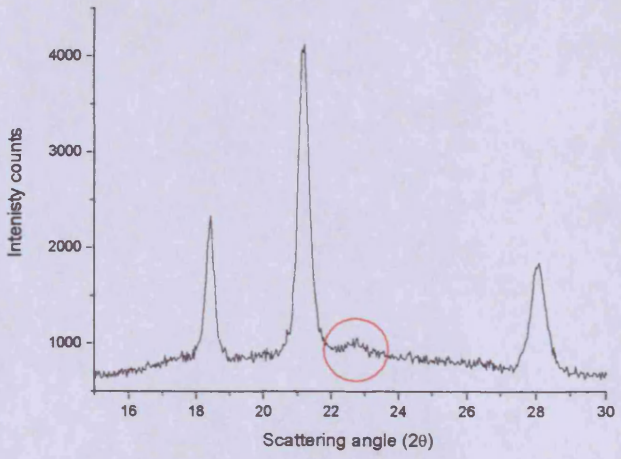

Fig 7.3: XRPD pattern of ω-$VOPO_4$ using the preparation procedure described in table 7.1 and 7.2. Traces of pyrophosphate are still present (reflection at 22.5° 2θ)

For this reason, optimisation has been necessary, not only to have a pure phase for catalytic tests, but also to give a phase useful for characterization studies and confirmation of the crystal structure. The final optimised conditions involve a further temperature cycle, reported in table 7.3.

Table 7.3
Purification of ω-$VOPO_4$, in air 60 mL min^{-1}, step2

Temperature step	Temperature (°C)	Time (seconds) to reach the assigned temperature	Stabilization time (seconds)	Acquisition time (seconds)
1	50	1800	300	900
2	200	600	300	900
3	300	600	300	900
4	400	600	300	900
5	500	600	300	900
6	**580**	**600**	**7200**	**900**
7	500	600	300	900
8	400	600	300	900
9	300	600	300	900
10	200	600	300	900
11	50	1200	300	900

This purification step leads to the following XRPD pattern in fig 7.4.

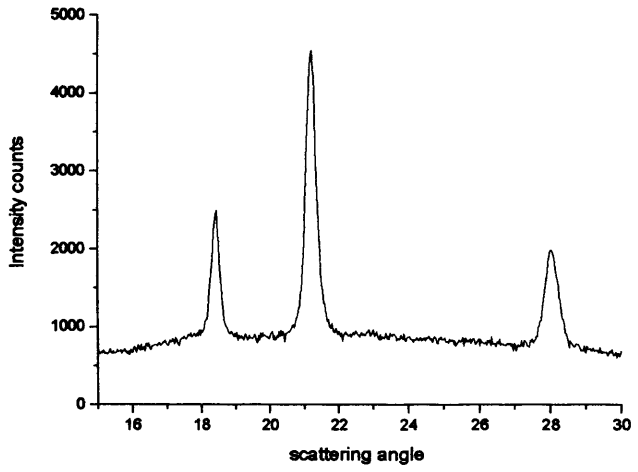

Fig 7.4: XRPD pattern of ω-$VOPO_4$ after purification (table 7.3), pyrophosphate is absent.

The main observed difficulties concern the minimum and maximum temperatures at which to carry out the purification and for how long. Further tests, showed that, using a lower temperature than 580, e.g. 550 °C, is insufficient for purification, as well as holding the temperature for less than 2 h. Particular care is necessary not to exceed 600 °C. It is worth underlining that in the first purification step (table 7.2) a temperature of

625 °C is necessary, but if further purification cycles are performed, the temperature for the observed phase transition decreases. This is in agreement with previous observations [28] and is confirmed here. At too high temperature, and the presence of oxygen can lead to γ-$VOPO_4$ although no reducing agents are used. In conclusion, the temperature range to effect the purification has to be considered quite narrow, and this can be assumed as further evidence of the difficulty of characterizing this crystal phase. Heating times longer than 4h at high temperature have not been investigated so far, but it could be useful to test the stability of the phase under these conditions. In fact, it is possible to state that the process is both temperature and time dependent.

It has been possible to demonstrate that the presence of small pyro-phosphate impurities do not affect the observed transformation from ω-$VOPO_4$ to δ-$VOPO_4$ when butane is used as reducing agent. However, it is quite significant to note, that this further thermal treatment, as well purifying the phase, leads to quite significant changes in morphology. This is clearly evident from TEM analysis of the ω-$VOPO_4$ obtained using the two different routes (figures 7.5, 7.6, 7.7 and 7.8)

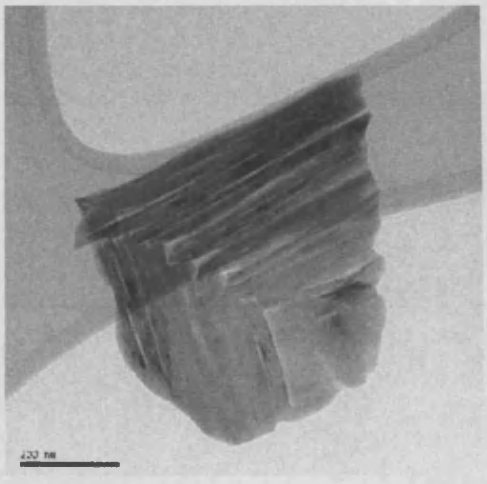

Fig 7.5: TEM (200 nm scale) of ω-$VOPO_4$ crystal obtained using the procedure without the purification step.

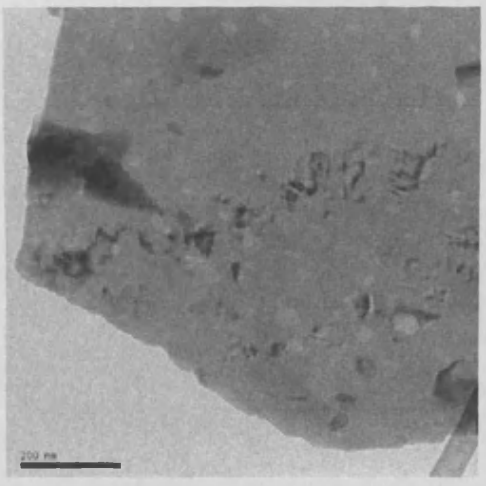

Fig 7.6: TEM (200 nm scale) of ω-$VOPO_4$ crystal obtained using the procedure with purification step. The pyramid shape is lost and dominions are present.

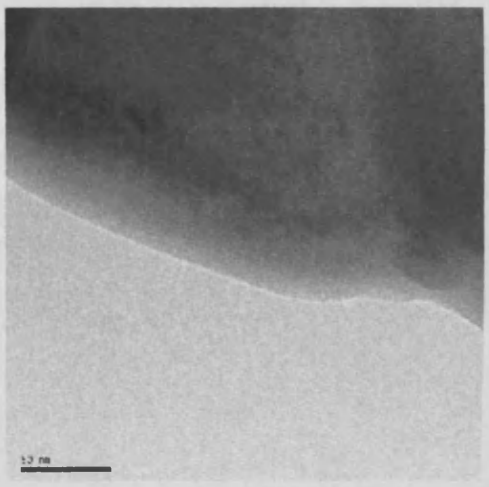

Fig 7.7: TEM details (50 nm scale) of ω-$VOPO_4$ crystal obtained using the procedure without purification step.

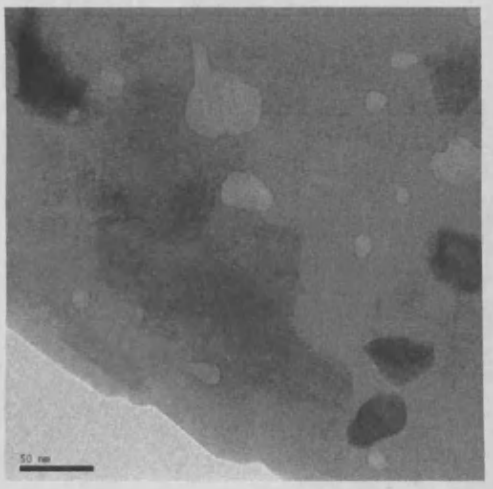

Fig 7.8: TEM details (50 nm scale) of ω-$VOPO_4$ crystal obtained using the procedure with purification step.

Using the preparation route without a purification step the final product has a morphology that looks like a monolith having a stepped pyramid shape (fig 7.5) while using the route with a purification step the final product appears as a set of spread dominions (fig 7.6). This is fully evident from the comparison of the TEM details of the ω-$VOPO_4$ obtained using the first route (fig 7.7) and ω-$VOPO_4$ using the second route (fig 7.8) respectively. It is reasonable to think that the final morphology it is not simply due to the absence of pyro-phosphate but also an effect of the temperature ramp used.

In addition, the optimised route allowed a material that is easier to recrystallise from omega samples at room temperature to be obtained. With a pure sample available it has been possible to reobtain the omega phase for reaction tests starting from room temperature simply by heating it at 550 –580 °C and afterwards cooling to the usual reaction temperature of 400 °C. It is possible to repeat the process many times, increasing the possibility of carrying out experimental tests on ω-$VOPO_4$, as well as the possibility of obtaining δ-$VOPO_4$ available for characterization from a well-defined ω-$VOPO_4$ precursor.

7.3 Reactivity of ω-$VOPO_4$ towards *n*-butane

The first, and most investigated substrate tested in this study, was the reactivity of ω-$VOPO_4$ towards butane under different conditions. As already mentioned the industrial process for maleic anhydride manufacture uses $(VO)_2P_2O_7$ at 380-430 °C. For this reason the first test was to study the behaviour of the phase at 400 °C using a mixture of 1.5 % *n*-butane in air with a total flow of 60 mL min^{-1}. The results are reported in figure 7.9 [21, 28]

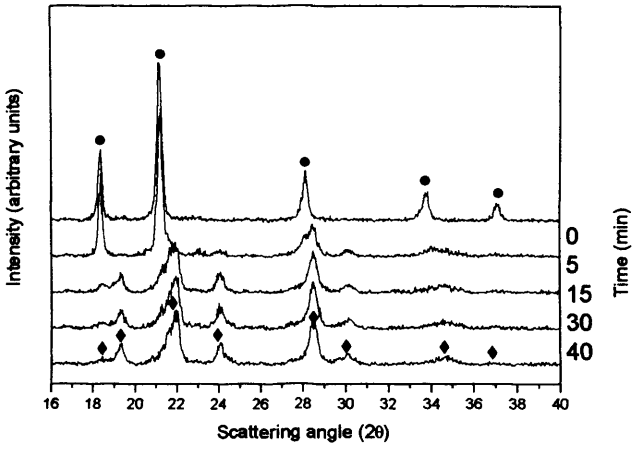

Fig 7.9: Phase transition of (●) ω-$VOPO_4$ at 400 °C using a mixture of 1.5 % n-butane in air to (♦) δ-$VOPO_4$

A phase transition occurs and the omega phase evolves quickly to a phase that has been identified as δ-$VOPO_4$ [16].

If the test is carried out in an inert atmosphere using nitrogen, the transformation is faster and the system can evolve to an amorphous material as reported in figure 7.10 [21, 28].

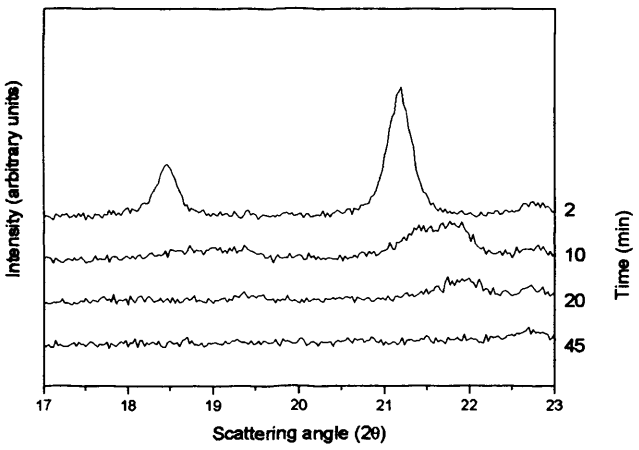

Fig 7.10: Phase transition of ω-$VOPO_4$ at 400 °C using a mixture of 5 % *n*-butane in nitrogen. The crystal phase quickly evolves to an amorphous material

The phase transformation is very fast, and is on the same timescale as the filling of the reaction chamber by the reactants. Moreover, if reaction occurs, it is reasonable to think that the oxygen necessary to carry out the reaction comes from the ω-$VOPO_4$ lattice, and this removal of oxygen is responsible for the observed transformation.

In order to test this hypothesis, catalytic activity tests have been carried out, both in aerobic and anaerobic conditions (see paragraph 7.4.1)

Concerning the observed transformation, important observations are necessary. If δ-$VOPO_4$ is treated again in presence of air only, not exceeding 600 °C, it is possible to re-obtain ω-$VOPO_4$, while the process does not occur if only nitrogen is used, and this is more evidence for the importance of lattice oxygen.

Moreover it has often been possible to recrystallise omega even from the disordered material using air treatment at 600 °C. Sometimes this has not been possible and it has to be considered as an indication of the destruction of the crystal lattice during the experiment if this is performed in anaerobic conditions for a long time. These aspects are summarized in the following scheme:

Scheme 7.1: Phase transitions between ω-$VOPO_4$ and δ-$VOPO_4$ by the effect of temperature and butane in different atmospheres (RT denotes room temperature)

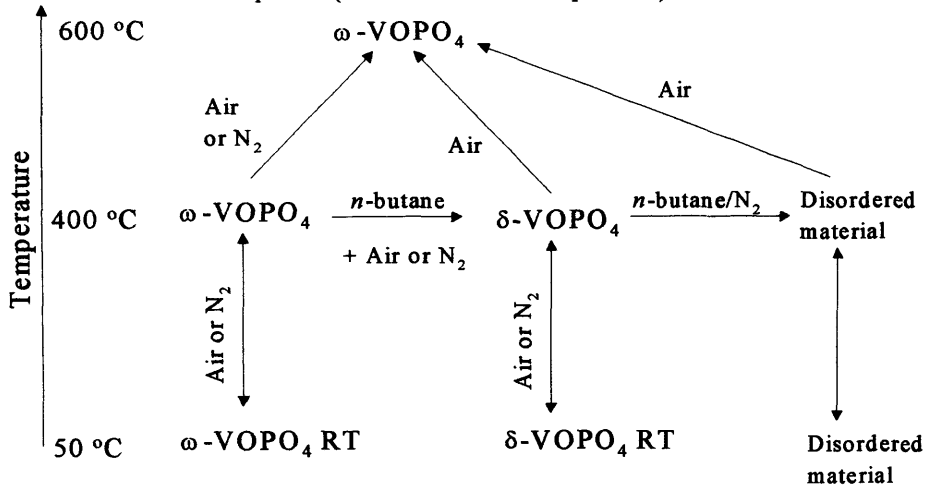

7.3.1 ω-$VOPO_4$ and δ-$VOPO_4$ at room temperature, and structural correlations

It is important to note that the observed process is not due to decomposition of ω-$VOPO_4$ when temperatures of 400 °C or below are used. In order to clarify this aspect, in fig 7.11 the XRPD patterns of ω- and δ-$VOPO_4$, both at 400 °C and room temperature, are compared with the effect induced from reaction.

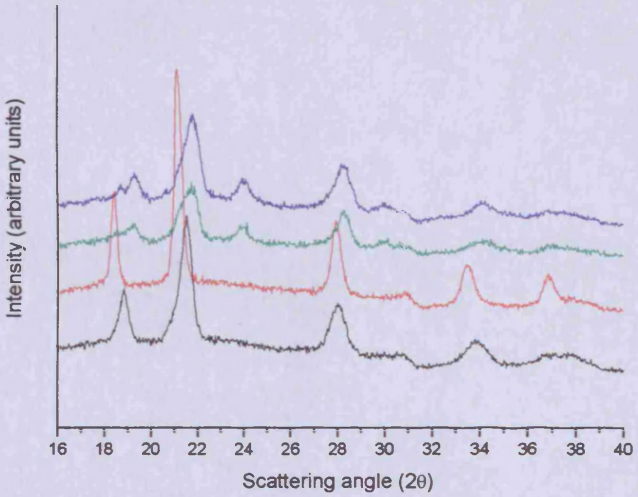

Fig 7.11: XRPD pattern of (—) ω-$VOPO_4$ at RT, (—) ω-$VOPO_4$ at 400 °C, (—) δ-$VOPO_4$ after reaction with butane at 400 °C and (—) δ-$VOPO_4$ at RT

ω-$VOPO_4$ and δ-$VOPO_4$ appear quite different at room temperature, the most significant differences are the most intense reflection at 21.5° 2-theta for ω-$VOPO_4$ and the absence of the reflection at 23.8° 2-theta. These details are important, because the presence of a fast transformation is proof of a close structural correlation between ω- and δ-$VOPO_4$. Both structures share the same three-dimensional arrangement of infinite chains of distorted trans-corner sharing VO_6 octahedra. However it has recently been possible to state [4, 17] that distortion of the octahedra is much more pronounced than in other $VOPO_4$ polymorphs, because the V···O distance is much longer in comparison. The most

notable difference between ω- and δ-$VOPO_4$ is that the ω-$VOPO_4$ structure is disordered with respect to both the orientation of the phosphate groups and the direction of the V—O bonds within the chains [4], whereas the δ-$VOPO_4$ structure is ordered. The difference in ordering may be related to the chains being straight in the ω-$VOPO_4$ phase but having a zigzag shape in the δ-$VOPO_4$ phase.

A schematic representation of the V-O-P chains viewed along the crystallographic axis *a* and *c*, top and bottom of the figure 7.12 respectively, is reported below [17]:

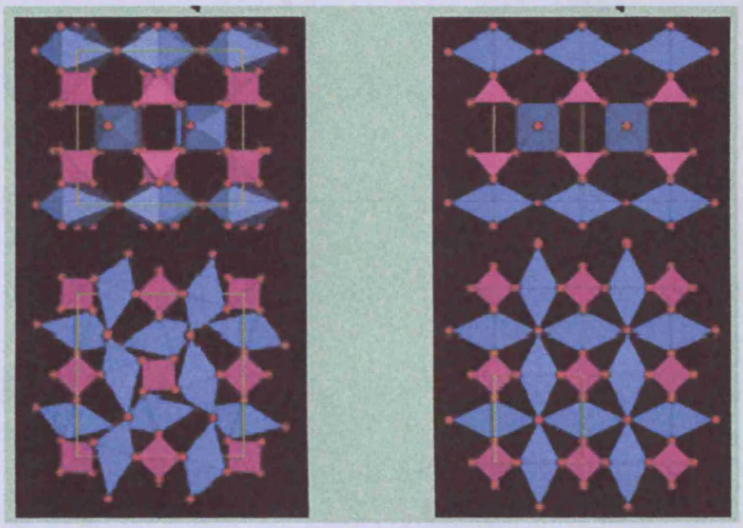

Fig 7.12: Different ordering between δ-$VOPO_4$ (left picture) and ω-$VOPO_4$ (right picture). A zig-zag shape is identified for δ, whereas a straight chain orientation is identified for ω along the *c* axis (bottom of the picture). Colour code: red, oxygen atom; blue VO_6 or VO_5 units; purple, PO_4 units

All these aspects lead to the conclusions that the observed transformation is a real transition phase, which is chemically induced by the organic substrate

In addition, from figure 7.11 it is evident how the reflection of ω-$VOPO_4$ at 400 °C is sharper when compared with the pattern collected at 50 °C, a direct indication that ω-$VOPO_4$ is more stable at high temperature.

7.4 Catalytic testing of ω-$VOPO_4$ in aerobic conditions

A catalytic activity test has been performed using ω-$VOPO_4$ as starting material. The sample was tested under fuel-lean conditions (1.5% butane in air) at a GHSV of 4500 h^{-1} and a reaction temperature of 400 °C for a total time on line of 14 hours.

The results obtained are shown in figures 7.13 and 714, and this is the first example of reactivity of vanadium phosphates using ω-VOPO4 as the precursor [21].

The total conversion was low, with an average value of 8%; nevertheless, the selectivity was high, with an average value of 57% for maleic anhydride. It has been possible to determine that ω-$VOPO_4$ is mainly comprised of V(V) centres [21] and this test is important because it is in agreement with previous experimental observation where V(V) centres are responsible for the selectivity towards butane oxidation [11].

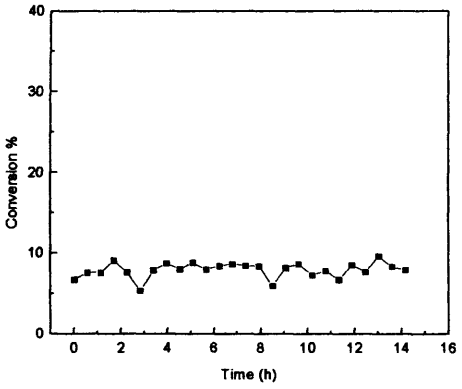

Fig. 7.13: ω-$VOPO_4$ activity test under fuel-lean conditions (1.5% butane in air), GHSV=4500 h^{-1}, and temperature= 400 °C

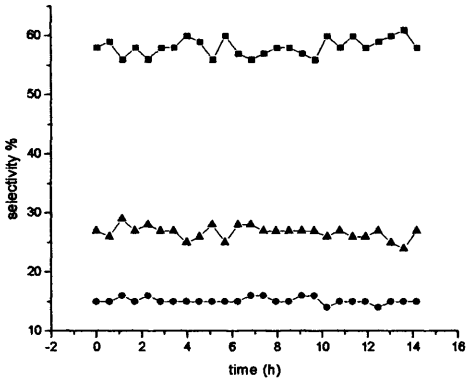

Fig 7.14: ω-$VOPO_4$ selectivity under fuel-lean conditions (1.5% butane in air), GHSV=4500 h^{-1}, and temperature= 400 °C, for: (■) maleic anhydride, (▲) CO, and (●) CO_2.

It should be noted that in the industrial catalyst V(V) centres are provided by δ-VOPO4, but whereas δ-VOPO4 is an active component ω-VOPO4 is not. This difference in reactivity should not be ascribed to a different surface area of these two phases, but to their different symmetry along the crystallographic *c* axis.

An important feature of the catalyst (fig. 7.15) is that, even at the end of the reaction

where XRD pattern of the sample shows rightly δ-$VOPO_4$, it is possible to obtain the ω-$VOPO_4$ phase again by treating the sample in air at 600 °C.

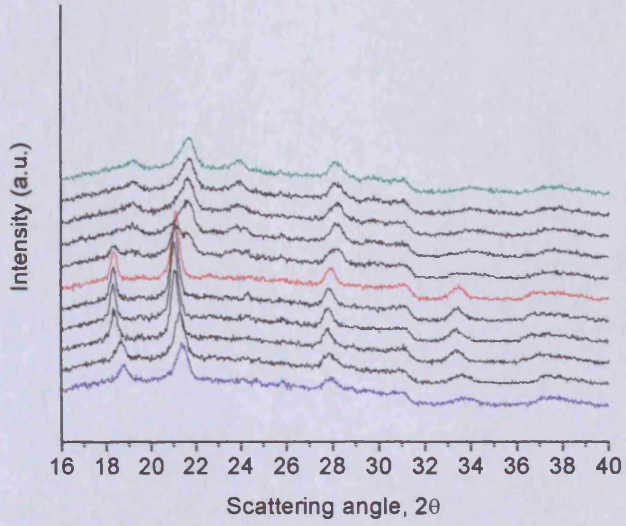

Fig 7.15: XRPD pattern of $VOPO_4$ sample after catalytic test. It is possible to re-obtain (—) ω-$VOPO_4$, from (—) δ-$VOPO_4$ at room temperature obtained after the test, under air flow, using a temperature ramp up to 600 °C. The material is also preserved at room temperature (—).

In order to collect more detailed information, Scanning Electron Microscopy (SEM) has been carried out on samples before and after catalytic testing (figs 7.16 and 7.17).

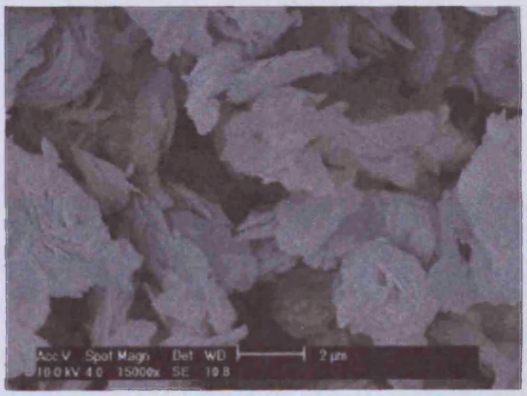

Fig. 7.16: ω-$VOPO_4$ before catalytic activity test, the product is highly homogeneous, with clean edges.

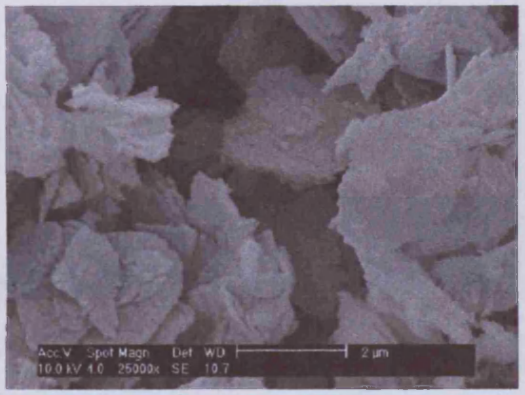

Fig. 7.17: δ-$VOPO_4$ after catalytic activity test (see XRPD pattern in fig 7.15), the product is still homogeneous, but completely fractured, with complete loss of the clean edges.

Before reaction a rosette shape with clean edges is present, while after reaction the VPOs crystals are fully fractured.

7.4.1 Catalytic test of ω-$VOPO_4$ using a periodic flow reactor

In order to verify that reactants like butane are oxidized by ω-$VOPO_4$ in the absence of oxygen catalyst testing using a periodic flow reactor has been carried out. The reactor was equipped with a six port sample valve fitted with a 250 μL sample loop positioned upstream of the reactor. Prior to the start of reaction the ω-$VOPO_4$ was heated to 600 °C for 2 hours, in a stream of flowing air to ensure the catalyst was fully oxidised at the start of the cycle, and then the temperature was decreased to 400 °C to carry out the experiment. Afterwards, butane and helium were introduced to the gas sample valve *via* a calibrated mass flow controller. Samples (250 μL) of this feed were fed to the reactor as discrete pulses using the injection mode of the sample valve.

Using anaerobic conditions, a butane conversion of 2.2 % was observed, and butane oxidation products were detected with the following selectivity: CO_2 (23%), CO (13%) and maleic anhydride (64%), which are similar to the values obtained using aerobic conditions. However, these values account for the first pulse only, where omega is present, but not for the further pulses, due to the phase transition.

These data show that the reaction is chemically induced by the organic substrate with chemical removal of oxygen from the VPO lattice.

7.4.1.1 ω-$VOPO_4$ under vacuum

In order to verify whether phase transition is physically induced and not chemically induced, ω-$VOPO_4$ was treated *ex situ* at 10^{-3} bar for 18 hours at room temperature and afterwards treated at 580 °C using nitrogen. The XRPD pattern recorded at 400 °C gave an identical XRPD profile to that preceding the vacuum treatment (fig. 7.18 below):

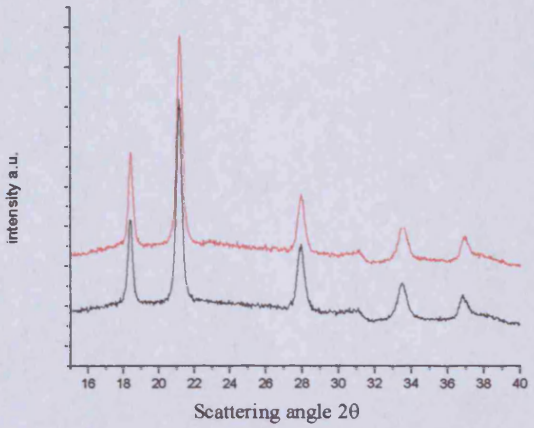

Fig. 7.18: XRPD pattern of ω-$VOPO_4$ at 400 °C (—) before and (—) after vacuum.

This leads to the conclusion that the removal of oxygen is associated with a chemical process, at least in the pressure range explored. Attempted of *in situ* experiments under vacuum have been carried out, but the cell available was not suitable for this purpose, so they provided little information.

7.4.2 Reduction of vanadium centres

The data described up to now indicate that removal of lattice oxygen is a process that has to occur. Such phase transitions of metal oxides are not new [32], however what is different in this study is that the reduction process cannot involve reduction of the bulk material, otherwise ω-$VOPO_4$ and δ-$VOPO_4$ could not be considered as polymorphs because there would have to be a change in stoichiometry. This aspect is crucial, and it makes this observed transition unique [21].

In order to investigate the reduction process XPS and electron paramagnetic resonance (EPR) techniques have been used. In this case EPR investigations proved quite useful, indeed although most of ω-$VOPO_4$ is made of V(V) centres, the V(IV) centres are EPR active with the vanadyl groups able to give hyperfine coupling spectra which can provide

structural information, as well as information on reduction processes [33]. In particular, *in situ* EPR investigations revealed slight differences in the crystal field parameters [21], indicating an increased extent of tetragonal distortion in the VO_6 units for the δ-$VOPO_4$ sample, as would be expected from the removal of lattice oxygen. Furthermore, an increased V(IV) signal intensity was observed for δ-$VOPO_4$ as compared to ω-$VOPO_4$ (from 1.0 to 1.2 arbitrary units), which is in agreement with the XPS observation (24 to 29%, respectively).

Taking into account these data, it is reasonable to think that a reduction of surface lattice oxygen leads to an avalanche effect able to change the whole crystal structure of the material. Another indication that only a minimum amount of lattice oxygen is involved in the process is that *in situ* Raman investigation revealed only small changes in V—O distances [21, 28].

7.5 Phase transitions using different substrates

Up to now, all the data collected and discussed are consistent with the extraction of surface oxygen from the lattice. However, it is quite important to consider a possible effect induced by the reaction products [34], as well as information on the timescale of the observed phase transition. Since the reaction is an oxidation of an organic substrate, the reaction could also be induced by H_2O, CO_2, CO, the maleic anhydride product, as well as acetic acid, that is often observed in trace amounts [2]. All these substrates have been investigated and the results are reported in figures 7.19-7.24. All the experiments were carried out at 400 °C with a total gas flow of 60 mL min^{-1}.

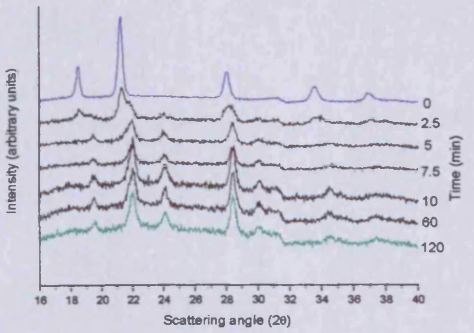

Fig. 7.19: XRPD pattern of (—) ω-$VOPO_4$ at 400 °C under a flow of acetic acid in air. A phase transition is observed and (—) δ-$VOPO_4$ is fully defined after 2 h.

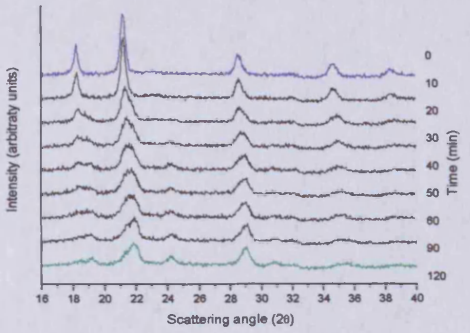

Fig. 7.20: XRPD pattern of (—) ω-$VOPO_4$ at 400 °C under a flow of 5% H_2 in nitrogen. A phase transition is observed and (—) δ-$VOPO_4$ is fully defined after 2 h.

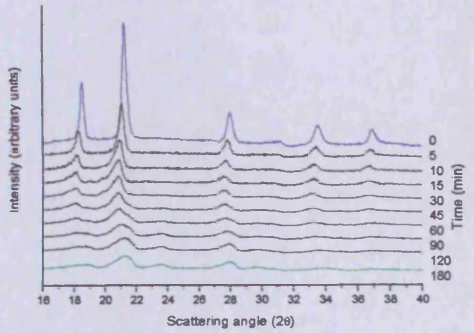

Fig. 7.21: XRPD pattern of (—) ω-$VOPO_4$ at 400 °C under a flow of 5% CO in argon. A phase transition is observed and (—) δ-$VOPO_4$ is fully defined after 3 h.

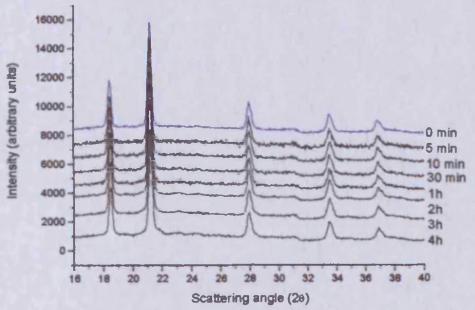

Fig. 7.22: XRPD pattern of (—) ω-$VOPO_4$ at 400 °C under a flow of 5% CO_2 in nitrogen; ω structure remains unchanged after 4 h of reaction on line.

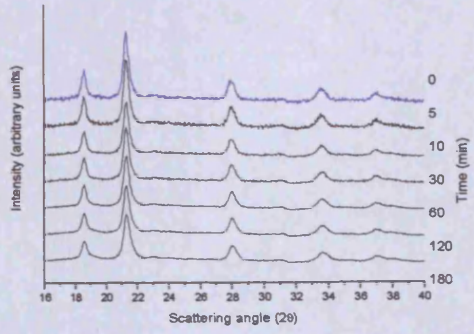

Fig. 7.23: XRPD pattern of (—) ω-$VOPO_4$ at 400 °C under a flow of water vapour in nitrogen; ω structure remains unchanged after 3 h of reaction on line.

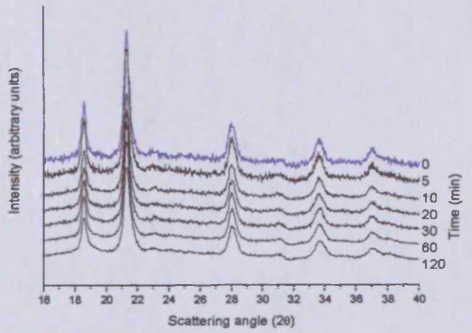

Fig. 7.24: XRPD pattern of (—) ω-$VOPO_4$ at 400 °C under a flow of maleic anhydride in the vapour phase in nitrogen; ω structure remains unchanged after 2 h of reaction on line.

Important considerations can be made. Acetic acid in air is able to induce the phase transition (fig 7.19) although over a longer timescale than *n*-butane, but H_2 in N_2 (fig 7.20) and CO in argon (fig 7.21) are also able to induce the process. These tests prove that the phase transition observed is definitely chemically induced and although a reduction is involved, it should not be considered as the main factor. Indeed, the transformation using 5% H_2 in N_2 has a shorter timescale than that observed for CO, and therefore, it is not simply the reducing nature of the reactant to be involved, but it could be also be the molecular symmetry of the reactant involved in the process that is important. In contrast, CO_2 (fig 7.22) is not able to induce the transformation, at least not after a time on line of 4 h.

The last two experiments, even though not inducing the phase transition, are in fact quite significant. Water, used in vapour phase, is not able to induce the transformation (fig 7.23) this is not a trivial observation because this means that no hydration occurs, and so the transition phase observed is not due to intercalation of H_2O to ω crystal planes, so a reaction really has to be involved. In fact, δ-$VOPO_4$ is known to have this property [35]. Moreover, the absence of reaction when maleic anhydride was used (fig 7.24), is an important result because it means the transition is not due to a template effect [34].

It is worth noting that the reaction using H_2 in N_2 is the easiest to control; and reducing the amount of H_2 to 3% or 1.5 % enables pure δ-$VOPO_4$ to be obtained for characterization. Indeed, once the reducing agent is removed, the lattice stays 'frozen' and it is possible to cool the sample for characterization then to heat it again at 400 °C and to obtain the same XRPD pattern. If hydrogen is re-introduced, the phase transition can carry on again. If the amount of H_2 in nitrogen is 1.5% the process can take up to 16 h before obtaining a good δ-$VOPO_4$, but the quality of the sample can be quite good.

An intriguing test involved the use of chloroform, both in air and in nitrogen. This chemical species has been used because contains carbon in a high oxidation state, but without oxygen atoms. Carrying out the reaction in the usual condition in nitrogen, the phase transition observed (fig 7.24) δ-$VOPO_4$ is well defined after 1 h of reaction time

and the material is fully disordered after 10 h. HCl is detected as a reaction product. However, if air is used, HCl is still detected but no phase transition occurs (fig. 7.25).

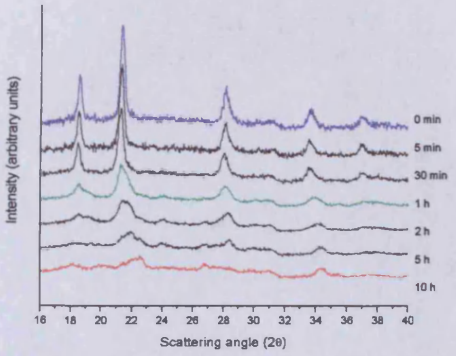

Fig 7.24: XRPD pattern of (—) ω-$VOPO_4$ at 400 °C under a flow of chloroform in the vapour phase in nitrogen; phase transition is observed, and (—) δ-$VOPO_4$ is defined after 1 h. However, if the reaction is carried out for 10 h δ-$VOPO_4$ evolves to (—) a disordered material.

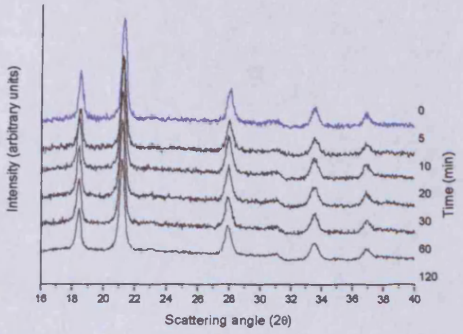

Fig 7.25: XRPD pattern of (—) ω-$VOPO_4$ at 400 °C under a flow of chloroform in the vapour phase in air; the phase transition is not observed after 2 h of reaction.

The reason for this chemical behaviour is still unclear; although when air is used it could be possible to assume a fast replacement of surface lattice oxygen for this particular case. However, possible reaction between the chloroform and the stainless steel walls of the reaction chamber at 400 °C should not be excluded when air is used. Indeed, the presence of HCl has been detected only qualitatively and not quantitatively.

A possible pathway that could lead to HCl is reported in scheme 7.2

Scheme 7.2: Possible pathway for HCl formation during reaction of $CHCl_3$ in nitrogen over ω-$VOPO_4$

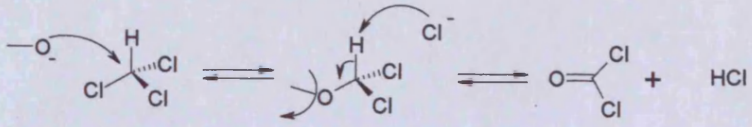

Another experiment worth noting is the use of CO_2 for long term reaction. If the usual reaction time on line of 4 hour is used no reaction occurs, as previously stated, (fig7.22)

but if the test is carried out for 22 h it is possible to observe the phase transition (fig 7.26).

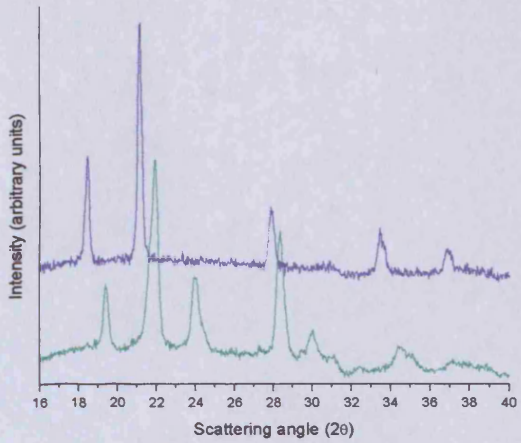

Fig. 7.26: XRPD pattern of (—) ω-$VOPO_4$ at 400 °C under a flow of 5%CO_2 in nitrogen; if XRPD is collected after 22 h it is possible to observe the phase transition to (—) δ-$VOPO_4$, while if a time on line of 4 h was used no transition was observed (fig. 7.22)

These results should not to be considered as a contradiction to the previous results but it has to be considered as another indication of the metastable nature of the ω-$VOPO_4$ phase. As previously observed, the amount of removed oxygen necessary to induce the transformation, must be minor, and over a long term, CO_2 could be able to do that. In addition, this is an indication that is not only the reducing power of the reagent used that is able to induce the transformation. However, has it has not been possible to determine the reaction products for this extended experiment, it has to be considered only as an indication of metastability.

7.6 Conclusions

The first achievement of this work has been to be able to obtain a reliable method for the synthesis of ω-$VOPO_4$, in contrast with other techniques that can give a pure phase, but display a lack of reproducibility. In addition, the method described uses as a starting

material the hemi-hydrate which when calcined, can lead to pyrophosphate and afterwards to omega phase and this has an immediate reflection on the industrial catalyst used to perform *n*-butane oxidation to maleic anhydride. In fact, the industrial conditions used to obtain the active catalyst are very close to the conditions described here to obtain ω-$VOPO_4$. This concern is not trivial, in fact it has been possible to show that the use of ω-$VOPO_4$ as a catalyst results in little conversion, although with good selectivity. Consequently, the best industrial conditions also discourage ω-$VOPO_4$ formation.

The second achievement has been the possibility to identify a fast phase transition between omega and δ-$VOPO_4$ when butane is used. This aspect is important because the existence of a fast phase transition as well as the possibility to regenerate omega when air is used at high temperature, means there is a close structural correlation between the two crystal structures. This experimental evidence helped to classify the vanadyl phosphate catalyst [17] with ω- and δ-$VOPO_4$ as part of the same 'δ family', both having a 3D network assuming a pyramidal view. This aspect in crystallography has been the subject of debate over the last 20 years. In fact, some authors proposed an edge-sharing pyramids or octahedra [35], while other authors, taking into account the possibility of hydration for δ-$VOPO_4$, proposed a 2D network [36]. It is useful to note that the experiments discussed here, as well as showing that ω- and δ-$VOPO_4$ are closely related, did not show any effect of water on ω-$VOPO_4$ (fig. 7.23).

Finally, and maybe this is the most important aspect, it has been possible to observe for the first time a solid state transition, which involves surface lattice oxygen, but preserves the polymorph nature of the two phases. This aspect is quite important because it means that the reduction process on a catalyst surface must be minor and an effect on the surface is able to induce a bulk transformation with a time scale that is the same time scale of the diffusion of the reactant. It is then proposed that the transition ω-$VOPO_4$ to δ-$VOPO_4$ is possible only with a certain minimum concentration of surface oxygen vacancies, in order to facilitate the oxygen mobility necessary to rearrange the structure. From the experimental evidence, it can be seen that the role of surface oxygen is significant since

ω-$VOPO_4$ can oxidize butane in anaerobic conditions, and the omega phase can be re-obtained from delta only when air is used, as well as from the amorphous material after reaction.

In addition, all these experimental observations indicate of the metastable nature of ω-$VOPO_4$. In fact studying the reactivity of ω-$VOPO_4$ towards different substrates such as: *n*-butane, CO, H_2, acetic acid, and the absence of reactivity towards maleic anhydride, helped to clarify the role of surface lattice oxygen. Indeed, in the present work it has also been possible to demonstrate that omega is well defined only at high temperature around 600 °C. Nevertheless, the lower temperature of 400 °C is used it is possible to observe the phase transition only if a suitable reducing agent is introduced, and when this happens the transition can be considered very fast, but only chemically induced. The best example is probably when *n*-butane is used, while when H_2 is used the process is slower and the change occurs in hours rather than minutes when anaerobic conditions are used. However, this last observation is quite useful to prepare a well-defined δ-$VOPO_4$ phase for characterization studies. It should be stressed that when the reducing agent is removed the transition is interrupted, and it can only continue when the reducing agent is re-introduced again.

In closing it can definitely be stated that vanadium phosphorus oxides are unique materials, which are able to provide fascinating fields of study.

7.7 References

[1] P. Amorós, D. Marcos, A. Beltrán-Porter and D. Beltrán-Porter, *Curr. Opin. Solid State Mater. Sci.*, 123, **4**, 1999

[2] G. J. Hutchings, *Appl. Catal.*, 1, **72**, 1991

[3] Z. G. Li, R. L. Harlow, N. Herron, H. S. Horowitz, and E. M. McCarron, *J. Catal.*, 506, **171**, 1997

[4] P. Amorós, M. D. Marcos, M. Roca, J. Alamo, A. Beltrán-Portera and D. Beltrán-Porter, *J. Phys. Chem. Sol.*, 1393, **62**, 2001

[5] G. Centi, F. Trifiro, G. Busca, J. Ebner and J. Gleaves, *Faraday Discuss.*, 215, **87**, 1989

[6] B. K. Hodnett, *Catal. Today*, 477, **1**, 1987

[7] J. G. Speight, *Chemical and Process Design Handbook*, McGraw-Hill, New York, 2002

[8] C. J. Kiely, A. Burrows, G. J. Hutchings, K. E. Bere, J. C. Volta, A. Tuel, and M. Abon, *Faraday Discuss.*, 103, **105**, 1996

[9] G. Centi, *Catal. Today*, 1, **16**,1993

[10] K. E. Birkeland, S. M. Babitz, G. K. Bethke, H. H. Kung, G. W. Coulston and S. R. Bare, *J. Phys. Chem. B*, 6895, **101**, 1997

[11] G. W. Coulston, S. R. Bare, H. Kung, K. Birkeland, G. K. Bethke, R. Harlow, N. Herron and P. L. Lee, *Science*, 191, **275**, 1997

[12] G. Centi, F. Trifiro, J. R. Ebner, V. M. Franchetti, *Chem. Rev.*, 55, **88**, 1988

[13] G. J. Hutchings, C. J. Kiely, M. T. Sananes-Schulz, A. Burrows and J. C. Volta *Catal. Today* 273, **40**, 1998

[14] A. Tuel and M. Abon, *Faraday Discuss.*, 103, **105**, 1996

[15] C. Cacela, A. Baudot, M. L. Duarte, A. M. Matos-Beja, M. Ramos-Silva, J. A. Paixáo and R. Fausto, *J. Mol. Struct.*, 143, **649**, 2003

[16] M. Schneider, M. Pohl, G.-U. Wolf and F. Krumeich, *Mater. Sci. Forum*, 960, **321-323**, 2000

[17] F. Girgsdies, T. Ressler, R. Schlögl, W.-S. Dong, G. Budroni, M. Conte, J. K. Bartley, G. J. Hutchings, G.-U. Wolf and M. Schneider, Poster presented at the XXXIX

Jahrestreffen Deutscher Katalytiker meeting, Weimar, Germany, 15 to 17 March 2006 (http://edoc.mpg.de)

[18] G. J. Hutchings, J. A. Lopez-Sanchez, J. K. Bartley, J. M. Webster, A. Burrows, C. J. Kiely, A. F. Carley, C. Rhodes, M. Hävecker, A. Knop-Gericke, R. W. Mayer, R. Schlögl, J. C. Volta and M. Poliakoff, *J. Catal.*, 197, **208,** 2002

[19] G. J. Hutchings, *J. Mater. Chem.*, 3385, **14**, 2004

[20] G. F. Benabdelouahab, J.C. Volta and R. Olier, *J. Catal.*, 334, **148**, 1994

[21] M. Conte, G. Budroni, J. K. Bartley, S. H. Taylor, A. F. Carley, A. Schmidt, D. M. Murphy, F. Girgsdies, T. Ressler, Robert Schlögl and G. J. Hutchings, *Science*, 1270, **313**, 2006

[22] H. Wibbeke, International Centre for Diffraction Data, Powder Diffraction File, Entry 37-809 (1996).

[23] P. Amorós, M. D. Marcos, J. Alamo, A. Beltrán and D. Beltrán, *Mat. Res. Soc. Symp. Proc.*, 391, **346**, 1994

[24] D. Beltrán, A. Beltrán, P. Amorós, R. Ibánez, E. Martínez, A. Le Bail, G. Ferey and G. Villeneuve, *Eur. J. Sol. State Inorg. Chem.*, 131, **28**, 1991

[25] P. Amorós, R. Ibánez, E. Martínez, A. Beltrán-Porter, D. Beltrán-Porter and G. Villeneuve, *Mater. Res. Bull.*, 1347, **24**, 1989

[26] P. Amorós, D. Beltrán, A. Le Bail, G. Ferey and G. Villeneuve, *Eur. J. of Sol. State Inorg. Chem.*, 599, **25**, 1988

[27] G-U. Wolf, B. Kubias, B. Jacobi and B. Lücke, *Chem. Comm.*, 1517, 2000

[28] G. Budroni (PhD Student) and G. J. Hutchings (Supervisor), *Preparation and Characterization of Catalysts*, PhD thesis, Cardiff University of Wales, 2004

[29] G. J. Hutchings and D. Lee, *J. Chem. Soc. Chem. Comm.*, 1095, 1994

[30] E. Bordes, J. W. Johnson and P. Courtine, *J. Solid State Chem.*, 270, **53**, 1984

[31] J. W. Johnson, D. C. Johnston, A. J. Jacobson and J. F. Brody, *J. Am. Chem. Soc.*, 8123, **106**, 1984

[32] T. Ressler, O. Timpe, T. Neisius, J. Find, G. Mestl, M. Dieterle and R. Schlögl, *J. Catal.*, 75, **191,** 2000

[33] M. Ruitenbeek, A. J. van Dillen, A. Barbon, E. E. van Faassen, D. C. Koningsberger and J. W. Geus, *Catal. Lett.*, 133, **55**, 1998

[34] G. J. Hutchings, A. Desmartin Chomel, R. Olier and J. C. Volta, *Nature*, 41, **386**, 1994

[35] E. Bordes, *Catal. Today*, 499, **1**, 1987

[36] F. Ben Abdelouahab, R. Olier, N. Guilhaume, F. Lefebvre and J.C. Volta, *J. Catal.*, 151, **134**, 1992

Chapter 8: CONCLUSIONS AND FUTURE WORK

8.1 Conclusions

In the present work different areas of heterogeneous catalysis have been explored, both investigating metal supported species and the use of material such as vanadium phosphorus oxides, which can display catalytic activity in the bulk state. Conclusions for these different fields and the related studied reactions are reported separately in the following paragraphs.

8.1.1 Low temperature CO oxidation

From what has been described in this thesis, it is evident that although low temperature CO oxidation is widely investigated in the field of heterogeneous catalysis, the real understanding of its nature and the molecular details operating over a catalyst surface have yet to be reached.

It has been possible to demonstrate that the presence of trace amounts of nitrate over Au/TiO_2 catalyst can lead to enhanced and long term activity improvements which are 20-30% better than the undoped catalyst. Although the origin of this effect is still unclear, it is significant, because it cannot be related to nitrates only, and it underlines once again the importance of the technique used to prepare a catalyst; if trace amounts of nitrate precursor are not removed, variable activity may result [1].

It is worth mentioning recent research, although not yet published, by Moma and Scurrell [2] indicating a dramatic increase of activity of Au/TiO_2 catalysts for CO oxidation after doping with sulphate ions. At the current state of knowledge it is not possible to state if nitrate and sulphate operate at the same level, for instance involving site blocking or the formation of new sites at the perimeter of gold nanoparticles, but it is evident that this is a field worth further investigation. In fact, up to now the role of promoters in gold catalysis

has received little attention, while studies like these could help to design a new class of heterogeneous gold catalysts with enhanced or tuned characteristics.

8.1.2 Hydrochlorination of acetylene using bimetallic gold catalysts

As for the effect of doping agents on catalytic performance of gold catalysts, the use of bimetallic system has been only partially investigated, but with a few important exceptions like vinyl acetate manufacture [3], and the possibility of active core shell structure bimetallic catalysts for primary alcohol to aldehyde oxidation [4].

In the present work it has been possible to support previous studies demonstrating that when gold only is used over carbon as support, it is the best catalyst towards the hydrochlorination reaction of acetylene when compared with metals like palladium, platinum, rhodium, iridium and ruthenium. Although these last metals display little catalytic performance, a positive synergistic effect can be present when they are used to give a bimetallic system with gold.

In particular, it has been possible to identify an enhanced initial activity for catalysts containing a small amount of palladium and iridium, and a long term enhanced activity when rhodium is used, while metals such platinum and ruthenium do not give reproducible results or enhanced activity.

Concerning Au/Pd catalysts, they can be considered superior to catalysts comprising gold only, in terms of initial activity, although quick deactivation by oligomer formation occurs. In addition, it has been possible to demonstrate that even by using the wetness impregnation technique the catalyst obtained is a real alloy system, with a higher amount of Au(III) than the original gold catalyst.

With the data available up to now, it is possible to conclude that the presence of palladium in low amounts can lead to more active catalysts, but due to an inefficient

desorption process the catalyst deactivates. Maybe the reaction occurs at the gold/palladium interface, and this could explain the synergistic effect observed. However, it has to be remembered that this phenomenon is support dependent. Even using carbon as the best support for hydrochlorination reactions, it has been possible to see that the use of different carbons can lead to enhanced catalytic activity, but with loss of the initial promotion effect by palladium.

In contrast with palladium, iridium and rhodium can lead to enhanced catalytic activity by using a higher amount of metal as in the bimetallic catalyst. In these cases, the final catalyst also presents independent bimetallic clusters, although when rhodium is used the bimetallic system is able to preserve high selectivity to vinyl chloride monomer. Also in these cases, the origin of these phenomena is still unclear. It has been possible to demonstrate that when the catalyst has a higher amount of Au(III), it displays higher activity, and all the bimetallic catalysts displaying this phenomenon can lead to enhanced performance.
A point of debate is that this effect is not a peculiarity of the second metal added. It has been possible to observe that catalysts containing gold only can have a significant amount of Au(III) and so good activity, but when the metal added is palladium, iridium or rhodium at low loading, the presence of enhance performance is systematic. Maybe also for iridium and rhodium, the reaction occurs at the metal/gold interface, or the added metal is in some way able to change the electronic structure of the gold cluster leading to enhanced performance. However, for these catalysts the support used is also important since it is possible to obtain different results using different carbons as for the case of the gold/rhodium system.

Bimetallic systems such gold/platinum and gold/ruthenium have been investigated only briefly, leading to poorly reproducible results. In addition, variability in gold catalysts can be present due to gradient effects during the preparation.

Nevertheless, further investigation of the use of gold catalysts towards hydrochlorination reactions, for instance identifying not only a second metal but also a suitable procedure to

increase the amount of Au(III), could be important for many reasons. The reaction product vinyl chloride monomer is one of the most synthesized chemicals in the world with an average production of millions of tons per year, and it is the main block for the production of polyvinyl chloride, which is used in a great number of everyday products. This aspect alone could justify attention to the processes for its synthesis, looking for more efficient routes in terms of yield, to find a cheaper production method, or for milder reaction conditions.

At the moment the use of a catalyst comprising gold only is not competitive in the balanced industrial process. But it has to be remembered that the selectivity obtained can be taken as virtually 100% under the reaction condition used: 1.1 bar for each reactants and a temperature of 180 °C are not too drastic when compared with other manufacturing routes, and it is a one step synthesis.

8.1.3 Hydrochlorination reaction mechanism and gold catalyst properties

A distinctive characteristic in the use of gold catalysts towards hydrochlorination reactions is its exceptional selectivity, which can be considered the highest among metal supported catalysts. Moreover, it is has been possible to demonstrate that gold catalysts can be regenerated off line by treatment using aqua regia, or on line with an activation and regeneration effect of the reactant HCl, while C_2H_2 plays a deleterious role independent of whether the reaction occurs or not. These tests, with the support of XPS data, lead to the conclusion that the active species responsible for the higher activity is Au(III) and it is probable that a redox mechanism involving equilibrium Au(III) ↔ Au(I) could be operating.

In order to explain these properties and the behaviour of the catalyst, the existence of a C_2H_2/Au/HCl complex over the catalyst surface has been postulated. In order to support this proposal, reactivity of gold catalysts towards different triple C-C bond containing substrates such as 1-hexyne, phenylacetylene and 2–hexyne have been tested, as well as using deuterated substrates.

These experiments lead to the conclusion that the highest activity is observed for acetylene only, however an appreciable activity around 10%, is observed also for the other substrates, but only in cases where they contain a terminal hydrogen. 2-hexyne displays an almost negligible activity. Nevertheless, selectivity towards Markovnikov products and mono-chlorinated adducts is preserved, making this property again unique for gold catalysts.

Experiments with deuterated substrates and molecular modelling investigations, lead to the observation an *anti* type addition, with final addition of H and Cl in trans positions on the final double C-C bond products. Such isomerism can be obtained only with a coordinate role of the reactants in a complex, although a route involving carbocation intermediate cannot be excluded and it could be explained proposing an oxidative addition pathway.

Although these results are not conclusive, they are important because they can be considered as the first examples of the existence of alkyne/Au/HCl complexes on heterogeneous gold catalysts, involving further possible reaction pathways by gold, and not only the simple electrophilic-nucleophilic interactions between gold and the organic substrate which are usually considered. In addition, the molecular modelling investigation carried out show very well the possibility of Au to activate triple C-C bonds substrate, predicting *anti* addition as well as the difficulty of desorption of the final product, which can explain the observed tendency for oligomer formation in cases where the reaction temperature is too low.

8.1.4 Hydrochlorination of double C-C bond containing substrates

In order to carry out hydrochlorination reactions on double C-C bonds containing substrates, it has been necessary to move from gold catalyst supported on carbon to gold catalyst supported on metal oxides. In fact, Au/C catalyst has been shown to be selective towards substrates containing triple C-C bonds only. In contrast, Au/ZnO and Au/MgO

catalysts are selective towards substrates containing double C-C bonds only.
However, none of these gold supported catalysts, both supported on carbon or metal oxides, are able to carry out the oxychlorination reaction, but investigation of the behaviour of Au/ZnO catalyst lead to the conclusion that the reaction occurring is hydrochlorination. What is even more important, is that the reaction is not catalysed by gold, but by $ZnCl_2$ formation on the catalyst surface. It has been possible to obtain more efficient catalysts by dispersing $ZnCl_2$ on silica. Nevertheless, it is worth mentioning that although gold displays a deleterious effect in terms of activity, it leads to a catalyst with higher selectivity than for the hydrochlorination of propene.

The use of $ZnCl_2$ based catalyst for the hydrochlorination reaction has, up to now, not been reported in the literature. Maybe this could be due to the poor conversion observed and coking phenomena affecting the catalysts, similar to the behaviour reported in literature for methylation reactions [5]. However, these catalysts show high selectivity towards the hydrochlorination of ethylene and isobutylene, as well as giving chlorinated species by the hydrochlorination of isoprene, which are difficult to obtain using other routes.

8.1.5 Phase transitions of ω-$VOPO_4$

Among vanadyl orthophosphates, the ω-$VOPO_4$ phase has been considered for a long time one of the most difficult to investigate due to its metastable nature. Nevertheless, it has been possible to develop a reliable preparation method via dehydration of the dihydrate precursor $VOHPO_4 \cdot 0.5H_2O$ to pyrophosphate $(VO)_2P_2O_7$ and afterwards thermal treatment in air. Such treatment has two immediate applications: firstly it is a pure phase available for further characterization studies; secondly the conditions used are close to the industrial conditions for *n*-butane oxidation to maleic anhydride. This last aspect is very important because δ-$VOPO_4$ is obtained from ω-$VOPO_4$ as precursor, which displays little activity, and so the industrial preparation conditions discourage ω-$VOPO_4$ formation.

After treatment with *n*-butane ω-$VOPO_4$ quickly evolves to δ-$VOPO_4$ and such transformation can be considered unique among vanadium phosphorous oxides [6]. In fact, although reduction is involved, this is minor in order to preserve the polymorph nature of ω- and δ-$VOPO_4$. This last aspect is considered crucial to clarify the role of surface lattice oxygen, without involving a Mars-Van Krevelen mechanism, and maybe it is not only limited to vanadium phosphorus oxides.

The investigation of this solid state phase transition, using reagents such as CO, H_2, acetic acid, and the absence of reactivity towards maleic anhydride, water and CO_2, helped to clarify the existence of a correlation between ω- and δ-$VOPO_4$. Indeed this provided useful information to determine the dimensionality of the phases, which have been identified as 3D networks for both phases, and to the rejection of the possibility of 2D networks. This helped to determine the crystal structure, i.e. indexing, of δ-$VOPO_4$.

8.2 Future work

Further investigations are possible for all the fields explored in this thesis. The effect of doping agents on gold based catalysts for CO oxidation suggests that the observed effect could not be limited to nitrates only, but other anions could also display similar phenomena. A systematic study on the effect of different anions, not limited to TiO_2, but also other metal oxides could be carried out.

Regarding the hydrochlorination reactions, the role of bimetallic catalysts could be investigated further to see whether improvements in the catalytic activity and the real understating of the electronic effect of the second metal on gold. It has been observed that the reaction is support dependent, even amongst carbons; therefore, it could be interesting to find a carbon able to give a lower deactivation rate, which could lead to a catalyst attractive for industrial applications.

The collected data support the hypothesis of C_2H_2/Au/HCl complex formation when gold

catalysts are used for the hydrochlorination of alkynes. More detailed investigation using molecular modelling procedures could clarify further aspects of the reaction mechanism, with specific considerations towards reactions using terminal alkynes.

Hydrochlorination of double C-C bond containing substrates, can be achieved using $ZnCl_2$ based catalyst. The conversion observed is low, but the selectivity is high, and a possible field of investigation, could be the identification of supports able to decrease the observed coking phenomena that at the moment are an obstacle for suitable applications of these catalysts.

Finally, further investigations are possible for the phase transitions of ω-$VOPO_4$, and vanadyl orthophosphates. Up to now, all research attention has been focused on the use of *n*-butane as a reducing agent, due to its importance in the maleic anhydride manufacture. However, the oxidation reaction could be extended to substrates containing double or triple bonds. Particularly, a series of tests using ethane, ethylene, and acetylene, could provide useful information on the oxidation properties of ω-$VOPO_4$, and to provide further information on the nature of the phase transition, perhaps finding a correlation with carbon hybridisation.

In addition, it could be interesting to evaluate the effect of different oxidizing agents such NO or NO_2 in the crystallization process of ω-$VOPO_4$, or it could be possible to find a preparation route to give ω-$VOPO_4$ directly from the hydrate, as in the case of β-$VOPO_4$. Also, metal cations such as Bi could be intercalated to evaluate the effect on catalytic activity and the kinetics of the phase transition.

8.3 References

[1] B. Solsona, M. Conte, Y. Cong, A. Carley and G. Hutchings, *Chem. Comm.*, 2351, 2005

[2] J. A. Moma and M. S. Scurrell, *Dramatic promotion of gold/titania for CO oxidation by sulphate ions*, talk presented at CATSA 2006, 14th-17th November 2006, Mossel Bay, South Africa

[3] D. J. Gulliver and J. S. Kitchen, BP. Chem. Int. Ltd., EU Patent #654301, 1995

[4] D. I. Enache, J. K. Edwards, P. Landon, B. Solsona-Espriu, A. F. Carley, A. A. Herzing, M. Watanabe, C. J. Kiely, D. W. Knight and G. J. Hutchings, *Science*, 362, **311**, 2006

[5] Z. Fu, Y. Yu, D. Yin, Y. Xu, H. Liu, H. Liao, Q. Xu, F. Tan and J. Wang, *J. Mol. Catal. A: Chem.*, 69, **232**, 2005

[6] M. Conte, G. Budroni, J. K. Bartley, S. H. Taylor, A. F. Carley, A. Schmidt, D. M. Murphy, F. Girgsdies, T. Ressler, Robert Schlögl and G. J. Hutchings, *Science*, 1270, **313**, 2006

[7] M. G. Willinger, D. S. Su, and R. Schlögl, *Phys. Rev. B*, 155118, **71**, 2005

Appendix A: REACTION WALLS PRODUCTS

A.1 Time evolution of reaction walls products

In chapter 4, when presenting the chromatogram of the hydrochlorination of acetylene (fig 4.13) has been indicated a small impurity which is always present when both reactants are present. As previously stated in the case of acetylene reaction this does not affect the final results, because the amount of acetylene reacting to the walls is less than 1%. Attempts of identification of these products, using 1H-NMR, allow identifying H bonded to double C-C bond only.

However it is to note that such products do not occur on reactor walls, which are made of glass, but on the stainless steel making the lab rig pipes. These products are observed even at room temperature and only when HCl is introduced.

In addition, these products are not distinctive of acetylene but they are present when ethylene is used as well. In chapter 6, fig 6.7, a small peak is indicated and claimed as impurity, but actually is again a reaction wall product. In the case of hydrochlorination of ethylene the conversion values are lower if compared with acetylene, therefore is easier to note these peak even without using an enlarged scale. For this reason, in the case of ethylene a more systematic treatment has been done in order to identify these products.

In figures A.1 and A.2 are reported 2 chromatograms on line, flowing the reactant through the by-pass of the lab rig at room temperature. The by pass used for this test is new in order to evaluate the evolution of these products during time.

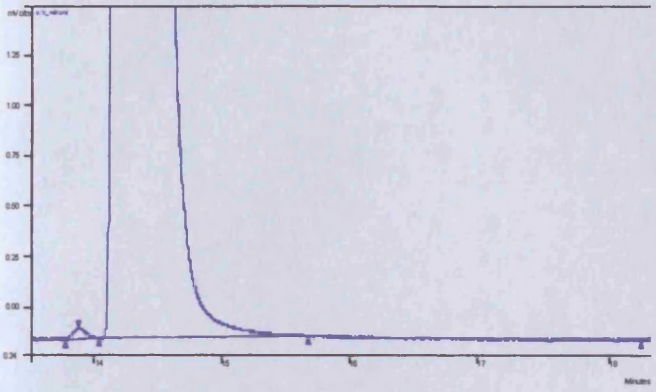

Fig. A.1: Chromatogram of He/C_2H_4 mixture through new by-pass

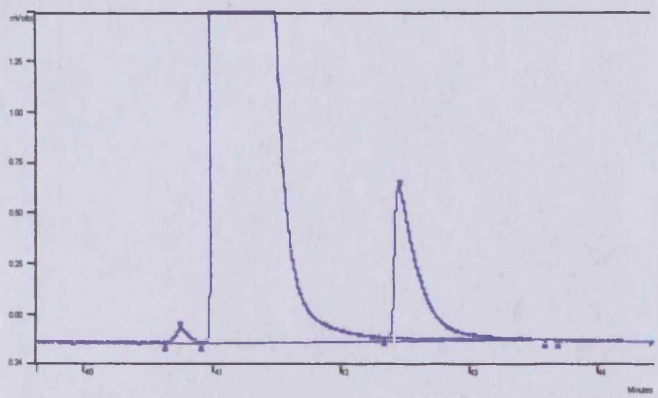

Fig. A.2: Chromatogram of HCl/C_2H_4 mixture through new by-pass

The scale is enlarged, the first very small peak is an ethylene impurity, the second is ethylene and the third the reaction products.

When the He/C_2H_4 mixture is used no reaction product is detected (fig A.1), but when HCl is introduced on line, they are (Fig. A.2)

The chromatogram below (Fig. A.3), has been obtained collecting all the chromatographic injections on line, the increasing trend of these reaction walls products during time is displayed.

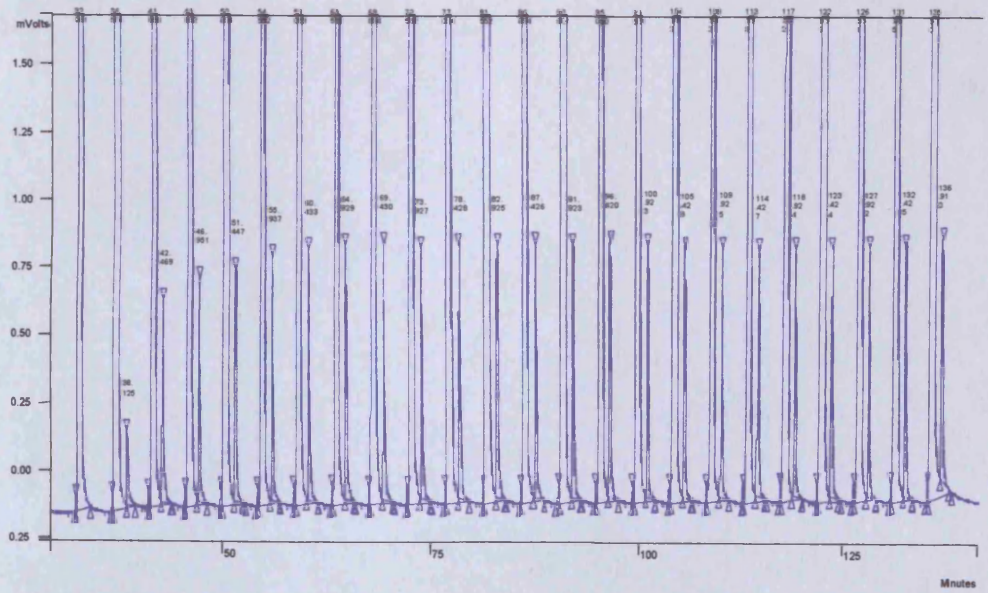

Fig. A.3: Trend formation of reaction walls product with time. The highest peak is ethylene, the smallest reaction walls product

Moreover, it is significant to note that when both of the reactants (C_2H_4 and HCl) are removed, while the ethylene signal decrease of thousands of times, the reaction walls products decrease of less than 50% (fig. A.4)

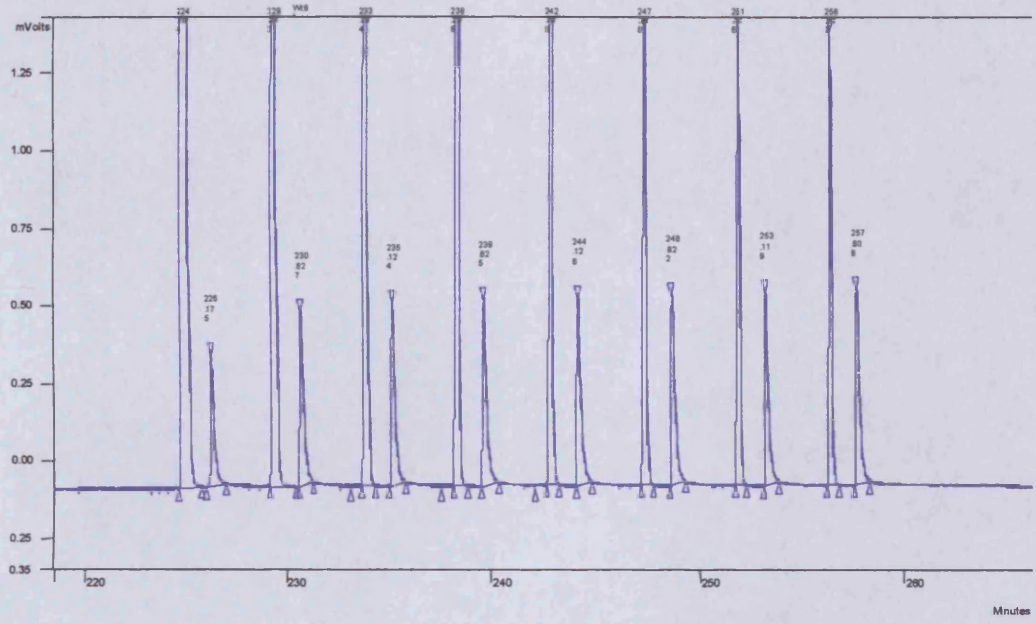

Fig. A.4: Chromatogram of He only through new by-pass after C_2H_4/HCl on line

A.2 Attempts of identification of reaction walls products

The reaction walls products present like a very fine green powder, but of different consistency than the oligomer vinyl chloride. They display a limited solubility in acetone and a very limited in chloroform, and this can explain why usually are not detected during NMR characterization of reaction products being used a chloroform trap.

Two different attempts in order to identify this product with GC-MS and NMR have been done. The first has been a GC-MS determination, while second ^{1}H-NMR in deuterated acetone.

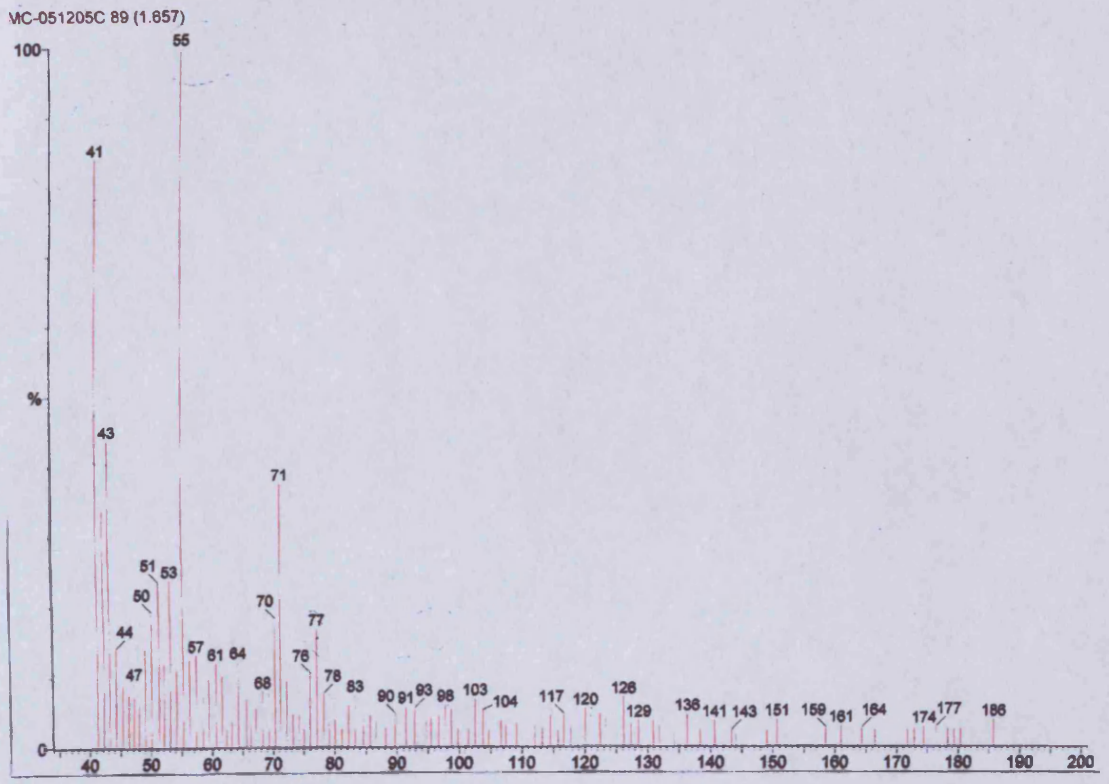

Fig. A.5: Mass spectrum profile for reaction walls product

From the MS pattern in fig A.5 it is possible to identify the ions: $C_3H_3^+$ (41), $C_3H_7^+$ (43), $C_4H_7^+$ (55), $C_5H_{11}^+$ (71), and $C_6H_5^+$ or $C_3H_6Cl^+$ (77), which are typical of chlorinated alkanes.

In addition, the peak at m/z 77 it is well known to be characteristics for benzene, and indeed also a peak at m/z 51 (loss of C_2H_2) is present. However the benzene formation can be considered as few reliable. Nevertheless it is difficult also that the peak at 77 is $C_3H_6Cl^+$ because, if so, also a peak at m/z 79 with 1/3 ratio should be detected (there is one peak but not with the expected ratio).

Collecting spectra in the range m/z 32-60 is possible to obtain the following pattern (fig A.6):

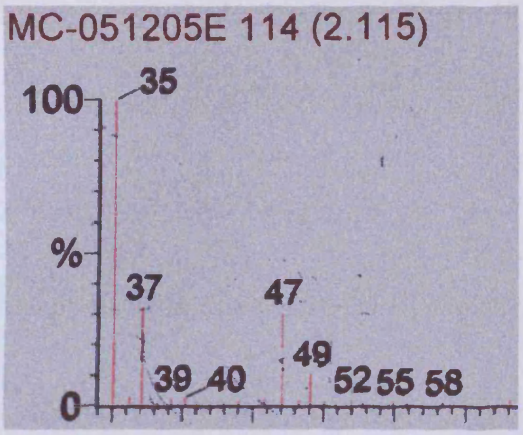

Fig. A.6: Mass spectrum profile of reaction walls product in the range m/z 32-60

The presence of chlorine is well evidenced by the peaks at m/z 35 and m/z 37 with 1/3 ratio and the two peaks at m/z 47 and 49 diagnostic of the CCl^+ fragment.

Using ^{1}H-NMR the only significant region is between 5.5 and 3 ppm, as reported in the spectrum below (fig. A.7)

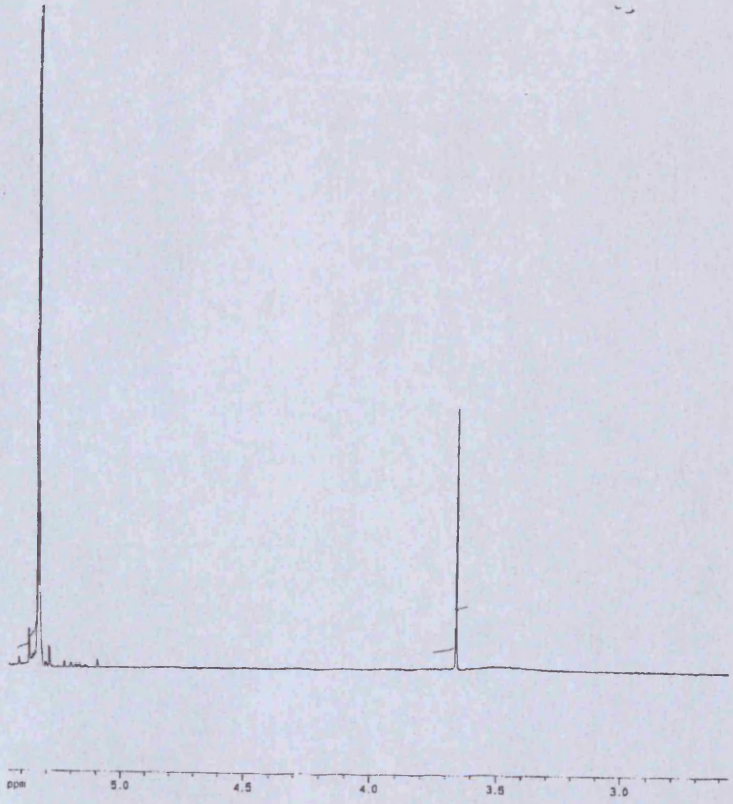

Fig. A.7: ^{1}H-NMR of reaction walls product in deuterated acetone. Spectrum obtained at 500 MHz.

From the NMR spectra it is possible to determine very well the presence of H bonded to carbon with double bond at 5.33 ppm (and as a singlet this could be also ethylene), and the peaks of CH_2 and CH_3 bonded to a strong electron attractor atom as oxygen or halogen at 3.66 ppm. No trace of benzene at higher ppm is detected. In conclusion the nature of this products is still unclear and it is possible only to state that they are chlorinated light products. Finally is to underline once again, that these product are detected only on stainless steel surface and not on inert surface used in the lab rig like glass of poly-tetrafluoro-ethylene.

Appendix B: CHARACTERIZATION OF REACTION PRODUCTS OF DOUBLE C-C BONDS CONTAING SUBSTRATES

B.1 Introduction

In this appendix characterization of the reaction products shown in chapter 6 is described. The description is mainly focused on the demonstration that chloral or 1,2-dichlororethane are not the products of the attempts of oxychlorination reaction of ethylene, but chloroethane and therefore the reaction that really occurs is hydrochlorination.

In addition, ^{1}H-NMR spectra of the other products carrying out hydrochlorination reaction on Au/ZnO and $ZnCl_2/SiO_2$ catalysts are described.

NMR characterizations have been carried out at 400 or 500 MHz, using an Avance DPX-400 Spectrospin Bruker and a Avance 500 Bruker Ultrashiled NMR spectrometers respectively. All the samples have been prepared in deuterated chloroform dissolving the reaction product previously collected in a chloroform trap. In most of NMR analysis the aim to detect products in trace level was present, as consequence for all the spectra afterwards described a number of 1024 scans on protons signal were used.

B.2 Chloral

Chloral, 2,2,2 trichloroaldehyde, is a byproduct always present when oxychlorination reaction occurs. However, it is a chemical that, when hydrate, can find applications such: hypnotic, antiseptic and drugs precursor.

Initially having ambiguous information of the nature of the reaction products over Au/ZnO catalyst, attention has been reserved in chloral formation or by-products.

Using a pure sample of chloral, the first test has been to determine the retention time. A chloral chromatogram is reported below (fig B.1)

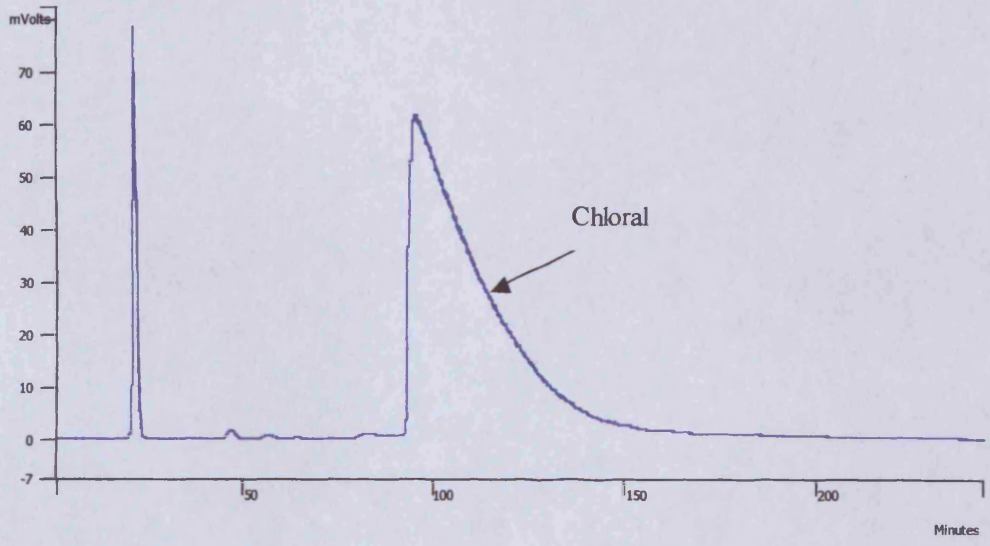

Fig. B.1: Chromatogram of a pure chloral sample using the same chromatographic conditions specified in chapter 4.

The detected retention time over 100 minutes it is not consistent with any expected product of oxychlorination of ethylene. While some doubts were present foe chloral impurities, but again with no match.

Chloral is know to be quite unstable, if exposed to air or light it can lead to not well defined species by hydrolysis or polymerisation.

^{1}H-NMR of a chloral sample stored in a vial exposed to light for 4 days led to the following ^{1}H chemical shifts (fig. B.2).

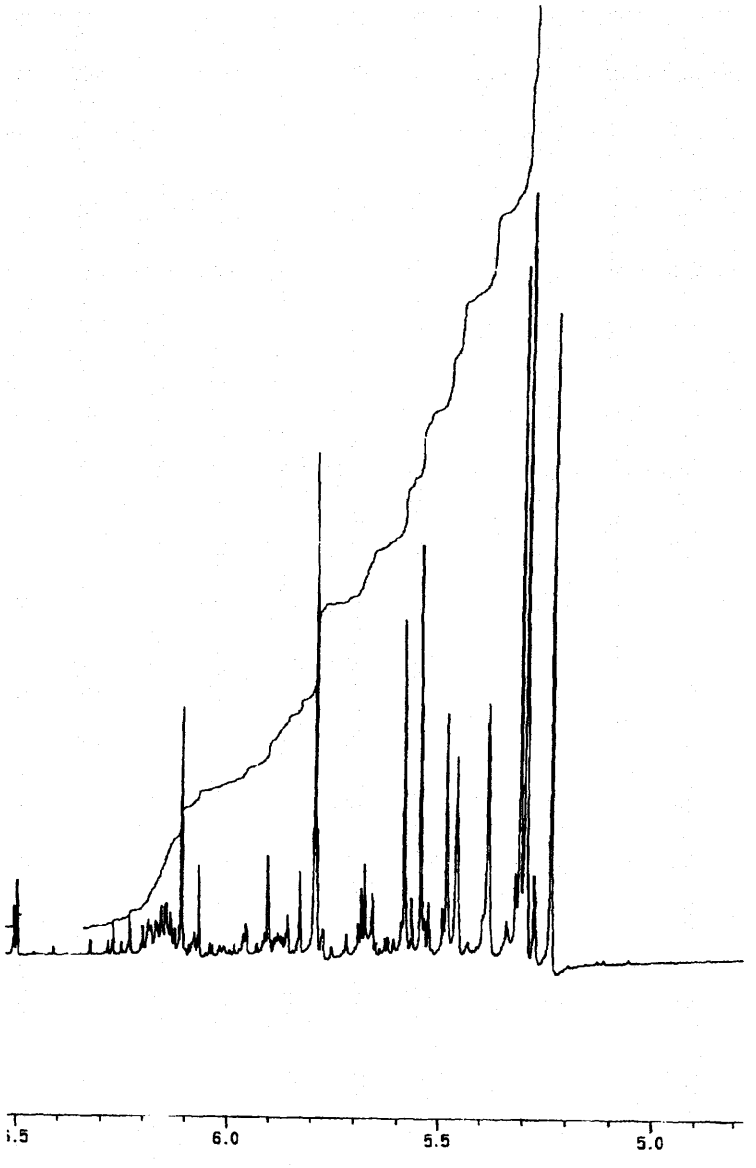

Fig. B2: ^{1}H-NMR of chloral after exposure to light for 4 days. Spectrum obtained at 500 MHz.

The NMR spectrum is quite complicated and displays the presence of diastereoisomers, but there is no match with the expected products as 1,2-dichlroethane, 1,1-dichloroethane, or chloroethane.

These evidences lead to conclude that chloral is absent when attempt of oxychlorination reaction were carried out, and from these data it has been decided to carry out experiments in absence of oxygen.

B.3 Hydrochlorination of ethylene on $Au/ZnO/SiO_2$

Taking into account the results above, and the poor activity over $Au/ZnO/SiO_2$ to carry out the oxychlorination reaction in presence of oxygen. A further test has been repeated using as reaction mixture containing ethylene and HCl only. Products have been collected in a chloroform trap.

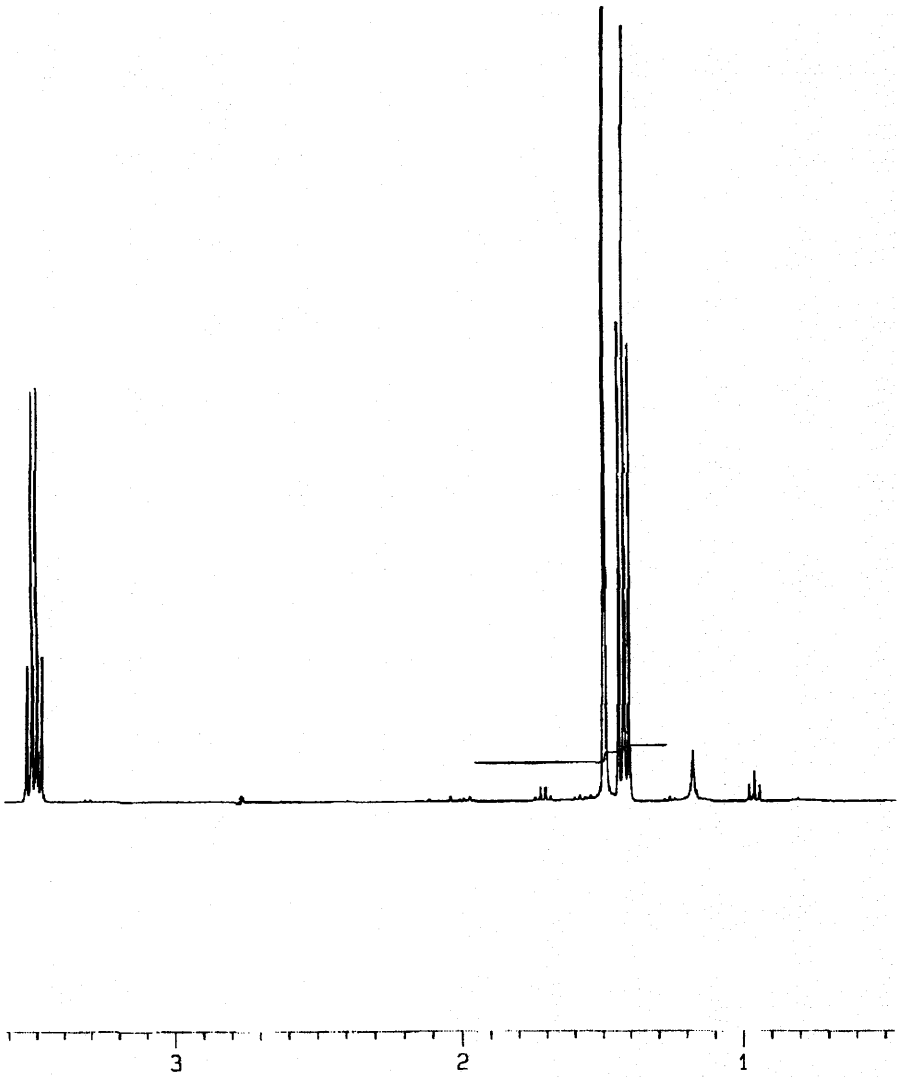

Fig. B.3: ^{1}H-NMR of chloroethane after hydrochlorination of ethylene on $Au/ZnO/SiO_2$ catalyst. Spectrum obtained at 400 MHz

This spectrum allowed unambiguous identification of chloroethane. The signal at 3.68 ppm is associated to the $-CH_2-$ group, while the signal at 1.42 ppm is associated to the CH_3 group. The coupling of this two signal has been confirmed also by using ^{1}H-COSY NMR. In addition for the test carried out, it is evident the presence of water, singlet at 1.49 ppm.

Having identified the product, the identification of chloroethane on Au/ZnO catalyst has been done using the chromatographic retention time. The same procedure has been used for the $ZnCl_2/SiO_2$ catalyst.

B.4 Hydrochlorination of propene on Au/ZnO

In this case characterization of reaction products have been carried out via mass spectrometry suing a Varian TurboMass Ariel spectrometer and a DB-Wax capillary column and initial isothermal conditions at 40 °C.

The main product has been identified as 2-chloropropane (figs B.4and B.5)

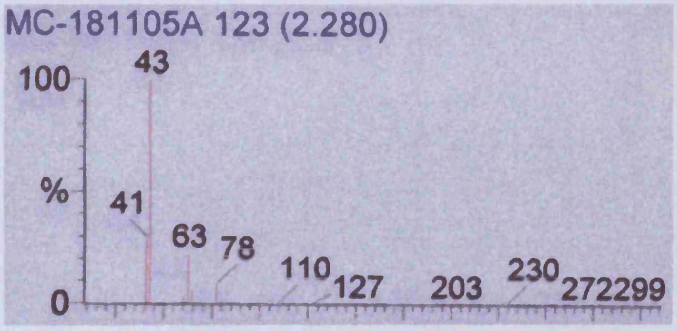

Fig B.4: Experimental mass spectrum profile of 2-chloropropane

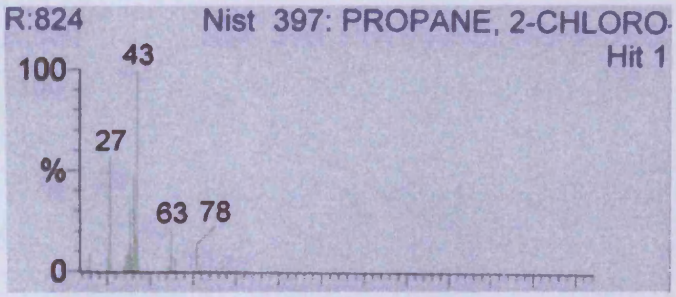

Fig B.5: Standard mass spectrum profile for 2-chloropropane

The anti-Markovnikov product, 1-chloropropane has been identified as well (figs B.6 and B.7) in traces level.

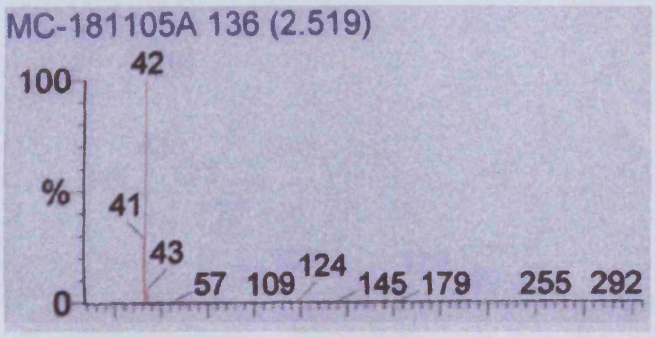

Fig B.6: Experimental mass spectrum profile for 1-chloropropane

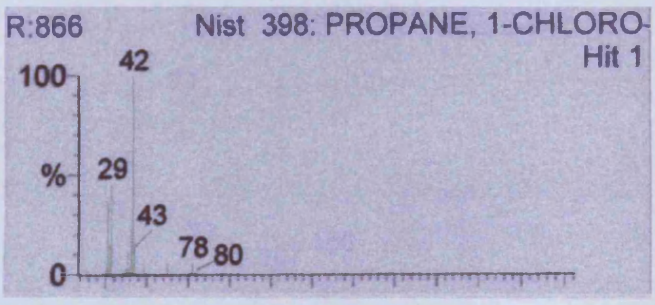

Fig. B.7: Standard mass spectrum profile for 1-chloropropane

However 1-chloropropane, has been quantified only in traces level, having obtained a signal more than 1000 times lower that the signal of 2-chloropropane.

B.5 Hydrochlorination of isobutylene on Au/ZnO

This reaction leads to 2-chloro-2 methyl-propane as the only detected product. In figure B.8 in indicated the singlet originated by the three $-CH_3$ groups at 1.55 ppm and the signal of the $-CH_3$ groups of the starting material isobutylene at 1.66 ppm.

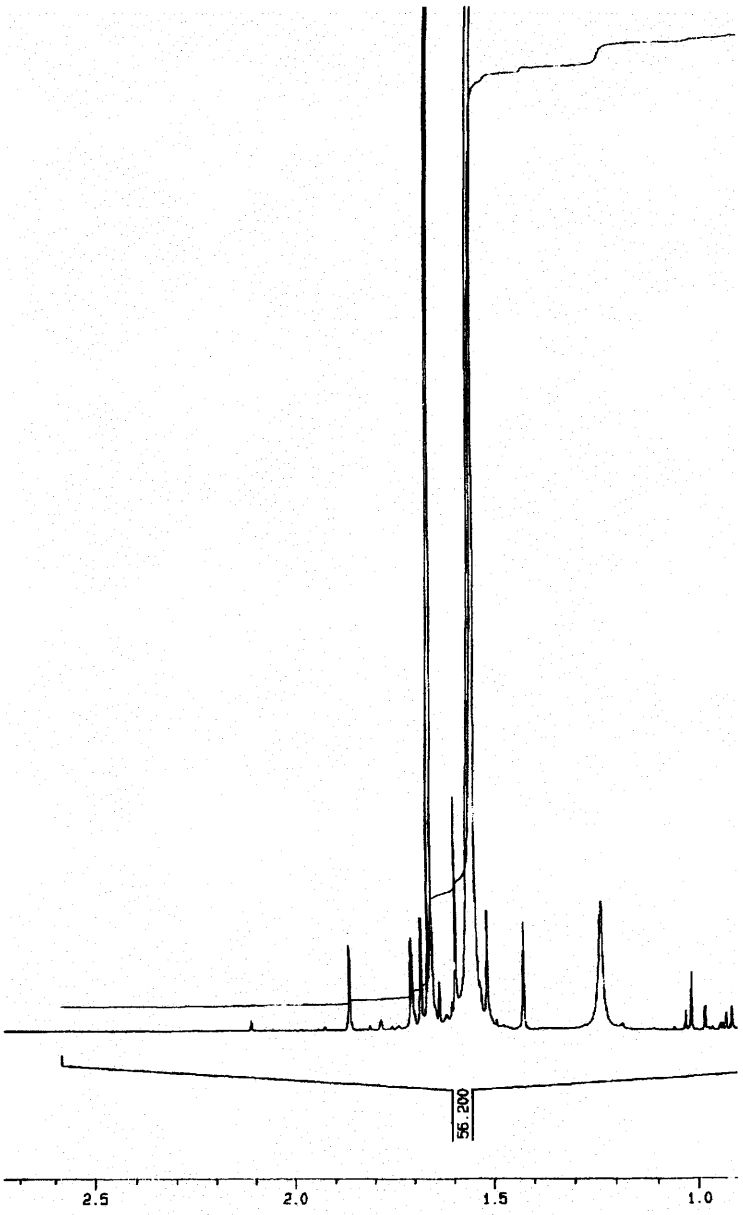

Fig. B.8: ^{1}H-NMR detail of 2-chloro-2methyl-propane and starting material isobutylene. Spectra obtained at 500 MHz.

B.6 Hydrochlorination of propene on $ZnCl_2/SiO_2$

In the figure B.9 below, is reported a ^{1}H-NMR detail of the reaction products of propene on $ZnCl_2/SiO_2$ catalyst. In contrast with the Au/ZnO catalyst, this time it is possible to detect also the presence of the anti-Markovnikov product.

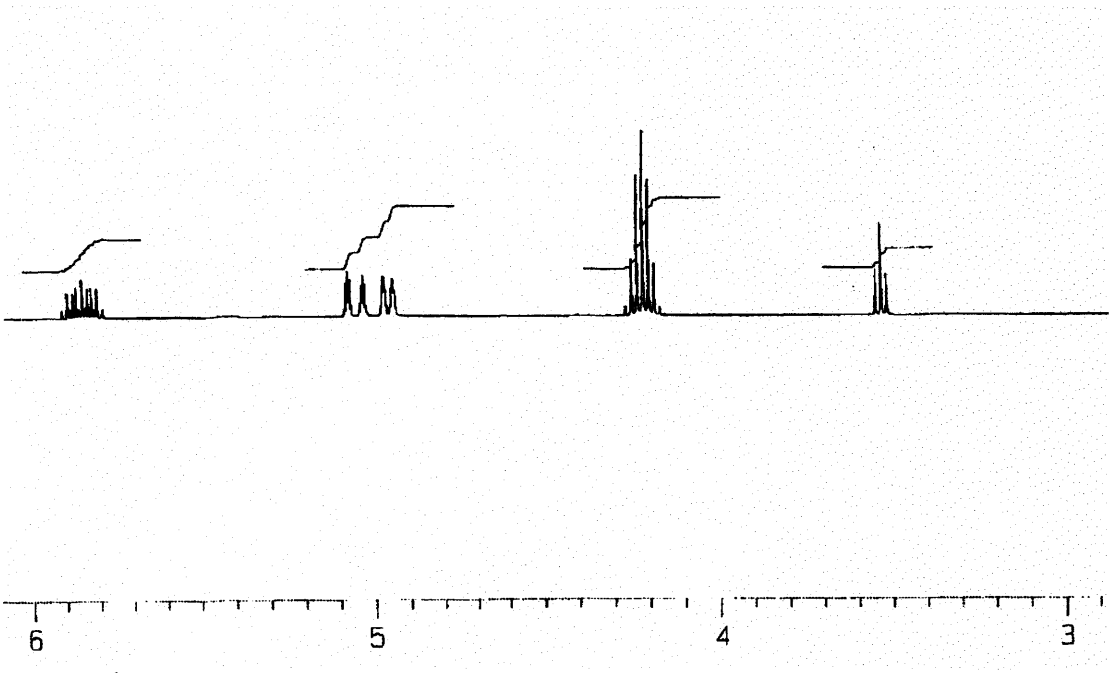

Fig. B.9: ^{1}H-NMR detail of hydrochlorination reaction product and starting material on $ZnCl_2/SiO_2$ catalyst.

The signal at 4.2 ppm is originated from the single proton in position 2 of 2-chloropropane, while the signal of the terminal CH_3 of 1-chloropropane is at 3.5 ppm. The signals at 5.87, 5.05 and 4.95 ppm are generated from the protons bonded on the double bonds of the starting material propene. The multiplet system observed is due to hyperfine coupling using a 400 MHz instrument.

B.7 Hydrochlorination of isobutylene using $ZnCl_2/SiO_2$

The only product detected is the Markovnikov adduct, 2-chloro-2-methyl propane that gives a singlet at 1.55 ppm, while traces only of the anti-Markovnikov 1-chloro-2methyl propane are present in the very small signal at 4.44 ppm (fig B.10).

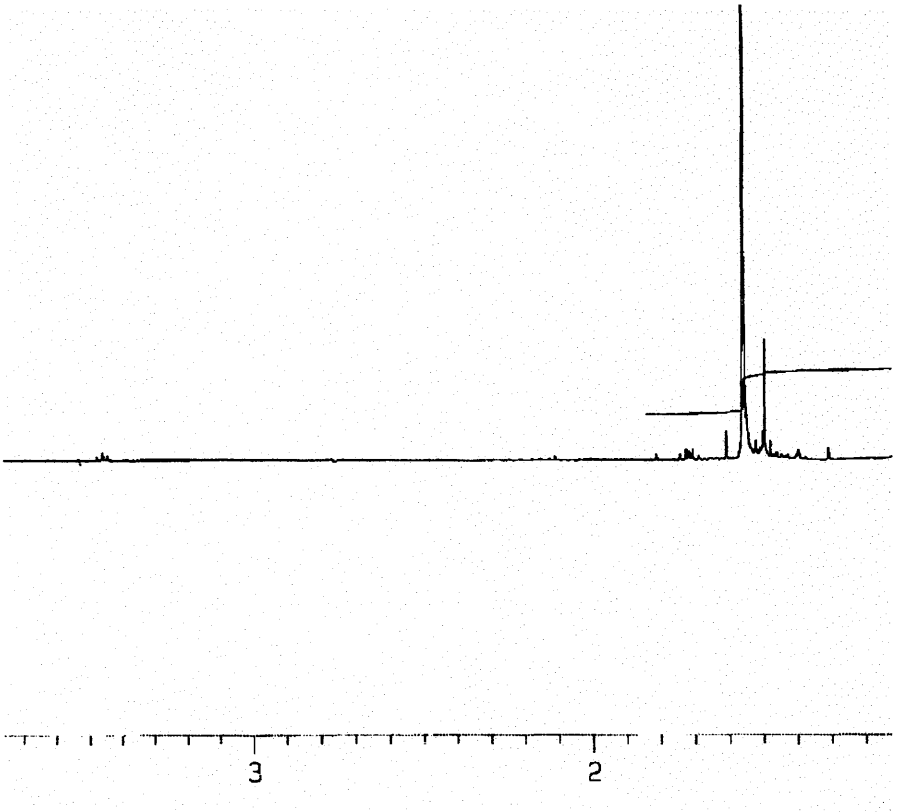

Fig. B.10: 1H-NMR of 2-chloro-2methyl propane. Spectrum obtained at 400 MHz

It is worth noting that in this spectrum the signal of the starting material isobutylene is absent due to evaporation in contrast with the sample used for the hydrochlorination of isobutylene on Au/ZnO

B.8 Isomerisation of chloropropane on $ZnCl_2/SiO_2$

Isomerisation products of chloropropane on $ZnCl_2/SiO_2$ are reported in the following spectrum (fig. B.11)

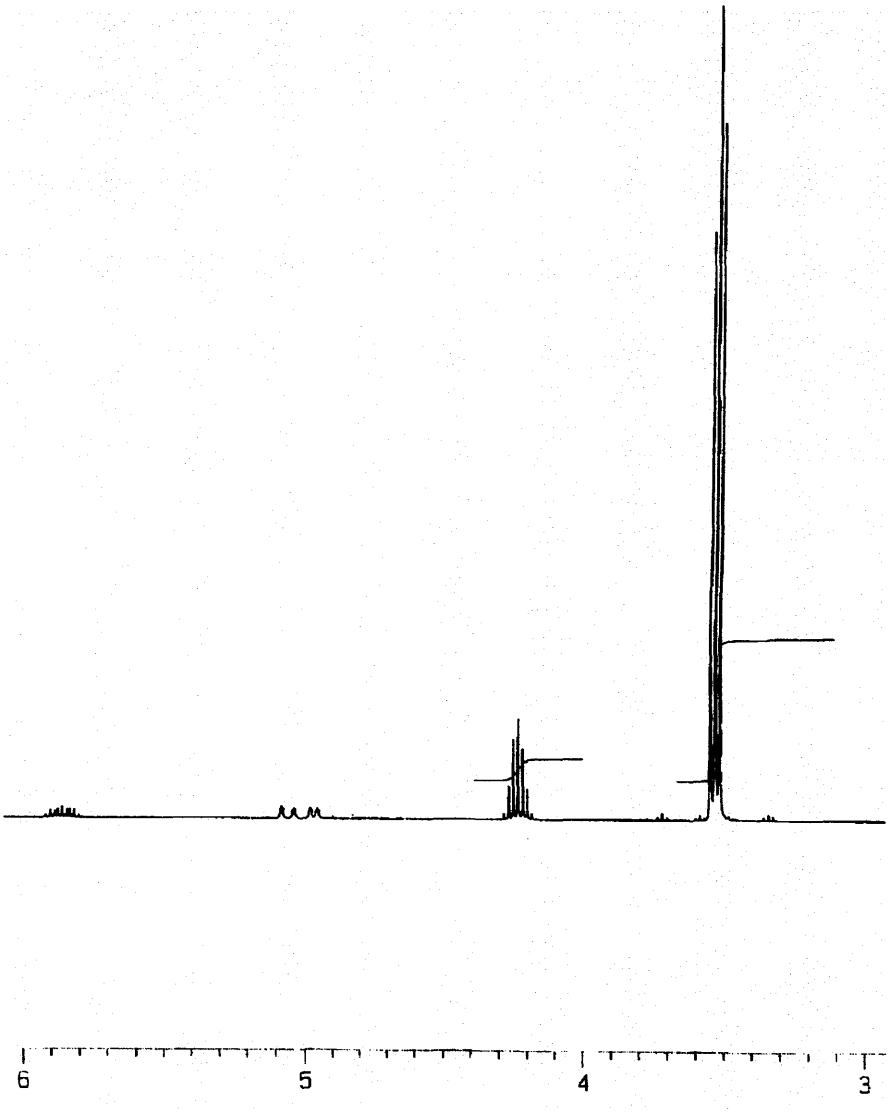

Fig. B.11: 1H-NMR of isomerisation products of chloropropane on $ZnCl_2/SiO_2$. Spectrum obtained at 400 MHz.

The triplet of the terminal methyl at 3.55 ppm identifies the starting material chloropropane, while the isomerisation product 2-chloroprapane is identified by the signal of the single proton in position 2 at 4.2 ppm. It is interesting to note that propene is detected as well, hyperfine coupling at 5.88, 5.05 and 4.95 ppm respectively for the hydrogens bonded to the double bond. Propene can be obtained *via* elimination reaction as described in chapter 6

B.9 Hydrochlorination of isoprene using $ZnCl_2/SiO_2$

Using a 400 MHz instrument several hyperfine coupling are present and the resulting spectra is complex. However presence of the starting material can be identified from the highest intensity peaks at 6.52, 5.28, 5.18 and 5.03 ppm. The smallest peaks systems are instead due to the hydrochlorination and elimination products at 6.15, 5.5 and 4.12 respectively (fig. B.12)

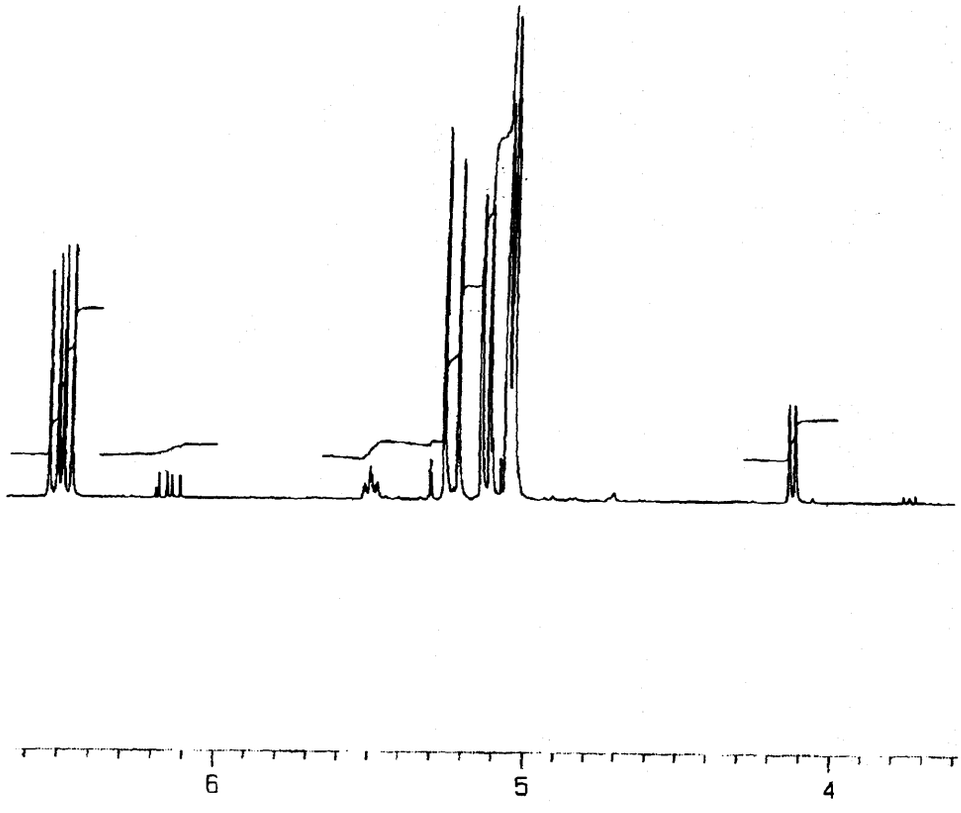

Fig. B.12: ^{1}H-NMR of isoprene hydrochlorination reaction. Spectra obtained at 400 MHz.